Low Velocity Edge Impact on Composite Laminates: Damage Tolerance and Numerical Simulations

by

Anjum Malhotra

A thesis submitted for the award for the degree of

Doctor of Philosophy

School of Engineering and Materials Science

Queen Mary

University of London

Mile End Road

London E1 4NS

August 2014

ABSTRACT

Composite laminates are increasingly being used in more complex structural applications where edges and cut outs are inevitable. These applications include wing skins of military and civil aircraft, further aerospace applications as well as automotive panels and critical structures. Composite components in such applications are highly susceptible to damage. Composites behave in a different manner to conventional metallic materials, which has introduced several design problems not previously encountered. One such problem has been the susceptibility of the material to accidental low energy impacts which frequently leave no visible mark on the impacted surface but considerable internal damage. Investigation of the residual strength and stiffness of composites after edge impact has become important for the design of aerospace components.

Previously, the research work involved central impact of composite laminates but in this research we are investigating edge impact behaviour of composite laminates as parts of composite structures are particularly vulnerable to impacts, including near the edge of an inspection port or other aperture. Furthermore, impacts to such areas may lead to more severe damage near the edge of the laminate rather than the surface. Thus the present work extends these investigations to impact on the edge of composite laminates.

The thesis includes both experimental investigations and finite element simulations of impact damage on the plane of the laminate near the edge (near-edge), and on the edge (on-edge) of composite laminates. A comparison with centre impact with on and near-edge impact is done to understand the damage on the edges and away from the edges. A new design has been developed and implemented to perform edge impact experiments.

The research investigated the effects of various parameters like thickness, absorbed energies, force-time histories and damage behaviour of composite laminate. The damage size and mechanisms have been explored. Impact simulation was carried out using finite element code Abaqus. Explicit solution technique of the code was used to analyse the edge impact phenomenon. Results of the finite element analysis were compared with experiments. The residual strength of the laminates under compressive and tensile loading has been measured. Tensions after impact (TAI) tests were conducted to evaluate the residual load carrying

capacity. The effect of edge impact on the low velocity impact response and the residual tensile strength is discussed via the test results.

This thesis also includes computed tomography as the main technique for micro level damage characterisation and investigates the study of damage mechanisms of glass/epoxy laminates subjected to edge impact with varying energy levels and thickness. Computed Tomography aims to provide damage behaviour such as internal damage state, delaminations during different types of edge impact.

ACKNOWLEDGEMENTS

With All God's grace, I am submitting my PhD thesis and would like to thank everyone who has contributed towards its completion.

First of all, I would like to express my sincere gratitude to my supervisor, Professor Felicity J Guild, for her continual guidance, motivation, financial support and encouragement throughout the project and it is due to her support I am able to complete my PhD. Furthermore, I am very grateful to my second supervisor Professor Martyn J Pavier for his invaluable advice. Also, I would like to thank Dr. Graham Davis for his excellent guidance in analysing damage in composites using Computed Tomography.

Furthermore, I would like to sincerely thank Prof. Mike Reece for supporting my studies in the SEMS department throughout the research in tough times. Many thanks to colleagues in the Department of Materials, Queen Mary, University of London, especially Dr. Kyriakos Berketis, Mr. Bill Godwin and Mr. Colin Langdown for experimental work and Choothum, Tu and Wei for their advice in Finite element simulations, without them I would have had a much harder time.

Finally, I am very grateful to my brother Anuj and my parents for standing by me and supporting me throughout my studies.

I am also thankful to my parents-in-law, brother-in-law and sister-in-law for all their blessings and best wishes for my PhD.

Last but not least, I would like to express many thanks to my wife Shweta for her love and kindness and for being my light in the darkness and showing me hope where there was none left for me to see.

And I am extremely glad that I am submitting my PhD thesis at the time when my baby Aayansh is one year old. With his love and being him on my side has always kept me energetic and motivated to complete my PhD.

PUBLICATIONS

- "Edge Impact of Composite Laminates : Experiments & Simulations"(2008) - Journal Of Material Science – Published.
  (Available on website: http://link.springer.com/article/10.1007%2Fs10853-008-2863-z)

- "Impact Damage of Composite Laminates: Effect of Impact Location" (2014) - Applied Composite Materials – Published.
  (Available on website: http://link.springer.com/article/10.1007%2Fs10443-013-9382-z)

CONFERENCES

- Deformation and Fracture of Composites (DFC-12) "Impact Damage of Composite Laminates: Effect of Impact Location", A Joint Sheffield-Cambridge-Manchester Conference, Queen's College, Cambridge, 8-11 April 2013.
- Invited Speaker on topic "Damage Tolerance of Composite Laminates subjected to edge impact" at Comptest conference held in 2008 at US Air Force Research Laboratory –Dayton, USA.
- Third Euro-USA Conference Presentation - "Stretching the Endurance Boundary of Composite Materials: Pushing the Performance Limit of Composite Structures", Madeira, Portugal- September 2007.

AWARDS AND POSTER PRESENTATIONS

- PhD Overseas Research Scholarship from School of Engineering and Materials Science, Queen Mary, University of London (2007-2012).
- Poster Presentation on "Edge Impact of Composite Laminates: Experiments & Simulations" at Queen Mary, University of London, September 2007.

Table of Contents

Table of Figures

Chapter – 1

Chapter – 2

Chapter – 3

Chapter – 4

Chapter – 5

Chapter – 6

Chapter – 7

Appendix A

Appendix B

Appendix C

Appendix D

Table of Tables

Chapter – 2

Chapter – 3

Chapter – 5

Chapter – 6

Appendix C

Chapter 1
Introduction

1. Introduction

1.1 Aerospace Composites Structures

Aerospace is an industry that has changed our lives significantly, an area that has developed extensively over the last hundred years. In the present scenario, the industrial and economic development of any country is critically linked to the high performance engineering materials. In a short span of time, the aerospace industries have significantly increased the usage of composite materials. Safety, environment and economy have always been very important parameters of concern for aerospace industry for a long time. Aerospace industries have realised the importance of using composites materials and thus these materials are now widely used in military and commercial aircraft due to their lightweight and their high strength under severe flight conditions. The aerospace is the predominant market for advanced composites today; the industrial and automotive markets will increasingly see the use of advanced composites in coming future. At present, both manual and automated processes are employed in making advanced composite parts (Abrate 1991).

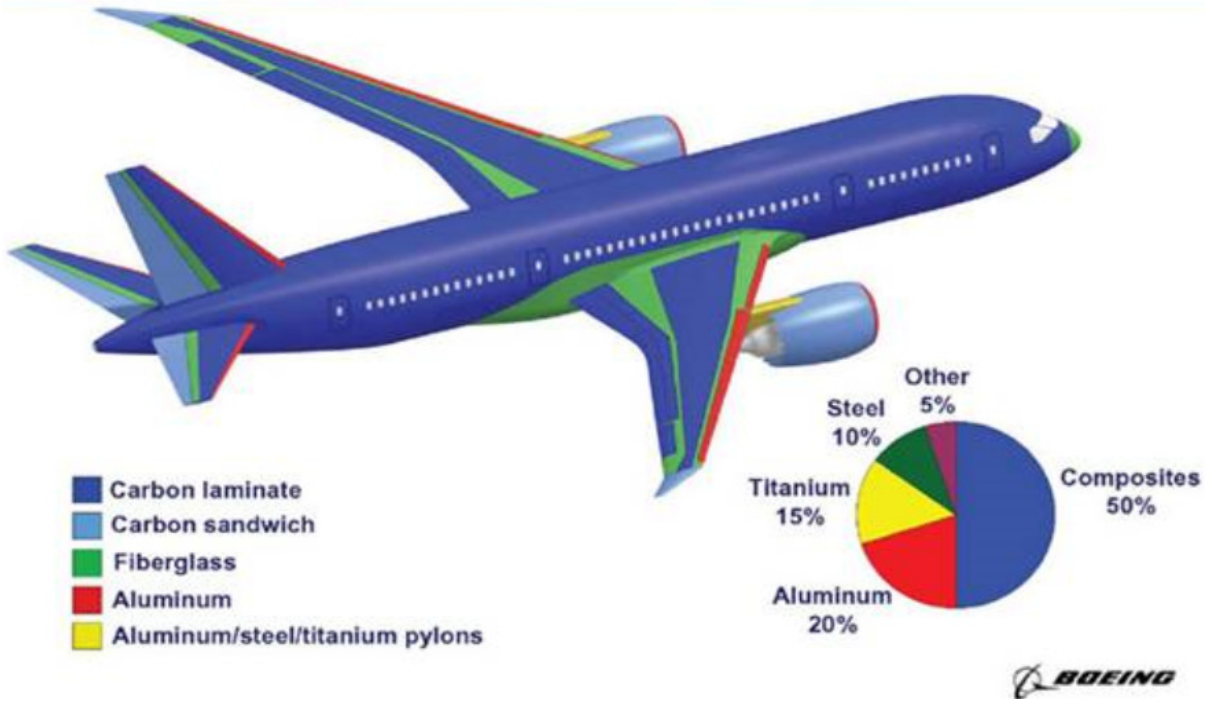

Figure 1.1 Composite materials for aerospace applications (Fidler 2007)

The major classes of aerospace structural composites used today consists of polymer matrix composites (PMC's), metal matrix composites (MMC's), ceramic matrix composites (CMC's), carbon-carbon composites (C/C) and hybrid composites. Figure 1.1 shows the

application of advanced composite materials for aerospace. These advanced composite materials are characterised by higher strength and higher stiffness, fatigue resistance, low weight, corrosion resistance, and useful thermal and electrical properties. The combination of these properties makes advanced composites very attractive for aircraft and aerospace structural parts. Of these classes of composites PMC's are the most widely developed and extensively used in aerospace industry.

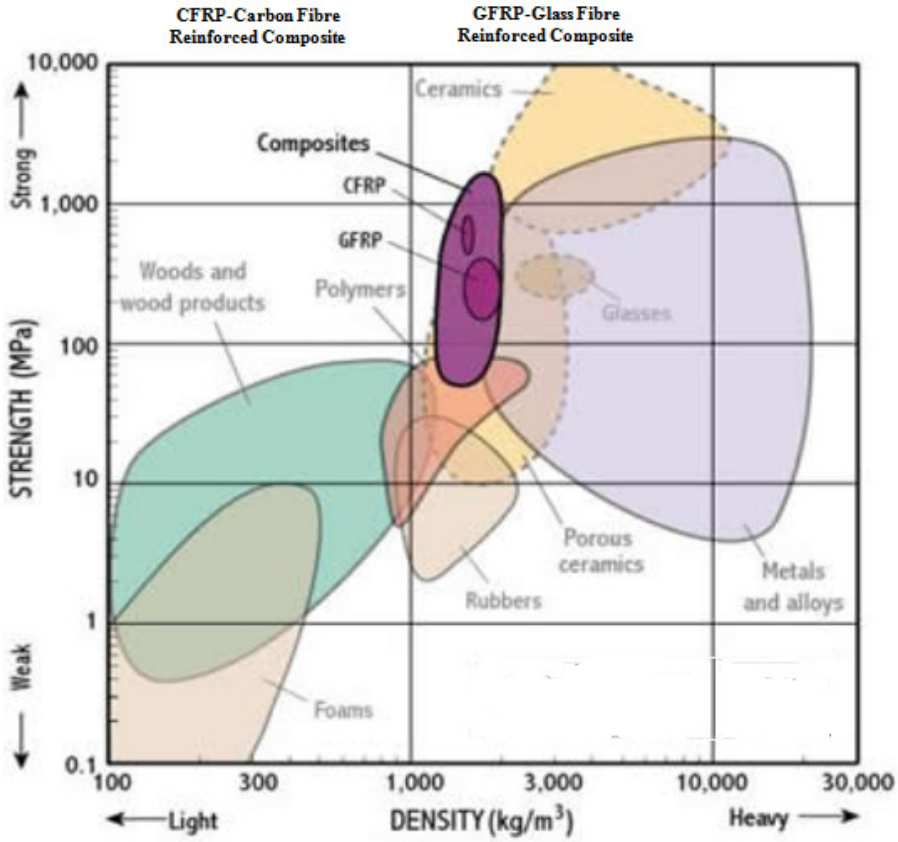

Figure 1.2 Mechanical properties of materials (Composite Primer)

Figure 1.2 shows the mechanical strength and relative values of density of different materials. Metals and alloys have high densities and lower strength compared to polymer matrix composites. These materials have the optimum values of density and relatively high strength while wood products have lower strength and density.

1.2 Motivation

Impact damage has been a major problem for composite structures and involves diverse disciplines and requires the combined knowledge skills in materials, maths, physics and computational finite element methods. Under low velocity impact composite laminates may

undergo various types of internal damage such as delamination, fibre fracture, matrix cracking, and fibre/matrix interfacial de-bonding. Composite parts in commercial and military aircraft are very susceptible to low velocity impact during in-service maintenance or tool dropping during manufacturing and during flight operating conditions such as flying debris, hail storm and lightning.

These impacts can cause internal damage which is not visible and often ignored during daily routine inspections. This internal damage is popularly known as barely visible impact damage (BVID). Figure 1.3 shows the finite element simulation of the various parts of the aircraft. Internal damage and failure mechanisms in composite materials can be modelled and simulated by using commercial finite element analysis (FEA) software such as Abaqus, Ansys, Nastran, I-deas etc. These simulation tools help to accurately predict the extent and location of the stresses and internal damage that could occur in composite components.

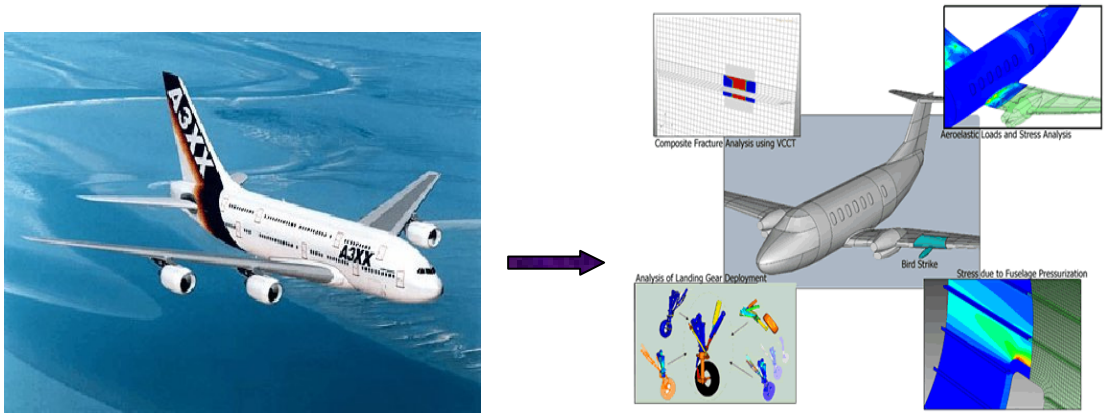

Figure 1.3 Finite element simulations of various parts of aircraft (Airbus - A3XX), (Abaqus 6.10)

With the higher usage of composite structures in the aerospace industry and because of their excellent high specific stiffness and strength ratios there are concerns about the vulnerability of performance of these materials under dynamic loading events. Predicting the vulnerability of the composite part to an impact event is crucial when designing a commercial composite product. These complex materials present new challenges understanding their mechanical behaviour under various types of impact loading.

1.3 Aims & Objectives

Aim:

The overall aim of this project is to develop a scientific understanding of the way in which accidental damage to a composite laminate free-edge, such as during manufacturing, transportation or routine maintenance is going to influence the long term integrity of the composite structure. This research aims to provide the reader with in-depth analysis of the serious effects of edge impacts. Research investigates different experimental methods, finite element simulation and non-destructive techniques such as computed tomography, to analyse impact damage on centre, near-edge and on-edge of composite laminates.

Objectives:

This research aims to provide an effective approach for the analysis of composite structures subjected to low velocity edge impact. To achieve this, programme objectives have been set up that will meet the overall aim of the project. The objectives set up for the research project are outlined as follows.

Project objectives:

- Investigate the effect of low velocity edge impact of the composite laminate with respect to various incident energies and thickness at different impact locations.
- Determine the effect of low velocity edge impact on the damage width and area with respect to impact energy levels and laminate thickness for different impact locations. Computed tomography is used to characterise fibre fracture, matrix cracks and delamination damage.
- Determine the damage tolerance and residual strength of composite laminates for a range of laminate thickness and impact energy subjected to centre, near-edge and on-edge impact.
- Investigate modelling and simulation of on-edge and near-edge impact. Discussion of various failure theories for the edge impact and the future development of further damage models.
- Comparison of experimental results and results from the finite element simulations of near-edge and on-edge impact.

Thus the aim and objectives of this research will be summarised and several conclusions will be drawn as per the tests results. Research will aim to provide useful information regarding the serious effects of low velocity edge impact and the subsequent damage tolerance of the

composite structures. These results will provide a gateway for effective prediction of edge impact damage at certain incident energy levels and the various factors involved in the failure processes.

1.4 Research Project Plan

Figure 1.4 shows the flowchart showing the experimental procedure for experiments and finite element analysis undertaken in this study. Glass fibre epoxy laminates were used throughout the project and were manufactured in the laboratory using vacuum infusion. Specimens of different thickness were prepared and assessed using different energy levels, impact locations and residual strength characterisation methods.

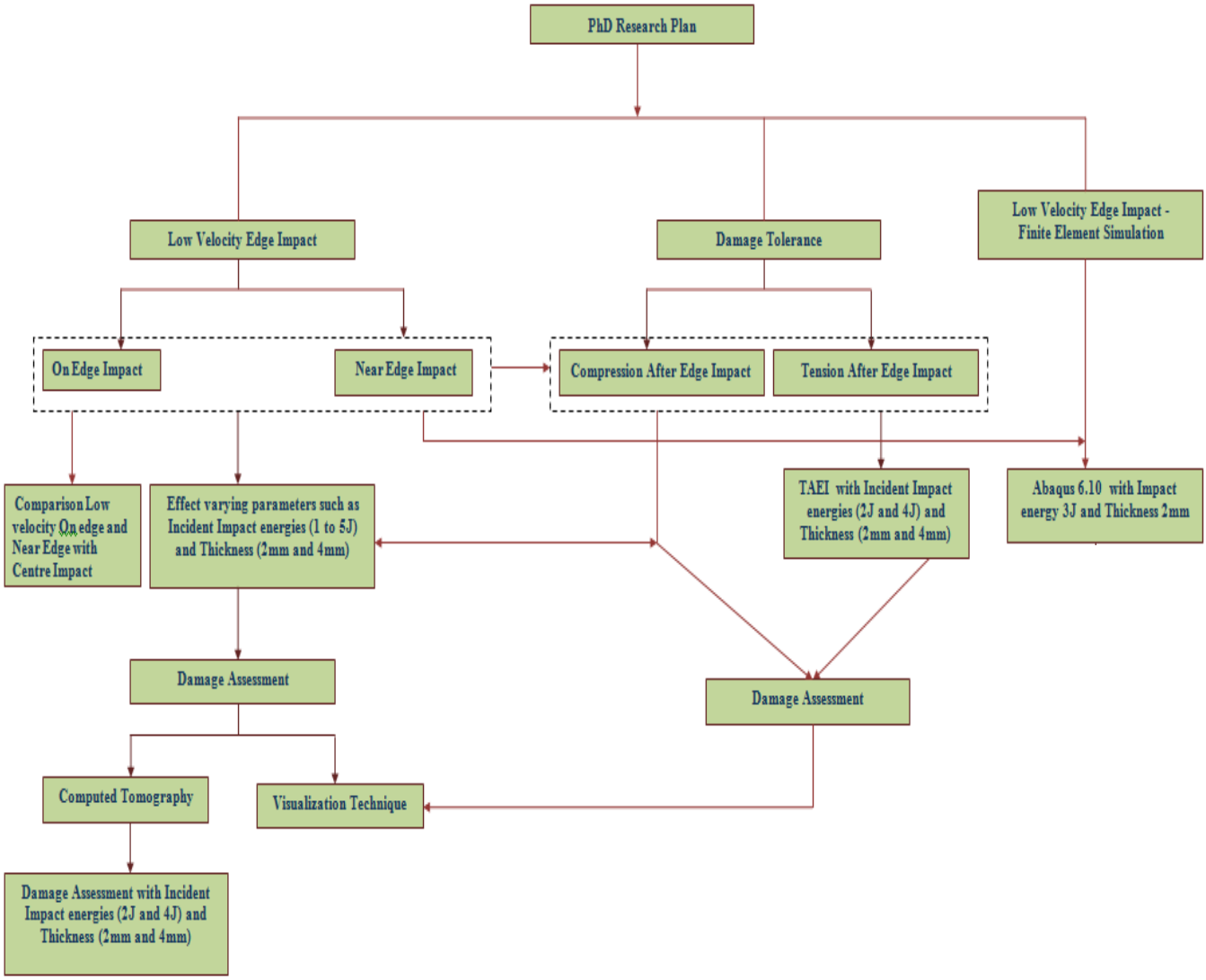

Figure 1.4 Research project plan

1.5 Structure of Thesis

The results of this research are divided into the following chapters.

- *Chapter 2* presents the literature review on the effect of low velocity impact in composites structures and introduces various non-destructive and finite element simulation techniques to analyse the subsequent impact damage.
- *Chapter 3* presents the experimental investigation on the effect of low velocity edge impact such as near-edge and on-edge impact and its comparison with centre impact on various parameters like thickness, impact damage, force-time history and absorbed energies.
- *Chapter 4* presents a detailed study employing computed tomography to investigate the presence of multiple fibre cracks, delamination and matrix failure and propagation direction during low velocity impact events on composite laminates at near or at on-edge locations. This chapter will provide the study of various parameters involved in computed tomography in finding the crack path and failure modes using tomography analysis tool such as Drishti (Drishti software).
- *Chapter 5* investigates the damage tolerance and the residual strength of composite laminates subjected to on-edge, near-edge and centre impacts. Experimental tests for compression and tension were realised after impact on the near-edge, on-edge and centre impact. These experimental results enable us to determine how the impact location affects the damage tolerance for varying impact energies and laminate thickness.
- *Chapter 6* presents the finite element analysis of composite structures subjected to low velocity edge impact. The simulations presented are from elastic analyses without failure mechanisms. Various failure theories are discussed, including Hashin damage criteria and cohesive damage modelling. Results obtained from experimental tests such as impact force/displacement–time histories are compared with those obtained by finite element models for both on-edge and near-edge impact.
- *Chapter 7* presents the overall discussion of all the experimental and simulation studies undertaken in this work. The chapter will discuss how the results have been related to overall aims and objectives of the thesis.
- *Chapter 8* outlines final conclusions, recommendations and future work related to low velocity edge impact on composite structures.

Chapter 2
Literature Review

2. Literature Review

2.1 Introduction

Composite materials are highly susceptible to impact damage, which introduces several design problems. One such problem has been the susceptibility of composite components to impact damage at accidental low energy impacts which frequently leave no visible mark on the impacted surface but cause considerable internal damage. Critical applications which may be susceptible to such damage include the wing skins of military and civil aircraft and panels for automotives (Cantwell et al 1991; Abrate 1991). A composite materials response to impact dynamic loads is a complex area of study, both theoretically and experimentally, involving different damage modes including fibre failure, matrix failure and delamination (Shyr et al 2003). Investigation of these failure mechanisms has received considerable attention from many researchers over the past two decades such as Chamis et al (1972), Bradshaw et al (1973), Beaumont et al (1974), Choi et al (1991), Davies et al (1994), Chun et al (1998), De Freitas et al (2000), Li et al (2002), Mitrevski et al (2004), Cesari et al (2007).

Impact damage can be introduced in various ways to composite laminates in aircraft structures; including during manufacturing processes and by low-velocity impacts in-service caused by tool drop or runway debris. Damage arising from such impact events can considerably reduce the strength and stiffness of structures of composites laminates (Abrate 1991). Previous work has typically been restricted to the study of normal, transverse impact away from an edge (Cantwell et al (1981), Zukas (1982), Choi et al (1991), Dowling et al (1999), Olsson (2003), Wang et al (2010). However, in-service impact events are often out-of-plane in nature and such impact events lead to more serious damage compared to normal impact (Butcher 1979; Ghaffari et al 1990). Such impact damage can lead to more severe delamination, which is difficult or even impossible to detect during visual inspections leading to premature compressive failure of the composite structure (Wiggenraad et al 1999). There is very little published work on low velocity impact on the edge of composite laminates. More recently it has been realised (Breen et al 2006) that such edges of composite structures are particularly vulnerable to impacts, including near the edge of an inspection port or other aperture.

Furthermore, impacts on the edge of the laminate may lead to more severe damage than impact on the laminate plane (Breen et al 2006). Under low velocity impact loading

conditions the load history can yield important information concerning damage initiation and growth (Zhang 1998; Belingardi et al 2002). The use of composite structures will increase in future if problems regarding impact damage on composites are solved but currently there may be restriction from the lack of understanding of the precise damage mechanisms occurring. Understanding the adverse effect of in-service impact events and subsequent damage evolution has become a critical necessity (Butcher 1979; Meo et al 2003). Accurate modelling and prediction methods must be developed to ensure designers are correctly informed, leading to safer structures.

2.2 Types of Composites

2.2.1 Classification of Composites

Depending upon the type of strength and weight requirements composites are classified into different categories such as particle reinforced, fibre reinforced and structural composites, see figure 2.1.

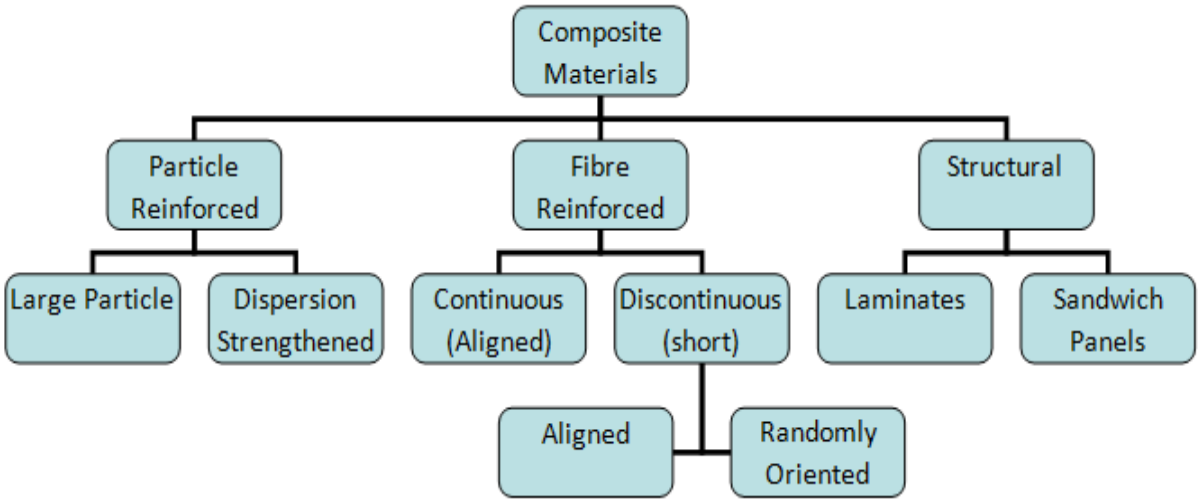

Figure 2.1 Classification for various types of composites (Callister 2006)

In fibre reinforced composites the applied load is transmitted and distributed to the reinforcement via the matrix phase. It is the control of the reinforcement geometry and distribution which are important parameters for high strength and stiffness to be attained (Callister 2006).

2.2.2 Structure of Composites

Composites are manufactured using a range of materials, such as carbon and glass fibres. The geometry and constituents of a composite material determines its mechanical properties. Thus it is important to understand the interaction of the matrix and fibre phase as the

properties of the composite depends upon both of these phases and various parameters associated with it.

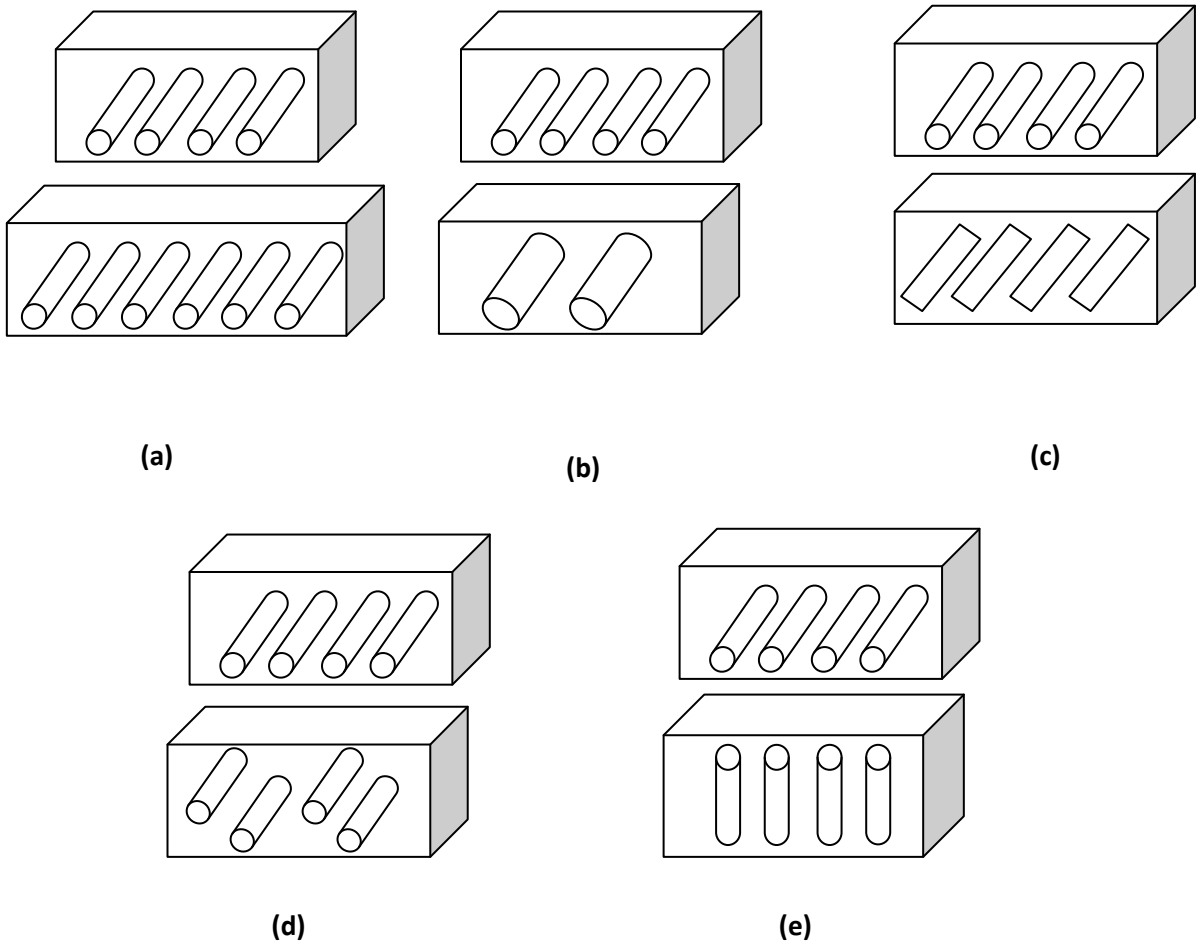

Figure 2.2 Parameters affecting the strength of composites (a) Concentration (b) Size (c) Shape (d) Distribution and (e) Orientation (Callister 2006)

Composite materials with the same matrix and fibre will behave differently when the other parameters are changed such as shape, size, distribution of the fibres in the matrix phase which is also known as the dispersed phase (see figure 2.2 (a)-(e)). Adhesion is necessary for achieving high level of mechanical properties of the composite. Thus the mechanical properties of the composites depend upon these parameters and good adhesion between the phases to provide load transfer (Callister 2006).

2.3 Manufacturing Process for Composites

There are several methods of manufacturing composite materials that are widely used in the aerospace industry. The method used depends upon the various project requirements such as low cost, less weight, good mechanical and physical properties. A brief discussion of the various techniques that are widely used within the composite industry will now be introduced.

2.3.1 Spray-up

In the spray-up process, the mould is waxed, sprayed with gelcoat, and then cured in a heated oven at approximately 50°C. After the gelcoat has cured, liquid spray of resin matrix and chopped reinforcing fibres are discharged simultaneously from a spray gun on the surface of a mould where they are deposited to form a uniform thickness (CCP Composites). Depending upon the product requirements the desired thickness (range 2-10 mm) of the composite product can be achieved (Ashby et al 2009). Sprayed mixture of fibre and resin is left to cure in the mould at room temperature and thus the desired composite product is produced. This technique is a quick method to cover large surface area. However this technique has limited use as the mechanical properties of the material are moderate and this method is unable to use continuous reinforcing fibres. Applications include truck bodies, storage vessels, lorry cabs and boat hulls (Gowariker 1986).

2.3.2 Filament Winding

The filament winding method involves a continuous filament of reinforcing material wound onto a rotating mandrel in layers at different angles. In this process continuous length of strand, roving or woven tape of the fibre is passed through a bath of resin and curing agent. As the strand comes out of the bath the excess resin is squeezed out. The resin dipped filament or strand is then wound over a mandrel of the required shape and subsequently cured under the influence of heat. The tension of the fibre and the pattern of the windings are very important factors as they influence the ultimate property of the finished product. Applications include high pressure cylinders storage tanks and rocket motor bodies (Callister 2006).

2.3.3 Autoclave Curing

Autoclaves are pressure vessels which are used to process composite materials under elevated pressure and temperature. Prepreg such as glass/epoxy is widely used for autoclave process. A prepreg is a pre-impregnated sheet containing both the reinforcing glass fibres and the epoxy resin (with hardener). The composite is layered on a flat plate and the composite and its plate are placed into a plastic bag, from which air is exhausted by a vacuum pump and then cured with application of vacuum pressure, temperature (60-120°C for glass/epoxy) and inert gas pressure. This operation removes air inclusions and volatile products from the moulded part. High processing pressures allow the moulding of thicker sections of complex shapes. Long cure cycles are required because the large autoclave takes a long time to heat up and cool down. The method is relatively expensive and is used for manufacturing superior quality structural components containing high fibre volume and low void contents such as high quality aerospace products (Carlsson et al 2014).

2.3.4 Pultrusion

The continuous strands are preheated by passing through a resin curative bath and then pulled through a die of a suitable profile. The die is heated and the compacted profile coming out of the die is heated externally. The cured profile is continuously pulled out of the die which provides the driving force for the impregnated strands to be forced through the die. The cured product is cut to the desired length by the cut-off saw. The pultrusion process has many advantages such as high productivity, process parameters are easily controllable, low manual labour cost, precise cross-section dimensions of the products, good surface quality of the products, homogeneous distribution and high concentration of the reinforcing fibres in the material is achieved (Gowariker 1986).

2.3.5 Vacuum Assisted Resin Transfer Moulding (VARTM) Process

VARTM is an advanced manufacturing process for polymer-matrix composites. The process involves the lay-up of a glass or carbon fibre fabric of desired length placed onto a rigid tool plate surface. The plate is surrounded and sealed by a vacuum bag. Vacuum is applied to remove any entrapped air inside the bag. Resin is then allowed to flow through the fibres under the vacuum. The resin can be injected through single or multiple inlet ports. The laminate is left to cure under constant temperature for the given time in a heated oven and then left to cure at room temperature. The process has advantages over other manufacturing

processes such as low tooling costs. Very large components can be manufactured with high fibre volume fractions and low void content (Carlsson et al 2014). This method of manufacture is used in this project.

2.4 Impact Mechanics

During the last few years the impact behaviour of polymer-matrix composites has been extensively studied by researchers on this subject. To name some authors, Doyle et al (1989), Cantwell et al (1989a, 1989b, 1989c, 1990a, 1990b, 1991), Abrate (1991), Sankar et al (1996), Olsson et al (2003) etc., have investigated the effects of impact events on composites.

Impact behaviour of various materials was studied throughout history. Goldsmith et al (1960) studied the impact behaviour of isotropic plates. Impact on an anisotropic laminated plate has been investigated by Sun et al (1975). Greszczuk (1975) investigated the response of composite plates to low velocity impact. Toland (1974) showed that during impact, time duration plays an important role. Pavier et al (1995) investigated the effect of impact velocity on impact damage on the composite laminates. Recently, Zaretsky et al (2004) studied stress wave progression on glass fibre reinforced polymer composites upon impact loading. This study showed that the level of the oscillations and frequency increase with stronger impacts while low intensity impacts resulted in the appearance of long period oscillations.

All these studies have illustrated that an impact response is a complex phenomenon and depends upon the nature and characteristics of the impactor and the structure, contact time, impactor velocity, thickness, wave propagation etc. All these variables have an effect on the structural response and integrity of the composite laminate. Furthermore, test variables such as mass, nose shape, diameter and velocity of impactor and composite variables such as lay-up, fibre volume fraction and geometry of the composite specimen and the boundary conditions will significantly influence the damage formation. Possible definitions for different loading conditions and impact duration are given by Chaturvedi et al (1997), in table 2.1 and shown in figure 2.3

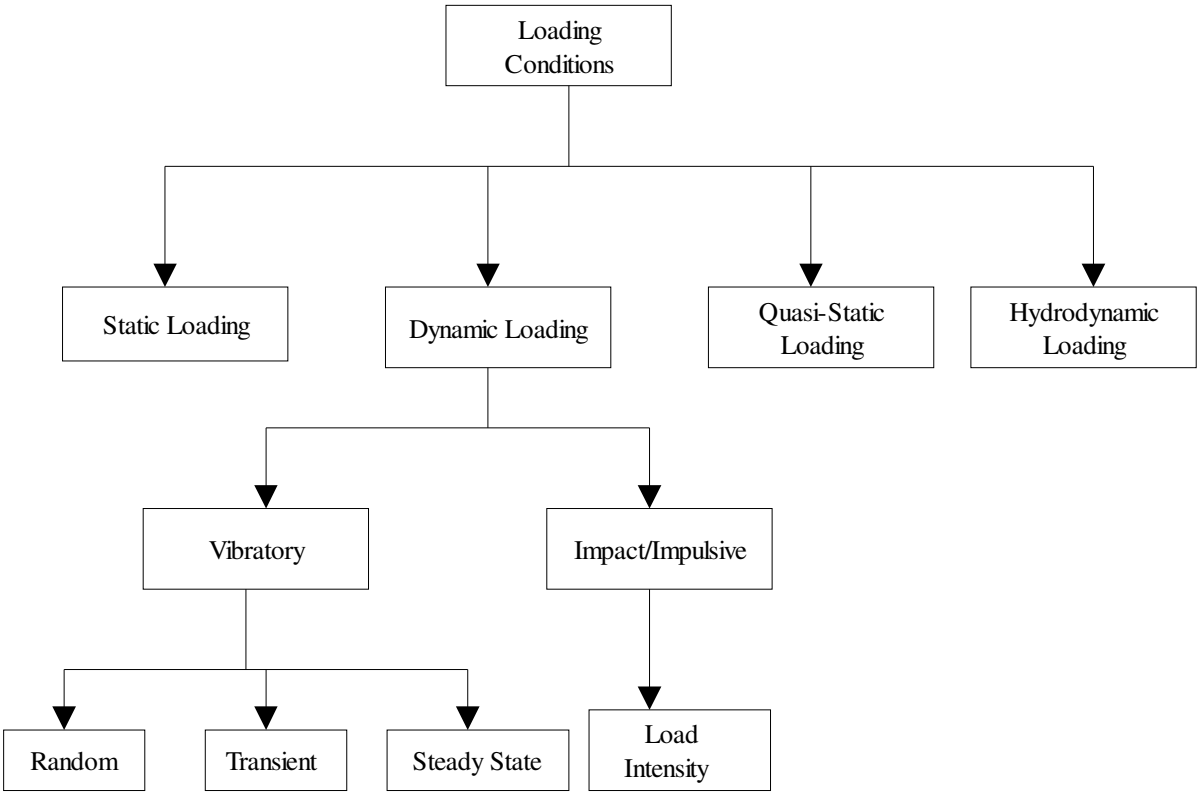

Figure 2.3 Different types of loading conditions (Chaturvedi et al 1997)

As indicated by Chaturvedi (1997), defining the role of the loading type becomes important for determining material structural response as the nature of impact loading conditions determines the initiation and propagation of the damage.

Regime	Pulse Duration/Natural Period (s)	Response
1	10^{6}-10^{4}	Static
2	10^{4}-10^{2}	Quasi-Static
3	10^{0}-10^{-6}	Dynamic
4	10^{-6}-10^{-9}	Hydrodynamic

Table 2.1 Material response regime and pulse duration/response (Chaturvedi et al 1997)

In real situations, a normal impact to the surface is considered to be an unlikely dynamic loading condition whilst there is very high possibility that the impact will occur at an edge and at an angle to the surface. In out-of-plane impact there is high level of shear and bending waves which propagate through the structure upon contact. These stress waves can produce high levels of contact stresses in the impacted region initiating delamination damage in

composite structures. In this situation, the magnitude of load and duration of impact play a very important role in the impact of composites.

2.5 Impact Damage Mechanisms

Composites behave in a different way as compared to conventional metallic materials. When traditional engineering materials such as steel and aluminium experience low velocity impact, the energy is typically absorbed through plastic deformation. However, this deformation is permanent, and it does not significantly reduce the load carrying capability of the structure (Bradshaw et al 1973).

Polymer matrix composites such as carbon fibre composites experience very little or no plastic deformation during a low velocity impact. This is because of the low strain to failure of the fibre and brittle nature of the epoxy matrix. During a low velocity impact, impact energy is absorbed through global bending of the composite laminate (Bradshaw et al 1973; Choi et al 1991; Lagace et al 1993).

Zhou et al (1995) performed a study to determine the influence of incident kinetic energy, damage mechanisms and the impact force during low velocity impact on glass fibre composite laminates. This research showed that the energy is absorbed by the composite laminate through various damage modes like delamination, fibre failure and fibre-matrix microcrackings. The authors observed that these damage mechanisms can be studied from impact force-time history, and concluded that damage mechanisms were geometry dependent. Later, Davies et al (1996) studied the post impact compressive strength of delaminated composites and concluded that their strength and stiffness was greatly reduced due to delaminations present between interfaces from low velocity impact.

These initial studies illustrated that composite damage resistance is very complicated and usually influenced by various factors, for example the lay-up-stacking sequence, geometry and thickness of the composites laminate. Shyr et al (2003) indicated that the impact energy is absorbed through various failure mechanisms and fracture processes such as fibre fracture or shear failure or driven by combination of these.

2.5.1 Damage Modes

The impact event generates two kinds of damage modes, a local response and a global damage response. Figure 2.4 show the effect of local and global damage modes (Chaturvedi 1997). In the flowchart it can be seen that the damage initiation critically depends upon the loading conditions, which in turn depends upon various geometrical and material parameters for composites.

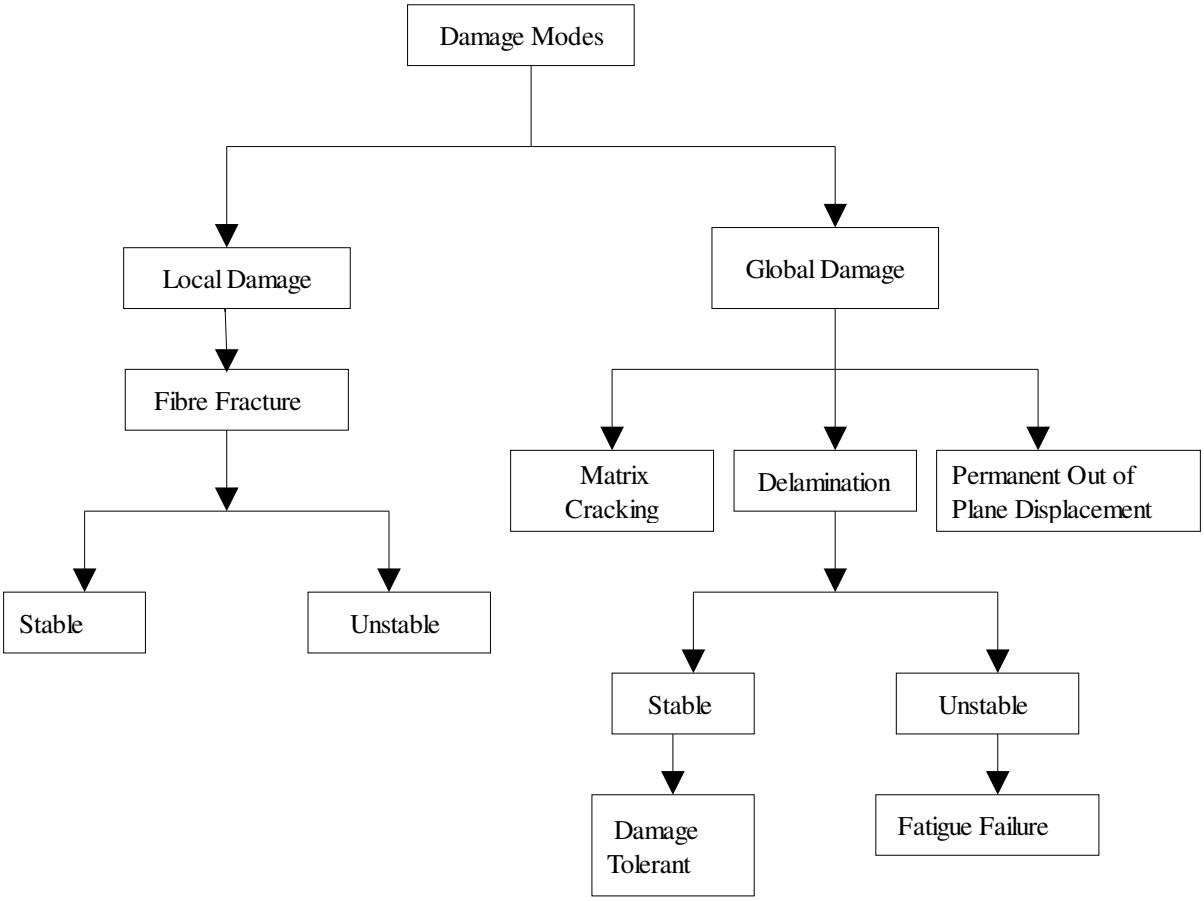

Figure 2.4 Effect of local and global damage modes (Chaturvedi et al 1997*)*

Local damage can be lead to fibre failure. A laminate which can withstand high operating loads after suffering impact damage can be defined as stable behaviour. Stable behaviour does not propagate to cause catastrophic failure; unstable behaviour propagates and leads to failure of the laminate. For example, fibre failure occurring in local damage is stable if the remaining fibres can sustain the load. However, fibre fracture in laminates which are unable to sustain the operating loads, leading to catastrophic failure can be defined as unstable behaviour.

Matrix damage and delamination is very hard to detect in service. Low velocity impact leads to complicated impact problems (Chaturvedi et al 1997) and can occur during aircraft landing and takeoff. The debris on the ground can cause a low velocity impact on the leading edge of the wing which can go undetected, thus creating an internal damage, leading to delamination and matrix damage.

Thus, definition of the damage modes guides us to evaluate damage mechanisms. Damage mechanisms in local and global modes include different kinds of failures. For the effective use of polymer-matrix composites for high-performance applications, understanding the causes and the formation of such damage arising from low-velocity impact and improving the damage-resistance characteristics of the laminates are important.

2.5.2 Damage Development

Abrate (1998) has proposed four principal damage mechanisms for fibre reinforced composites subjected to a low velocity impact event (see figure 2.5). These different mechanisms will now be discussed.

Contact Stresses and Matrix Cracks: During impact, when contact stresses have exceeded the relevant strength of the matrix material, matrix cracks are formed on the first ply which grows progressively with the increase of load within a small time scale. In this case, upon impact, cracks form in the matrix material perpendicular to the direction of the fibres. Under low velocity impact a composite absorbs enough energy to form cracks in the matrix material. Matrix crack can occur due to bending or shear stress waves. Figure 2.5 (a) and (b) shows the contact stresses and the formation of cracks during the low velocity impact event.

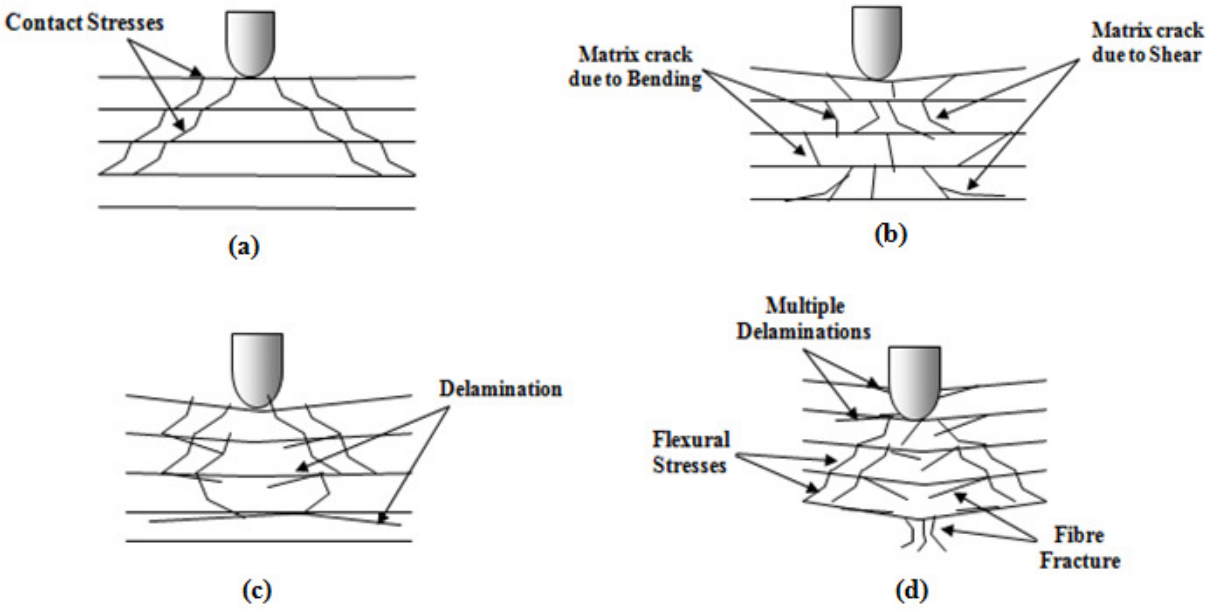

Figure 2.5 Four principal damage mechanisms for low velocity impact: a) Contact stresses b) Matrix cracking c) Delamination d) Fibre failure (Abrate (1998), Richardson et al (1996))

Delamination: The next mode of damage is delamination between plies of the composite, see figure 2.5 (c). This type of damage can occur both at low and higher impact energies with the damage occurring inside the composite laminate. When stresses are sufficiently large they cause failure at interfaces between the plies with much of the energy absorbed dissipated through the formation of delaminations. These delaminations seriously reduce the compressive strength of the composite and also allow more paths for progressive failure of the composite structure with time. Critically the delamination pattern is dependent upon lay-up of the laminate (Abrate 1998).

Fibre Failure: The next mode of failure is the fibre failure, see figure 2.5 (d). After the laminate has suffered the matrix damage and delamination, the extra energy is absorbed by the formation of flexural stresses and fibre damage which finally leads to fibre failure (Abrate 1998, Richardson et al (1996)).

2.6 Low Velocity Impact

In composite laminates, low velocity impacts can cause barely visible impact damage which is difficult to detect during routine inspections. Many researchers have carried out experimental studies on low velocity impact of composite structures. The residual tensile and compressive strengths of composite laminates are influenced by the damage area and mechanisms induced by this impact mode. The contact time plays an important role since the contact time between the impactor and the composite is considerably less at higher velocities, resulting in a localised response with no global deformation, whilst at lower velocities the impact global response becomes dominant (Cantwell 1981; Cantwell et al 1990a, 1990b). Olsson et al (2000) investigated the effect of large and small mass impactors and observed that a large mass impactor generated a quasi-static response, whereas a small mass impact response was wave controlled. Later, Olsson et al (2003) suggested criteria for classifying low and high velocity impact events. For impact velocities below 5 m/s (low velocity impact) the impact response is governed by impactor/plate mass ratio rather than by impact velocity while at higher impact velocities the short impact time results in a response governed by wave propagation phenomena.

2.6.1 Low Velocity Impact Test Methods

To evaluate the various types of impacts, materials, and structures a wide variety of accepted impact tests are extensively used in the industry. Materials behave differently depending on the type of impact they are subjected to. Therefore, it is important to conduct impacts tests that most closely model the actual types of impacts the material structure will be exposed to during use (Wang et al 1998).

The impact test methods most widely used in the industry include the Charpy pendulum, Izod pendulum and Drop weight test machine. Typically low velocity impacts (up to 20 m/s), such as a dropped tool, are generally utilised using a pendulum test (Charpy or Izod), or a drop-weight impact (Cantwell et al 1991).

2.6.1.1 Drop Weight Impact Tests

A method to simulate low velocity impact events observed in operational composite structures is the drop weight impact test, which employs a free fall weight dropped on to the specimen surface from a desired height. Low velocity impact testing gives the allowable impact energy that the structure is able to withstand and to assess the typical failure modes encountered during this type of loading. This test has been extensively used in the testing of materials by several authors including Cantwell et al (1989a, 1989b, 1989c, 1990a and 1990b).

Winkel et al (1985) conducted experiments with drop weight test fixtures to characterise the difference in impact damage between several types of composite laminates. Strain gauges were the most common tools used for instrumenting of drop weight impact tests in earlier experiments. Piezoelectric transducers were then introduced and implemented in the drop weight impact test (Graham (1972, 1974)). The piezoelectric effect causes an electric charge to be generated by the application of mechanical stress to a solid material. Drop weight impact tests are very useful for modelling the types of impacts experienced by the composite materials for aerospace and automobile applications. Also, the drop weight test allows for a greater variety of specimen geometries, which is an advantage over the Charpy and Izod impact tests.

In this project, drop weight impact device will be used to determine the edge impact behaviour of the glass/epoxy composite laminates. The free flight drop tower test is similar to the impacts that would occur from a dropped tool during in-service maintenance on the composite laminate. Depending on the type of impact loading, various impactor shapes and boundary conditions can be used with the drop height adjusted to achieve the desired impact velocity and conditions to duplicate realistic impact events (Abrate 1998).

2.6.2 Internal Damage

During low velocity impact stress levels are very low but important. Figure 2.6 shows the development and progression of internal damage during low velocity impact events. For this case the impactor is assumed to be rigid and the target is assumed to be multilayer, orthotropic solid (Zukas et al 1982). Also it is assumed that impact duration is long and the impact is normal to the target surface.

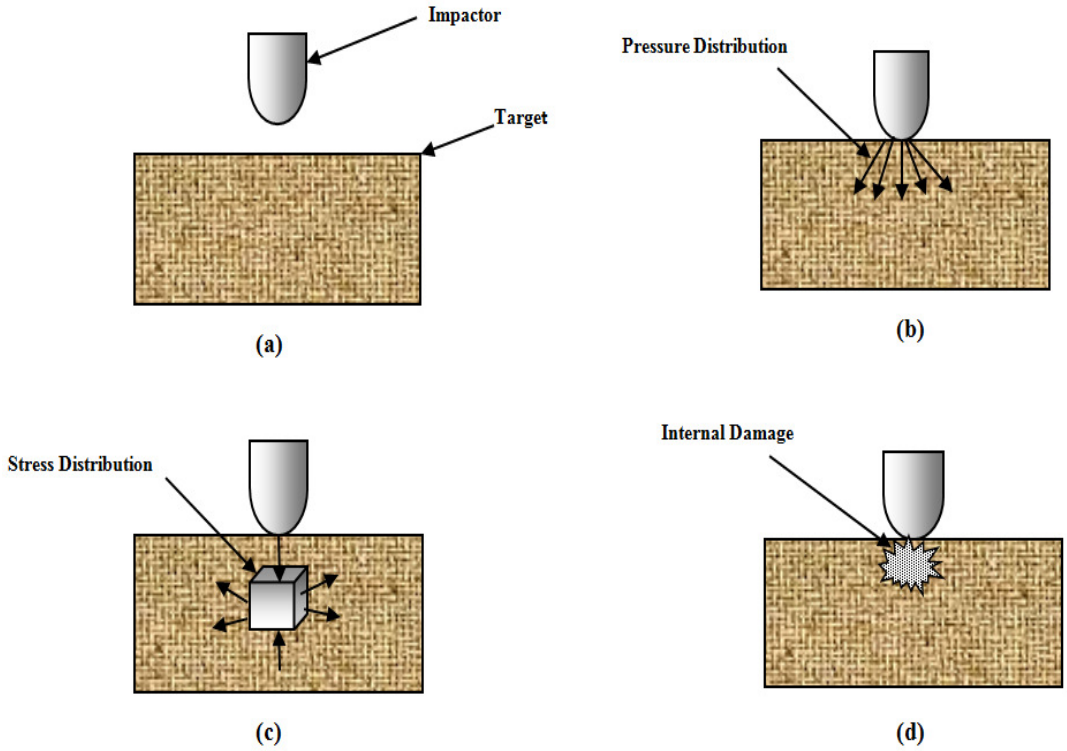

Figure 2.6 Internal damage stages on low velocity impact a) Impactor-target b) Pressure distribution c) Stress distribution d) Internal damage (Zukas et al 1982)

As figure 2.6 (b) suggests, as soon as the impactor comes in contact with the target, stress waves propagate away from the point of contact and pressure is distributed around the area of contact. The time-dependent pressure creates 3-dimensional internal stresses in the composite laminate (Zukas et al 1982) as can be seen from figure 2.6(c). Figure 2.6(d) shows that the stresses induced damage initiation within the composite laminate.

2.6.3 Impact Force-Time Histories

The force-time histories, generated from the drop weight impact test can be used to determine when the damage both initiates and propagates through the specimen. Force-time graph indicates the various damage states that occur during low velocity impact. Figure 2.7 illustrates the force/time curves at different time intervals which can be used to determine the overall impact damage within the specimen and as a prediction for the extent of damage and its mechanisms, and damage thresholds for each specimen. For higher impact time duration the laminate transverse stresses will be higher.

Stage 1

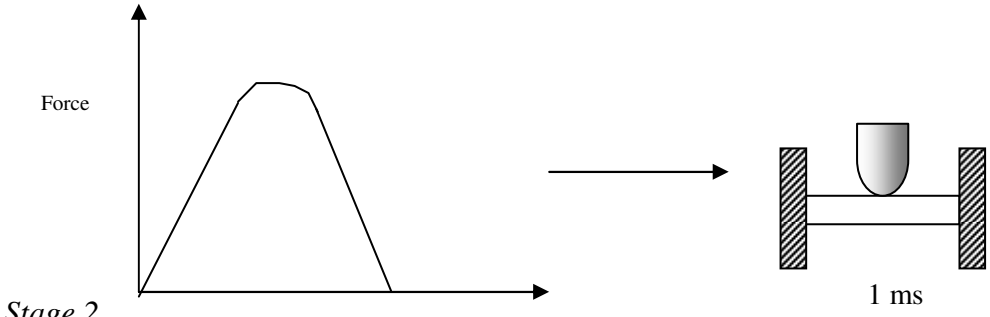

Stage 2

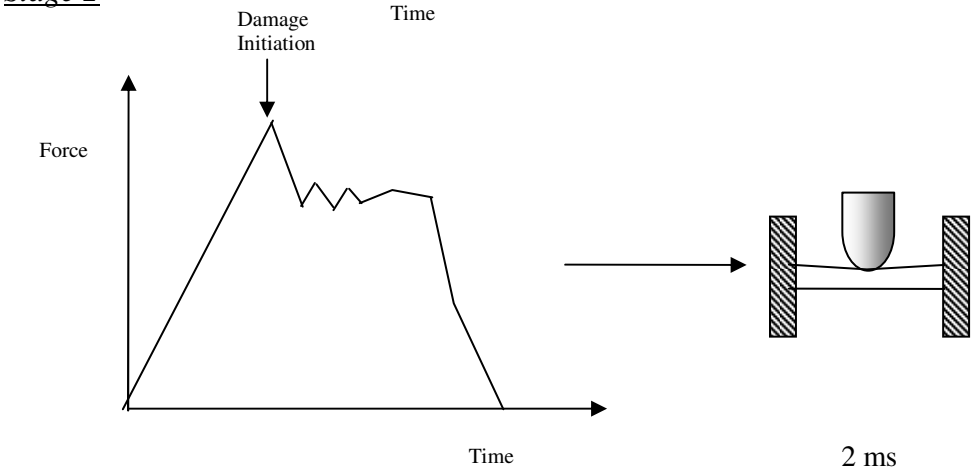

Stage 3

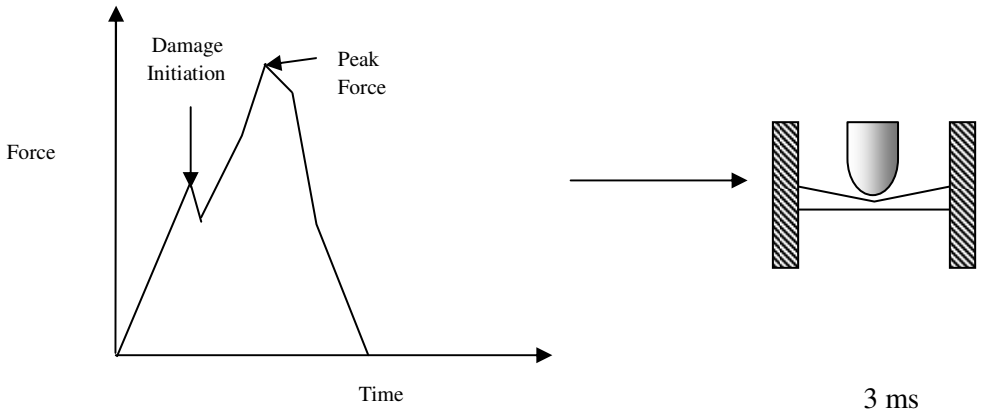

Stage 4

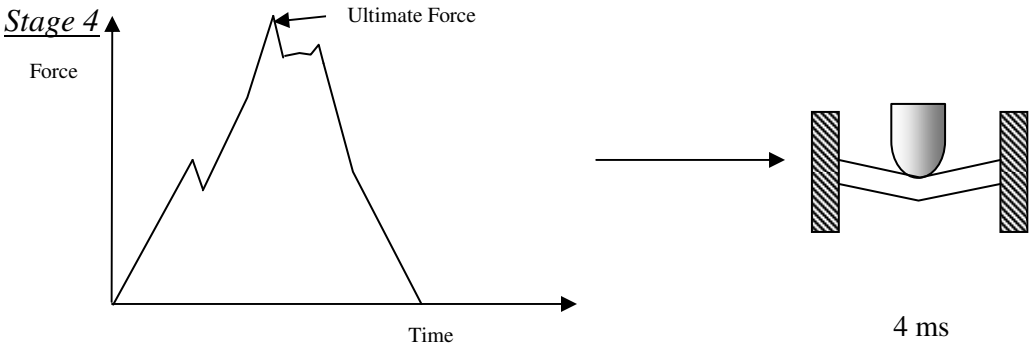

Stage 5

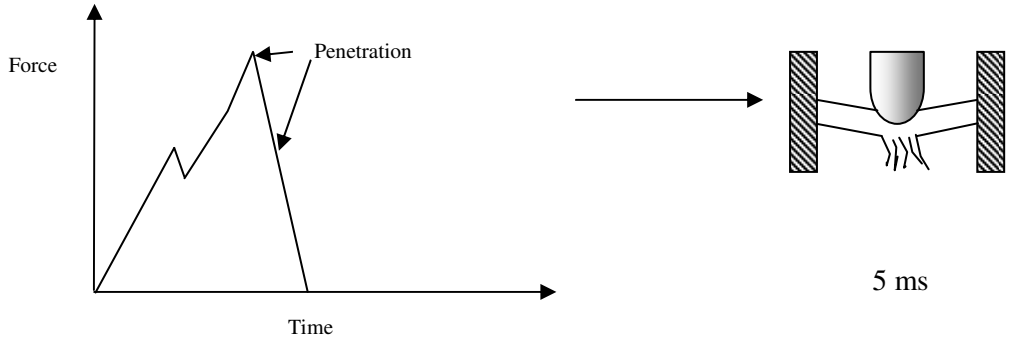

(a) **(b)**

Figure 2.7 Damage stages on low velocity impact a) Force-time curves b) Impact deformation (Zhou et al 2000)

Stage 1 shows an elastic impact with no damage present. In this stage impact introduces contact stresses but damage has not been initiated at this time interval (1ms).

Stage 2 represents that damage is initiated but the impact energy is not enough to cause failure beyond damage initiation. This stage is also known as damage threshold limit, when matrix cracks have been formed and small delaminations may exist but remain stable.

Stage 3 occurs when more energy is available to increase damage beyond damage initiation in stage 2. In this stage multiple delaminations have occurred. The shear stress generated at the interface by the impact may be sufficient to cause shear failure.

Stage 4 represents the maximum ultimate force that the material is able to withstand. Beyond this stage the failure process starts.

Stage 5 represents the penetration of the material. In this stage material failure occurred and the material is unable to absorb energy after full penetration.

The force-time histories can provide useful information for the damage initiation and propagation of different damage modes within the composite structure (Zhou et al 2000).

2.7 Types of Impact Damage

When a composite is subjected to a low energy impact, the plate deformation absorbs the energy of the striker elastically at first and subsequently by a combination of micro-fracture processes and further elastic deformations (Abrate 1998). Polymer-matrix composites are known to be highly susceptible to internal damage caused by transverse loads even under low-velocity impacts. Out-of-plane impact induces bending deformation and this introduces shear, tensile and compressive stresses on the composite structure. The composites can be damaged on the surface and beneath the surface by relatively light impacts causing barely visible impact damage, while the surface may appear to be undamaged to visual inspection.

2.7.1 Geometrical and Material Parameters

The initial mode of impact damage depends upon various factors like geometrical and material properties, laminate support conditions, impactor nose and shape, geometry of the specimens and loading conditions. To illustrate the interdependency of the geometrical and material parameters on the damage initiation within the composite laminate, figure 2.8 has been produced.

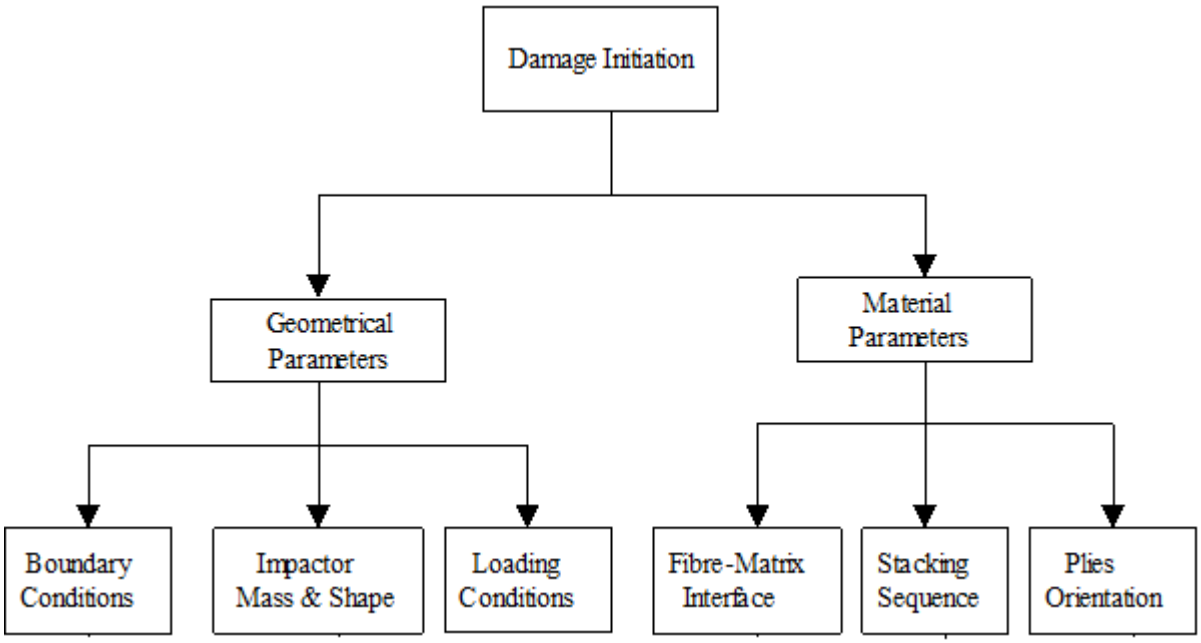

Figure 2.8 Effect of various parameters for damage initiation (Chaturvedi et al 1997)

2.7.2 Impact Velocity

Impact velocity is a very important parameter in determining the failure mechanism of composite laminates. Figure 2.9 shows the effect of impact velocity on the overall damage of the composite structure as reported by Mikkor et al (2006). This research indicated that as the impact velocity increases the overall damage area increases and the impact time duration decreases.

Low velocity impact velocities range in the region of 5-20 m/s. In this range stress waves start originating from the point of impact and transfer the load to the rest of the structure. At impact velocities greater than 20 m/sec, the impact can be considered as high velocity impact (Chaturvedi et al 1997). For higher impact time duration, the laminate transverse stresses will be higher.

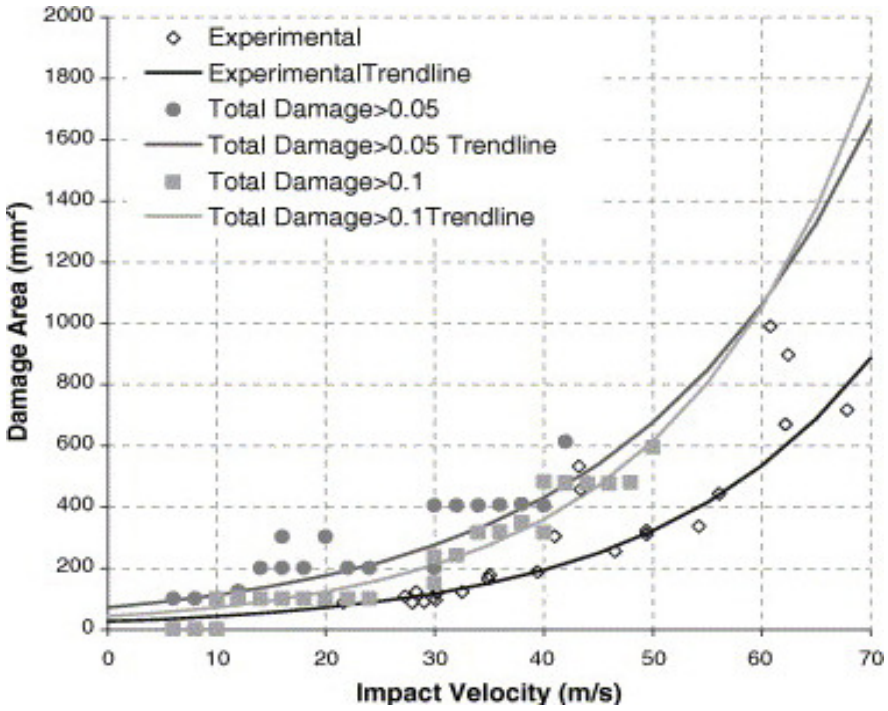

Figure 2.9 Effect of impact velocity on overall damage area (Mikkor et al 2006)

2.7.3 Thickness

The magnitude of the impact damage is also affected by the thickness of the composite laminate. When composite laminates are subjected to low velocity impacts there is a pressure distribution around the area of contact which induces complex state of stresses. In this state contact and bending stresses become important.

For thin laminates the bending deformation stresses are very important, since the damage tends to occur between the internal plies due to the flexibility of the laminate. Conversely, when thick laminates are subjected to low velocity impacts, the bending deformations are less important and the damage remains located around the outer plies. The damage at these plies is due to higher contact stresses and propagates to the inner plies. The delaminations increase the flexibility of the structure and new intra-ply damage occurs close to the delaminations. When the impact energy is insufficient to activate any failure mechanism, the progressive failure process stops (Abrate 1998).

Cantwell et al (1985c) carried out research on impacted CFRP composite targets of varying thickness with the same stacking. As the target thickness is increased delamination area was found to vary non-linearly with the increase in thickness. Research carried out by Zhou et al (2000) showed the effect of damage area as a function of incident kinetic energy on the thickness and concluded that energy needed for damage area was most affected by the laminate thickness.

Tai et al (1999) investigated the effect of thickness on the residual tensile strength of the composites after low-energy impact loading. Investigations showed that residual tensile strength of thinner laminates has more significant influence on tensile strength than for thicker laminates. Laminates with higher thickness showed less extension of the damage.

An investigation by DeMorais et al (2004) explored the effect of laminate thickness and how the distribution of load and energy absorption plays an important part within the composite. Sutherland et al (2004) investigated the impact behaviour of thin and thick laminates using an instrumented drop weight tests. They concluded that during impact lower deflections and higher contact loads are seen for the thicker laminates. The thin laminates were significantly affected by higher bending deflections.

2.7.4 Delamination

Delaminations occur between stacked fibrous layers and tend to have a very adverse effect on the mechanical performance of the composite structures. The delaminations are barely visible and cannot be detected easily under operation conditions of the composite laminates. Delamination has different types of shapes and the majority of delamination shapes which depend upon the stacking sequence of the composite structures and the impact energy. Figure 2.10 shows a representative elliptical shaped delamination following the ply orientation within a composite laminate.

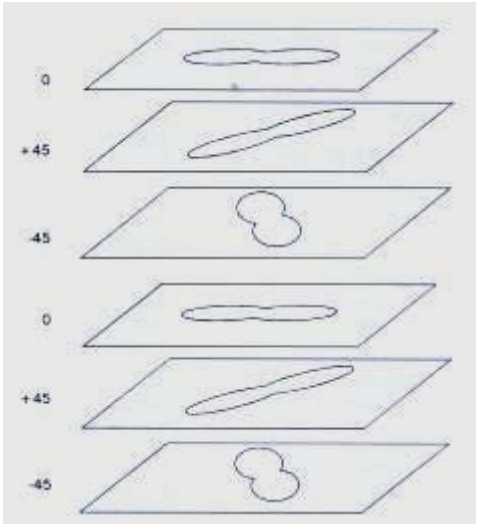

Figure 2.10 Shapes of delamination at different oriented plies (Abrate 1998)

Plies with +/- 45^0 are in similar pattern but opposite in direction while for 0^0 plies the delamination shape is in longitudinal direction (Abrate 1998).

2.7.5 Impactor Shape

Impact responses are generally affected by interactions between impacting bodies and the composite structure. There is a relationship between factors like the mass, geometry of the impactor and target stiffness, geometry and rigidity. Impact velocity of the impactor affects the global response of the composite structure, the interfacial bond between fibre and matrix and stress wave effects. In past research (Cantwell et al (1989a, 1989b, 1989c, 1990a, 1990b, 1991)), the most common impactor shape used has been hemispherical for drop weight impact, although in actual practice this is not an actual representative of a dropped tool on a composite panel during routine maintenance.

Mitrevski et al (2004) investigated the effect of different impactor shapes: flat, hemispherical, ogival and conical ended (see figure 2.11). The force-time histories of different impactors at high velocity impact on carbon epoxy laminates were compared. This research showed that the hemispherical impactor produced the largest peak force and shortest contact duration. Also, flat and hemispherical impactor produced similar energy dissipation and failure mechanisms within the composite specimens.

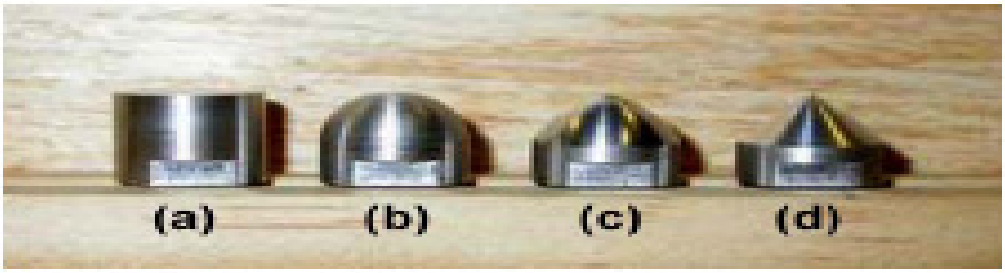

Figure 2.11 Impactor shapes (a) Flat (b) Hemispherical (c) Ogival (d) Conical (Mitrevski et al 2004)

Specimens impacted by the conical impactor absorbed the most energy and produced the largest penetration depth. The damage threshold load (DTL) was highest for the hemispherical impactor followed by the ogival and conical impactors respectively (Mitrevski et al 2004).

Research carried by Zhou et al (1995) found that for the impact with hemispherical impactor on various types of GFRP laminates initiated matrix cracking first, followed by fibre fracture. With the flat indentor there was widespread stress concentration underneath the impactor and thus ply shear-out was found to be the dominant failure mechanism with this particular geometry.

Research carried out by Mines et al (1999) founded that under static conditions the flat and hemispherical impactors produced larger delamination areas compared to a conical impactor for laminates of varying thickness and they suggested that the damage caused by conical impactor is more localised.

2.8 Compression after Impact

2.8.1 Introduction

After low impact has taken place it is important to investigate how the composite laminate behaves under compressive or tensile loads. Generally some composite laminates that are in commercial use in their lifetime will suffer impacts either during manufacturing, maintenance etc., so it is important to know what level of damage tolerance the composite laminate can sustain after an impact event. In general, compression after impact (CAI) in particular has gained much attention especially from the aircraft industry to characterise the structure's performance after damage occurrences. A number of approaches have been considered in the literature. These will now be discussed.

2.8.2 Types of CAI Fixtures

2.8.2.1 NASA CAI Fixture

The NASA fixture (shown in figure 2.12) consists of four separate assemblies and the specimen is simply supported from four sides, each clamping onto an edge of the specimen and thus allowing the specimen to stabilise against buckling.

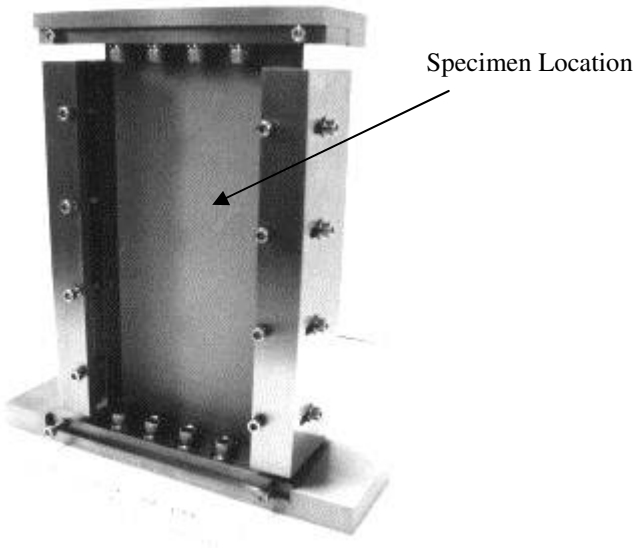

Figure 2.12 NASA compression after impact fixture (NASA 1983)

The fixture consists of top plate and support fixture and in between it can accommodate the loading specimen. The specimen height varies from 254 to 318 mm and width from 127 mm to 178 mm. The impactor diameter is 12.7 mm. The mass is set to 4.5 kg and the drop height to 0.61m which allows attaining maximum energy of 27 J. Loading is set at 1.27mm/min (NASA 1983).

2.8.2.2 Boeing CAI Fixture

The Boeing fixture was developed by the Boeing Company in year 1988 (see figure 2.13). According to Boeing CAI standard (Boeing 1988) the specimen dimensions should be 152 mm x 102 mm with a thickness between 4 mm to 5 mm and with layup $(45/0/-45/90)_{ns}$. Hemispherical impactor with 15.75 mm diameter and mass which varies from 4.5-6.8 kg impacts prior to compression.

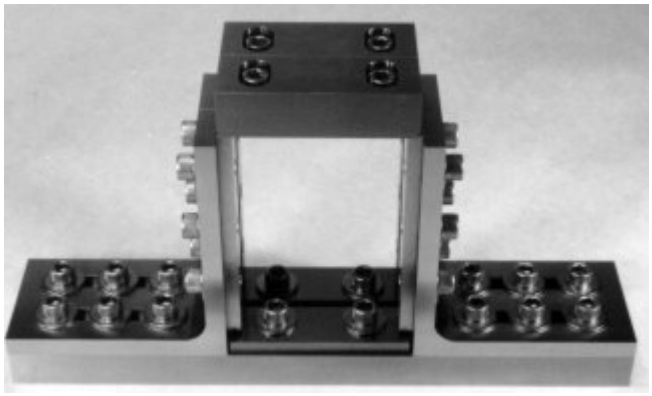

Figure 2.13 Boeing compression after impact fixture (Boeing 1988)

The specimen is clamped by all four sides in the steel frame from the top. The top of the loading plate sits over the top edge of the test specimen to provide simple support to the loading specimen (Boeing 1988). It is supported by a cut-out frame square size of 127 x 76 mm. The loading rate is set at 0.5 mm/min. The vertical sides of the fixture have knife-edge like supports. The unsupported gauge length is 5 mm. The fixture design is very flexible and can be adjusted such that it can accommodate small variations in specimen width and thickness. The side supports can be fixed to different positions along the base plate. Major advantage of these rigs is that specimens with different dimensions as well as curved panels can be tested accurately. Boeing version has been standardized by ASTM whereas the NASA version has not.

2.8.2.3 BAE Systems CAI Fixture

A new CAI rig was designed and built by BAE Systems for testing for large dimension specimens and panels thus allowing analysing larger damage regions and attainment of higher impact energy (figure 2.14).

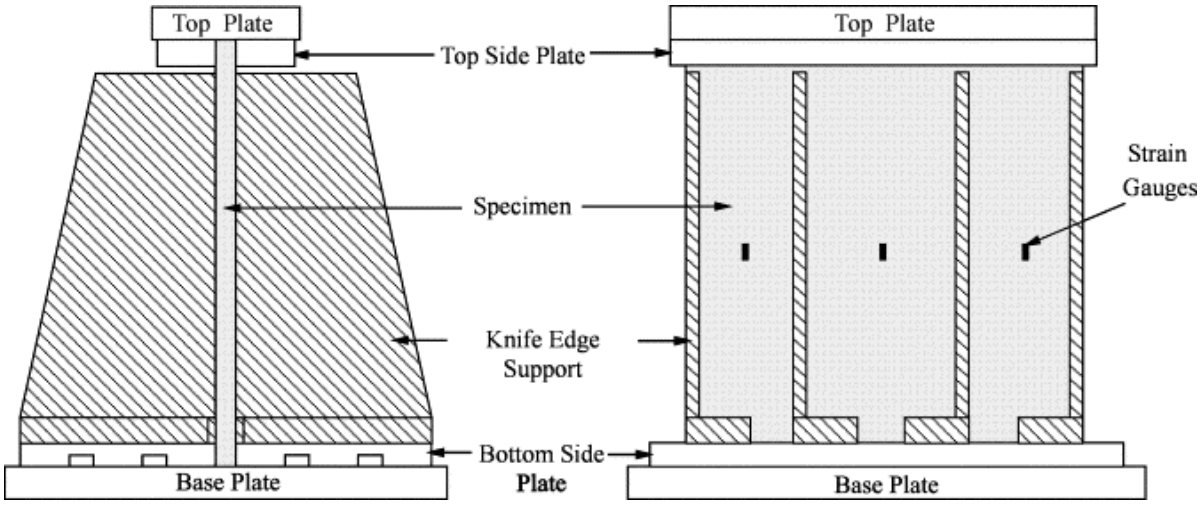

Figure 2.14 BAE Systems compression after impact fixture (Habib 2001)

It consists of both top plate and bottom plate which are clamped with no side supports but only front and back supports so it can accommodate specimens and adjust the dimensions. As the top plate has no guides it can cause early buckling. The rigs and fixture is capable of accommodating test specimens of variable thickness and width (Habib 2001).

2.8.2.4 Airbus CAI Fixture

Airbus has developed their own CAI design in Europe (AIRBUS AITM 1-0010). Figure 2.15 show Airbus compression after impact fixture. According to Airbus standards for CAI, the specimen dimensions should be 100mm x 150mm with a thickness approximately 4 mm and with layup $(45/0/-45/90)_{ns}$. This is quite similar to Boeing CAI rigs. The prescribed thickness is 6.35 mm for lay-up $(45/0/-45/90)_{ns}$. The impactor diameter is 16 mm. The mass ranges from 1 to 3kgs or 4 to 6 kg. The energy levels obtained varies from 9 to 40 J.

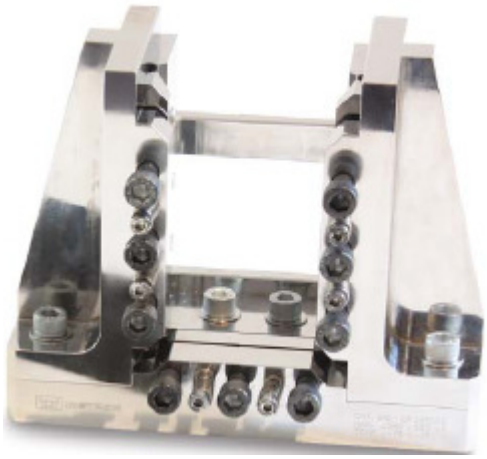

Figure 2.15 Airbus compression after impact fixture (AIRBUS, AITM 1-0010)

Support is given at four sides by a steel frame of size 125x75 mm. End loading rate is 0.5 mm/min and the loading rate is adjusted such that the failure is achieved very quickly. The specimen clamping arrangement differs from the Boeing CAI rig. The top clamping plate is smaller than the specimen width. There are two side support knife edges and the side supports run the full height of the specimen. The compressive load area on the top is smaller than the bottom area. Clamping arrangement is important for the design for the CAI test as it eliminates misalignment.

2.8.2.5 CAI Fixture Summary

Table 2.2 shows the summary of the various geometrical, support conditions and loading parameters of various major compressions after impact fixtures.

Companies - CAI Fixtures	Material Thickness and Lay-Up	Impactor Tup and Support Conditions	Compression After Impact		
			Specimen Dimensions	Loading Arrangement	Loading Rate ($mm.min^{-1}$)
NASA	t= 6.35 mm $(45^0/0^0/-45^0/90^0)_{ns}$	Tup Diameter: 12.7 mm Mass: 4.5 Kg Height: 0.61 m Energy: 27 J Support: 127 mm	(254-318 mm) x 178 mm (cut to 127 mm post impact)	End Loaded	1.27
BOEING	t= 4 to 5 mm $(45^0/0^0/-45^0/90^0)_{ns}$	Tup Diameter: 15.75 mm Mass: 4.5/6.8 Kg Energy: Any Support: 127 x 76 mm	152 mm x 102 mm (cut to size before impact)	End Loaded	0.5
AIRBUS	t= 4 mm $(45^0/0^0/-45^0/90^0)_{ns}$	Tup Diameter: 16 mm Mass: 1-6 Kg Energy: 9-40 J Support: 125 x 75 mm	150 mm x 100 mm (cut to size before impact)	End Loaded	0.5

Table 2.2 Summary of compression after impact fixtures

2.8.3 Parameters affecting the compressive strength

Compressive strength of the impacted laminates is affected by various parameters such as the impactor diameter, thickness of the laminate, material strength, incident impact energy levels, boundary conditions, and degree of delamination. To understand the effect of impact damage it is important to know the residual strength of the composite laminate, where residual strength is defined as the ratio of average strength of the damaged specimen to that of the undamaged specimen of the composite laminate.

The post-impacted compressive strength of thin composite laminates was investigated by Sanchez-Saez et al (2005). They used three different laminates, cross ply, quasi-isotropic and woven laminate (see figure 2.16). The strength of the damaged laminate was normalised with respect to the strength of the undamaged laminate.

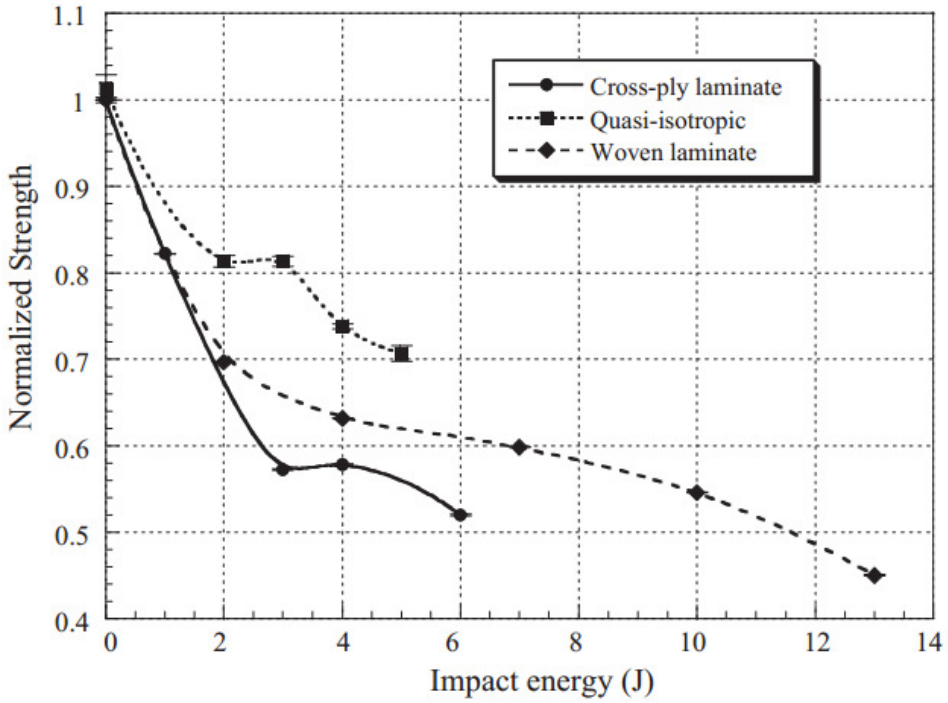

Figure 2.16 Normalised compressive strength vs impact energy (Sanchez-Saez et al 2005)

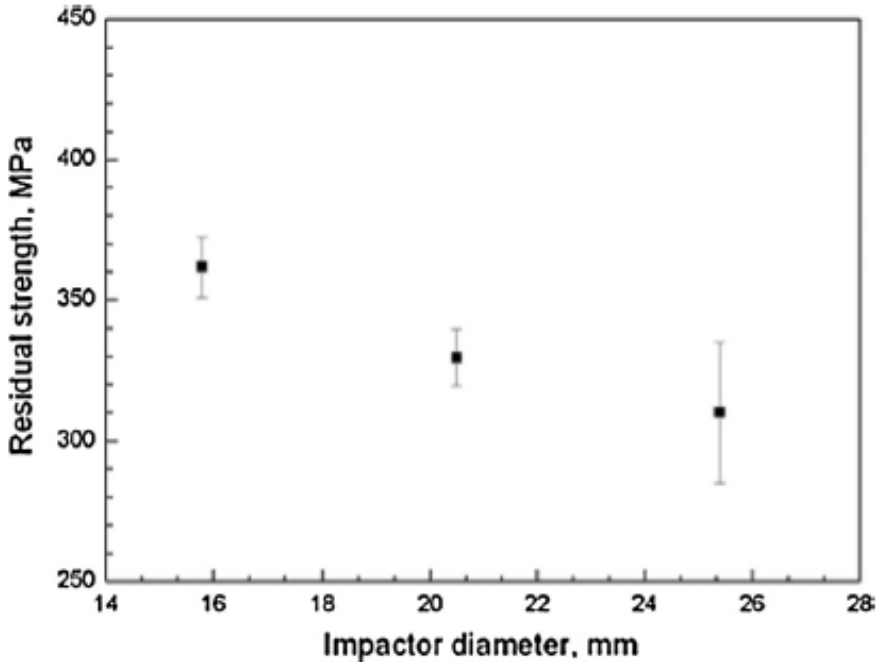

Figure 2.17 Effect of impactor diameter on the compressive residual strength (Koo et al 2013)

For all the layups, there is a reduction in normalised strength with increased impact energy. The cross-ply laminate shows the greatest reduction in normalised strength at 4J impact. This

reduction is due to the 90^0 orientation of the inner plies which makes the centre of the laminate less stiff, and thus the laminate fails under a much lower load. The smallest reduction in normalised strength is observed in quasi-isotropic laminate and this may be due to $+45^0/-45^0$ plies, which protect the load bearing 0^0 plies against the impact damage (Sanchez-Saez et al 2005).

Recent research investigated by Koo et al (2013) suggested that the impactor greatly affects the residual strength of the composite laminates. From figure 2.17 it is clear that as the diameter of the hemispherical impactor nose is increased approximately from 15.8 mm to 25.4 mm under constant impact energy of 23 J and impactor mass of 5 kg then the residual strength decreases drastically. This decrease in residual strength was due to the increase in damage area due to the increase in the impactor radius. These results were found to differ from the results obtained by Shim et al (2005) who concluded that the area of damage increases with the decrease of the impactor radius. Koo et al (2013) study showed that this difference arose from the different boundary conditions.

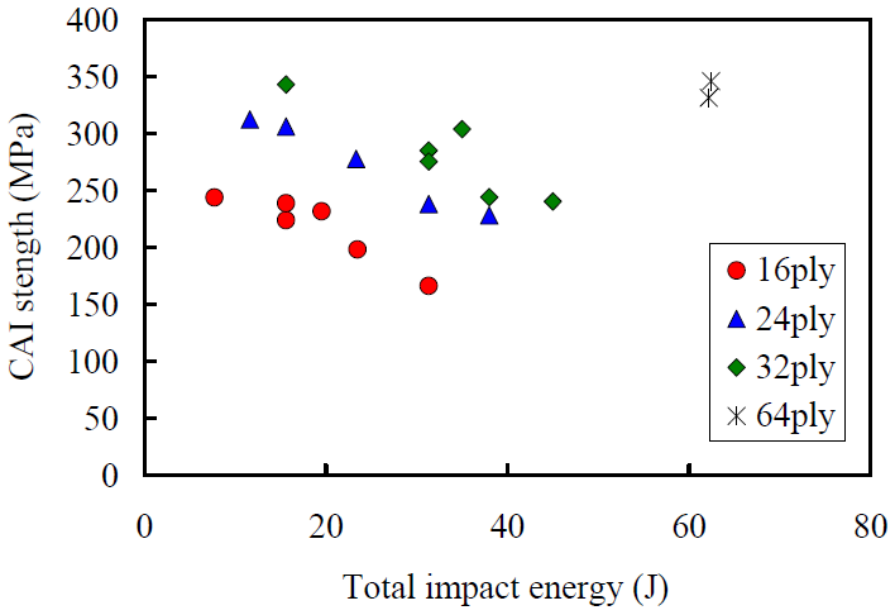

Figure 2.18 Effect of thickness: CAI strength vs. total impact energy (Aoki et al 2009)

The effect of thickness has been investigated by Aoki et al (2009) for quasi-isotropic laminates; the results are summarised in figure 2.18. Each ply thickness is approximately 0.145 mm. The nominal thickness for 16 ply is 2.3mm, 24 ply is 3.4 mm, 32 ply is 4.7 mm and 64 ply is 9.3 mm. The reduction in CAI strength with impact energy is higher for the thinner laminates.

The presence of delamination significantly reduces the residual strength and the damage tolerance of the composite structure and thus makes composite susceptible to premature failure upon compressive loading (Short et al 2001, 2002). Another study by Wang et al (2005) indicated that the related multiple delaminations lead to a higher reduction in compressive strength than the single delamination. Delaminations were incorporated at different locations of the laminate to study this effect. From the trend in figure 2.19 it can be clearly seen that as the number of delaminations increases the compressive failure load of the composite laminate decreases.

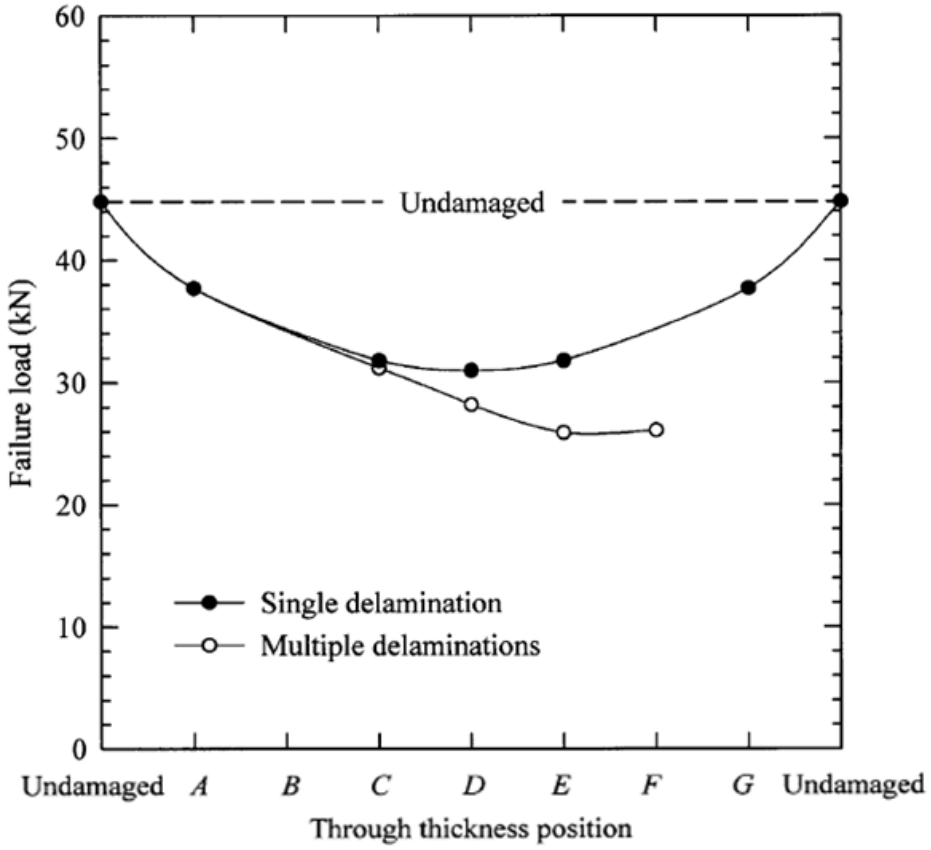

Figure 2.19 Effect failure load on multiple delaminations (Wang et al 2005)

2.9 Damage Assessment Techniques

There are various types of techniques to locate the damage in composite laminates. Non-destructive techniques (NDT) are extensively used on composite structures to detect the delaminations, manufacturing flaws and adhesive debonding. In industries, NDT is applied during manufacturing as well as during in-service maintenance. The most widely used NDT method is the ultrasonic testing but with the advancement of technology various other NDT methods have gained importance in the composites industry for example computed

tomography, shearography and thermography (Zhou et al 2000; Abrate 1998). We will discuss some of the damage assessment techniques that have been used in the literature.

2.9.1 Computed Tomography

2.9.1.1 Introduction

The word "tomography" is derived from the Greek tomos (slice) and graphein (to write). Physicist Cormack (1963) conducted first experiments using reconstructive tomography on research in medical applications by developing a unique method of calculating radiation absorption distributions in the human body. Kuhl and Edwards (1963) introduced the concepts of emission computed tomography. In 1972 the first practical implementation of computed tomography was achieved by Hounsfield (1973), who is recognised as the inventor of computed tomography. His research team collaborated with British firm EMI Ltd. and originally computed tomography was known as the "EMI scan". With the new developments in the medical research area it became popularly known as computed axial tomography which was limited to acquiring images in the axial plane. But later with the development of multi-detector CT scanners with near isotropic resolution, it was possible to produce data that could be reconstructed in any plane with minimal loss of image quality (Hounsfield 1973).

Computed tomography can be defined as the collection of slices/data by transmission or reflection on the object or specimen by cross-sectional imaging. Object projections can be obtained by using various types of computed tomography techniques. Computed tomography (CT) refers to the cross-sectional imaging of an object from either transmission or reflection data. The process involves reconstructing an image from its cross-sectional projections (Slaney et al 1984). CT has become an important tool in medical science with many applications such as detecting cancer, heart scans, full body scans, fracture, brain problems like tumors, bone trauma and complex fractures (Abel et al 2012).

There has been a rapid advancement in the technology mainly in terms of better computational algorithms to construct the image from the projection data. This has resulted in better image quality through a greater number of pixels and higher spatial resolution offering increased clarity, number of grey shades and higher contrast resolution (Slaney et al 1984) is possible now. In recent years X–ray CT has also found increased use in non-medical

applications, especially for Non-Destructive testing of materials (Summerscales 1990; Schilling et al 2005; Scott et al 2010).

2.9.1.2 Types of Computed Tomography

There are various types of tomography depending on the type of technique used to obtain the projections, i.e. X-ray Computed Tomography, Ultrasound Computed Tomography and Magnetic Resonance Imaging (MRI).

All of these different tomographic techniques are essentially based on the same principle that is to reconstruct the cross-sectional image using some material parameter such as the attenuation coefficient. Computed tomography scanner uses X-rays to produce tomographic images at specific areas of the scanned object allowing user to view the scanned area in three dimensions. As X-rays are non-diffracting whereas sound waves are diffracting, the reconstruction algorithms are developed differently for X-rays and sound waves. Thus the selection of techniques depends upon the kind of the object or materials to be analysed and its interaction with matter through which they pass.

Both 2D and 3D reconstructions can be generated for both MRI and CT. In CT the contrast in images can be done only by using X-ray attenuation while MRI can generate cross-sectional images in any plane and uses electromagnetic waves produced due to magnetic resonance of the nucleus in an atom which are used to obtain the projections and images. In MRI there is a variety of parameters that can be altered for the best contrast for specific region of interest thus providing enhanced images. MRI is best suited for medical applications and has found its applications in cases when a patient is to undergo the examination several times successively in the short term (Dalvi et al 2007) as compared to CT which is limited by the hazard of exposing patient to the ionizing radiation.

2.9.1.3 Advantages and limitations over other conventional techniques

X-ray computed tomography can be used for detailed damage characterisation of composite laminates. The technique can be used to identify and locate both manufacturing and in-service defects. When a beam of X-rays strikes glass/epoxy laminates the composite laminate undergoes an absorption which depends upon the following parameters.

1. Nature of the materials that is densities of fibre and polymer matrix (linear absorption coefficient);
2. The thickness of the laminate;
3. The incident intensity of the radiation.

Conventional radiography or optical microscope gives information of the surface topography. Delamination is difficult to detect because when the beam strikes the surface of the composite material it reflects a plane projection so cracks perpendicular to the beam are able to escape without detection (Kapdia, TWI Ltd.). However computed tomography with 3D partition has the advantage of viewing the defect at different angles of rotation. By this it is possible to know the absorption density of any point within a given volume which is not applicable in other conventional techniques. CT is more powerful as compared to scanning electron microscopy (SEM) as with CT we can obtain 3D volumetric data that greatly enhances material differentiation. CT investigates and identifies fractures, structural damage, crack area, crack density initiation and propagation developed through in-service loadings.

However there are certain limitations associated with the use of computed tomography sources for observing micro-level damage in composites. The major limitation is the sample size and shape. The specimen size has to be small in order to fit into the specimen holder. The small size limits the possibility of thorough investigation of damage in composite material. Also the complex shapes are difficult to mount for the tomographic scan so special rotating mounts with the new design are required for specific projects (Symons et al 2000).

2.9.1.4 Theory of Computed Tomography

The absorption of X-rays by composite materials depends on the energy of the photons, the electronic configuration, the thickness and the density and volume fraction of matrix and fibre content of the composite specimen. When X–rays pass through different types of composite laminate they lose their intensity and get attenuated. This can be represented by the attenuation coefficient or linear absorption coefficient μ of the material. The Lambert-Beer's law states that slices of equal thickness and equal material (same density) in the beam path will absorb the same amount of radiation (*Standard Guide for CT, 1995*). So when the X-rays pass through a component, depending on the internal geometry and the type of constituents, they will get attenuated to varying degrees.

The change in intensity of X-ray beam or the linear absorption coefficient is given by (*Standard Guide for CT, 1995*).

$$I = I_0 e^{-\mu x}$$

$$I = I_0 e^{-\int \mu(s).ds} \tag{2.1}$$

Rearranging equation (2.1) we get

$$-\ln(I / I_0) = \int \mu(s) \cdot ds \tag{2.2}$$

In this equation (2.1) $\mu(s)$ is the linear absorption coefficient at every point on the X-ray path. Rearranging equation (2.2) with respect to incremental angle θ and position *n*, we get final equation,

$$P(\theta, n) = -\ln\left[\frac{I_s(\theta, n)}{I_o}\right] = -\int_s \mu(x, y) \cdot ds \tag{2.3}$$

From equation (2.2) and (2.3), I_o is the intensity of X-rays originating from the source. I_s is a measurement of the intensity during the orientation of the detector with respect to the object with the incremental angle θ and position *n* and $\mu_s(x, y)$ is the 2D distribution of the linear attenuation coefficient for the object and ds is an element of the distance along the X-ray path through the object with respect to an angle θ and position *n*.

During the rotation, the attenuation of the intensity of the X-ray beam is measured in finite number of angular increments. If the specimen exhibits a complex geometry or consists of a high density material, smaller angular increments can be used. The process is continued until the data from 180^0 of specimen rotation have been recorded. For complex shapes and geometries 360^0 sweep is required. Data is analysed by the computer that carries the image of the object. The grey level of each pixel in the image matrix corresponds to the different attenuation of the X-rays. Increasing the number of grey scales simplifies detection of even small changes in attenuation. Each pixel actually contains information about a 3D volume element often referred to as voxel. Defects such as matrix cracks, delamination, fibre rupture and variations in the density could be detected with CT Technique (Zhou et al 2000).

2.9.1.5 Industrial and Research Applications

Damage assessment using CT is important compared to the usual NDT techniques because of higher X–ray absorption coefficients of the materials to be analysed. The greater attenuation

difference between the constituents makes it easy to identify material integrity, defects and access manufacturing quality such as void contents and fibre distribution in MMC and ceramic matrix composites (Geandier 2003, Justice 2003).

In recent years X-ray Computed Tomography (CT) has found lots of application in industrial research. Euro Copter Deutschland (ECD) was the first helicopter company which applied CT as a non-destructive inspection method for the testing of helicopter composite components (Oster 1997). The company was able to utilise CT as a means to investigate and analyse the delamination and damage behaviour of the test specimen. After the successful detection and investigation of the damage characteristics of the composite materials, the company has applied CT in different applications in design and development, series production and maintenance of helicopter main rotor blades (Oster 1997). ECD used a medical scanner and investigated the effects of fatigue, bending behaviour on composite structures such as delamination, fibre cracks, failure of adhesive joints and low volume fibre fraction. Figure 2.20 shows the tomographic medical scanner and a typical specimen being evaluated.

:

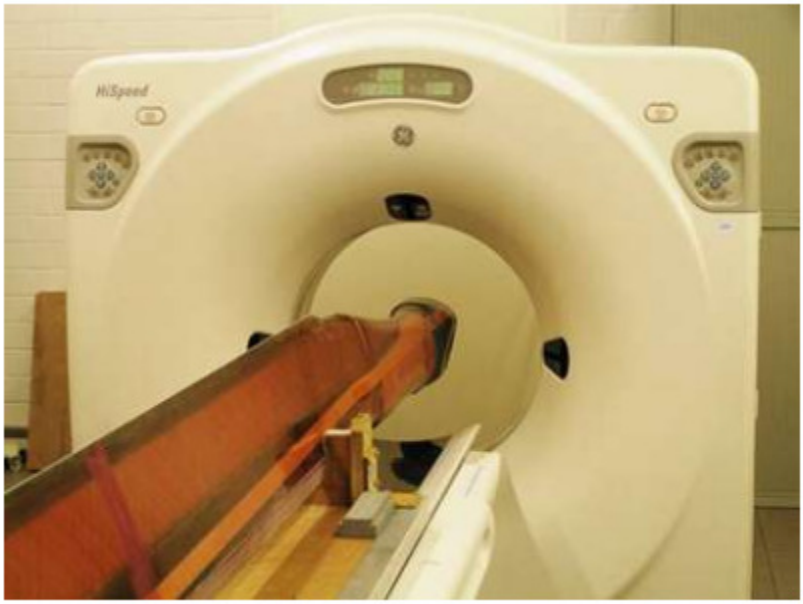

Figure 2.20 Tomographic medical scanner (Oster 1997)

More recently with increase in developments in CT with the contrast and geometric resolution the researchers have focused their attention for studying damage in polymeric matrix composites plies.

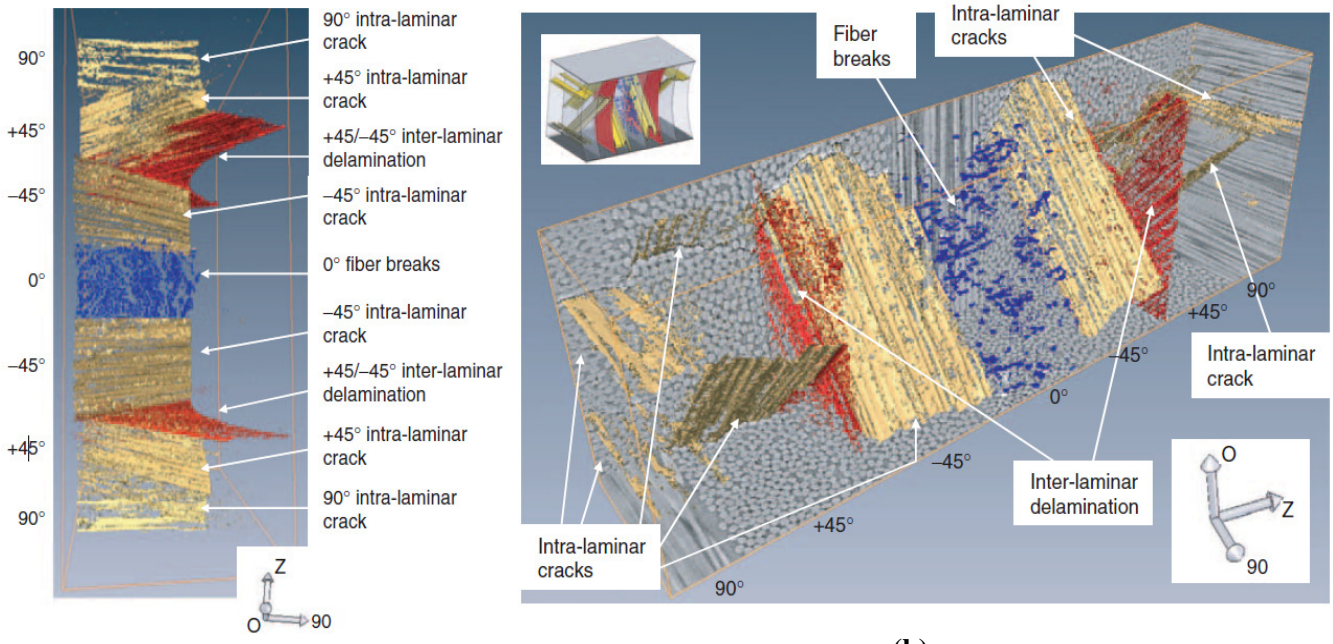

Figure 2.21 Cropped computed tomography volume showing segmented cracks, delaminations and fibre breaks with the fibre orientation within each ply ahead of the notch (a) 2D view (b) 3D view (Wright et al 2008)

Damage in notched Carbon/Epoxy Composite laminate has been investigated using Ultra High Resolution Computed Tomography (Wright et al 2008). The laminate plates with a $(90^0/+45^0/-45^0/0^0)_s$ lay-up configuration were subjected to applied loads. With the application of computed tomography the 3D rendering of damage regions near the damaged notch of composite laminate has been undertaken. Fibre orientation of each plies, cracks, delaminations and fibre breaks at notch tip are observed, as shown in figure 2.21 (a) and (b). 0^0 plies underwent fibre breakage cracks that follow the fibre direction within that ply and 90^0 plies suffered intra-laminar cracks while $-/+45^0$ plies suffered both extensive intralaminar and interlaminar cracks and delamination. These differences were not previously observed in non-destructive testing. X-ray CT can be used to provide detailed investigation of propagation of damage mechanism and its correlation with matrix-fibre breakage (Wright et al 2008).

In another case study (Dunkers et al 1999), an investigation of the effect of impact damage on epoxy/unidirectional E-glass composite laminates was carried out by slicing sections at different depths using computed tomography. This research lead to understanding the

behaviour of damage mechanisms inside composite laminate subjected to impact damage. Figure 2.22 (a) shows the volumetric presentation of the epoxy/unidirectional E-glass composite. The composite cross-section is shown along the x-z plane.

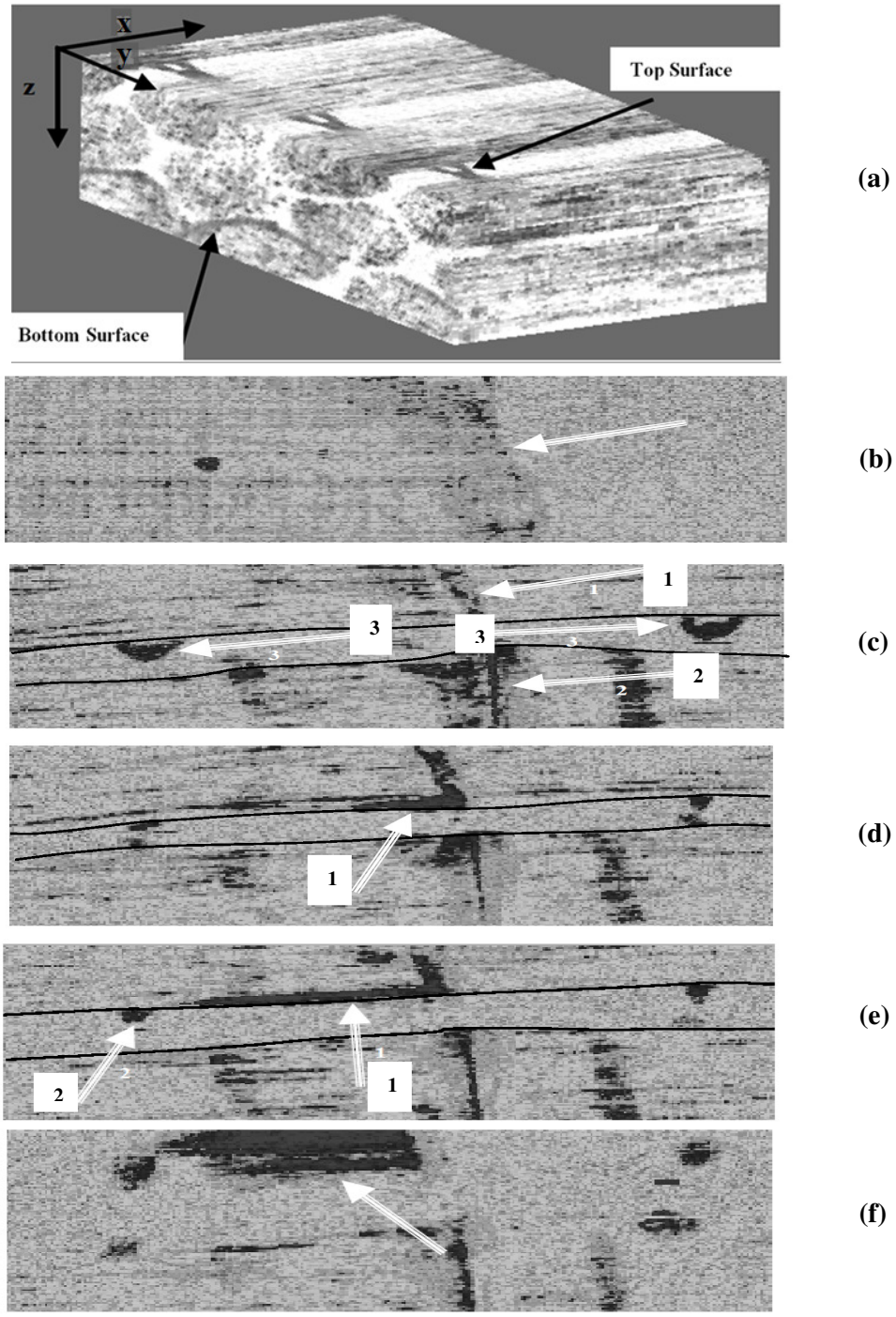

Figure 2.22 View of impact damaged epoxy/unidirectional E-glass composite at a depth (a) Laminate cross-section along the x-z plane (b) Top surface (c) 337 µm from surface (d) 460 µm from surface (e) 550 µm from surface (f) 652 µm from surface (Dunkers et al 1999)

Figures 2.22 (b)-(f) show the impact damage of the epoxy/unidirectional E-glass composite to detect the surface crack using computed tomography (Dunkers et al 1999). The x-axis is the 0^0 unidirectional fibre direction. The damage at the top surface of the composite laminate is shown by the arrow in figure 2.22 (b) while figure 2.22 (c) shows a slice of the impact damage composite laminate 337 μm below the surface of the composite laminate. Arrows 1 and 2 show fibre tow crack paths and propagation while arrow 3 indicates polyester crossing threads that primarily function as holding the top layer together. The black lines in the figures indicate the path and direction of the fibre tows. Figure 2.22 (d) shows impact damage at 460 μm below the surface of the composite laminate. Arrow 1 shows the initiation of the crack at the interface and crack propagation along the fibre tow and resin boundary. Figure 2.22 (e) shows impact damage at 550 μm below the surface of the composite laminate. The crack extends to 1.8 mm long as shown by arrow 1. Arrow 2 indicates the presence of polyester stitching. Figure 2.22 (f) shows the presence of delamination at the interface of fibre and matrix region during impact damage at a depth below the surface of composite laminate and extensive size and widening of the crack is seen at the bottom of the fibre tow of the composite laminate and the delaminated area. The delamination is about 1.9 mm wide and 0.50 mm high and 652 μm from the surface. Thus the computed tomography is important for the study of impact damage as we get information of behaviour of how the damage initiates and propagates from the surface to bottom by the fibre glass tows path and how the interface crack that is at the boundary of fibre and matrix leads to delamination. Thus the damage in composite laminates can be understood clearly by tomography reconstruction and re-slicing of impact damage through the thickness of the composite. This re-slicing of the image data reveals the progression of cracking and delamination within the composite (Dunkers et al 1999).

There are very important applications of CT in defence research work of different metallic/non-metallic materials. Recently, the Army Research Laboratory investigated the behaviour of ceramic matrix composites for armour material applications. In figure 2.23 (A) the CT image at 18.18 mm from section surface of impacted titanium carbide (TIC) disk is shown clearly visualising the crack damage (William et al 2001).

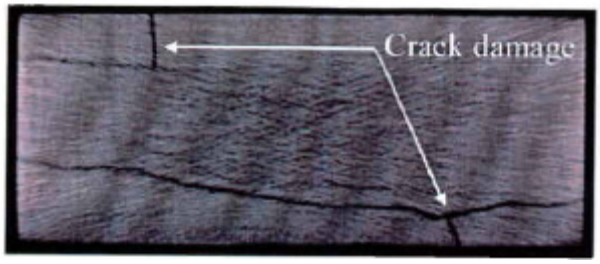

Figure 2.23 (A) CT image at 18.18mm from section surface (William et al 2001)

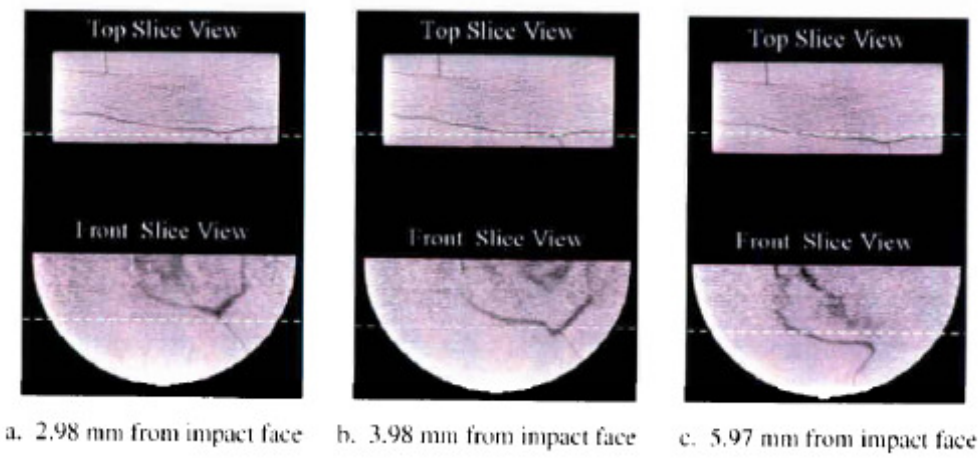

(a) **(b)** **(c)**

Figure 2.23 (B) CT of the top and the front slice from different distances of titanium carbide (TIC) during impact (William et al 2001)

In figure 2.23 (B) the material is sectioned into different slices in order to investigate the damage behaviour. The image shows the path and direction of initiation and propagation of the crack damage from left to right. The figures 2.23 (B) - (a), (b), and (c) are top slice and front slice views with different distances from the impact face. At greater depth from the impact face the behaviour of the crack changes in shape, size and dimensions (William et al 2001). Extensive crack behaviour can be seen at 5.97 mm from the impact face location however the damage patterns seem to be following the point of initiation and propagation with the increasing depth of the damage from the impact face front slice locations. The series of side views shows how damage in the thickness direction changes with distance from the line of impact. The sectioned surfaces are an excellent way to visualise damage.

In another case study (Symons et al 2000) the impact behaviour of the composite laminate for medium to severe levels of impact was examined using computed tomography. The images in figure 2.24 (a) and (b) show four slices through the centre of the damaged zone taken at 0.58 mm intervals. Figure 2.24 (a) shows cross-sectional views. Here barely visible damage can be seen at a medium energy level while figure 2.24 (b) shows a more severely impacted specimen (Symons et al 2000). It is clear that in the moderately impacted specimen damage starts from the surface and propagates inside through the thickness of the laminate but no extensive damage is found at the bottom of the plies while with severe level of impact the upper plies as well as bottom plies have been broken severely. Extensive delamination can be observed in all successive four slices of the composite laminate. Clearly damage can be seen by visual inspection on the surface of the specimen. This information together with fatigue test data can be used for inspection of in-service components and can provide the threshold and damage tolerance limit of the composite laminate in-service (Symons et al 2000).

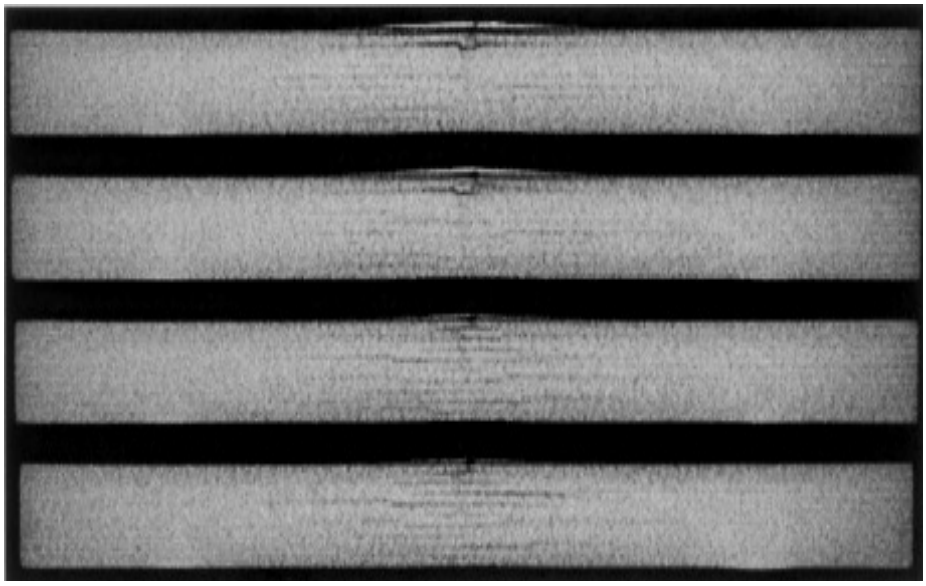

Figure 2.24 (a) X-ray computer tomography showing four slices and cross-sections of medium damage (Symons et al 2000)

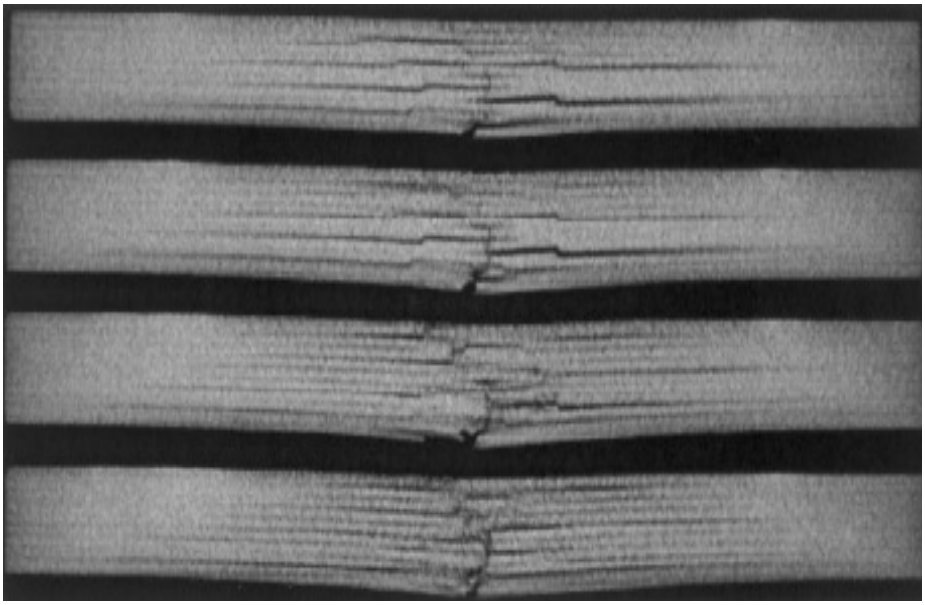

Figure 2.24 (b) X-ray computer tomography showing four slices and cross-sections of severe damage (Symons et al 2000)

The application of CT in composites can help determine fibre defects, in-homogeneities and crack behaviour. Figure 2.25 show 3D volumetric reconstruction (Schilling et al 2005) of GFRP specimen in which we could see fibre tows/bundles and voids present in the composite laminate. In order to see the direction and path of unidirectional fibre tows (bundles) the matrix is rendered invisible while the fibre tows are shown in light grey. Voids are also seen clearly which helps us to understand the in-homogeneity of composite laminate.

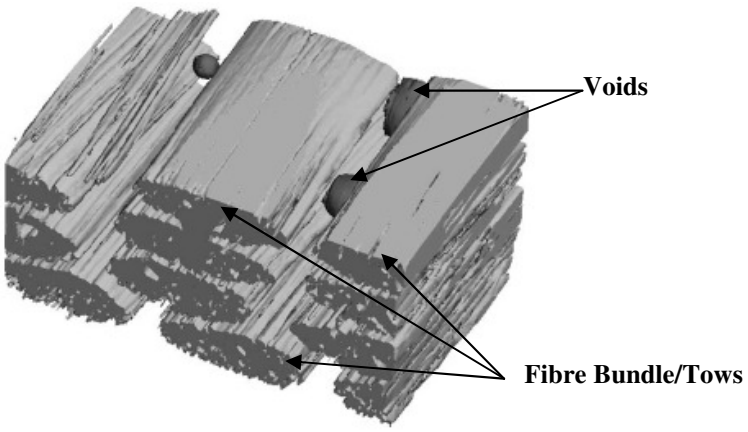

Figure 2.25 Three-dimensional volumetric models of S-glass unidirectional fibre bundles (lighter grey) and voids (darker grey) and the matrix is rendered invisible (Schilling et al 2005)

Damage mechanisms such as delamination, micro-damage and lateral damage in bolted Graphite/Epoxy specimens have been studied (Schilling et al 2005).

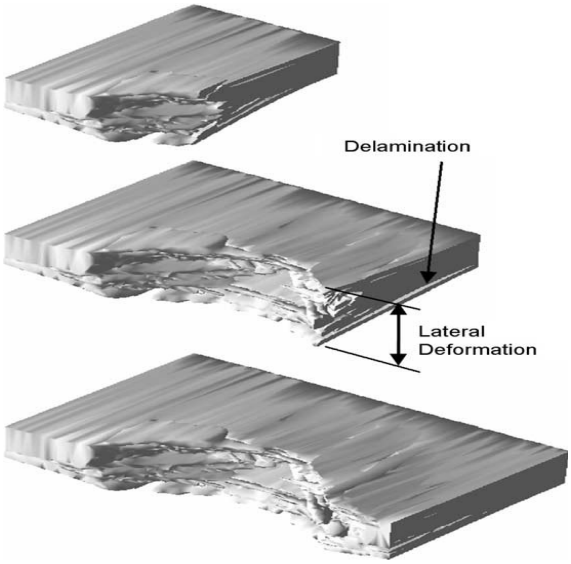

Figure 2.26 Bearing failure damage around the bolt hole in a graphite/epoxy laminate (Schilling et al 2005)

The reconstructed volume and two smaller sections of this research are shown in figure 2.26, revealing delamination and lateral deformation. The investigation showed how the composite laminate undergoes delamination near the edge of the bolt hole and indicates the unstable behaviour due to fibre crushing. Using CT techniques the damage is reconstructed in the three-dimensional model as shown in figure 2.26, permitting the lateral deformation and delamination around the bolt hole to be seen from different sections and locations.

2.9.2 Ultrasonic Method

Ultrasonic method is a widely used method for the detection of delamination, flaws, fibre matrix failure and debonding in composites materials (Zhou 2000). Ultrasonic usually have the frequency range of 1 -20 MHz. C-scan is a two-dimensional presentation of ultrasonic data where colour represents the signal data at a point. Depending upon the probe position the amplitudes are recorded. D-scan is a three-dimensional presentation of data and is similar to C-scan. In this echo time of flight is recorded depending upon the probe position. There are different types of ultrasonic techniques used for various applications.

- Water Immersion Coupled Ultrasonic technique.
- Direct Contact Ultrasonic technique
- Non-contact Ultrasonic technique.

There are two methods using water immersion coupled ultrasonic technique:

- Pulse-Echo method
- Transmission method

The overall ultrasonic data processing and analyses can be done in three basic steps.

- Image Domain
- Time Domain
- Frequency Domain

Direct Contact Ultrasonic

In this method there is a contact between probe and specimen. C-Scan is produced by x-y representation of the amplitude or time of flight of ultrasonic waves through the material whereas D-scan can be produced only with the time flight data. Time of flight data can be obtained using pulse-echo method or double transmission. A D-scan is a three dimensional x-y-z representation of the structure where on the z-axis the relative time of flight is shown (Summerscales 1990).

Non-contact Ultrasonic

Non-contact ultrasonic scanning is a technique used for material characterisation during and after manufacturing process. This method does not require traditional ultrasonic coupling and mechanical contact and is adapted for surface wave testing in MHz frequencies that enable impact damage/defect detection in surface plies of the composite materials (Djordjevic 2000).

2.9.3 Radiography Technique

Radiography is another important technique used widely. The basic principle is that specimens are subjected to X-ray electromagnetic beams with wide range of wavelengths (Abrate 1998, Matthews 2000). The X-rays penetrate through the composites, thus producing photographic images of the internal structure of the specimen. Figure 2.27 shows a typical radiography image for impact damage for carbon fibre composite laminate.

Figure 2.27 Radiography technique used to detect impact damage on carbon fibre composite laminate (Capriotti et al 2000)

Capturing of fine photographic images of the internal structure of the specimen depends upon the correct adjustment of voltages, currents, film to focus distances and exposure times (Capriotti et al 2000).

2.9.4 Visualisation Technique

Impact damage can be also be detected by visualising the translucent materials such as glass epoxy composite with the use of strong backlighting. Other composites that are opaque such as carbon epoxy composites cannot be detected by the visualisation method but internal impact damage can be detected by using various ultrasonic techniques. They have the advantage that they are able to predict the extent of the impact damage and its exact location.

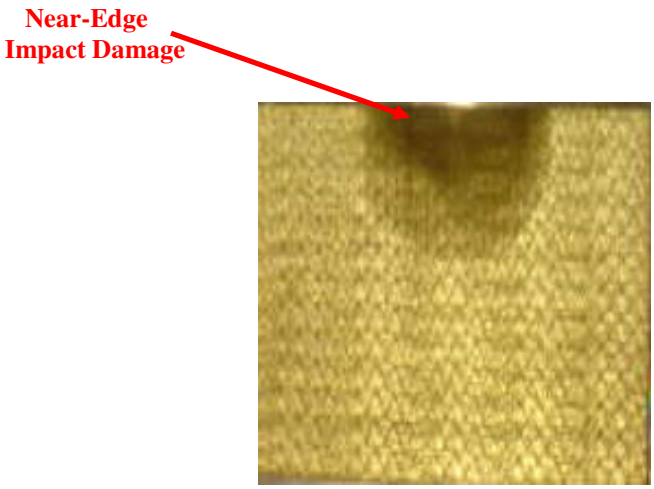

Figure 2.28 Visualisation technique for impact damage of glass fibre composite laminate

Figure 2.28 show near-edge impact damage on glass fibre composites using visualisation technique. The size and shape of impact damage and matrix crack can be detected by visual observation. Several researchers have used this simple technique effectively especially on glass fibre composites for understanding the morphology of impact damage and impact damage development (Zhou 2000, Abrate 1998).

2.10 Finite Element Modelling of Impact of Composites

In the last few decades, finite element simulations have become a very important tool to predict damage initiation and propagation in composite laminates under low velocity impact. Various software such as Abaqus/Explicit, LS-Dyna, Patran/Nastran etc., have become available in order to conduct such numerical simulations. Finite element simulations tools accurately model the composite laminates. Various options are available for performing low velocity impact simulations such as defining the loading and contact conditions and various composite failure criteria can also be incorporated into the models. Simulating the impact damage accurately may significantly reduce the experimental testing costs on composites.

Numerous low velocity impact models have been investigated using the finite element approach and then validating the results with experimental work. Wu and Chang (1989) conducted a study on transient dynamic analysis of laminated composite plates subjected to transverse impact. Research investigated the displacements, the transient stress and the strain distributions through the thickness of laminate during the low velocity impact. Lakshminarayana et al (1994) simulated and accurately predicted low-velocity impact damage using Abaqus. Ganapathy et al (1998) conducted failure analysis of laminated composite shell panels subjected to low velocity impact. Furthermore, Cho and Zhao (2002) studied the effects of geometrical and material factors on the mechanical behaviour of composite laminates under low velocity by implementing a finite element program developed in the laboratory. Aslan et al. (2002 and 2003) conducted comparisons of finite element simulations and experimental analysis to investigate the effect of the thickness, impactor mass and velocity for low-velocity impact on composite laminates. The research concluded that as the thickness of the laminate is increased the peak force in an impact event increases and the contact time is significantly reduced. Tiberkak et al (2008) investigated the effect of transverse/normal shear stresses and matrix damage in different plies under low-velocity impact by using the finite element approach.

Sosa et al (2012) conducted a study on modelling the damage in fibre reinforced composite laminates subjected to low velocity impact. The research investigated prediction of the delamination, the damage initiation and damage propagation. In another recent study, Kreculj et al (2013) studied the effect of impact damage on laminated composite aircraft structures. The research concluded that the most common impact damage mechanisms occurring in composite laminate are matrix cracking, fibre failure and delamination. Various failure criteria for composite materials including Tsai-Wu, Chang-Chang and Hashin were implemented in order to predict the extent of damage, fracture and failure of composite structures. The finite element simulations accurately predicted the experimental results.

In order to predict the impact damage composite failure theories have to be incorporated into the finite element models. Numerous failure criteria have been developed for composite materials for different applications but the most widely used for impact damage on composites is Hashin type failure criteria. Hashin proposed a set of failure criteria for predicting failure of unidirectional composites based on each failure mode. Hashin failure criteria involves both fibre and matrix failures with four different failure modes that are fibre tension, fibre compression, matrix tension, and matrix compression (Hashin and Rotem, 1973; Hashin, 1980). Usually Hashin criteria are implemented in two dimensions but the criteria can be extended to three dimensions.

In order to predict delamination, the cohesive modelling approach has recently become very popular for impact problems. Delamination is simulated using cohesive elements at the interfaces of the composite plies. The cohesive modelling approach allows selection of cohesive interface surfaces within a finite element mesh and application of traction-separation failure criteria at these interfaces. Cohesive elements act like nonlinear springs linking the nodes at interfaces.

In this thesis elastic simulations have been conducted on near-edge and on-edge impact. The mathematical formulations of Abaqus/Explicit code and contact algorithm are described in Appendix B. Abaqus/Explicit code is used. The contact between the impactor and laminate is defined using a contact algorithm.

2.11 Effects of low and high velocity impacts to commercial aircraft

2.11.1 Stress Waves

During impact initial incident energy is lost and is utilised in creating the damage, overcoming the frictional forces, noise and vibration of the entire system and some part of energy is lost in generating the stress waves. Stress waves are complicated phenomena in composites due to limitations such as internal defects, delamination, voids and impact damage in composites (Sansalone et al 1987). Wave propagation and impact in composite materials have been studied extensively previously using analytical and computational techniques (Moon 1973). Propagation of stress waves depends upon various parameters such as intensity and the angle of impact, boundary conditions and material properties i.e., laminate modulus, Poisson's ratio and the density (Ghomi 2011).

During the impact the stress waves are transmitted through the composite laminate at the location just under the impactor. Three different types of stress waves are generated and propagated i.e., dilatational or pressure wave (P-wave), distortional or shear wave (S-wave) and Rayleigh or surface wave (R-wave). All these stress waves travel with different speeds and can be longitudinal or compressive motions depending upon the type and the intensity of impact. P-waves and S-waves travel through the plate and surface waves (R-wave) travel away from the impact location. R-waves travel along the surface and include both longitudinal and transverse motions. R-waves decreases exponentially in amplitude as the distance from the impact surface increases. S-waves travel as a shear or transverse wave, so motion is perpendicular to the direction of wave propagation. P-waves travel as a pressure wave and the motion is parallel to the direction of wave propagation. P-waves propagate fastest followed by S-waves and finally slowest for R-waves. The particle motion of R-waves is larger than that of P-waves and S-waves, thus causing more damage to laminate (Impact-Echo Instruments (2001)).

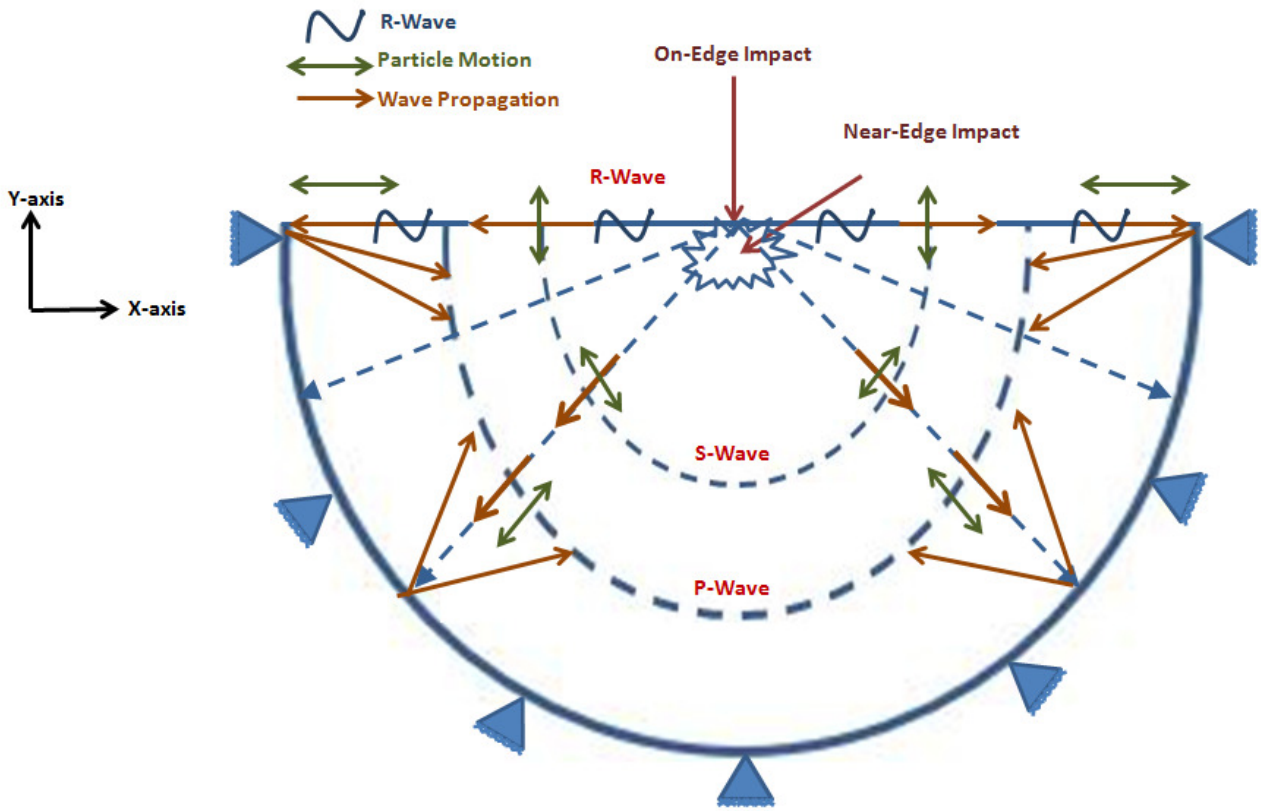

Figure 2.29 Distribution of stress waves during on-edge and near-edge impact (Impact-Echo Instruments (2001))

Figure 2.29 shows a surface stress wave (R-wave) generated during edge impact which travels along and away from the edge impact location while P-waves and S-waves travel through the plate with spherical wave fronts. In S-waves, the particle motion moves perpendicular to the wave propagation while for P-wave the particle motion moves parallel to the wave propagation. The boundary conditions greatly affect the nature of the wave mechanics during edge impact. Scattered stress waves reach the edge of fixed end boundary and then are reflected. At boundary edges, P-wave is reflected at different oblique angle thus distributing pressure wave around the boundary edges. This indicates more energy is absorbed by the laminate through these stress waves thus leading to more damage on this unconstrained area (Ghomi 2011).

2.11.2 Crashworthiness of aircraft

The term "crashworthiness" in aircraft design can be defined as a measure and ability of the aircraft structure to show impact resistance and protect the occupants from injury during a

survivable crash. Crashworthiness is an important parameter to include in different design stages during the manufacturing of the aircraft (Maia 2005). The design of an aircraft structure should be such that it satisfies the requirement of crashworthiness. One of the most important part of the aircraft design phase is the different types of impacts that an aircraft can undergo during its flight path. Figure 2.30 shows the different types of centre and edge impacts that a commercial aircraft can undergo during its flight life span.

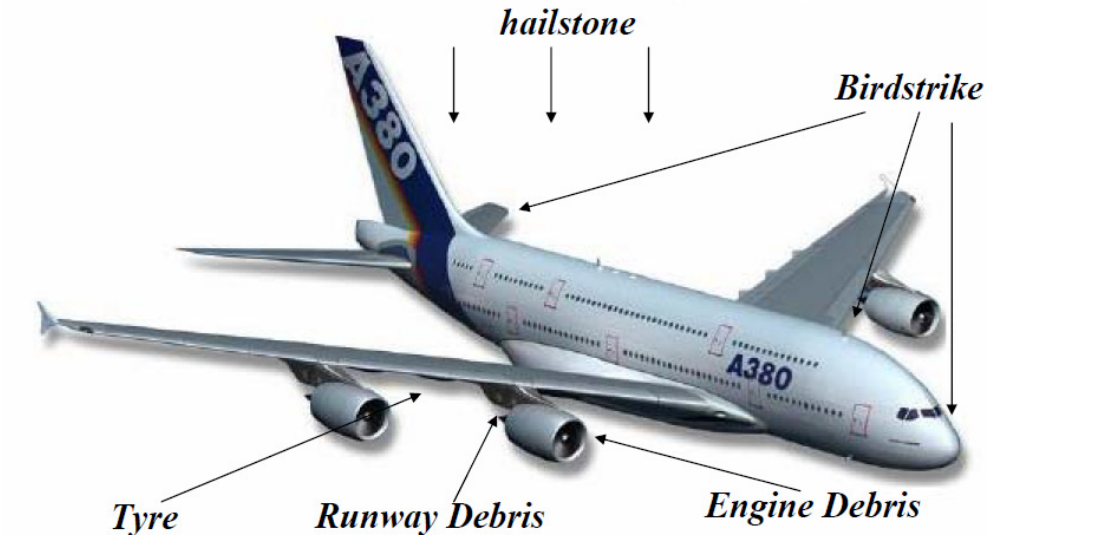

Figure 2.30 Crashworthiness of aircraft at high velocity impact (Brown 2006)

These potential impact threats can be considered as impactors. Impactor types can be hailstone, tyres, bird impacts, runway and engine debris etc (Brown 2006). Crashworthiness experiments are difficult, time consuming and expensive to conduct as they require similar impact and structural conditions as would occur in real impact event during plane crash. Finite element analysis is a useful tool to predict the structural responses and provides design guidance for aircraft regarding crashworthiness.

This research covers the damage response of a composite laminate to low velocity impacts on the centre, on-edge and near-edge. In some real case scenarios, centre and edge impacts can occur at a very high velocity. Some case studies can be related to edge impacts for example near-edge impact can be related to space shuttle Columbia, which crashed during the shuttle re-entry into the earth just minutes before the final landing. This example can be related to near-edge impact of the shuttle wing. Figure 2.31 (a) shows the foam striking fibreglass composite panel near the leading edge.

(a) **(b)** **(c)**

Figure 2.31 Foam is striking fibreglass composite panel near the leading edge (Columbia Accident Investigation Board 2003)

During launch a large piece of foam insulation from Columbia's external fuel tank struck underside the leading edge of the left wing (see figure 2.31 (b) and (c)) at approximately 530 mph, damaging the Shuttle's thermal protection system as shown in the figure. Initial research conducted by Columbia Accident Investigation Board showed that the foam impacted on a section of a fibre glass reinforced leading edge panel at approximately 530 mph. Tests showed visible and significant impact damage near the edge of the panel leading to damage propagation to failure (Columbia Accident Investigation Board 2003). Figure 2.32 and 2.33 shows two types of on-edge impact leading to crash.

Figure 2.32 On-edge impact on Boeing 737-33V HB-III aircraft wing (Federal Aircraft Accident Board 2003)

Figure 2.33 Bird striking the leading on-edge impact of the wing (Phoenix Airport Bird Control Services)

Figure 2.34 Centre impact on the Airbus A380-842 aircraft wing (Australian Transport Safety Bureau 2010)

Figure 2.32 shows the impact of hailstone striking on to the edge of the wing (Federal Aircraft Accident Board 2003). Figure 2.33 shows the bird striking and penetrating into the leading edge of the wing (Phoenix Airport Bird Control Services) while figure 2.34 shows centre impact of debris from the turbine engine penetrated on to the leading edge of the wing (Australian Transport Safety Bureau 2010). In all these cases the hail, debris and bird strike can be considered as impactors striking on the edge of the wing panel. Thus all these cases can be considered to be related to centre and edge impacts. In real case scenarios, the edge impacts can be a combination of both on-edge and near-edge impact. The probability and frequency of these edge impacts is highest during aircraft take-off and landing.

2.12 Literature Conclusion

This chapter outlined the importance of composite structures in the aviation industry and the effect of impact damage on the structural integrity of the composite structure. The following observations can be drawn from the literature review.

- Various manufacturing techniques have been discussed. For this work, quasi-isotropic lay-up of E-glass fibres was available. So, the manufacture of the laminates was carried out using the VARTM technique; the procedure is detailed in Appendix C.
- Various methods of impact testing for low velocity impact have been used in published research on impact of composite laminates, with drop-weight impact testing being the most used method. An impact test rig was available for drop-weight testing, and the drop-weight impact machine had suitable software available. The testing was carried out using this rig, modified for different impact locations as described in chapter 3.
- The literature review has demonstrated that the residual strength of damage laminates is an important parameter for design of composite structures. In this work, the residual strength of the damaged laminates was tested in both compression and tension. The methods of detection of impact damage have been discussed. The laminates used in this project were transparent so visualisation of the damage could be carried out. X-ray Computed Tomography was available and a preliminary study using this technique has been carried out.
- Finite element simulations are developing into an important method to predict impact damage. In this project, a preliminary finite element study has been carried out which could be developed to include fracture mechanisms in future work.
- Impact damage of composites is a growing concern for the aerospace industry. New effective tools and methods have to be explored and developed in order for industries to be fully confident about the full implementation of composite materials.

Chapter 3

Low Velocity Impact: Near-edge, On-edge and Centre Impact on Glass/Epoxy Composite Laminates

3.1 Introduction

The objective of the study is to investigate low velocity impact behaviour of a composite laminate during near-edge and on-edge impact events. Drop weight edge impact tests were performed and load, velocity, displacement and energy history were recorded during the impact events. The laminates were prepared as described in Appendix C. The experimental investigation will permit both a quantitative and qualitative assessment of the damage behaviour of near-edge and on-edge impact phenomenon. In particular, the progressive damage process observed in the composite laminate during the impact event will be considered. In the following sections we will discuss the results obtained during this experimental investigation.

3.2 Experimental Test Methodology

In this project glass/epoxy composites laminates were used. Drop weight low velocity impact machine (Instron) was used to investigate and understand the effect of thickness, absorbed energy and failure damage/modes involved in the impact process of near-edge and on-edge impact.

3.2.1 Impact Conditions

Low velocity impacts tests are usually simulated experimentally as normal impacts as this is the most favourable condition of impact. But generally low velocity impacts are out-of-plane in nature. This type of impact is very complicated as the type of impact damage is not visible. Figure 3.1 shows the different low velocity edge impact conditions used in this research.

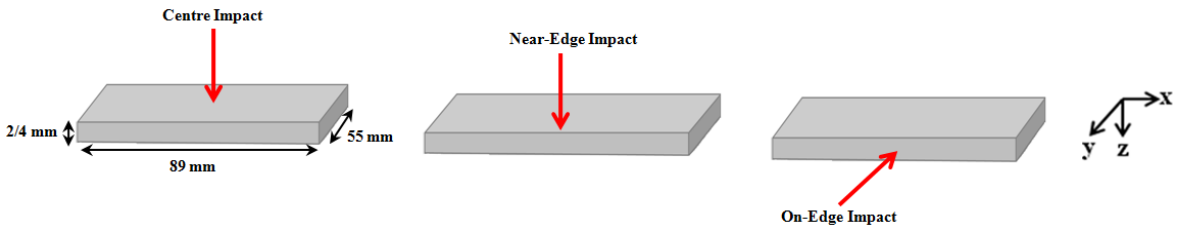

Figure 3.1 Edge impact conditions (x is 0^0 fibre direction)

3.2.2 Impact Test Method

The impact tests were carried out using a CEATIS Dartvis 6790 drop weight impact testing machine with computer data acquisition unit DAS4000, which has the capability of a 1MHz sampling rate. The piezoelectric dart striker provides force measurement with respect to time. The velocity of impact is measured using a triggered photocell and the control includes a pneumatic anti-bounce mechanism. The velocity, displacement and energy are calculated by the software programme installed in the impact machine. The drop weight impact machine is shown in the figure 3.2. Drop weight impact machine allows the free fall of the impactor on to the composite laminate. At the point of contact the gravitational potential energy of the impactor is converted into kinetic energy. So it can be written as during point of contact

Kinetic Energy = Gravitational Potential Energy

or $$\frac{1}{2}mv^2 = mgh \qquad (3.1)$$

or $$\frac{1}{2}v^2 = gh \qquad (3.2)$$

or $$v = \sqrt{2gh} \qquad (3.3)$$

Where m = mass of the impactor

v = velocity of the impactor
h = height of the impactor from the composite specimen
g = gravity

From the equation (3.1) – (3.3), we can find the incident velocity v if we know mass m and height h (see table 3.1). The tests were carried out for 5 different incident energy levels: 1J, 2J, 3J, 4J and 5J. The impactor mass was constant, 0.74 kg, with variable height. Therefore the impact velocity is controlled to produce the correct incident energy. The conditions used are shown in table 3.1

Incident Energy (J)	Initial Height (m)	Incident Velocity (m/s)	Impactor Weight (kg)
1	0.138	1.64	0.74
2	0.276	2.32	0.74
3	0.413	2.85	0.74
4	0.551	3.29	0.74
5	0.689	3.68	0.74

Table 3.1 Details of low velocity impact under different incident energies

Low velocity impact testing machine details are given as follows:

1. Striker load cell range : 24 kN
2. Piezoelectric dart striker provides force measurement with respect to time.
3. Measure of velocity by trigger photocell.
4. Pneumatic anti-rebounce mechanism as it passes the photocell
5. It can measure:
   - Maximum impact velocity up to 3.7m/s
   - Maximum energy up to 30J
   - Maximum height up to 700mm

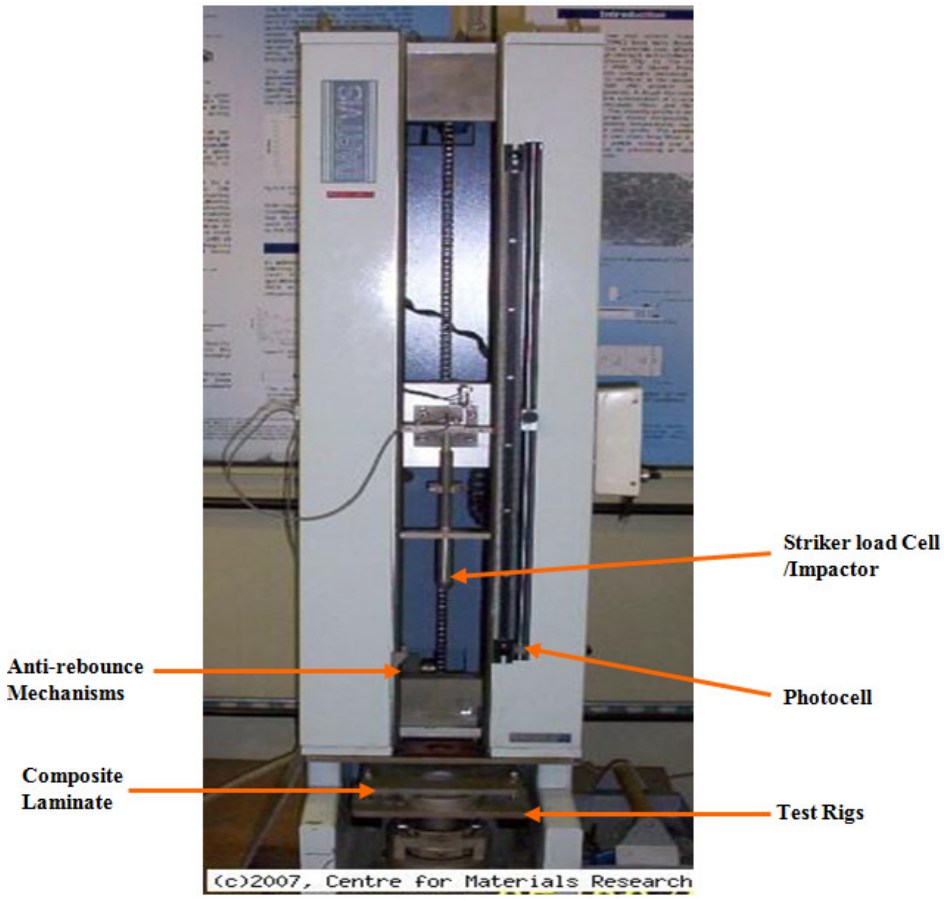

Figure 3.2 Low velocity impact testing machine

3.2.3 Rig Design for Edge Impact

The drop weight machine is generally used for face or central impact rather than on-edge impact. So the aim was to find the optimum structural configuration for edge impact under known loading and boundary conditions.

3.2.3.1 Issues in design

Several issues were considered during the prototype design of the edge impact experiments. Rigs were designed according to maximum loading conditions of the impact machine. The following issues were identified in the design process.

- Control of the multiple impacting of the striker due to increase of height of the clamped rig fixture for the on-edge impact.
- Shape and contact of the striker with the laminate for near-edge impact.
- Type of impactor shape and its contact with laminate for on-edge impact.
- Effect of boundary conditions that is the constraints of the laminate during edge impact.
- Effect of damage width during compression and tension after impact.

3.2.3.2 Design for Near-edge Impact

Figure 3.3 shows (a) the top view (b) side view and the design for near-edge impact. The laminate is fully constrained around a half-circle window of radius 20 mm.

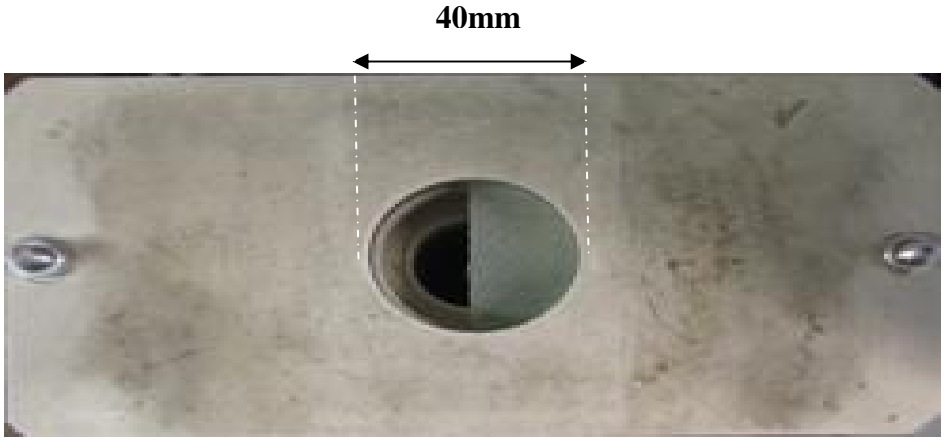

(a)

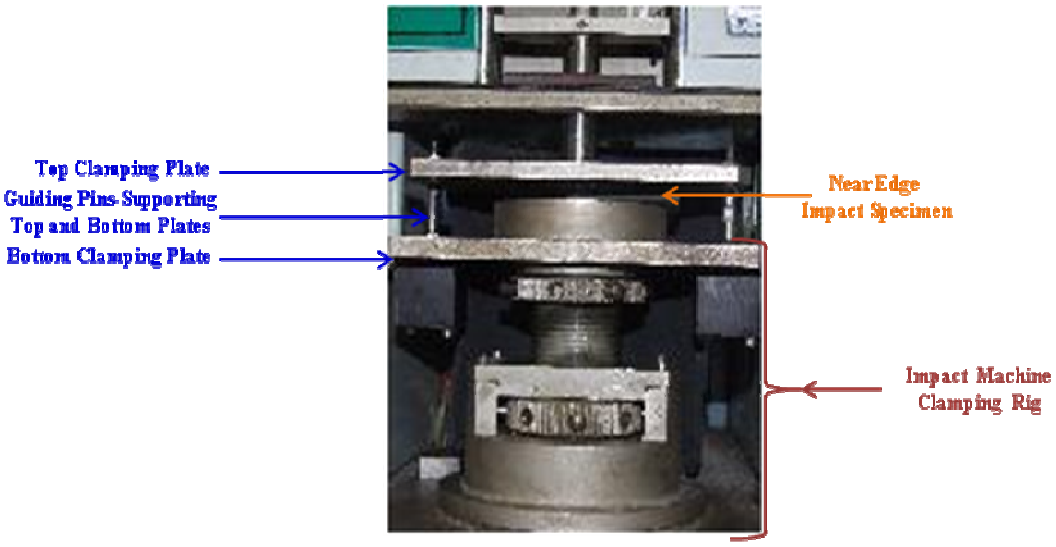

(b)

Figure 3.3 Rig design for near-edge impact a) Top view b) Side view

The 20 mm diameter tup arises from the original design of this rig for central impact in a 40 mm diameter window. Rigs are designed such that both thin and thick laminates can be adjusted.

3.2.3.3 Design for On-edge Impact

Figure 3.4 shows the design of a rig for an on-edge impact. The fixture was designed so that it can be clamped on the impact machine. The screws were tightened with a torque wrench to a set load.

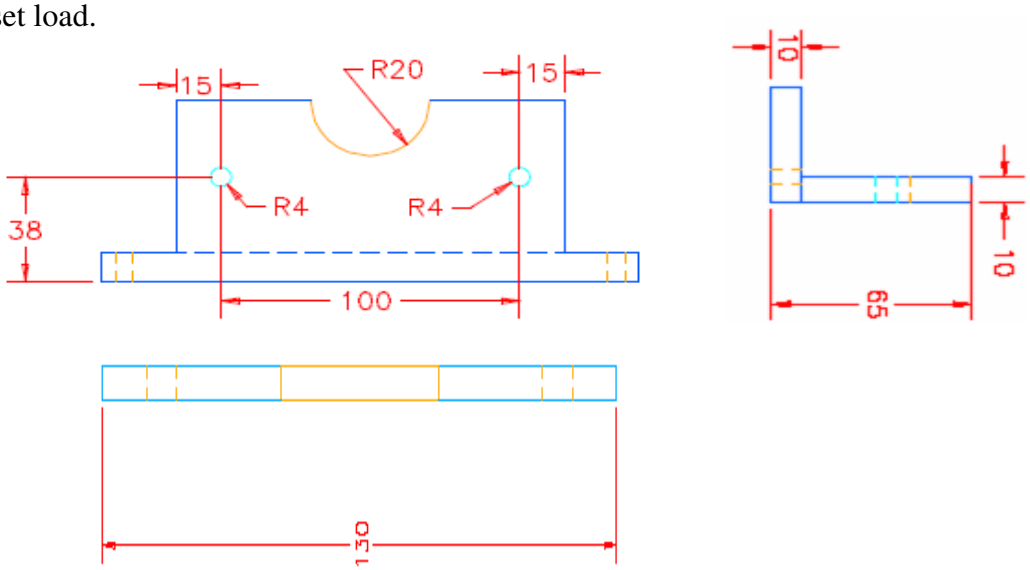

Figure 3.4 Balanced boundary condition rig design for on-edge impact

The impact machine will work when the minimum pressure is above 140 kPa and does not exceed the maximum pressure of 690 kPa. By default, the impact machine is set with air pressure of 580 kPa and all the experimental tests are performed under this air pressure. Figure 3.5 shows the implementation of the rig design.

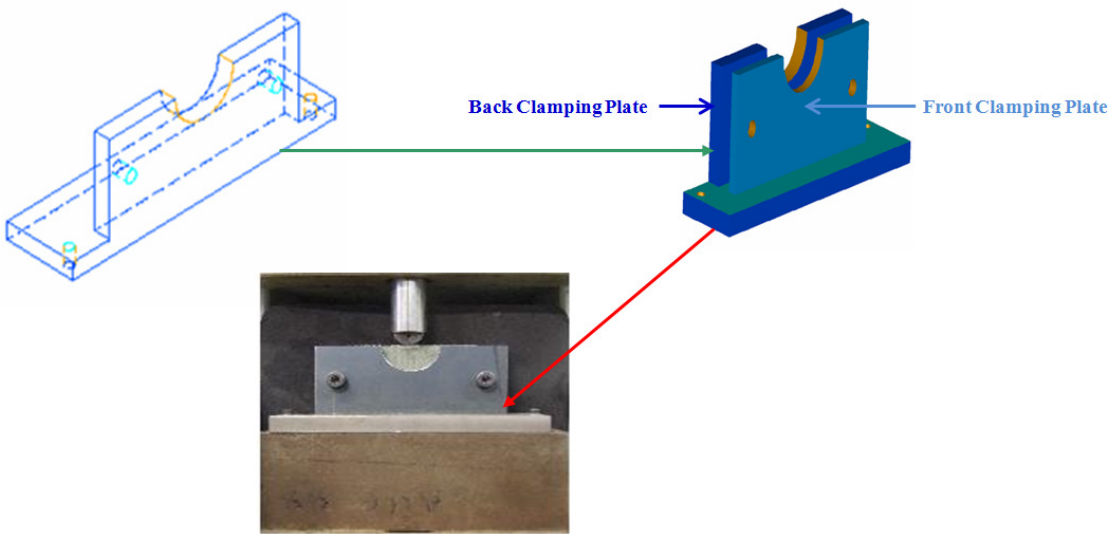

Figure 3.5 Implementation of rig design for on-edge impact

The design for both on-edge and near-edge impact makes the laminate fully constrained around a half-circle window of radius 20 mm. This rig was developed from the original central impact rig to reproduce similar boundary conditions. Clamping pressure using the nuts (see figure 3.5) was applied until the laminate was fully constrained without damage, using a torque wrench.

3.2.3.4 Impactor Shapes for Edge Impact

Figure 3.6 (a) show the impactor shape for centre and near-edge impact while figure 3.6 (b) show the impactor shape for an on-edge impact. The shape of the impactor for on-edge impact was chosen to ensure even impact at the edge of the laminate. The diameters of both impactors are 20 mm. The impactor diameter was required for this Instron impact machine. For the near-edge and on-edge impact the same impactor diameter was used as for the central impact. The length of the near-edge impactor is 15 mm. The impact experiments were performed with same impactor diameter; this was done to compare the different types of edge impact under similar parameters and conditions.

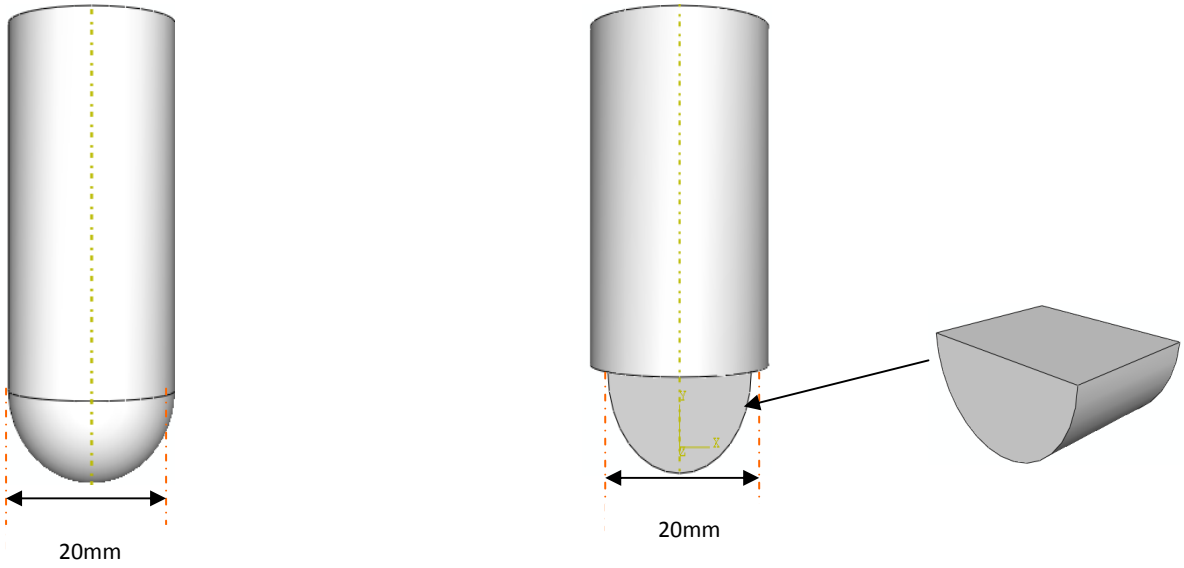

(a) **(b)**

Figure 3.6 Impactor shapes for edge impact a) Centre and near-edge impactor b) On-edge impactor

3.2.4 Material and Geometrical Parameters

3.2.4.1 Ply Architecture

Lay-Up: Two laminate thicknesses have been used that is 2mm and 4mm. Each ply is approximately 0.25mm thick. The lay-up was $[0^0/+45^0/90^0/-45^0]_s$ for the 2mm thickness and $[0^0/+45^0/90^0/-45^0]_{2s}$ for the 4 mm thickness.

3.2.4.2 Manufacturing Method

Appendix C provides the manufacturing and technical details of the composite laminate used. Multiaxial E-Glass Fabric is used for the project. Multiaxial fabric is made up of four layers of fibres stitched together with a light thread and the epoxy matrix is infused into the fibres.

3.2.4.3 Specimen Geometry

After the composite has been manufactured, the next stage is cutting. All test specimens were cut from the laminates using a cutting machine with a diamond saw. During the cutting of specimen to the desired size industrial oil lubricant is added in order to reduce frictional heat and ensure smooth cutting.

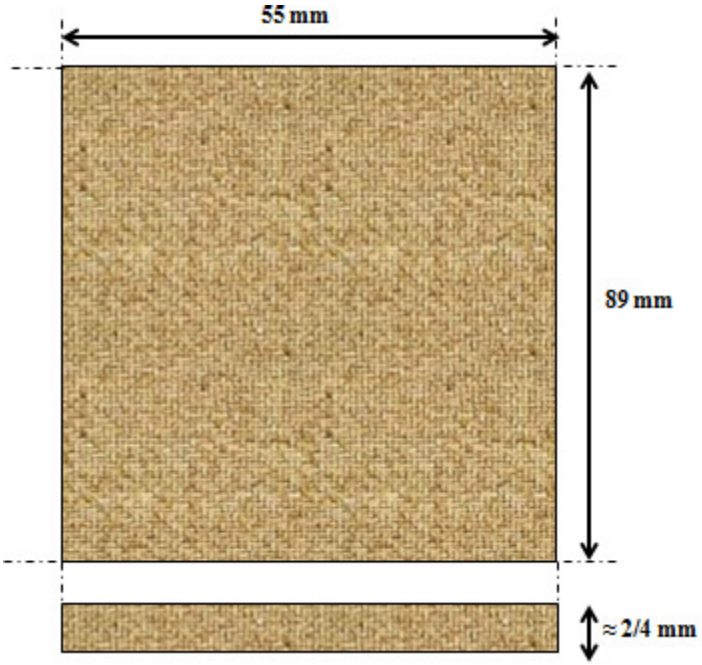

Figure 3.7 Dimensions of test specimen

The dimensions of the specimens were cut such that fixture could accommodate and perform impact tests and compression tests after impact as per the design developed by Prichard and Hogg (1992) at Queen Mary, University of London. The dimensions of the cut specimen are shown in figure 3.7.

3.3 Results and discussion

In this section we will discuss the experimental results obtained from the drop weight impact with respect to various parameters.

3.3.1 Reproducibility

All tests were carried out at ambient temperature, between 22 and 24 ^{0}C. An important aspect of experimental testing is that the results are repeatable. Three tests were carried out for each condition and excellent reproducibility was obtained. An example of this reproducibility is shown in figure 3.8 representing the force/time results for 3-J on-edge impact to a 4-mm laminate.

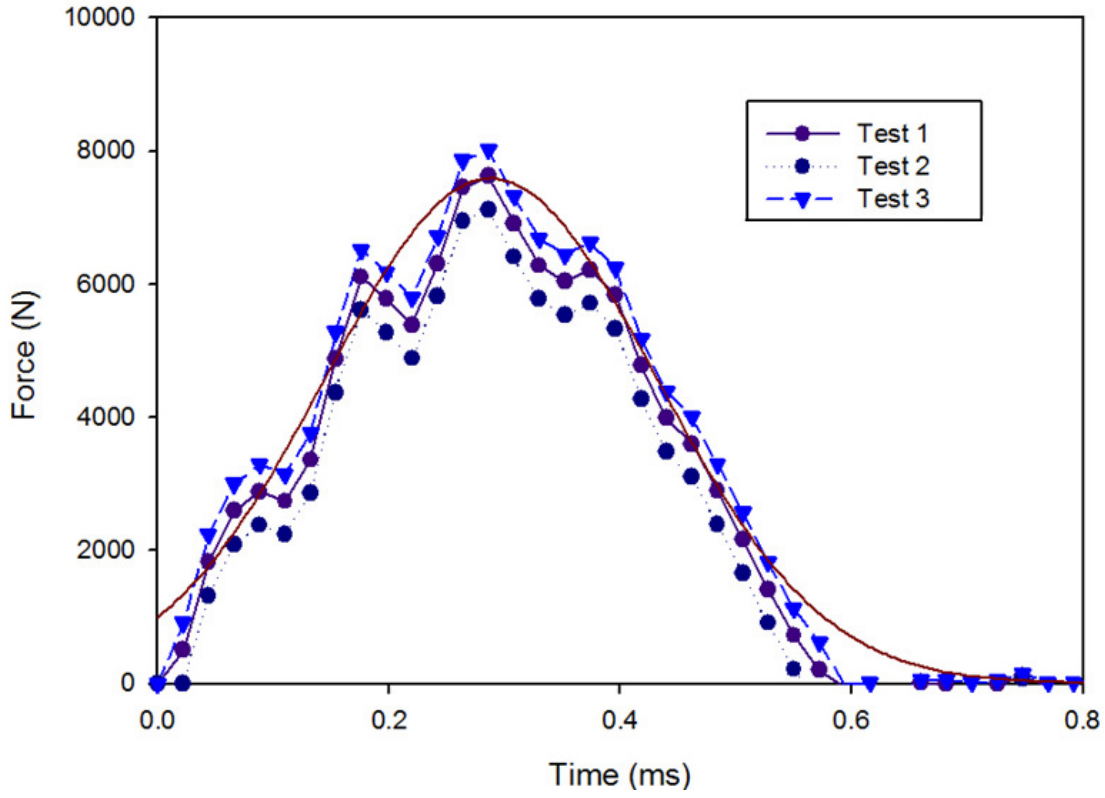

Figure 3.8 Comparison of experimental results for identical conditions: Force/time traces for 3-J on-edge impact to 4-mm laminate

3.3.2 Force-Time Results

3.3.2.1 On-Edge Impact

Figure 3.9 shows the force-time graphs during on-edge impact of composite laminates. These curves for the thin laminates show very high level of oscillations indicating progressive impact damage. Regular discontinuities in all the 1J results were found which are believed to arise from vibration of the specimen. The force/time results for 1J impact energy may be invalid and not included in figure 3.9; the results are valid for 2-5J impacted specimens only. The maximum impact force for these energy levels lies between 4000 to 8000 N. At approximately 0.05 to 0.1 ms initial contact occurs and the damage has initiated.

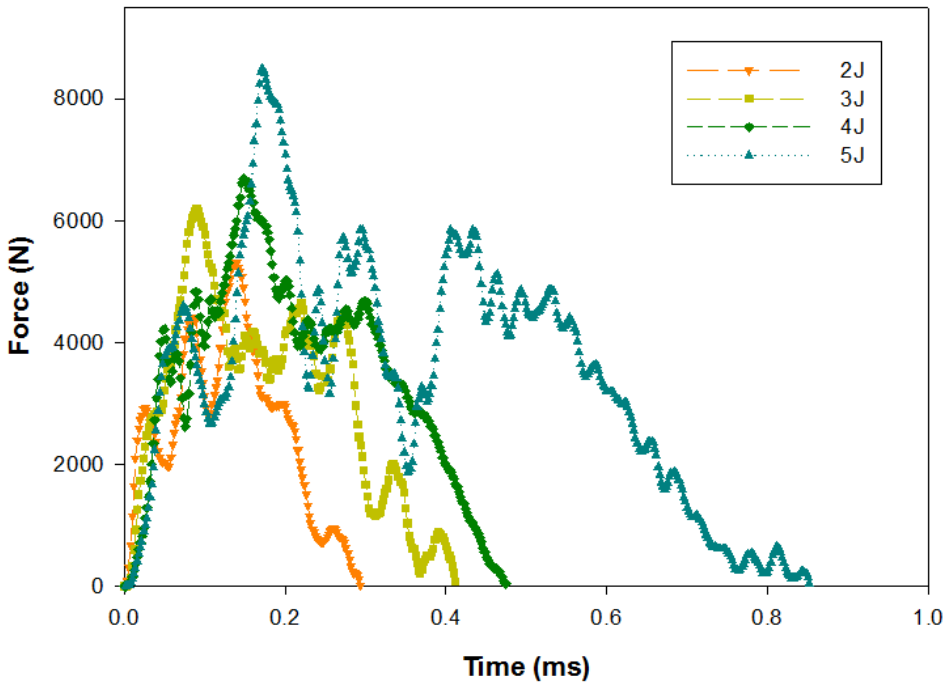

Figure 3.9 Force-time curves: On-edge impact (thin laminates)

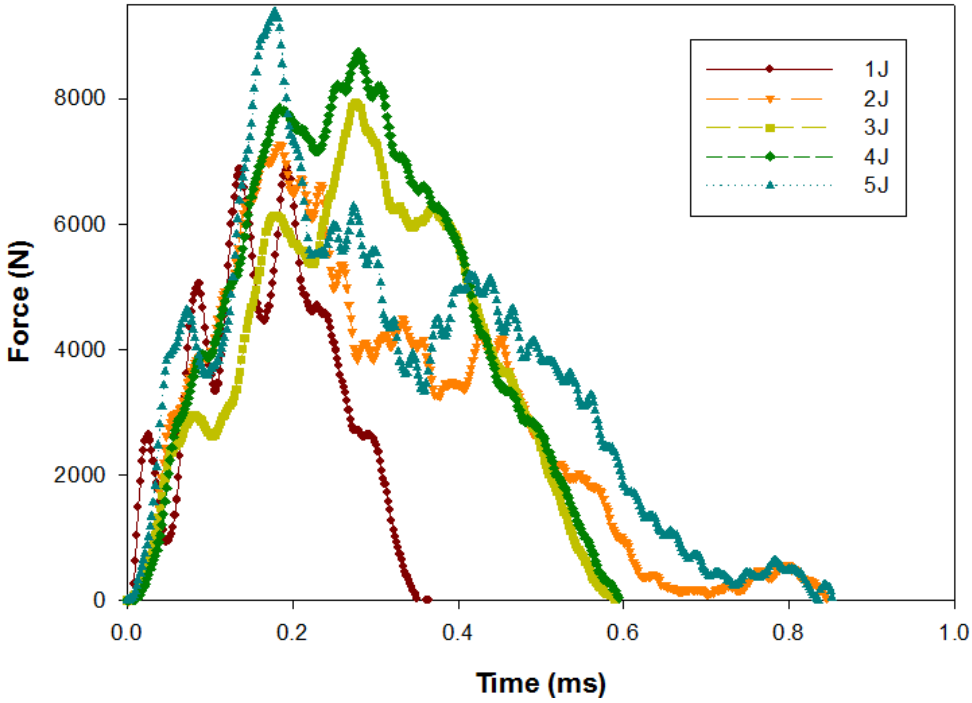

Figure 3.10 Force-time curves: On-edge impact (thick laminates)

The impact force increases rapidly after initial contact and there is a region of oscillations that are of high frequency between the times at around 0.1 to 0.7 ms during on-edge impact at all the energy levels. The time duration of the whole on-edge impact phenomenon for the composite laminate was around 0.8 ms. Thicker laminates show higher impact force indicating higher stiffness as can be seen from figure 3.10. The maximum impact force at

various energy levels lies between 7000 to 9000 N. The discontinuities in the 1J results are fairly regular, but the first discontinuity arises at a similar load level to other results; the validity of the 1J results is questionable. At approximately 0.1 ms initial contact occurs and the damage has initiated. After damage initiation the impact force increases with oscillations in the force-time graphs similar to those in thin laminates. The time duration of the whole on-edge impact phenomenon for the composite laminate was around 0.8 ms. However thicker laminate showed lower oscillations than the thin laminates during on-edge impact which may indicate less damage or less vibrations. The small vibrations visible in the curves may arise from out-of-plane vibrations. These vibrations were observed in the finite element simulations (see chapter 6).

3.3.2.2 Near-edge Impact

Figure 3.11 shows the force-time graph during near-edge impact of composite laminates. These curves for the thin laminates are very smooth with few oscillations indicating lower growth of damage. The maximum impact force at various energy levels lies between 1000 to 2500 N. Initial contact is indicated between 0.1 to 0.2 ms. The impact force increases constantly after about 0.5 ms and the force-time graph is smooth indicating lower growth of impact damage. The time duration of the whole edge impact phenomenon for the composite laminate was around 2.5 ms. After reaching the peak value of impact force there is an constant drop of the impact force value from time 1.2 ms to about 2.5 ms for all energy levels. Figure 3.12 shows the force-time curves for the thick laminates which are smooth curves but with some oscillations indicating the growth of some delaminations. The maximum impact force at various energy levels lies between 1500 to 3500 N. Initial contact is indication between 0.02 to 0.1 ms. The impact force increases rapidly after initial contact and reaches maximum at approximately 0.6 ms for all energy levels. The time duration of the whole near-edge impact phenomenon for the composite laminate was around 1.7 ms. After reaching the peak value of impact force there is a constant drop of the impact force value from time between 0.6 ms to 1.6 ms for all energy levels.

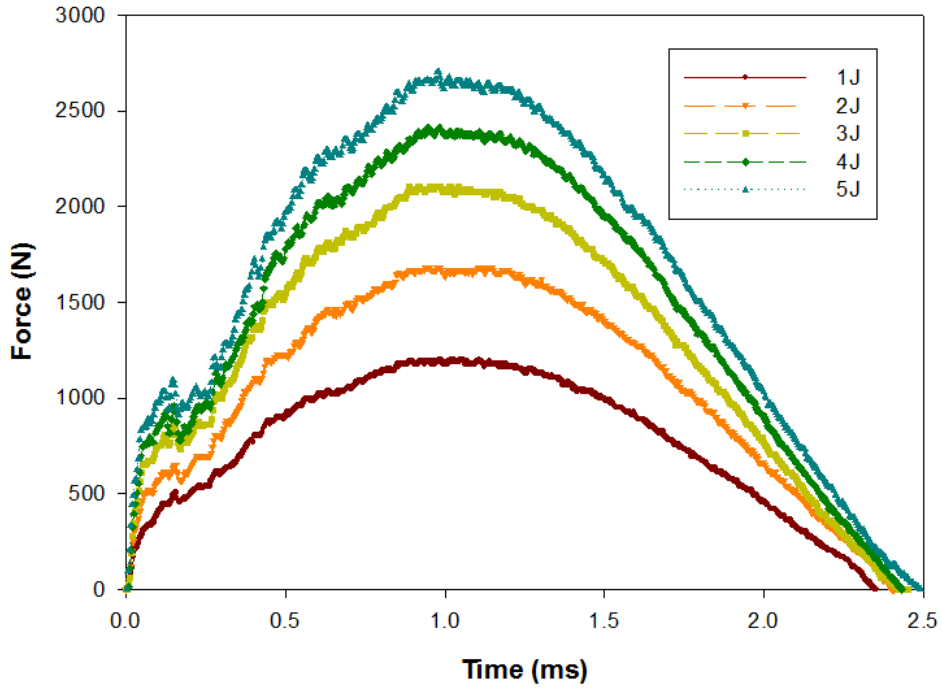

Figure 3.11 Force-time curves: Near-edge impact (thin laminates)

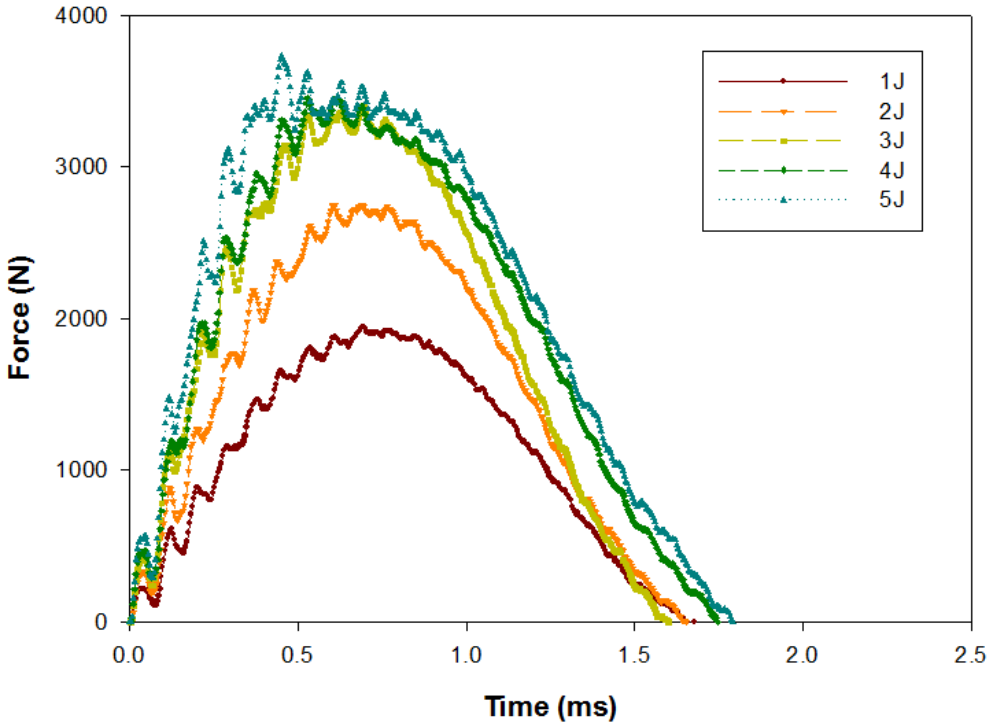

Figure 3.12 Force-time curves: Near-edge impact (thick laminates)

3.3.3 Edge Impact Summary Results

3.3.3.1 Damage Initiation

During impact the most important parameter for detecting the damage in the laminate is the damage initiation. Damage initiation can be defined as the first data point where the force values drops and recovers for further damage propagation. The results for on-edge impact are shown in table 3.2 which provides a summary of the damage initiation approximate values for the on-edge impact for the two thicknesses. The results are plotted in figure 3.13 (a). Taking the scatter into account, figure 3.13 (a) indicates that the damage initiation force is a constant value between 1 or 2 and 3 J for both thicknesses. Above 3J the value increases with higher values for the thinner laminate.

	OE-Damage Initiation Force (N)					
	Specimens	F_{DI}-1J	F_{DI}-2J	F_{DI}-3J	F_{DI}-4J	F_{DI}-5J
2mm	Specimen 1		3270	3008	4216	6120
	Specimen 2		2916	2856	4272	4596
	Specimen 3		4100	3734	4870	6790
4mm	Specimen 1	3096	3450	2774	2752	5054
	Specimen 2	2628	2988	2952	3912	4620
	Specimen 3	3946	4380	3130	3260	4396

Table 3.2 On-edge damage initiation force data for thin and thick laminates

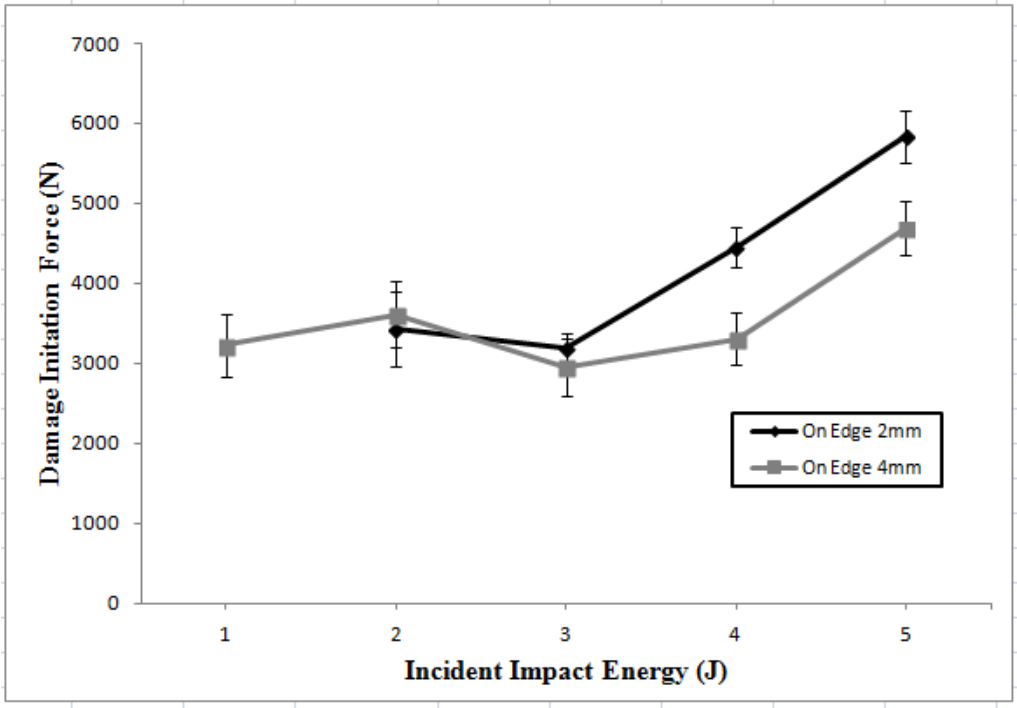

Figure 3.13 (a) On-edge impact damage initiation force vs incident impact energy

The results for the near-edge impact are shown in table 3.3 which provides a summary of the damage initiation values for the two thicknesses; note that there is uncertainty regarding the validity of the 1J result for the thin laminate. The results are plotted in figure 3.13 (b) which shows near linear increase in values over the whole range of impact energies, with thin laminates having higher values than thick laminates.

	NE-Damage Initiation Force (N)					
	Specimens	**F_{DI}-1J**	**F_{DI}-2J**	**F_{DI}-3J**	**F_{DI}-4J**	**F_{DI}-5J**
2mm	**Specimen 1**	**428**	**464**	**594**	**680**	**766**
	Specimen 2	**504**	**516**	**660**	**756**	**852**
	Specimen 3	**606**	**588**	**752**	**848**	**954**
4mm	**Specimen 1**	**184**	**290**	**386**	**422**	**508**
	Specimen 2	**216**	**336**	**432**	**468**	**564**
	Specimen 3	**266**	**378**	**466**	**496**	**610**

Table 3.3 Near-edge damage initiation force data for thin and thick laminates

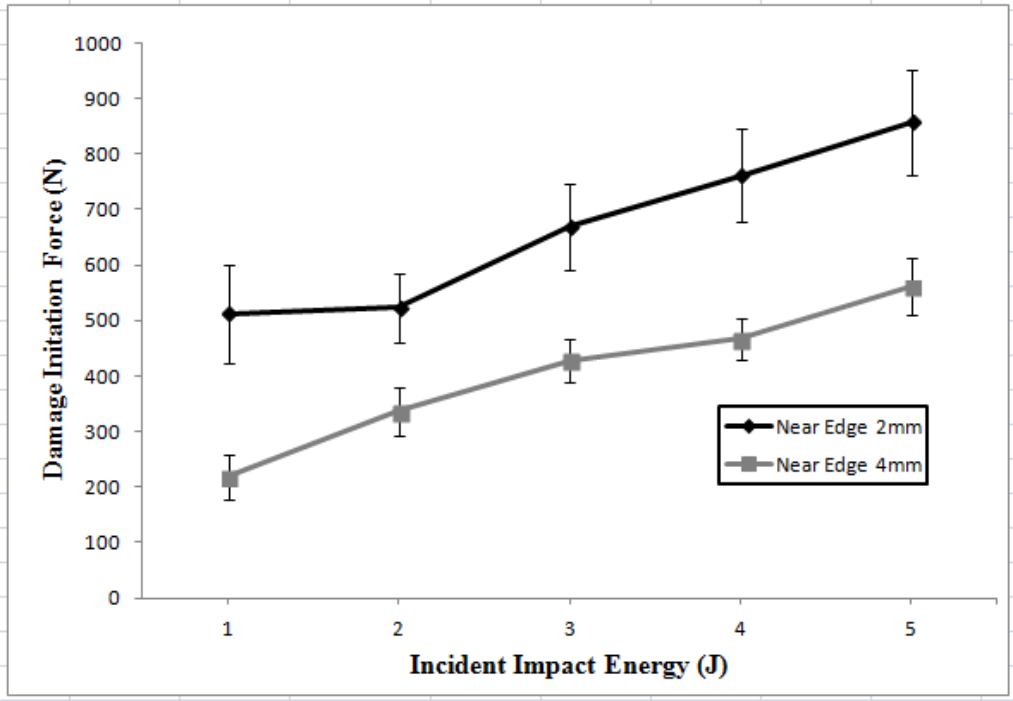

Figure 3.13 (b) Near-edge impact damage initiation force vs impact energy

3.3.3.2 Peak Force

The peak force is the maximum contact force between the impactor and the composite in an impact event which is important in analysing the severity of the edge impact damage in the composite laminate. Peak force is captured from the maximum value of data point in force-time curves for different impact energy levels and thicknesses. The peak force measurements are important in providing damage information about the different types of impact.

	OE-Peak Force					
	Specimens	F_{Max}-1J	F_{Max}-2J	F_{Max}-3J	F_{Max}-4J	F_{Max}-5J
2mm	Specimen 1	4094	4872	5858	6686	8056
	Specimen 2	4452	5316	6204	7056	8484
	Specimen 3	4830	5854	6680	7470	8974
4mm	Specimen 1	6574	6960	7466	8386	8952
	Specimen 2	6888	7272	7944	8724	9372
	Specimen 3	7170	7736	8420	9222	9784

Table 3.4 On-edge impact peak force data for thin and thick laminates

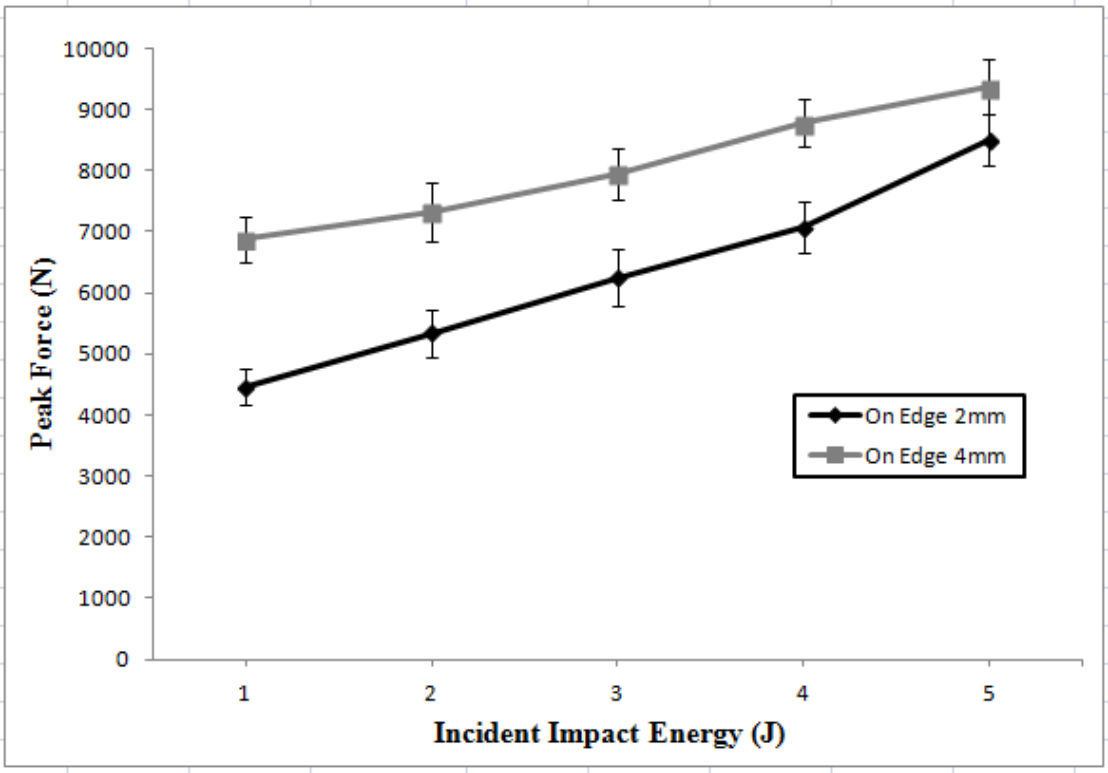

Figure 3.14 Peak force vs incident impact energy-On-edge impact

Table 3.4 show the data for the on-edge impact. The result for 1J edge impact is included since this result is believed to be valid. The peak force measured for all edge impact tests is

plotted as a function of incident impact energy in figure 3.14. Taking into account the scatter bands, the rate of increase of peak force with incident energy appears the same for both thicknesses of laminate. There may be a trend towards the same values for the two thicknesses at higher impact energies, but this trend cannot be confirmed from these results.

	NE-Peak Force					
	Specimens	F_{Max}-1J	F_{Max}-2J	F_{Max}-3J	F_{Max}-4J	F_{Max}-5J
2mm	Specimen 1	1020	1512	1890	2170	2430
	Specimen 2	1200	1680	2100	2412	2700
	Specimen 3	1442	1914	2394	2704	3026
4mm	Specimen 1	1750	2472	3134	3214	3358
	Specimen 2	1944	2748	3408	3456	3732
	Specimen 3	2216	3028	3598	3668	4042

Table 3.5 Near-edge impact peak force data for thin and thick laminates

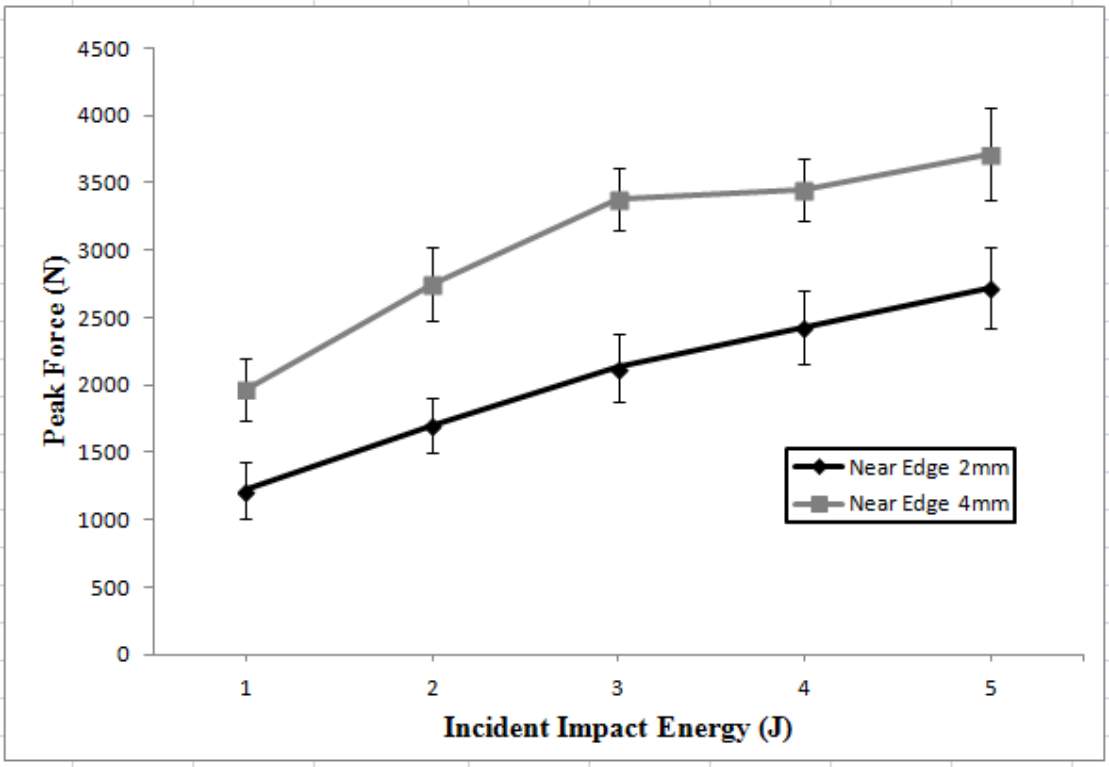

Figure 3.15 Peak force vs incident impact energy-Near-edge impact

Table 3.5 shows the peak force data for the near-edge impact. The peak force measurements for the thin and thick laminates for near-edge impact are compared in figure 3.15. Taking into account the scatter bands, the rate of increase in value of peak force is the same for the two thicknesses.

3.3.3.3 Discussion: Force-Time Results

During the low velocity impact, the initial contact between the impactor and composite laminate transfers the impactor incident energy to the composite laminate and this transferred energy is then used for the damage initiation and its progression. The impact response of laminated plates is commonly described in terms of force-time curve. The shape of the force-time curves usually indicates the damage initiation and its propagation. Contact force histories as a function of time for the on and near-edge impacted specimens are compared in figure 3.16 (a)-(b) impact. The contact force rise is much higher for on-edge impact than for near-edge impact.

We will now discuss the results of on-edge impacted specimens at 5J. From figure 3.16 the force-time history provides important information concerning damage initiation and growth. Point P_1 in on-edge impact indicates the limit of elastic response at this point the load reaches the first peak value and damage has been initiated. At P_1 point three different types of stress waves are generated and propagated i.e., pressure wave (P-wave), shear wave (S-wave) and Rayleigh or surface wave (R-wave). There is a first sudden drop in the force, indicating the initialisation of delamination and loss of stiffness from unstable damage development (Davies et al 2000). Between points P_1 and P_2 shear waves are more dominant and oscillations can be seen indicating that the laminate suffered multiple delaminations and reduction in stiffness of the composite laminate (Shyr et al; Schoeppner et al 2000). The S-wave is converted into P-wave just before reaching point P_2. The P-wave is more dominant at this point and has reached the edges of the boundary. Delamination areas are created at point P_2 for both thin and thick laminates. After reaching peak force P_2, there is a sudden drop in the impact force from point P_2 to P_3. At this stage the pressure wave is reflected from the constrained boundary edges and the damage is in the propagation stage. The delamination is expanding. At point P_4 reflected P-wave coincides with the existing surface waves and shear waves and thus more energy is absorbed, creating the damage. At point P_4 the velocity of the impactor reduces abruptly and approaches towards zero. Thus at P_4 the energy absorbed by the laminate reaches its maximum.

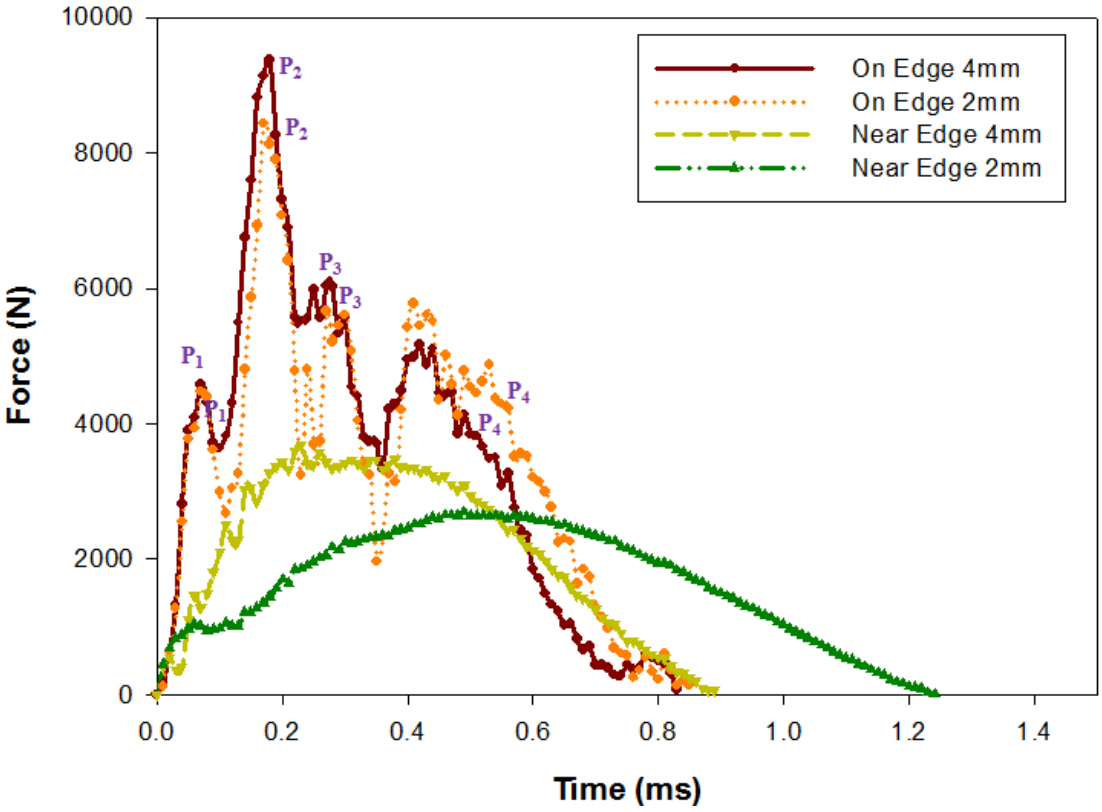

Figure 3.16 Force/time comparison of near-edge and on-edge 5J impact

Figure 3.16 shows that the impact response of the near-edge impacted laminate is almost sinusoidal that is the force–time curves exhibits a relatively smooth and symmetrical appearance without the evidence of sharp peaks for both thin and thick laminates. This lower peak force gives a clear indication of lower damage in the plane of the laminate as compared to on-edge impact. For near-edge impact the force-time curves for thick laminate contain some small oscillations at higher energy levels. The minor peaks in the curve are primarily due to elastic wave responses and vibration of the specimen (Schoeppner et al 2000). The impact duration for near-edge impact is much higher than on the edge impact. This arises since the bending stiffness of the laminate is much lower for near-edge impact. The similarity in response from the two thicknesses for on-edge impact, at this higher impact energy is indicated, but cannot be confirmed.

3.3.4 Force-Displacement Results

3.3.4.1 On-Edge Impact

Force-displacement curves are useful for analysing energy absorbed by the displacement of the composite laminate during impact. During the impact event, the impact force and displacements are measured as soon as the impactor comes in contact with the composite specimen.

Figure 3.17 shows the force-displacement curves during on-edge impact of composite thin laminates. Note that the 1J results are omitted due to the vibrations observed. The force-displacement curves for on-edge impact show very high level of oscillations indicating vibration of the specimen. These oscillations are of high frequency between displacements in the range around 0.05 to 0.25 mm for all the energy levels. The sharp drop in the peak force represents the damage progression and loss of stiffness of the composite laminate. Peak drop represents damage is accumulated and the energy is absorbed through impact.

In thick laminates after damage initiation the impact force increases with oscillations in the force-time curves similar to those in thin laminates but thicker laminate showed lower oscillations than the thin laminates during on-edge impact because they are stiffer. The displacement for thin and thick laminate lies in the range 0.14 to 0.24 mm and 0.38 to 0.60 mm respectively (see figure 3.18). It is seen that for both thin and thick laminates force-displacement curves have lots of high frequency vibrations during the initial elastic phase while less vibration is seen during the inelastic recovery phase.

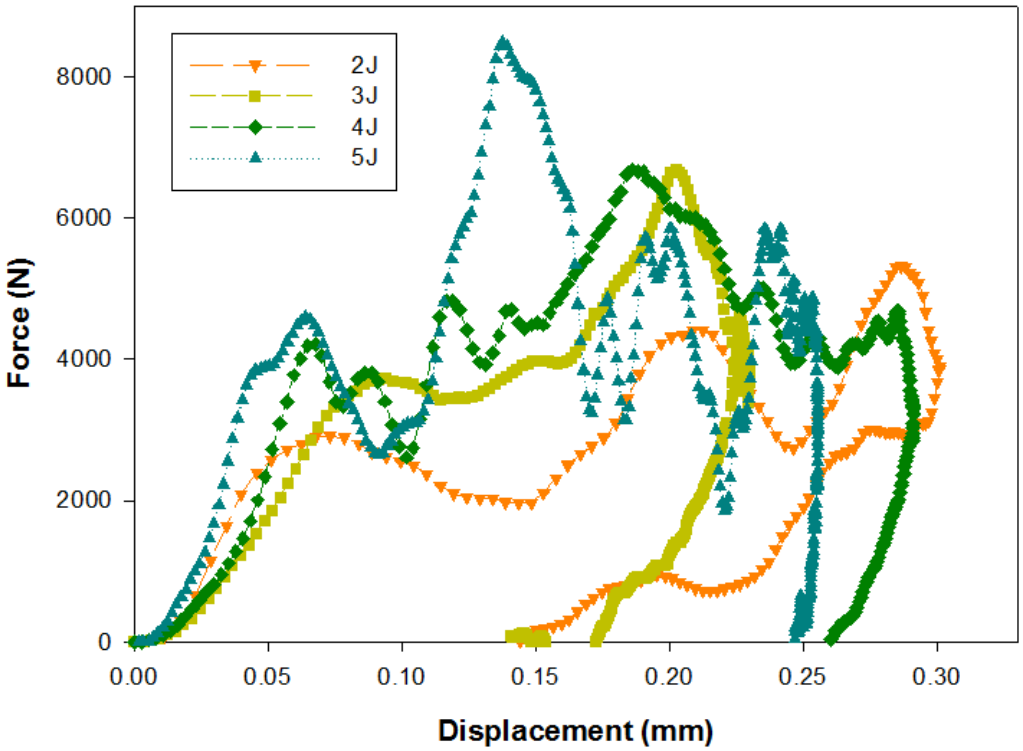

Figure 3.17 Force-displacement curves for on-edge impact (thin laminates)

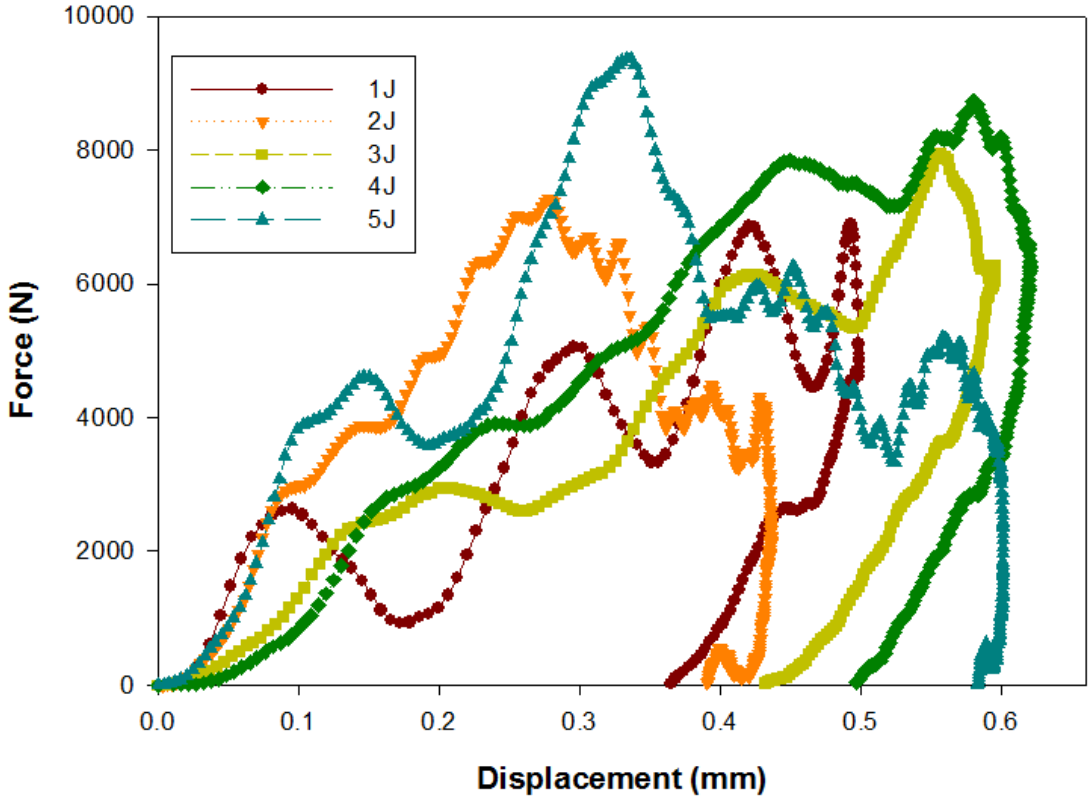

Figure 3.18 Force-displacement curves for on-edge impact (thick laminates)

3.3.4.2 Near-edge Impact

Figure 3.19 shows the force-displacement curve during near-edge impact of thin composite laminates. During near-edge impact, force-displacement curves are relatively smooth and monotonic as compared to on-edge impact which showed large vibrations and fluctuations. Minor peaks are developed during the elastic phase of the force-displacement curve while the inelastic recovery phase is much smoother. These trends can be seen at all the energy levels.

The maximum impact force lies between 1000 and 2500 N. Damage initiation for near-edge impact starts from displacement at 0.1 to 0.5 mm. The impact force increases constantly after displacement of 0.5 mm. The maximum displacement lies in the range of 0.5 to 2.8 mm. After reaching the peak value of impact force there is a monotonic drop of the impact force value for all energy levels at approximately the same rate.

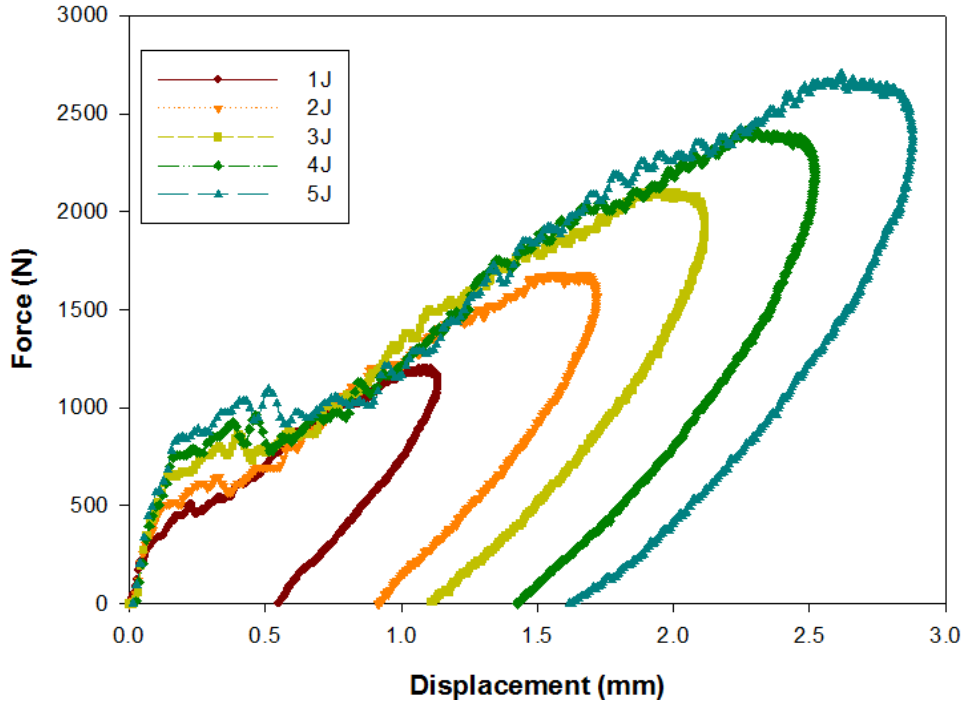

Figure 3.19 Force-displacement curves for near-edge impact (thin laminates)

The results for the thick laminates show similar trends (see figure 3.20). However the elastic phase of the curves shows show more marked minor peaks. These peaks probably indicate the growth of delaminations since peaks arising from vibrations are expected to be less prominent for the thicker laminates. The oscillations are present up to the peak force. The recovery phase is much smoother with very little oscillation. The maximum impact force lies between 2000 and 3500 N. After reaching the peak value of impact force there is a monotonic

drop of the impact force value for all energy levels, at similar rates. The displacement at various energy levels lies in the range between 0.4 to 1.4 mm.

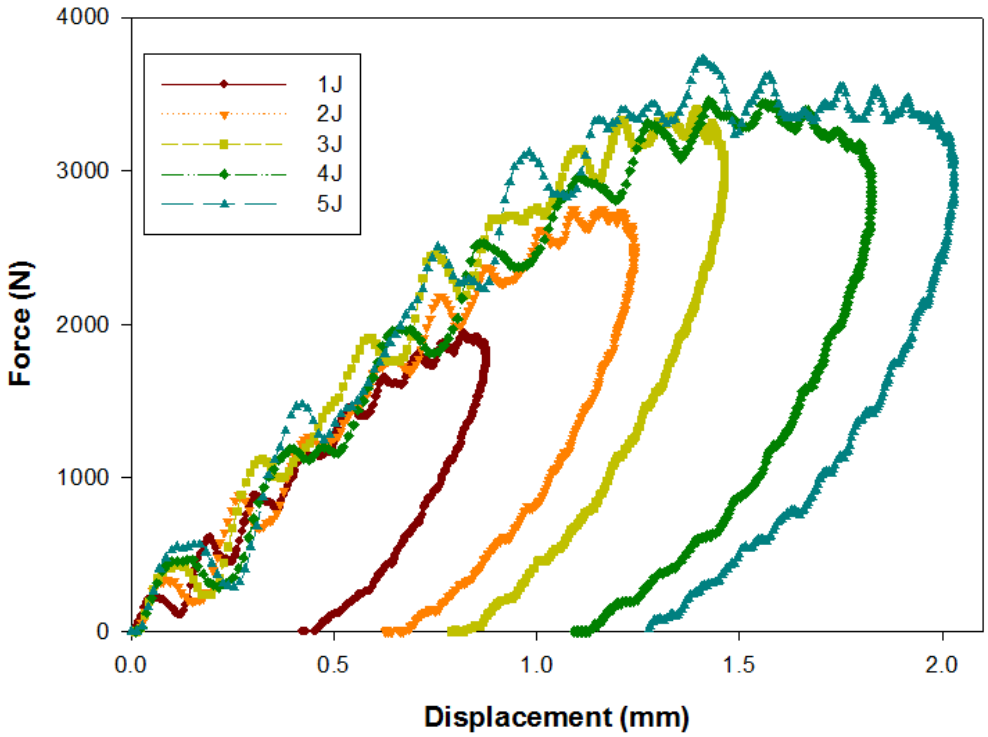

Figure 3.20 Force-displacement curves for near-edge impact (thick laminates)

The force-displacement curves provide useful information regarding energy absorbed by the laminate during impact. Thus elastic phase of the curve indicates that the part of this energy is mostly used in deformation of the laminate while in inelastic or the recovery phase the remaining energy is absorbed as damage.

3.3.5 Comparison of Near and On-edge Impact with Centre Impact

In this section near-edge and on-edge impact is compared with centre impact. As discussed in the literature review extensive research had been carried out on centre impact and so this comparison of near and on-edge impact with centre impact will provide useful information how the composite laminates behave in different types of impact conditions. Two results from two impact incident energies 2J and 4J are discussed.

On-edge, near-edge impact are compared with centre impact with respect to two thicknesses 2 mm and 4 mm. Figure 3.21 (a) shows force-time curve for 2J impact. We will first consider the case of thin laminate (2mm). It is clear from the curves that the maximum impact force for the centre impact is very similar to near-edge impact but much smaller then on-edge

impact. On-edge impact has the highest impact force which is almost three times the impact force value as compared to near and centre impact. However the impact duration for the centre impact is higher than that for near-edge impact, and far greater than in the case of on-edge impact.

Figure 3.21 (b) shows force-time curves for 4J impact. Similar trends are seen in force-time curve as the incident energy is increased from 2J to 4J for on-edge, near-edge and centre impact.

Thickness has a greater effect on the impact force and impact duration for the centre and near-edge impacts compared to on-edge impact. The impact duration for centre and near-edge impacts decreases as we increase the thickness from 2mm to 4mm since the thinner laminate is more flexible; the maximum impact force is approximately doubled for the thicker laminate. On-edge impact shows some reduction in the impact duration and increased impact force with increasing thickness.

For near-edge and centre impact, the different mechanisms of damage growth can be compared for the different impact locations. Centre impact has higher area of potential damage around the impact point. At lower impact energies, the damage is greater for the centre impact. However, near-edge impact causes more delaminations, which become unstable at higher impact energy levels. Thus at higher impact energy, damage for near-edge impact may be greater than for centre impact.

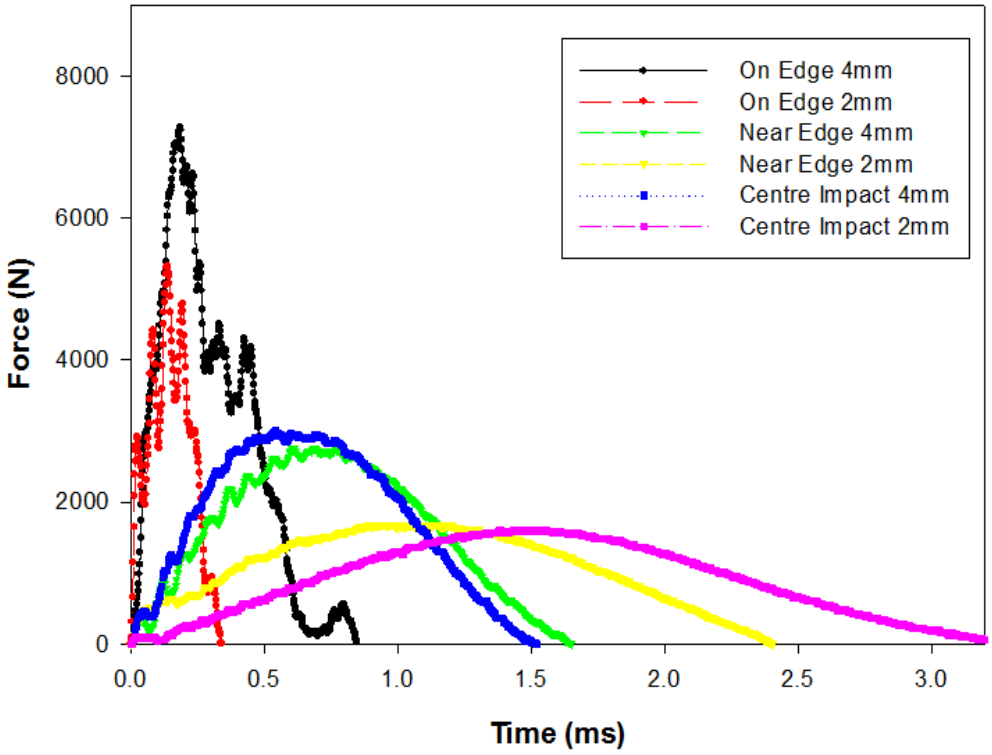

(a)

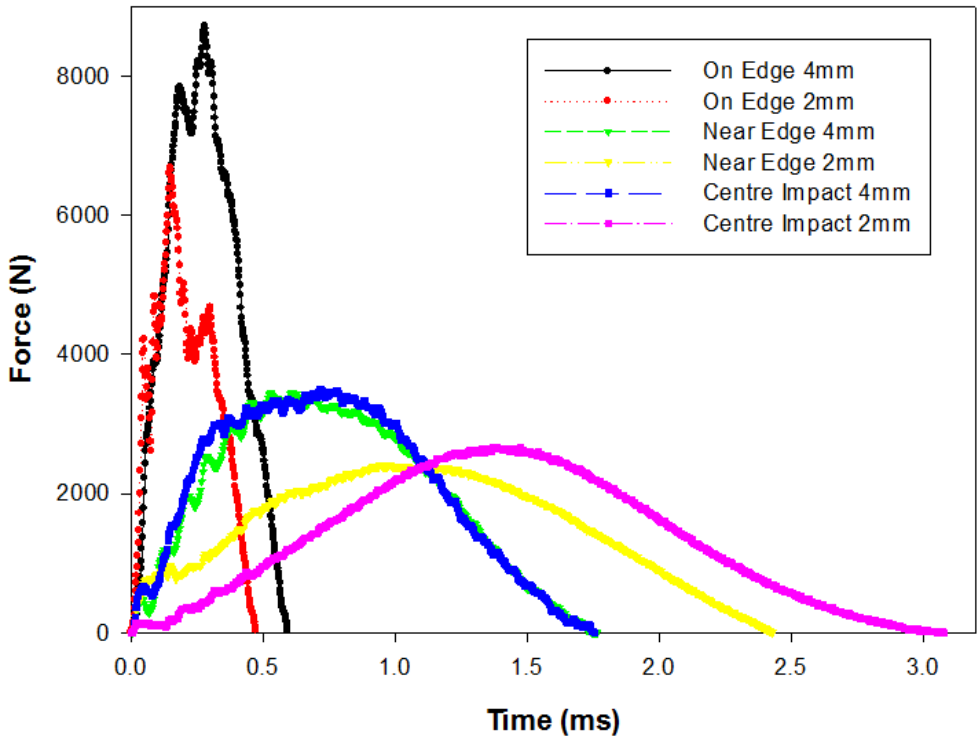

(b)

Figure 3.21 Comparison of force/time curves for on-edge, near-edge and centre impacts a) 2J b) 4J

3.3.6 Effect of Various parameters with respect to thickness

Composites absorb large amount of energy where some part of the energy is dissipated in the form of friction heat and other part of the energy is used in developing the damage resulting in fracture areas and reduced strength and stiffness of the laminate. The magnitude of the impact forces and displacement are directly proportional to the impact energy and increase in energy absorption can be linked with increase in damage accumulation. The absorbed energy is calculated by integrating the force displacement curve. Energy dissipation due to friction due to edge impact in the laminate and impactor are relatively small and may be assumed negligible.

In this section we will discuss in near and on-edge impact with respect to various parameters such as

- Normalised vs incident impact energy
- Damage width

These parameters are compared with respect to thickness.

3.3.6.1 Normalised vs Incident Impact Energy

Normalised absorbed energy can be defined as the impact energy absorbed by the laminate (area under the force-displacement curve) divided by the incident impact energy. The normalised absorbed energy indicates the damage accumulated during the impact event. The values of normalised absorbed energy for edge impact are shown in figure 3.22. It was found that thick laminates absorb higher normalised absorbed energies during on-edge impact as compared to thin laminates. At higher incident energy the values of normalised absorbed energy are similar for both thin and thick laminates and are close to one. The 1J on-edge result is included here, but may not be accurate because of the oscillations observed in the force/time curve.

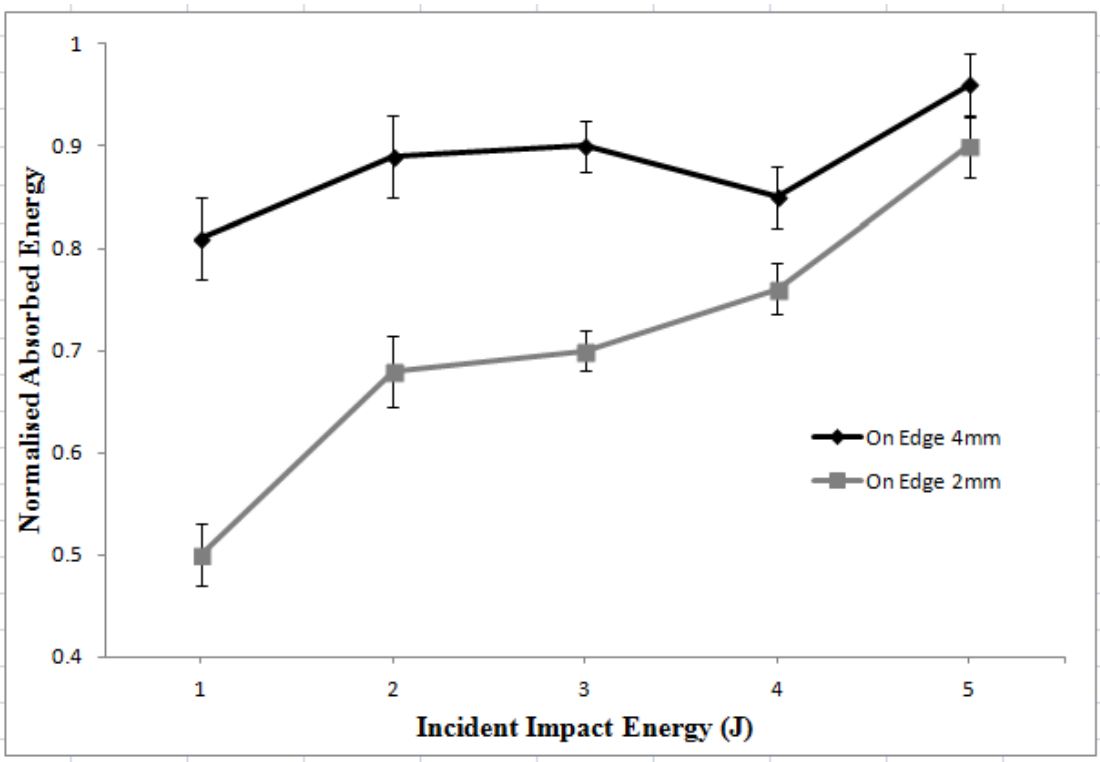

Figure 3.22 Normalised absorbed vs incident energies: On-edge impact

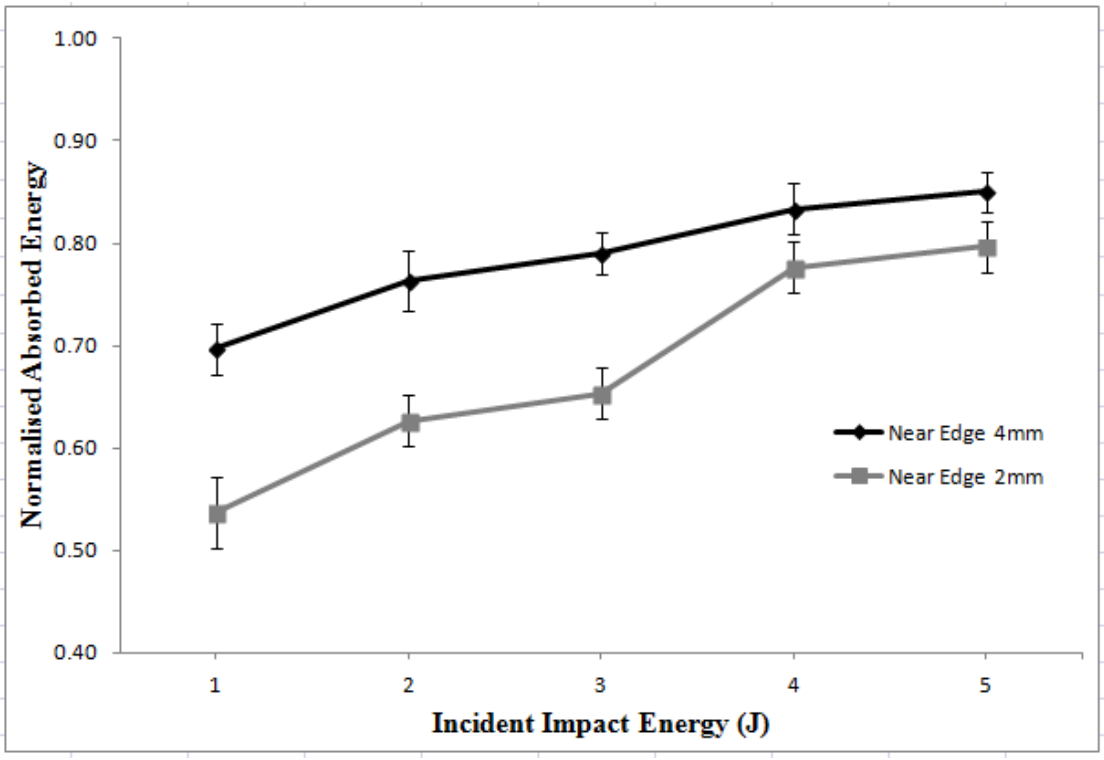

Figure 3.23 Normalised absorbed vs incident energies: Near-edge impact

The normalised absorbed energy results for near-edge impact are shown in figure 3.23. It is clear that the thick laminate absorbs higher amount of energy as compared to thin laminate

for near-edge impact. Values for both thick and thin laminates increase with increasing incident impact energy and are approaching one. Thus increasing the thickness of the laminate higher energy is absorbed and thus offers better resistance to impact damage and that accounts for the variation in the failure mechanisms of the same material at different thicknesses.

3.3.6.2 Damage Width

Damage width can be defined as the maximum length of the damage zone from visual inspection measured along the edge of the laminate. The damage width of the composite laminate is examined for successive energy levels and the two thicknesses. Figures 3.24 and 3.25 compare the relationship between damage width and impact energy for the on-edge and near-edge impact for the two thicknesses.

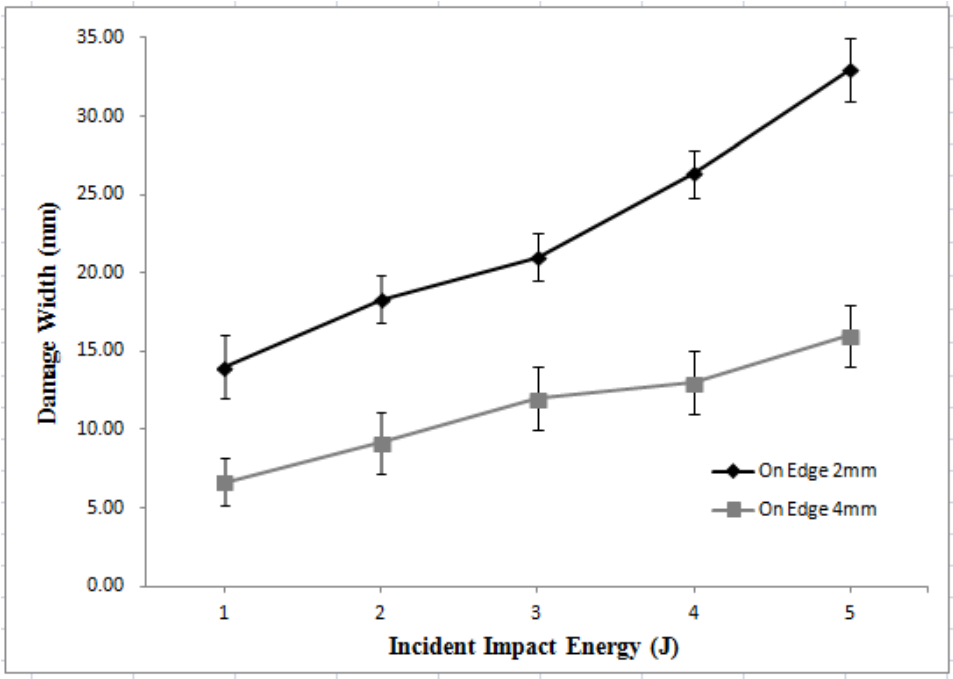

Figure 3.24 Damage width vs incident impact energy: On-edge impact

From figure 3.24 it is clear that as the energy level increases the damage width increases linearly for thin and thick laminates. Thin laminates show higher damage width as compared to thick laminate. At 1J incident energy the damage width for thin laminate is almost double as compared thick laminate whereas at 5J the damage width for thin laminate is around three times that for thick laminate. This difference arises from the large decrease in stiffness for thin laminates.

Taking into account the scatter bands, the rate of increase in damage width is linear for both values of thickness. However, the rate of increase is higher for the thinner laminates. These measurements are not expected to be affected by stress waves since the wave motion arising from on-edge impact is very high. The high difference with thickness for high impact energy arises from the damage mechanism of fibre failure; the amount of fibre failure is higher for the thinner laminate and this difference increases at higher values of impact energy.

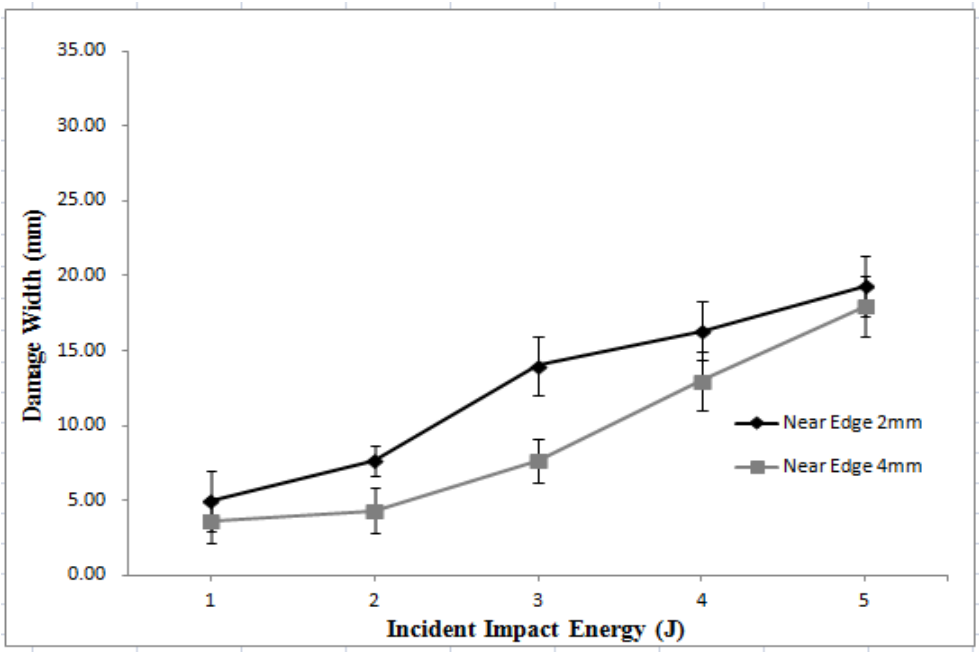

Figure 3.25 Damage width vs incident impact energy: Near-edge impact

Figure 3.25 shows the relationship between the incident energy and damage width for the near-edge impact. The damage width for near-edge impact thin laminate is larger at all energy levels. However the difference is smaller than that found for on-edge impact. At 5J the damage width almost coincides for thin and thick composite laminate.

The difference with thickness in damage width for near-edge impact is highest for the mid-range of impact energies. At low impact energy, the damage width is small and hard to measure. At higher impact energies the width is restricted by the boundary conditions which are within 10 mm of the edge of the damaged zone. Three types of waves are generated i.e.,P-wave, S-wave and R-waves which are reflected due to constrained boundary conditions (for more details refer to literature review section 2.11). Most of this damage is delamination growth, which will be influenced by the stress waves at high values of impact energy.

Thus from these results, it is found that damage width on-edge impact is higher than near-edge impact and damage width increases as the thickness of laminates is decreased. The damage width is influenced by the thickness and also the incident energy level. The influence of thickness is more marked for an on-edge impact.

3.3.7 Discussion

Force/time and force/displacement histories are useful to compare structural responses of the composite laminate from different types of impact. The high fluctuation during the elastic loading phase indicates force–displacement curves have a stiffness reduction due to impact (Wardle et al 1983; Belingardi et al 2002). The maximum displacement is obtained when the laminate starts oscillating at the first fundamental mode of vibrations and at this time the maximum amount of energy has been transferred to the laminate from the impactor.

Research done by Breen et al (2006) investigated the effect of impact velocity for central and near-edge impact on thick laminates (up to 12 mm). That work cannot be directly compared to the work here due to differences in lay-up and impact velocity. Localisation occurred in that work, which did not occur in the work here. However, the same trends in impact duration and displacement with impact velocity have been found, and lower impact duration was found for the thinner laminates as found here. Similar differences in impact damage were found comparing central and near-edge impact, with more bending and thus longer delaminations found for near-edge impact. Finite element analysis was used in Breen's work, but his models were unable to reproduce the precise lay-up, unlike the finite element models developed in this work (see chapter 6).

Thinner laminates show lower impact forces but higher displacements while thick laminates due to their higher bending stiffness are less likely to experience displacement due to bending but are more likely to experience shear displacement directly under the nose of the impactor. For centre, near-edge and on-edge impacts, the effects of laminate thickness and incident impact energy showed the expected trends. The thicker laminates had lower impact duration than thinner laminates for all types of impact. The impact duration was lower for the on-edge impact. Impact duration always increased with higher impact energy but the increase was very small for the near-edge impact. In particular, a higher proportion of energy is absorbed for higher incident energy. Energy absorbed by on-edge impact is higher as compared to

centre and near-edge impacts. On-edge impact experience large amplitude oscillations during the entire loading phase. These oscillations may be attributed to oscillations or the propagation of damage.

3.4 Impact Damage Assessment

The assessment of the edge and centre impacted laminates can be done using visualisation and optical microscopy techniques. However they provide limited information about internal damage, matrix/fibre damage but better insight into external impact damage.

3.4.1 Visualisation Technique

The figure 3.26 shows the near-edge impact damage from 1 to 5J incident impact energy for the 2mm thickness. Similar results were found for the 4mm thickness. From the figure 3.26 we can see that there is a linear increase in the near-edge impact damage as the incident impact energy increases. The values of aspect ratio for near-edge impact are given in table 3.6. Initially, at lower energy levels there is change in the aspect ratio but at higher incident impact energy the aspect ratio appears to be same.

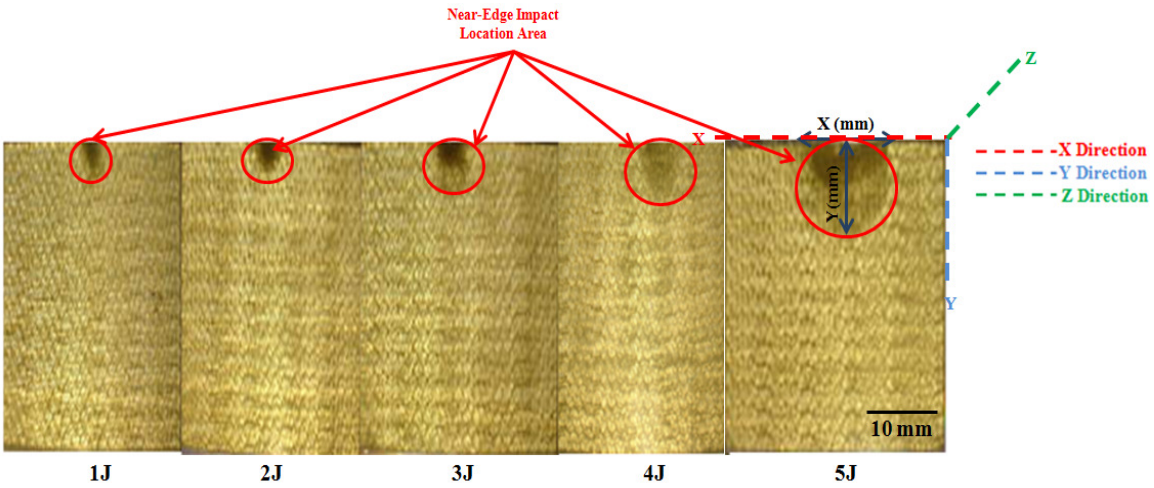

Figure 3.26 Near-edge impact damage-incident energy levels 1-5J thin laminate

Incident Impact energy Levels	1J	2J	3J	4J	5J
X (mm)	5	9	14	17	20
Y (mm)	5	6	10	12	16
Aspect Ratio	1.0	1.5	1.4	1.4	1.3

Table 3.6 Damage width aspect ratio for near-edge impact damage (thin laminate)

Figure 3.27 shows the centre impact damage at 2J and 4J incident impact energy for 2mm laminate. The damage area for 2J impact is 100 mm^2 approximately while for the 4J impact it is 500 mm^2. Clearly, the damage area is increased five times as the incident impact energy is increased from 2J to 4J.

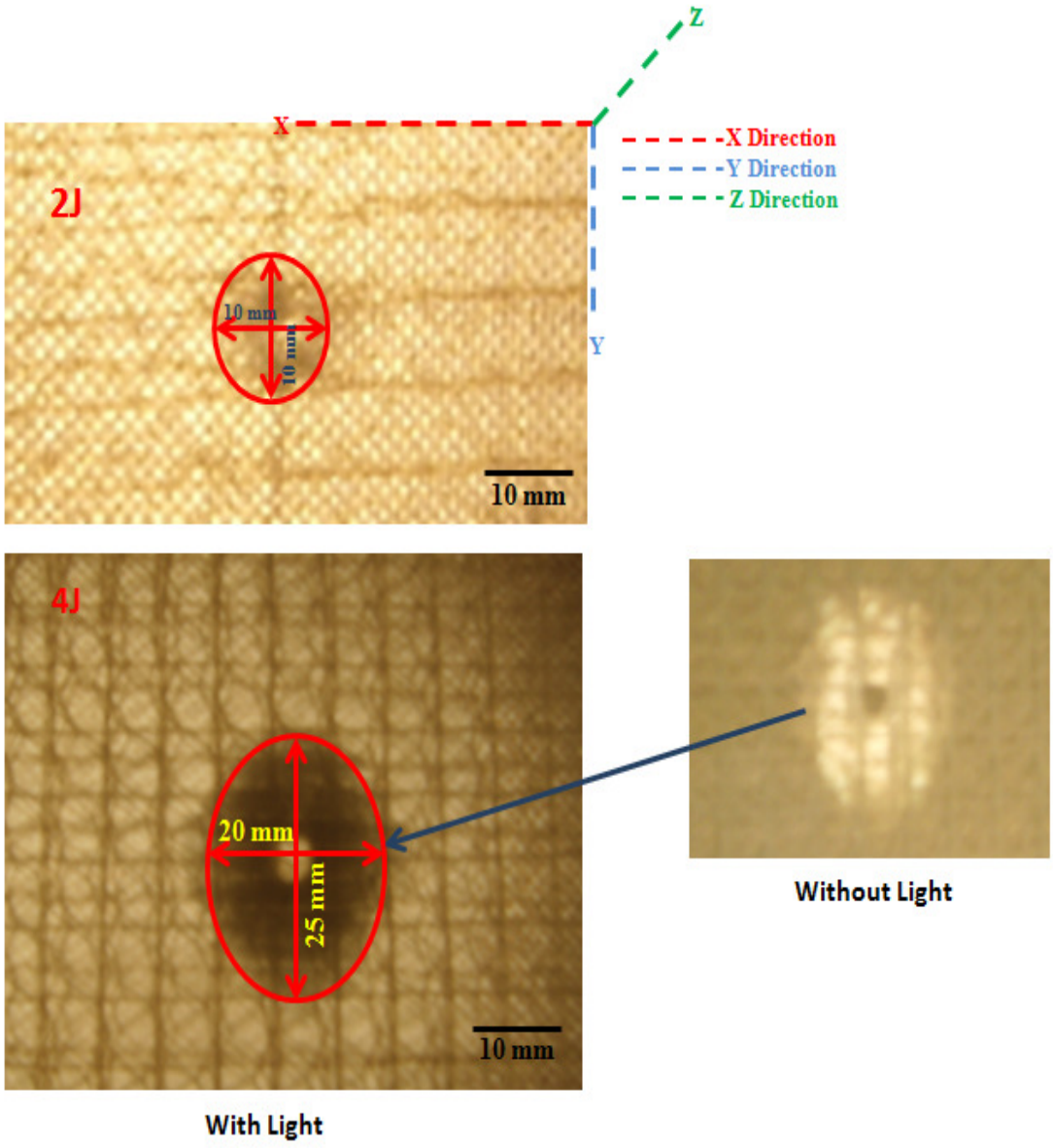

Figure 3.27 Centre impact damage-incident energy levels 2J/4J thin laminate

3.4.2 Optical Microscopy

On-edge and Near-edge impact damages are observed under the optical microscope. Figures 3.28 represent the near-edge impact damage at incident energy levels of 2J and 4J for the thin and thick laminate. The presence of delaminations at 2J energy level can be seen clearly in near-edge impact and delaminations tend to increase at higher energy level. While the damage induced by on-edge impact shows different behaviour with respect to near-edge impact and seems to dissipate a large amount of energy by matrix/fibre crushing as clearly seen from the observation of the damage. The damage consists of matrix/fibre cracks in the lower layers, some delaminations and fibre debonds/fracture. In near-edge impact, the delaminations initiate and propagate in the $+45^0/-45^0$ plies and in the middle layer. On-edge impact laminate shows multiple delaminations and an extended fracture area throughout the thickness.

Overall observation with respect to thickness indicates that in the thin laminates larger amount of fibres are broken for both near and on-edge impact. Fibre fractures tend to be initiated around the edge impacted area, where high contact internal damage stresses between the impactor and the specimen occur. While it seems that the thicker laminate showed lower delaminations as compared thin laminate for both near and on-edge impact but however the matrix damage information is not available through this technique. From figure 3.28 (a,b) we can say that the near-edge impacted thin and thick laminates the delamination starts initiating and propagating at the interface plies while for on-edge impact multiple delaminations can see and seems to spread widely at different layers of the interface.

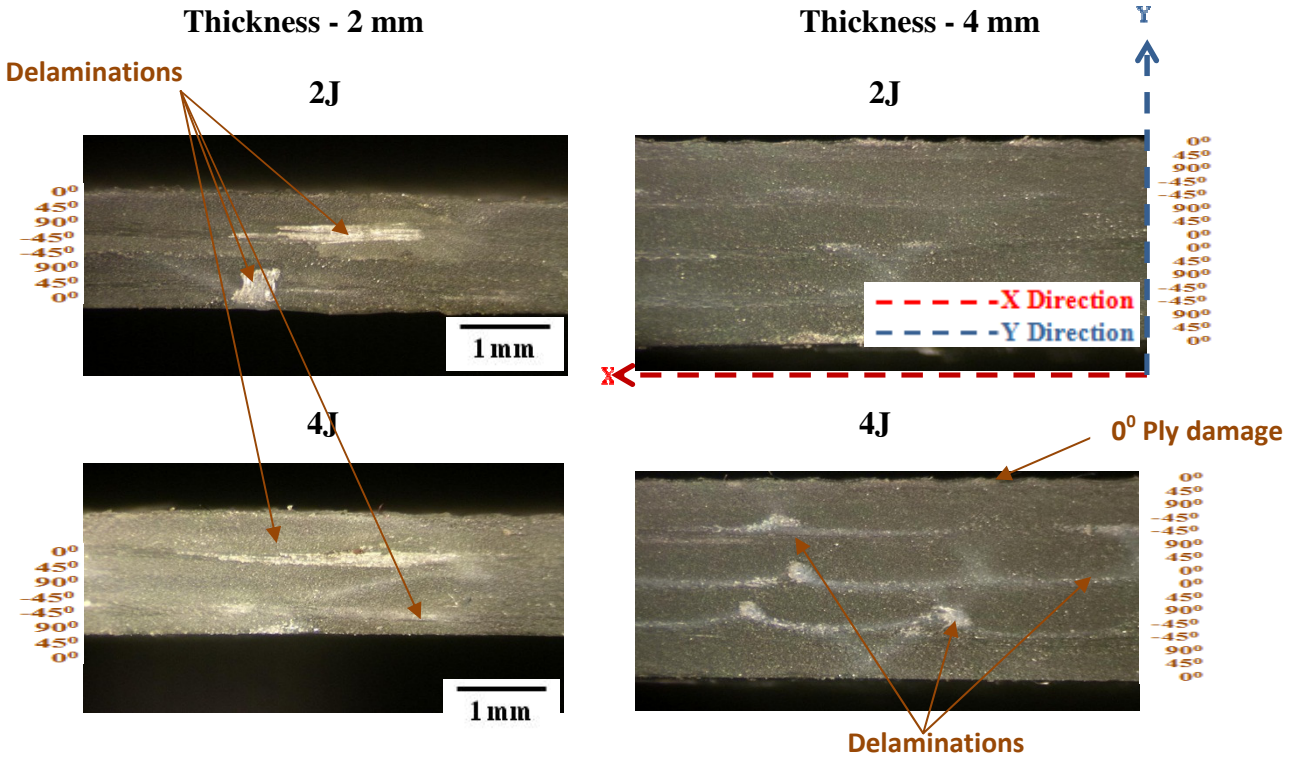

(a)

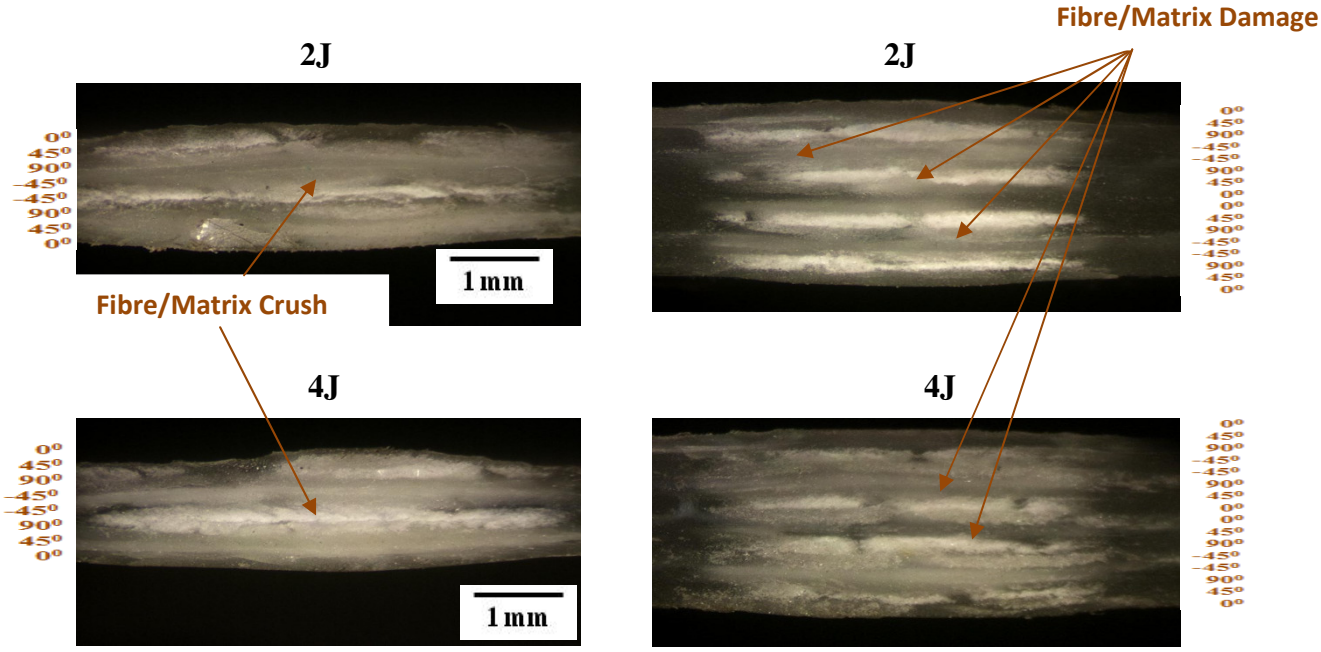

(b)

Figure 3.28 Optical microscopy techniques - Edge view
(a) Near-edge impact (b) On-edge impact

3.5 Conclusion

The significance of impact location has been highlighted by these results. Centre and near-edge impact produce similar responses, but it is notable that the centre impact results in an area of damage surrounding the impact area (see figure 3.27), while the near-edge impact has damage surrounding the impact area along one edge of the laminate (see figure 3.26). The main difference between these impact locations is in the impact duration. Typically, the impact duration for centre impact is double the duration for near-edge impact under the same conditions. This difference probably arises from the lower stiffness of the centre impact since it is more remote from the boundary conditions. At higher impact energies the impact width for near-edge impact may be restricted by the presence of the boundary conditions which are within 10 mm from the edge of the impact damaged zone. This restriction and the associated wave reflections may increase the level of damage at higher energy levels for near-edge impact. Both the force/time and force/displacement curves show discontinuities which can be associated with the formation of damage and energy absorption. The expected trends with thickness have been found for both centre and near-edge impact, with lower impact force and higher impact duration for the thinner laminate.

On-edge impact, as might be expected, behaves very differently to impacts on the plane of the laminate. The stiffness of the laminate to the impact on the edge is much higher than for impacts on the plane. The impact duration is lower, around half that for the near-edge impact. Both the force/time and force/displacement curves show significant discontinuities, indicating the formation of damage as the force is increasing and after maximum force. The discontinuities in the 1J results are very regular and may arise from vibration of the specimen; these results may be invalid. Values of normalised energy absorbed are generally higher for on-edge impact despite the higher stiffness. This must indicate differences in the damage processes. The effect of thickness was much less apparent for on-edge impact, with a measurable increase in peak force for the thicker laminate (see table 3.4) but no measurable change in impact duration. At the highest energy level the values of peak force for the two thicknesses are nearly identical; this must arise from interaction with the boundary conditions at this energy level. The lack of discernible effect of thickness on impact duration must arise since this effect would be small for this stiff direction for both thicknesses.

Chapter 4

X-Ray Computed Tomography of Glass/Epoxy Composite Laminates subject to Edge Impact

4.1 Introduction

In this chapter the three-dimensional nature of edge impact damage and its evolution is investigated and the extent of intra and inter laminar damage is explored using computed tomography. Visualisation of edge impact damage in 3D at a micro-level is captured. The objective of this chapter is to experimentally investigate the damage during on-edge and near-edge impact.

4.2 Experimental Details

Glass/epoxy laminates with near and on-edge impacts at 2J and 4J on composite specimens with thickness of 2mm $(0/45/90/-45)_s$ and 4mm $(0/45/90/-45)_{2s}$ have been investigated. The aim is to investigate the search areas of potential edge impact fibre/matrix damage using the different tools. Also it should be noted that every impact has a different impact history so in this chapter the comparison of near-edge and on-edge impact damage is not feasible due to the type and nature of the impact but the same techniques and steps to evaluate the damage behaviour of both configurations are used. Similar approach can be used for all the other energy levels for varying thicknesses.

4.2.1 Specimen Mounting Design and Preparation

To perform the computed tomography experiment, the coupon size glass/epoxy laminates are cut from original size of 89x55 to 89x10 mm^2. The cutting of the laminate captured the damage area since the cutting was orthogonal to the damage width. Figures 4.1 (a) and (b) show the sample holder and specimen dimensions respectively. The three glass/epoxy composite specimens with same thickness of 4 mm, undamaged and 2J and 4J impacted, are clamped from top and bottom with space of 2 mm in between. Composite laminate with near-edge impact zone is shown in figure 4.1 (c) with zoom area with Z-axis as 0^0 fibre direction while X-axis as 90^0 fibre direction.

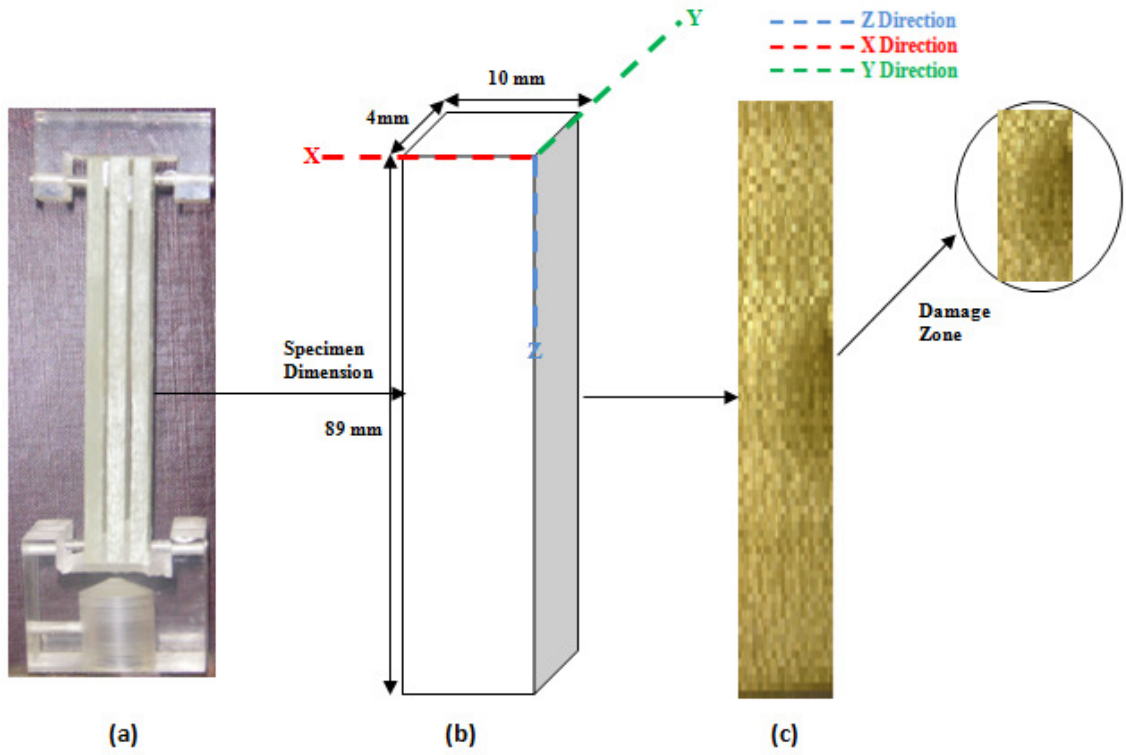

Figure 4.1 Sample preparations for X-ray scanning (a) Sample holder (b) Specimen dimensions (c) Damage zone (zoom area)

The rotation stage is fitted with a kinematic mount containing three V-blocks. The sample laminate can be fitted very easily in these mounting disks and this allows placing them in identical positions. The mounting plate is such that it can accommodate specimens with different thickness. At the rotation stage the specimen is mounted such that the scanned volume is at a considerable height. In order to have high resolution the specimen has to be mounted close enough to the source to obtain the necessary geometric magnification. The edge impacted laminate was positioned close to the X-ray source.

4.2.2 Computed Tomography (CT) facility

The MuCat scanner is a modified version of the existing available medical CT scanners. Dr.Graham Davis developed the MuCat scanner at QMUL for research into various medical applications. The MuCat scanner is a research tool with higher spatial resolution and greater sensitivity to differences in the intensity of X-ray beams. This enables the viewer to distinguish between old bone, new bone and ceramic sponge. MuCat scanners are set with an acceleration voltage from 0 kV to 225 kV ultra-focus X-ray generators. These scanners are

placed in a shielded cabinet. The camera is manufactured by Spectral Instruments company. Voltage is applied such that it controls the maximum energy of the X-ray spectrum and to maximise the contrast between glass/epoxy laminates (see figure 4.2).

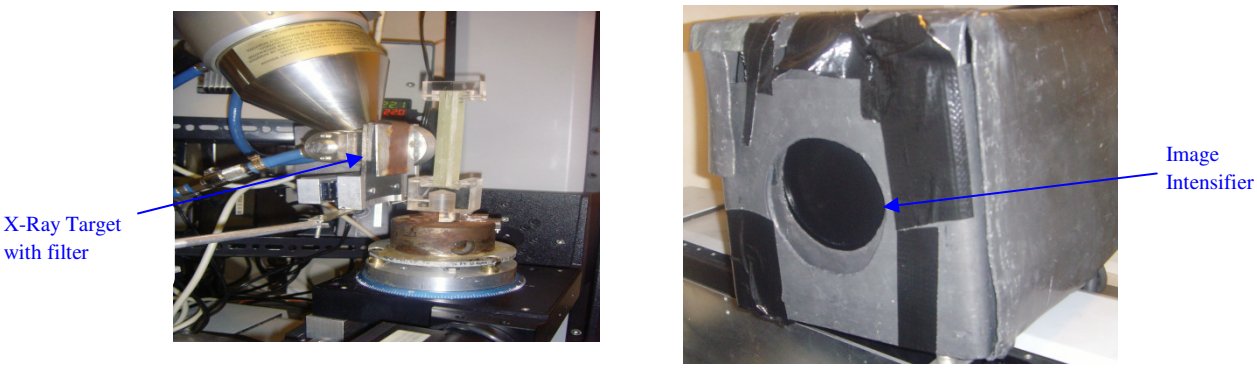

(a) **(b)**

Figure 4.2 CT experimental set-up (a) X-ray target with filter and sample holder (b) image intensifier (CCD 485 sensor)

Computed tomography device has parallel fibre-optic coupling system and has a sensor with 100 µm thick columnated scintillator. The fibre-optic faceplates have to be selected to have minimum distortion as most types of distortion cannot be corrected after acquisition. Two Physique Instrumented M-531 linear motion stages are used. The first controls the source to specimen distance and specimen height and the second is used to translate the camera to achieve the high resolution imaging. As the camera moves, the image is read out from the serial register of the CCD. The image is read such that the rate of movement of charge across the CCD exactly matches the motion of the image. The time taken for the image to move the length of the CCD is known as the exposure time. Thus to set the X-ray exposure time both motion rate and readout rate has to be adjusted. Physique Instrumented M-061 model is utilised for the rotation stage. It is .tom file voxel size is 15.0 with a voltage of 60.0 and current 0.27. Four blocks of 1601 projections are created which is a large file.

4.3 2D-Computed Tomography Edge Impact Damage Image Analysis

The following section will discuss the generation of initial results for on and near-edge impacted laminates. Damage images will be saved in high resolution mode.

4.3.1 Tomographic Edge Impact Files

Tomographic input file contains all data necessary for tomographical reconstruction. The datasets are collected from the computed tomography. These datasets are collected at each slices of the edge impacted laminate and are saved as a tomography (.tom files) files as a single data. These files contains the three dimensional datasets for edge impacted laminate and provides information about the fibre/matrix behaviour in XY, YZ and XZ planes. These .tom files are then imported into the Drishti Importer software where a two dimensional slice of a model file is created. The 2D files are further converted and saved into different format which is referred by "Filename.plv.nc". The final processed stack is then exported as a single volumetric file for a Drishti tool for rendering which allows displaying tomography set with a full 3-D visualisation effect and thus capturing the opacity and histogram of the edge impacted laminate.

4.3.2 Calibration of 2D radiographic images

Two dimensional radiographic images are captured to locate the damage in glass/epoxy laminates in XY, YZ and XZ planes. Each 2D radiograph provides average depth and view of the specimen in a particular direction. Different sections and slices of radiographic images are recorded as the composite specimen revolves slowly to 360^0 revolutions. It should be noted that Z is the 0^0 fibre direction, X is the transverse direction, 90^0 fibre direction while Y is the through thickness direction. Thus figures 4.3 (a)-(c) show 2D-three orthogonal slices from the reconstruction in XY, YZ and XZ planes of undamaged glass/epoxy specimen of 2 mm thickness.

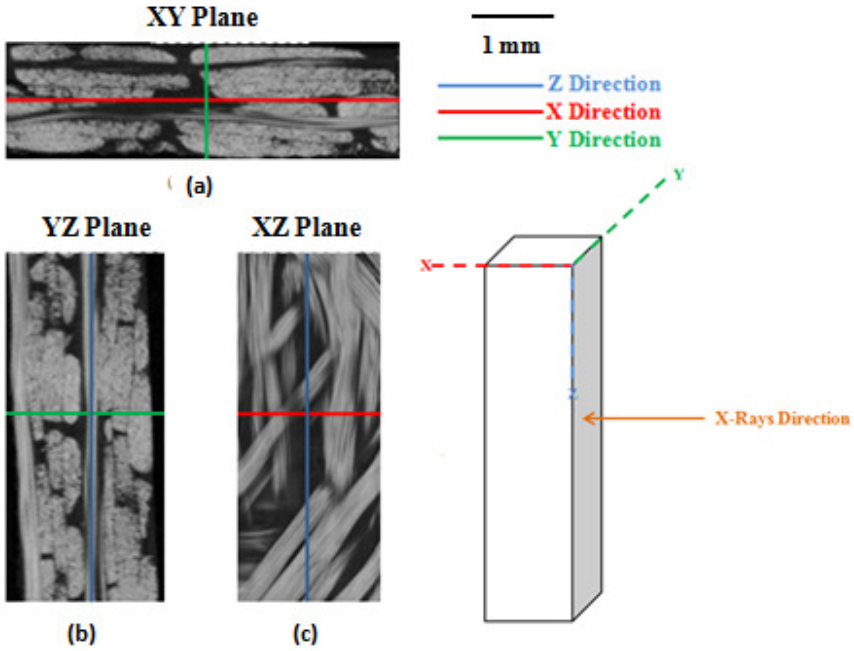

Figure 4.3 Two dimensional slices of 2mm undamaged glass/epoxy laminate reconstruction (a) XY plane (b) YZ plane (c) XZ plane

4.3.3 Damage Detection in XY, YZ and XZ planes

4.3.3.1 On-Edge Impact

In order to determine the crack geometry and its propagation a slicing of successive sections through the specimen is required. Three levels of grey colour can be identified in the images, representing three different densities. Dark grey/black colour represents the resin matrix while the white/white grey colour represents the highest density of fibre tows/bundles. Figures 4.4 (a)-(c) show on-edge 4J impacted (2mm thickness) with three orthogonal slices in XY, YZ and XZ planes from the tomography reconstruction with varying grey levels. The various fibre bundles are embedded in epoxy matrix. Large number of damaged fibre/matrix and crack paths can be found as shown in figure 4.4. In the XY plane, the on-edge impact damage opening can be seen. In the YZ plane, the matrix crack path is visible and in the XZ plane, multiple fibre fracture and deformation can be seen.

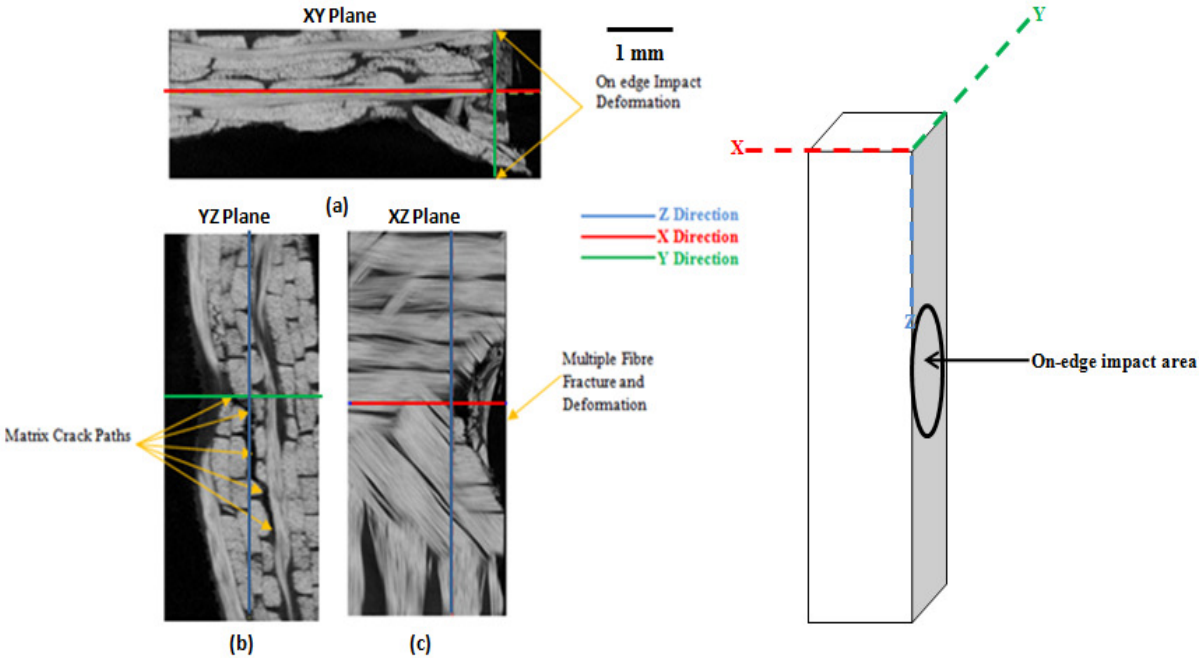

Figure 4.4 Two dimensional slices of 2mm on-edge 4J impact from the 3D reconstruction in the composite structure (a) XY plane, (b) YZ plane and (c) XZ plane

4.3.3.2 Near-Edge Impact

Figure 4.5 (a)-(c) shows near-edge impacted three orthogonal slices in XY, YZ and XZ planes. Figure 4.5 (c) shows the fibre breakage at the point of contact in XZ plane. In XY plane the delamination location can be detected. In YZ plane the matrix crack can be seen clearly. Thus different damages are seen in all the three different directions.

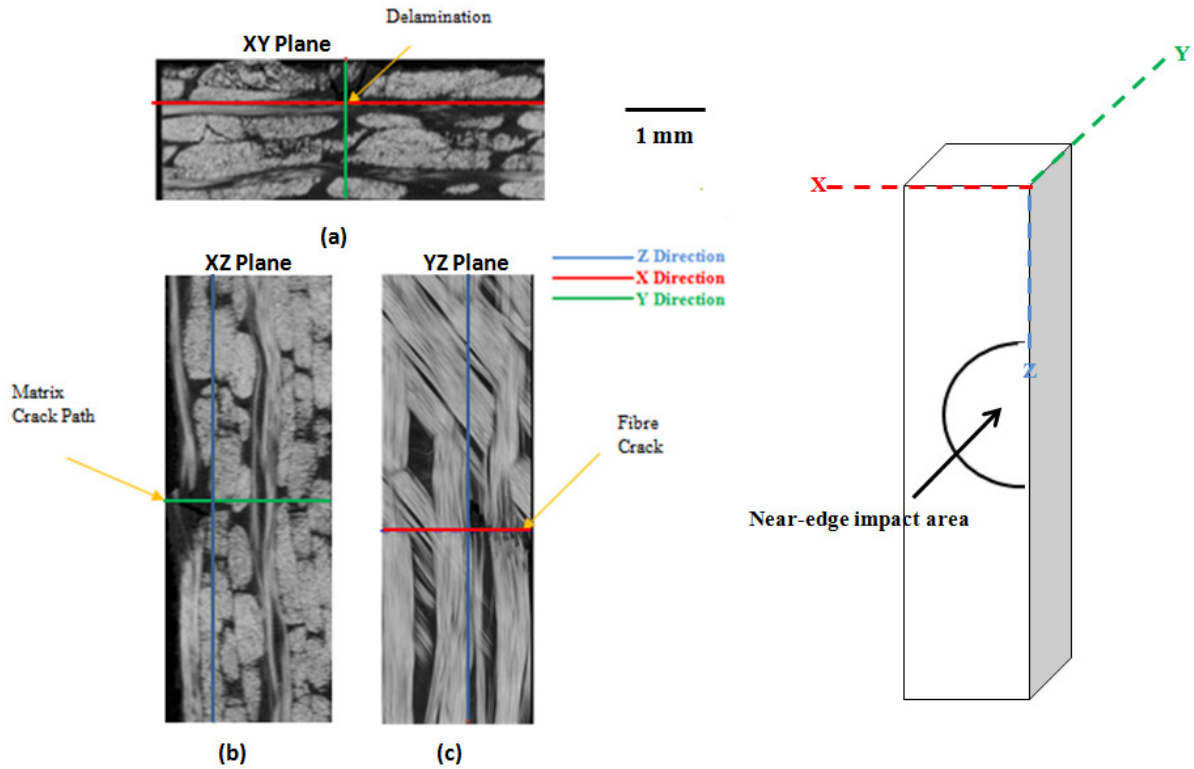

Figure 4.5 Two dimensional slices of 2mm near-edge 4J impact from the 3D reconstruction in the composite structure (a) XY plane, (b) YZ plane and (c) XZ plane

4.4 3D-Edge Impact Rendering Results

4.4.1 Undamaged Laminate

4.4.1.1 Fibre Bundles/Tows

Figure 4.6 (a) shows the volumetric model of fibre bundles using Drishti Tool for the undamaged 4mm thick laminate. The matrix is invisible and the distribution of fibres can be clearly seen. Figure 4.6 (b) shows the inside view of the 4mm thick laminate.

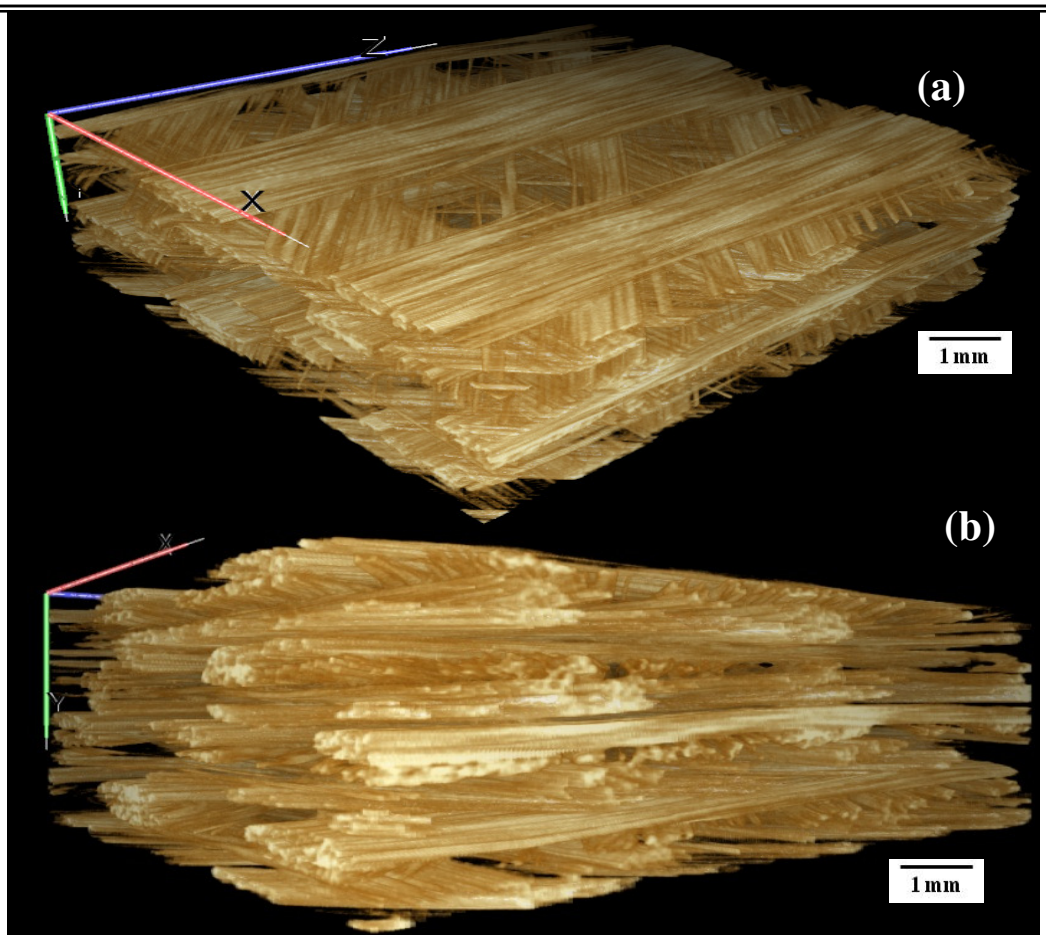

Figure 4.6 (a) and (b) Three-dimensional volumetric models of undamaged E-glass fibre bundles with 4mm thickness

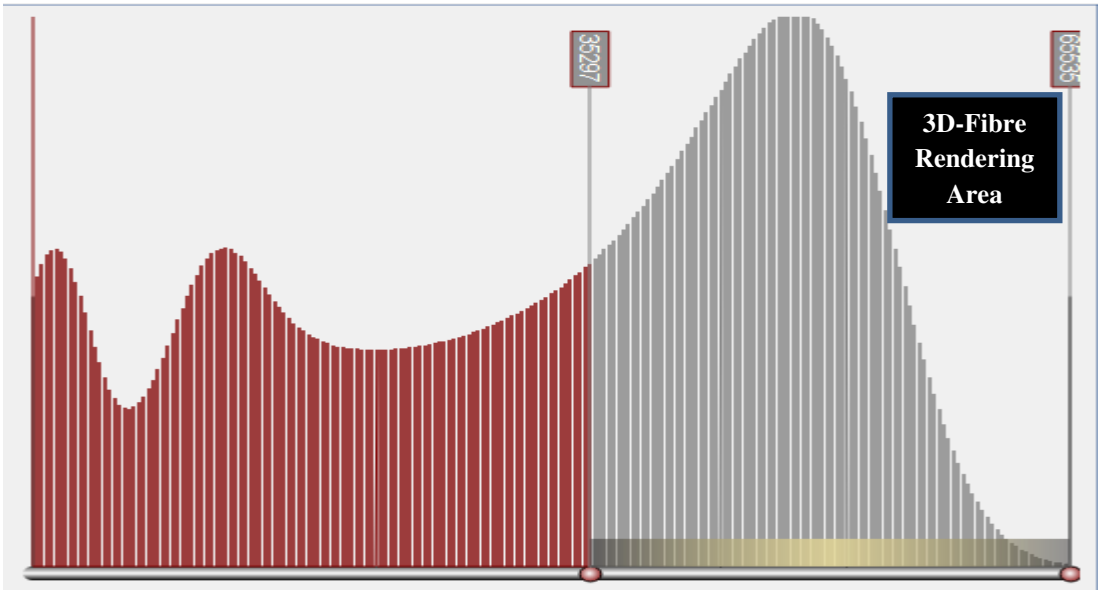

Figure 4.6 (c) Three-dimensional fibre rendering area for undamaged 4mm laminate

Figure 4.6 (c) shows the histogram for the whole laminate. The visibility of fibres can be achieved by considering the area shown in this figure 4.6 (c) making fibre visible and matrix invisible.

4.4.1.2 Undamaged Matrix

Figure 4.7 (a) shows the volumetric model of matrix distribution. The fibre is now rendered invisible and the distribution of matrix can be clearly seen. It should be noted that the direction and distribution of matrix is with respect to the laminate stacking sequence. The matrix rendering analyses the location, size, and geometry of the damage zone in three dimensions.

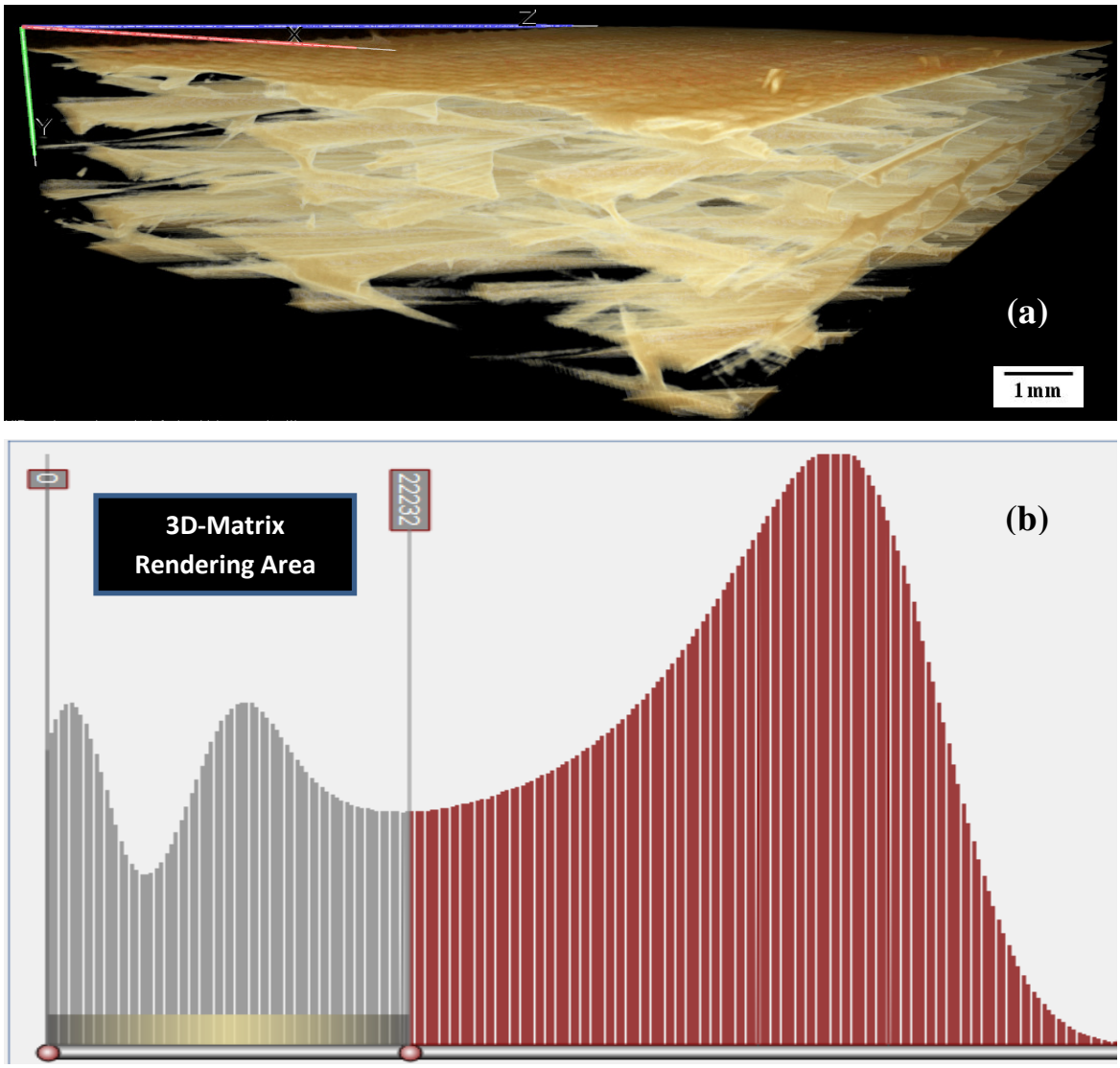

Figure 4.7 Three-dimensional matrix rendering for undamaged 4mm laminate
(a) Laminate matrix (b) Histogram - Matrix rendering area

Similarly the visibility of matrix can be achieved by considering the area shown in figure 4.7 (b). The results of the next section are obtained by the same approach.

4.4.2 Near-Edge Impact

4.4.2.1 Damage Profile Generation

Profile generation determines the intensity profile along the path length. Depending upon the edge impact damage the intensity profile can be generated at that particular location. Any number of points can be added along the damage path that is from 0 to 100. The results in the following sections will generate many profiles along the damage path to capture the various internal damage states.

4.4.2.2 Shear Damaged Fibre Bundles

Figure 4.8 shows the shear damage fibre bundle for near-edge 4J impact and thickness of 4mm. Three points are added along the shear damage fibre bundle path to capture profile curves along this path. All profiles show the intensity (number of pixels) as a function of the path. Another profile data is generated for the undamaged fibre path length and is denoted by B. This is to compare the damaged fibre and the undamaged fibre path profiles. Point 0, 1 and 2 are shown in figure 4.8. Damage path curve A from point 0 to 1 shows a peak curve of value of approximately 12599 indicating shear failure of the fibre. The empty area around this peak indicates the fibre removal between these two points. Similarly between the points, 1 to 2 (see figure 4.8) the peak value 18899 and the rest of the area around this curve is empty and thus the intensity of pixels is zero. For undamaged profile path B the peak value is between 15933 and 44849. This is far higher than for the damaged profile data. This indicates the higher intensity of pixels and absorption coefficient for the undamaged fibre bundle. Higher frequency of pixels along this path is seen due to higher absorption coefficient of fibre bundles. Every single fibre has different pixel magnitude and thus has different profile data.

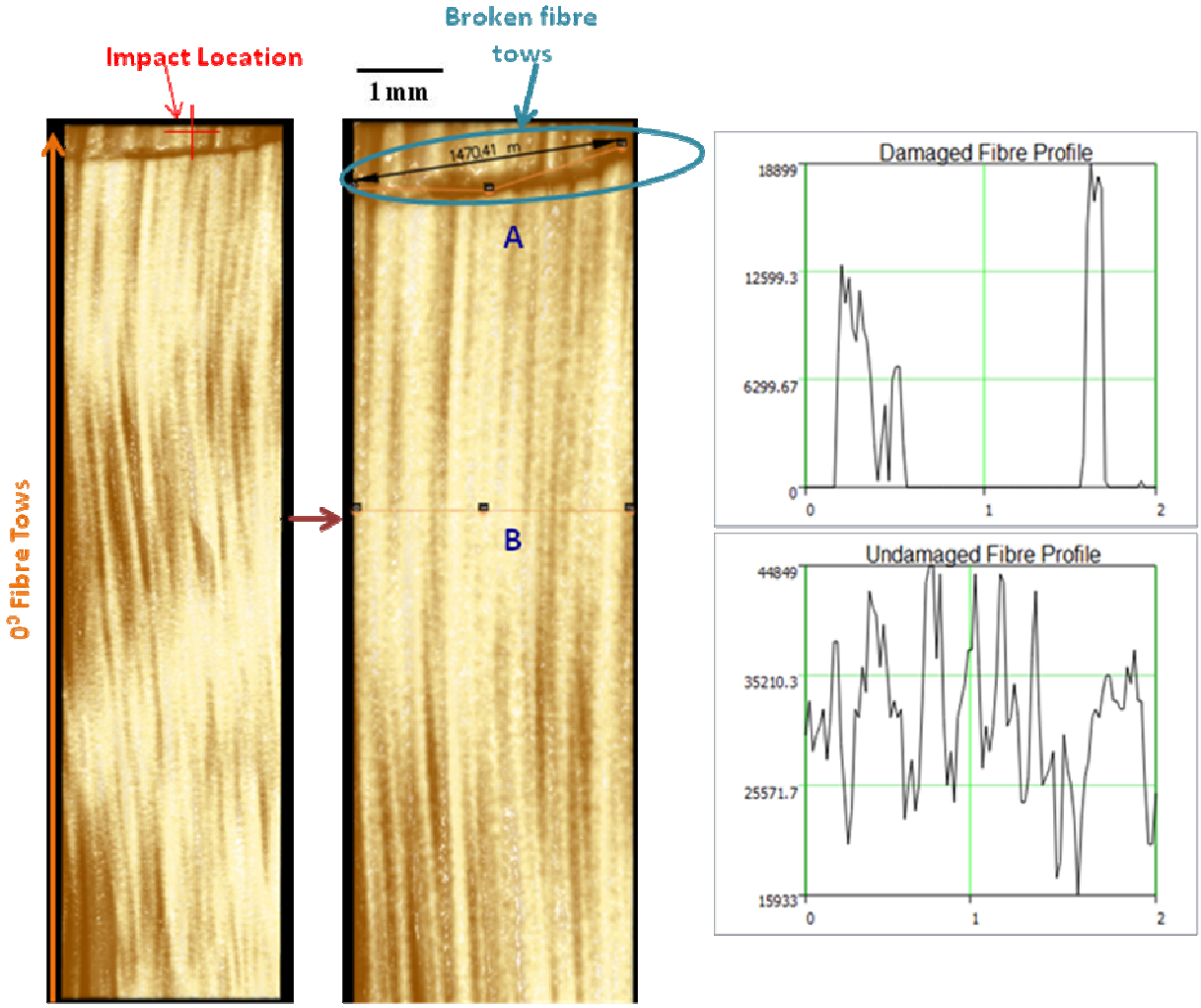

Figure 4.8 Near-edge 4J impacted with thickness 4mm-shear damaged fibre bundles with opacity and profile data

4.4.2.3 Displaced Fibre Angle and Path Length

The damage arising from the bending in the impact event may be characterised by the angle of displaced fibres. To test this method, two fibre angles have been measured. The angle was measured under the impactor for the near-edge impact (see figure 4.9). The angle of fibre disorientation measured at point B was found to be about 35°. This is a potential method to quantify the severity of impact damage.

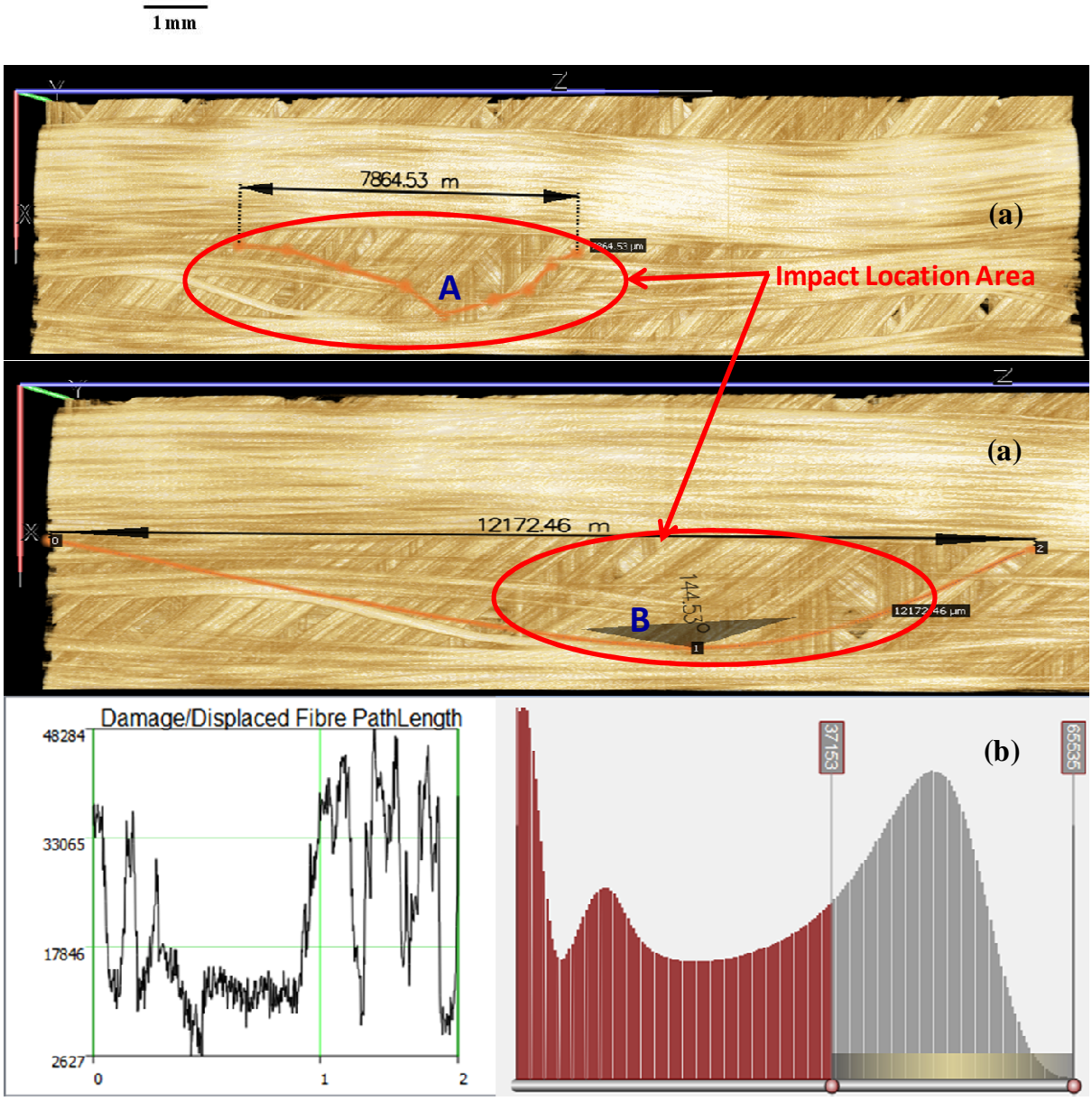

Figure 4.9 Near-edge 2J impacted with 2mm thickness (a) Displaced fibre angle and path length (b) Histogram and profile data

The displaced fibre length is approximately 12172 microns (12.172 mm). The profile data is generated along this curve. The numbering starts from point 0 with approximate value of 33065 and starts decreasing along this path showing fibre cracks while point from 1 to 2 shows higher intensity profile data indicating multiple fibres along this path and reaches a peak value of 48284.

4.4.2.4 Fibre/Matrix Damage Area and Load Path

The damage area is examined under the impactor. Figure 4.10 shows the near-edge 4J impacted with laminate thickness of 2 mm. Fibre breakages are clearly seen in figure 4.10. The fibre break can be divided into two parts the right hand part which is denoted by A and left hand part is denoted by B. We will consider path A first. The path A of fibre breakage has a length of 5988.56 microns (5.988 mm). For fibre bundle 1 all fibres in the bundle are broken and for fibre bundle 2 multiple fibres break while other fibres are displaced from their original position. Along path A twelve points and an intensity profile is generated along this path. Profile data shows high pixel intensity with a minimum value of 7049 and a maximum of 57008. The minimum value seen between the points 0 and 1 indicates shear cracks and fibre breaks while the maximum value is seen in between the points 3 and 4. Points 8 to 12 have higher intensity values.

Similarly in figure 4.11 path B has thirteen points and an intensity profile is generated along this fibre path. Zoom area is shown in figure 4.11. Profile data shows intensity profile with the minimum value of 6742 to maximum value of 53943. Minimum value is seen at points 8 and 9 due to the transition from the 1^{st} fibre bundle to the 2^{nd} while the maximum value is seen in between the points 11 and 12. Other points indicate higher absorption coefficient of the fibres.

In figure 4.12, the fibre area is invisible and matrix area visible, at the same position as figure 4.11. We can see clearly the near-edge impact matrix damage location. Shear matrix cracks are clearly seen around this area.

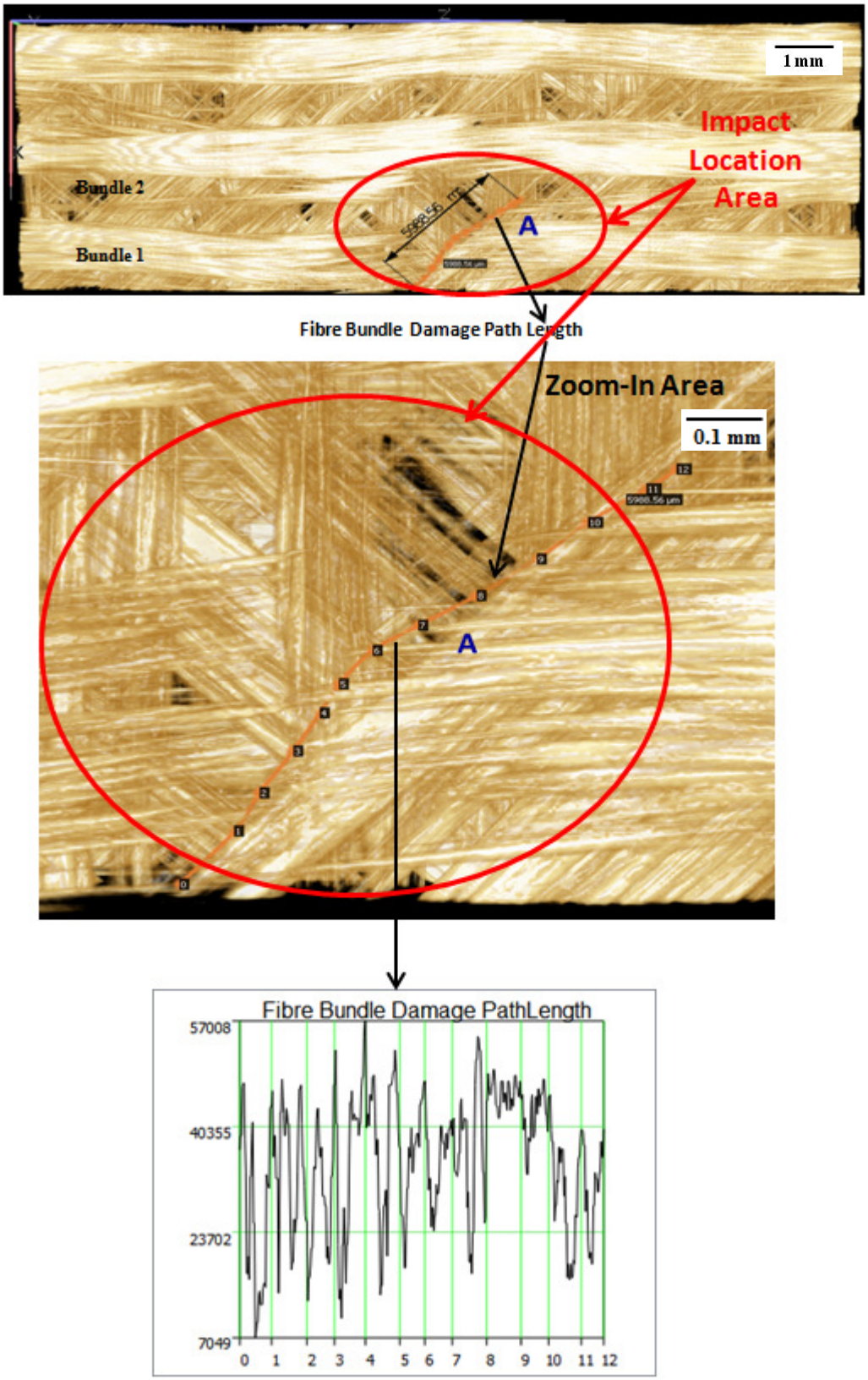

Figure 4.10 Near-edge 4J impacted with thickness 2mm-fibre bundle damage load path with profile data for point A

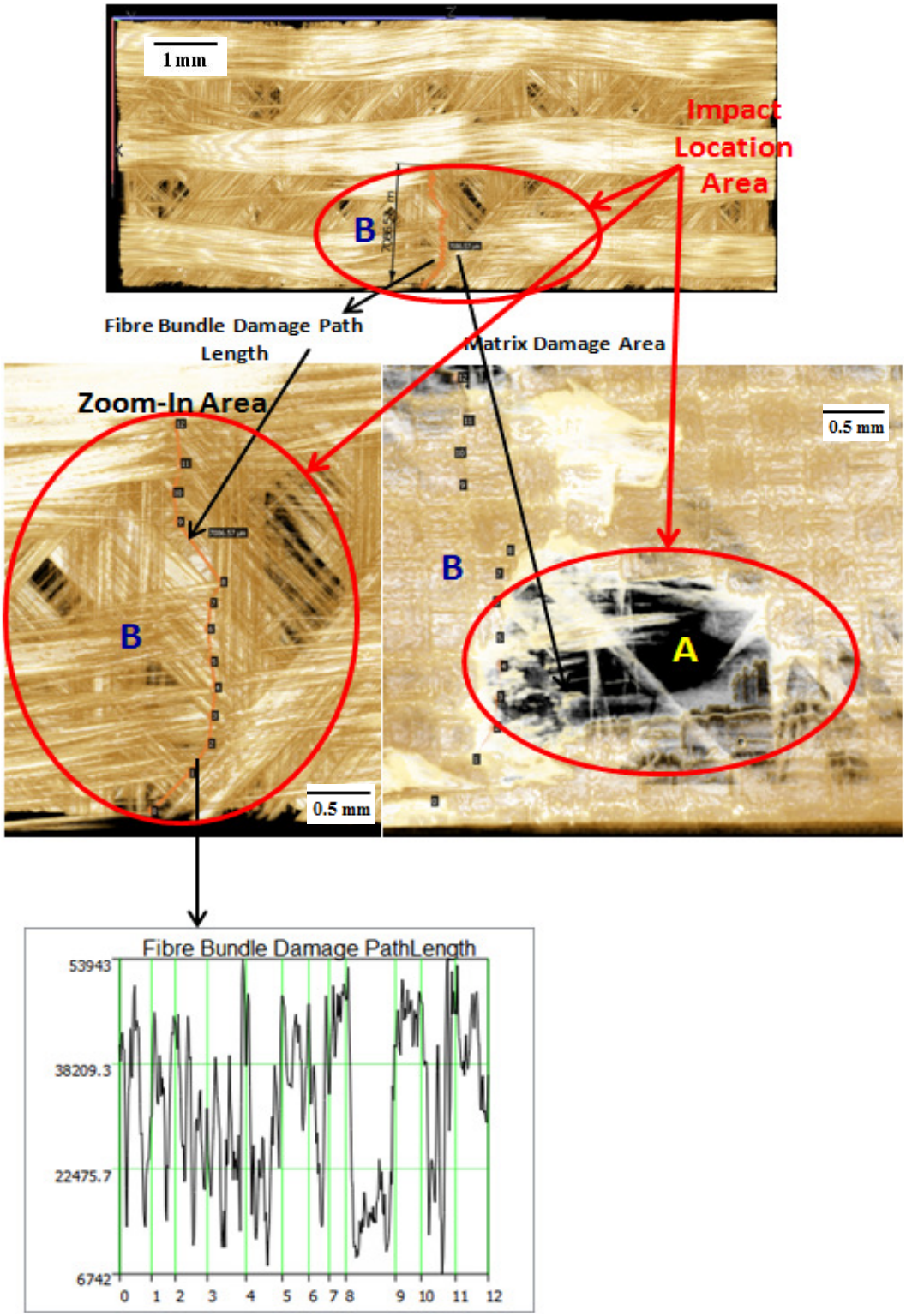

Figure 4.11 Near-edge 4J impacted with thickness 2mm-fibre bundle damage load path with profile data for path B and matrix damage at point A

Various matrix damage positions are seen in figure 4.12 (a). In some areas delamination starts and the matrix is completely removed while in other areas the matrix damage initiated. Matrix damage propagates along the path length from point 0 to 13 of path B. Beyond the point 13 of path B the matrix damage spreads across the whole bottom of the laminate. Top ply captures this behaviour clearly. Delamination can be seen to develop around the matrix damage as shown in figure 4.12 (b).

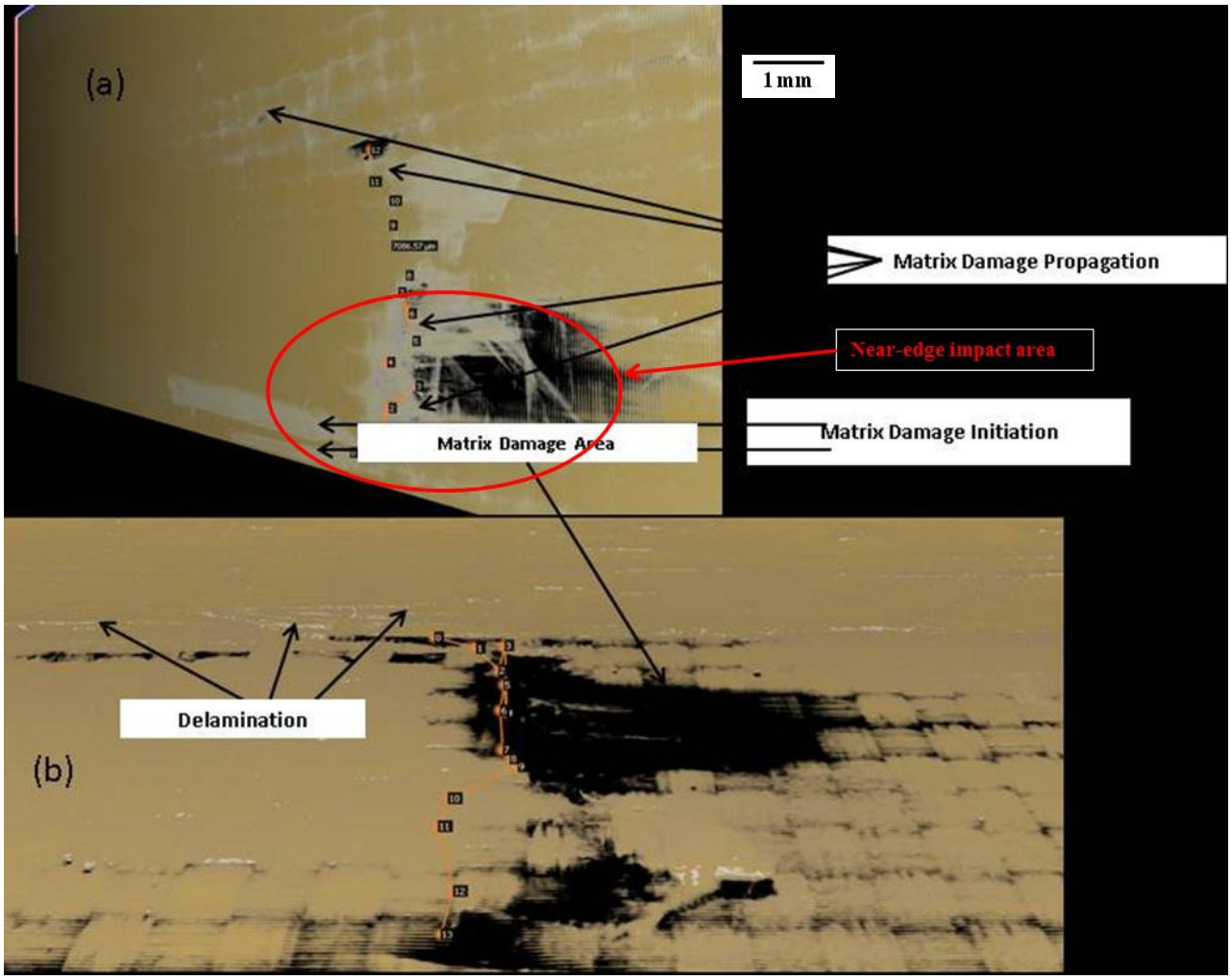

Figure 4.12 Matrix damage and delamination location for near-edge 2J impacted with thickness of 2mm (a) Matrix damage locations (b) Delamination near matrix damage area

4.4.2.5 Delamination and Matrix Damage Areas

Figure 4.13 shows the matrix damage for near-edge impact 2J and 4mm thickness. Fibres are rendered invisible. The white regions in the laminates are the development of delamination as shown in figure 4.13.

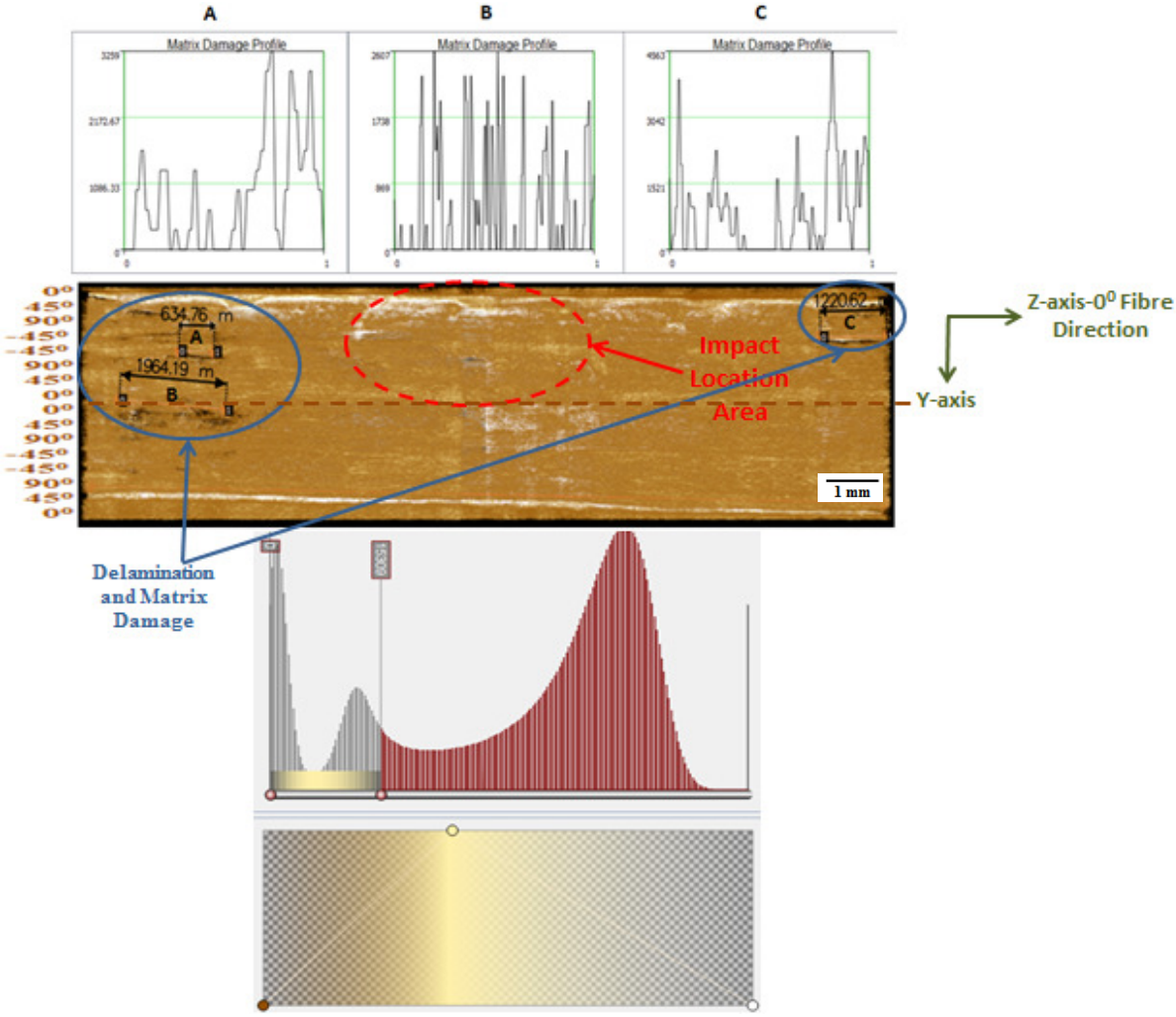

Figure 4.13 Delamination and matrix damage location with opacity and profile data for near-edge 2J impacted with 4mm thickness

The paths A, B and C show the matrix damage profile for the path from 0 to 1. The intensity values are very low for path A which is 3259. For path B it is 2607 and for path C it is 4563 indicating matrix damage has taken place. The matrix damage is generally seen on the top plies around the point of contact while delamination is just under the top plies and also seen on the bottom plies, see figure 4.13. The histogram is also shown for different opacity levels for matrix rendering for accurate prediction of delamination and matrix damage.

Another way to capture the hidden delamination and matrix damage is to embed the fibre phase. To do this the transfer function in the histogram is expanded to maximum in which it captures the whole laminate under consideration. This technique is also helpful to get an overview of the internal damage which cannot be seen by the above mentioned technique. We will consider the same case and from figure 4.14 we can see that with the black and white damage profile of the fibre embedded in the matrix. Paths A and B show the underlying matrix damage and delamination. However this does not provide an accurate picture of the damage as both the fibre and matrix are rendered together. The lower values in the profile data show that damage and delamination have started in these potential areas.

However the colour profile data with matrix rendering only provides different information that is not captured in black and white rendering. Figure 4.15 shows the matrix damage and delamination for the near-edge 2J impact with 2mm thickness. Delamination can be seen clearly at interfaces $0^0/45^0$ and $-45^0/-45^0$. Path A has a length of 5296 and path B has length of 7778 microns. Shear matrix damage is also seen for the thin laminate with the matrix damage path length of 14118 microns for path C. The zoom area of path C is shown in figure 4.15. Underlying matrix damage of 2976 microns and shear matrix cracks of 543 microns can be seen clearly. The captured image consists of grey intensity that corresponds to different densities within the composite laminate. Voids however are difficult to detect in composites due to the matrix embedded in the fibres. However using the Drishti tools one can determine the voids by rendering the fibres invisible and matrix visible. Shear cracks were determined using this approach. The path is created between the region of interest and the area under the peak curve of the histogram determines the density of the specimen. If there are no or very low peaks or no change in the grey levels in that path it can be assumed as voids. High opacity points and levels are required to capture these results as shown in figure 4.15.

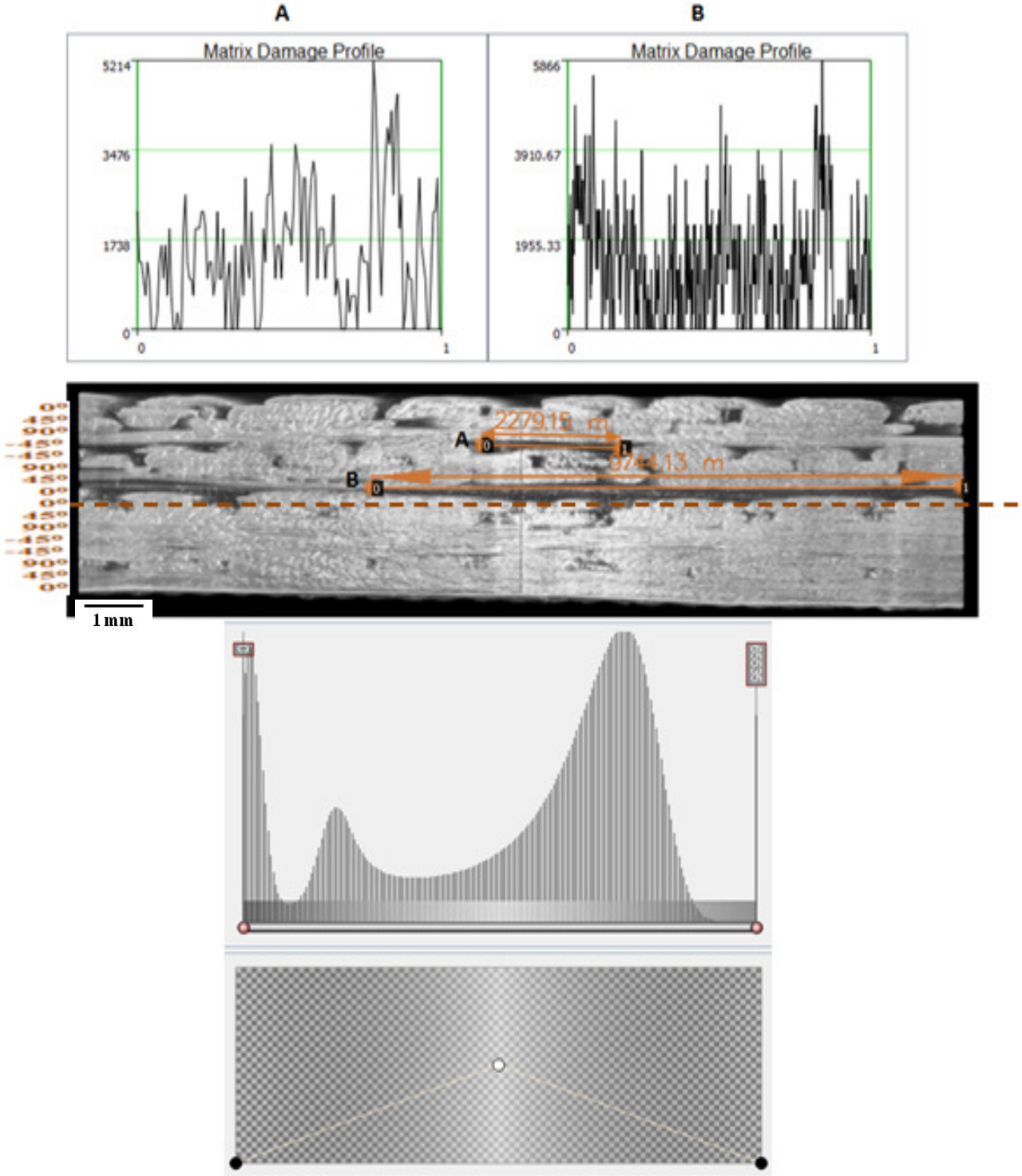

Figure 4.14 Delamination and matrix damage location with different opacity and transfer function – 4J impact and 4mm thickness

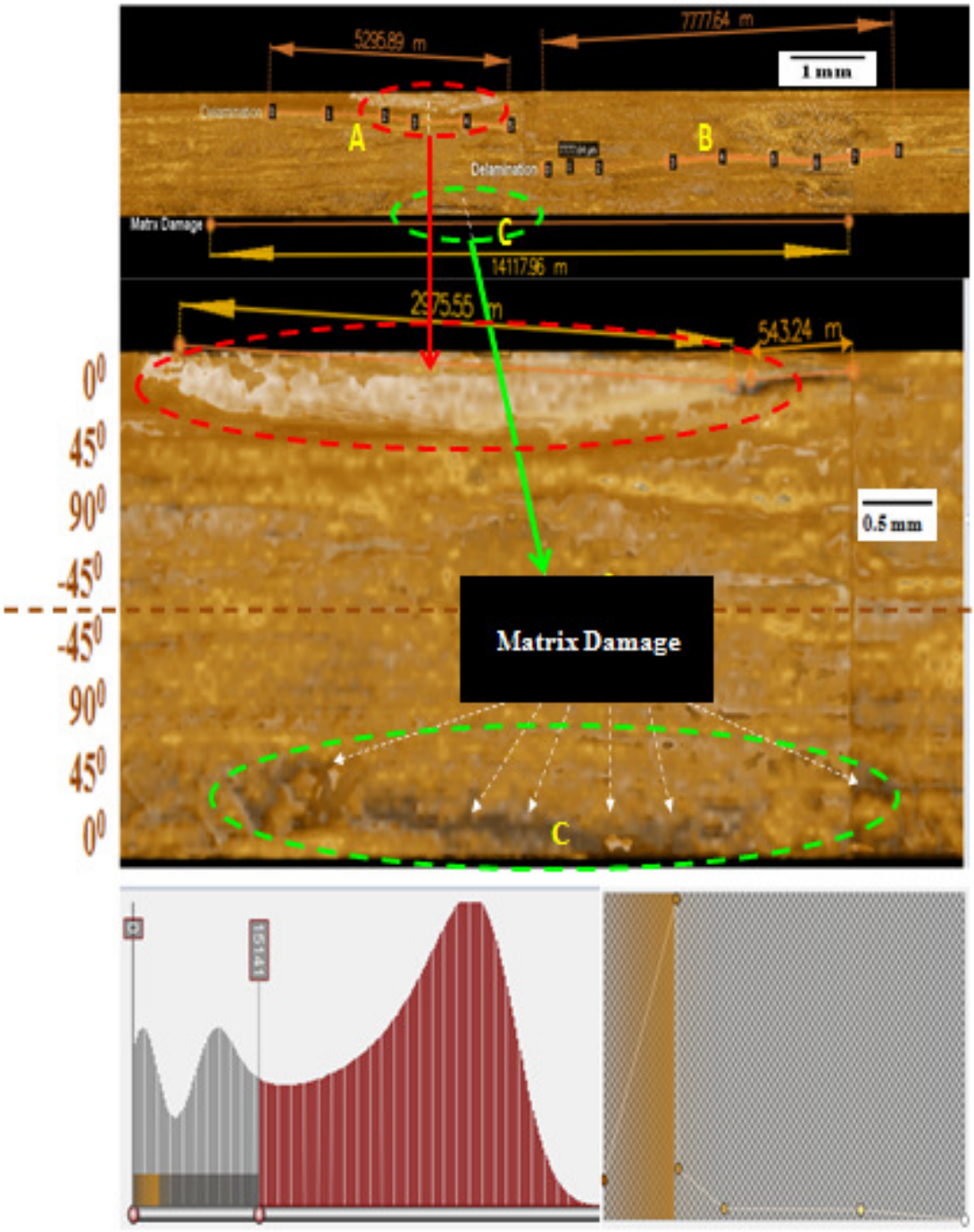

Figure 4.15 Matrix damage and delamination rendering for the near-edge 2J impact with 2mm thickness

4.4.2.6 Matrix Damage

Figure 4.16 shows the near-edge 2J impact damage with 4mm thickness. For path A the fibre is rendered then no fibre damage is observed but as we embed the matrix the matrix damage is observed as shown in path B in figure 4.16. The matrix damage path length is observed from number 0 to 8. As we can see from A and B that the path length is the same but the matrix/fibre rendering is the only difference. Thus damage is captured as we embed the matrix in the fibre bundle. The lower figure shows the isometric view of the 4mm thick laminate and shows that the fibre is embedded in the matrix. Profile data is captured showing high fluctuations which are due to the different areas having different absorption coefficients. The maximum value of the intensity is 14440 and the minimum value is 0.

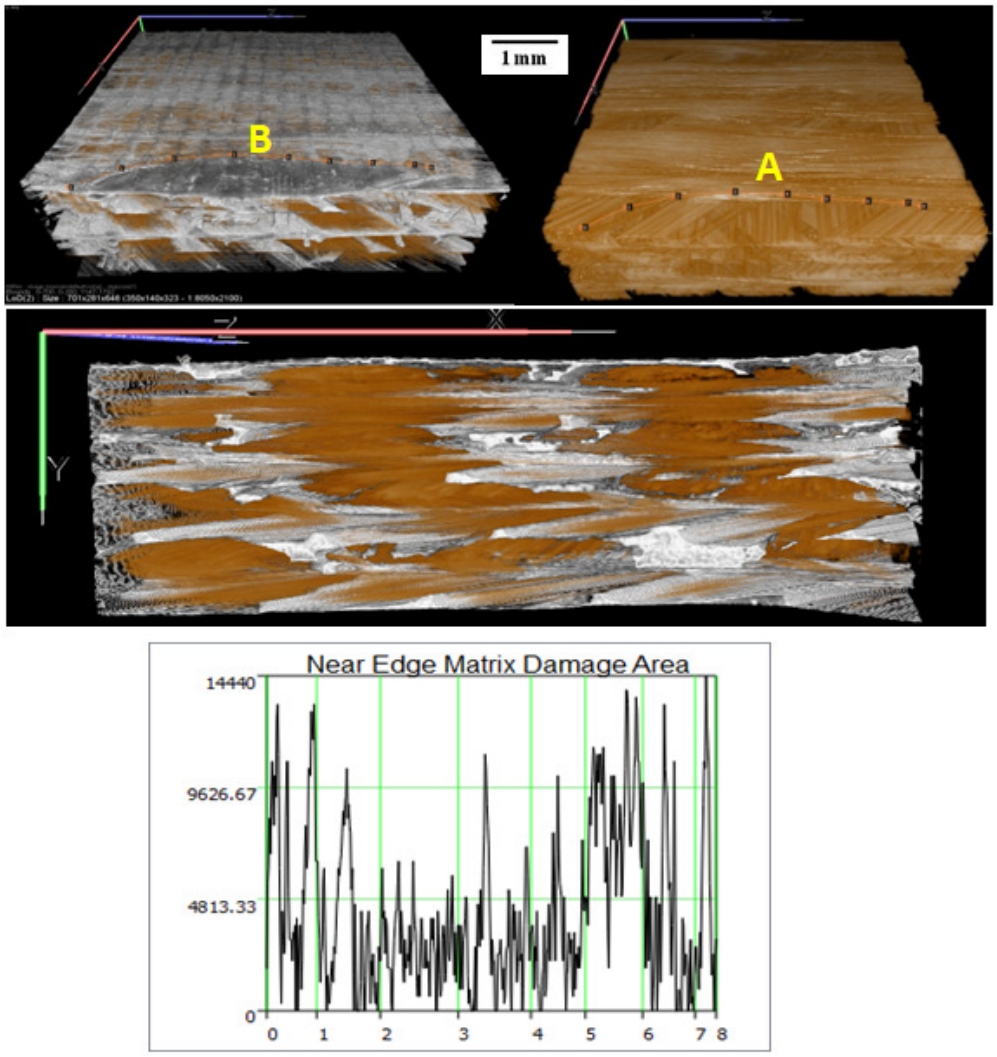

Figure 4.16 Near-edge impact 2J impacted with 4mm thickness-matrix damage with damage profile data

4.4.2.7 Matrix Damage Propagation

Figure 4.17 shows the near-edge impact with 4mm thickness. The behaviour is well captured. Path A shows that both the matrix and the fibre phases are embedded together and path B shows that no fibre cracks are observed. For path B the rendering shows that the underlying material is the fibre and the top layer is the matrix as can be observed from figure 4.17.

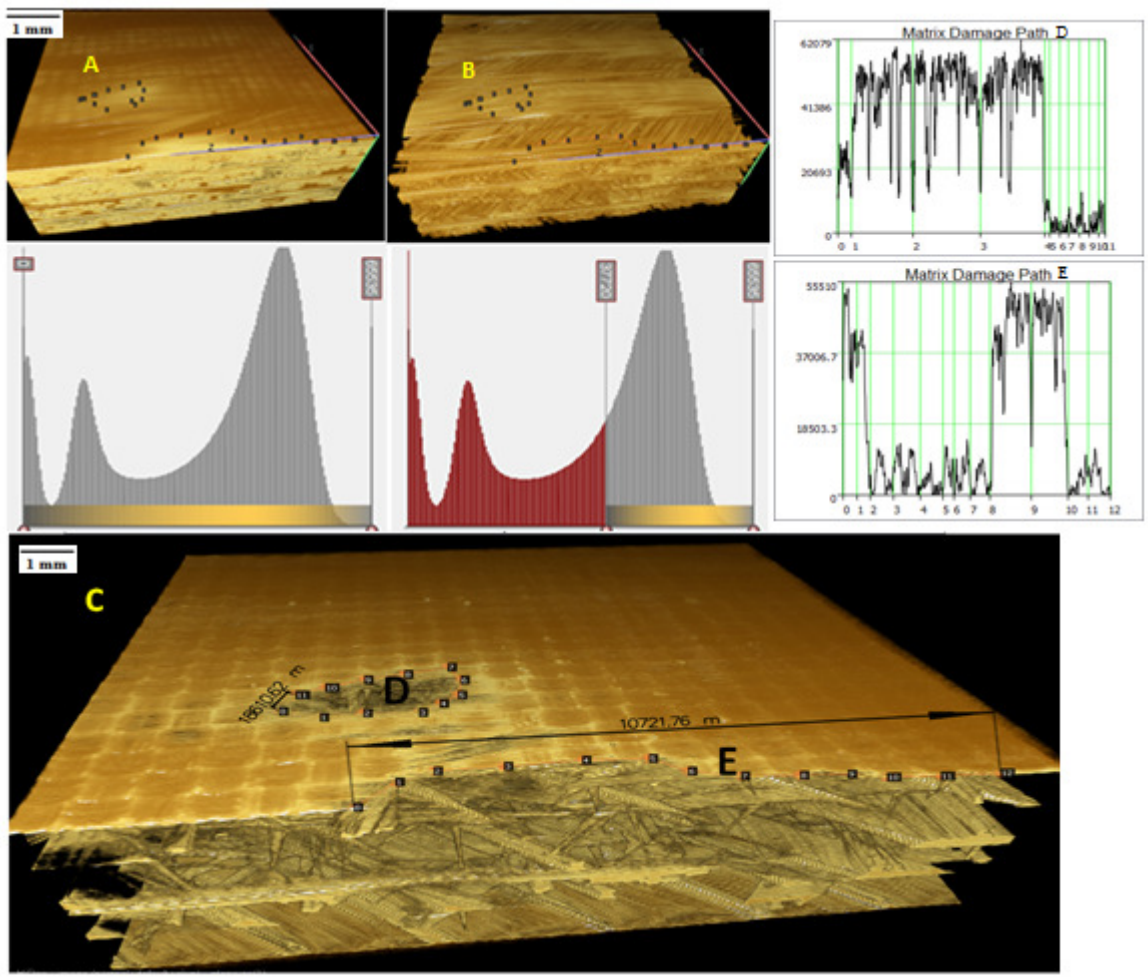

Figure 4.17 Near-edge 4J impact with 4mm thickness–matrix damage propagation

Thus at path A, although we can see the damage in pale yellow, we cannot figure out the exact nature of the damage while along path B no information about matrix behaviour is given. Picture C in figure 4.17 gives an accurate representation of matrix damage. Thus path D is defined from damage path number 0 to 11 and has the damage path length value of 18610.62 microns while path E is defined by the path number from 0 to 12 and has the damage path length value of 10722 microns. Along path E near-edge impact damage takes place and the damage progresses further to the area of path D where the matrix removal takes place. There is some matrix damage removal near the edge of the laminate. The matrix damage profile data is captured for the path E thus at points 2 to 8 we can see the value

approaching to zero indicating the matrix removal followed by points 10 to 12 while for path D the similar profile is observed from point 4 to 11 as shown in figure 4.17.

4.4.3 On-Edge Impact

4.4.3.1 Through Thickness Multiple Fibre/Matrix Damage Zone

Figure 4.18 shows the on-edge impacted with 4J with 2 mm thickness. During the on-edge impact damage the top ply bulges out and deplys from the other plies. Under this area fibre and matrix are crushing. Understanding the through thickness damage requires the section of the laminate to be cut into different sections in order to investigate the different types of damage that occur during edge impact. In order to study the underlying damage, the section is cut through-thickness from point A to B. The through-thickness behaviour is shown in figure 4.18.

Analysing this section will require two transfer functions. First transfer function will render matrix behaviour and the other transfer function will render fibre behaviour. This is done to capture different damage at the specific locations as shown in the histogram. The first histogram in figure 4.19 shows the matrix rendering which is done half way and the other is the fibre rendering which is fully done. For the histogram of matrix distribution, the matrix is only visible on the top plies and the fibres bundles are invisible in this region as seen in figure 4.19. This has been undertaken to understand the matrix distribution and the damage propagation during the on-edge impact. Matrix distribution is captured between points 0 to 9 (see figure 4.18 and 4.19) with the length of 8922 microns. The on-edge impact damage opening was captured with the shear matrix/fibre damage opening of 21.16^0. Similar behaviour, which has not been quantified, was observed for the 2J on-edge impact. Delamination opening is seen with the damage path length of 1494 microns. The fibre de-bonding is shown in figure 4.18 with de-bond length of 1113 microns. Shear failure was observed at angle of 45^0 to the direction of impact. Matrix crushing is seen at the point of contact and this will be discussed in more detail in the following section. For the matrix damage the pixel intensity has the value of approximately 10531 while for the delamination the pixel intensity has the value of 52346. Profile data clearly shows delamination is taking place at this point while matrix damage is taking place at the other point.

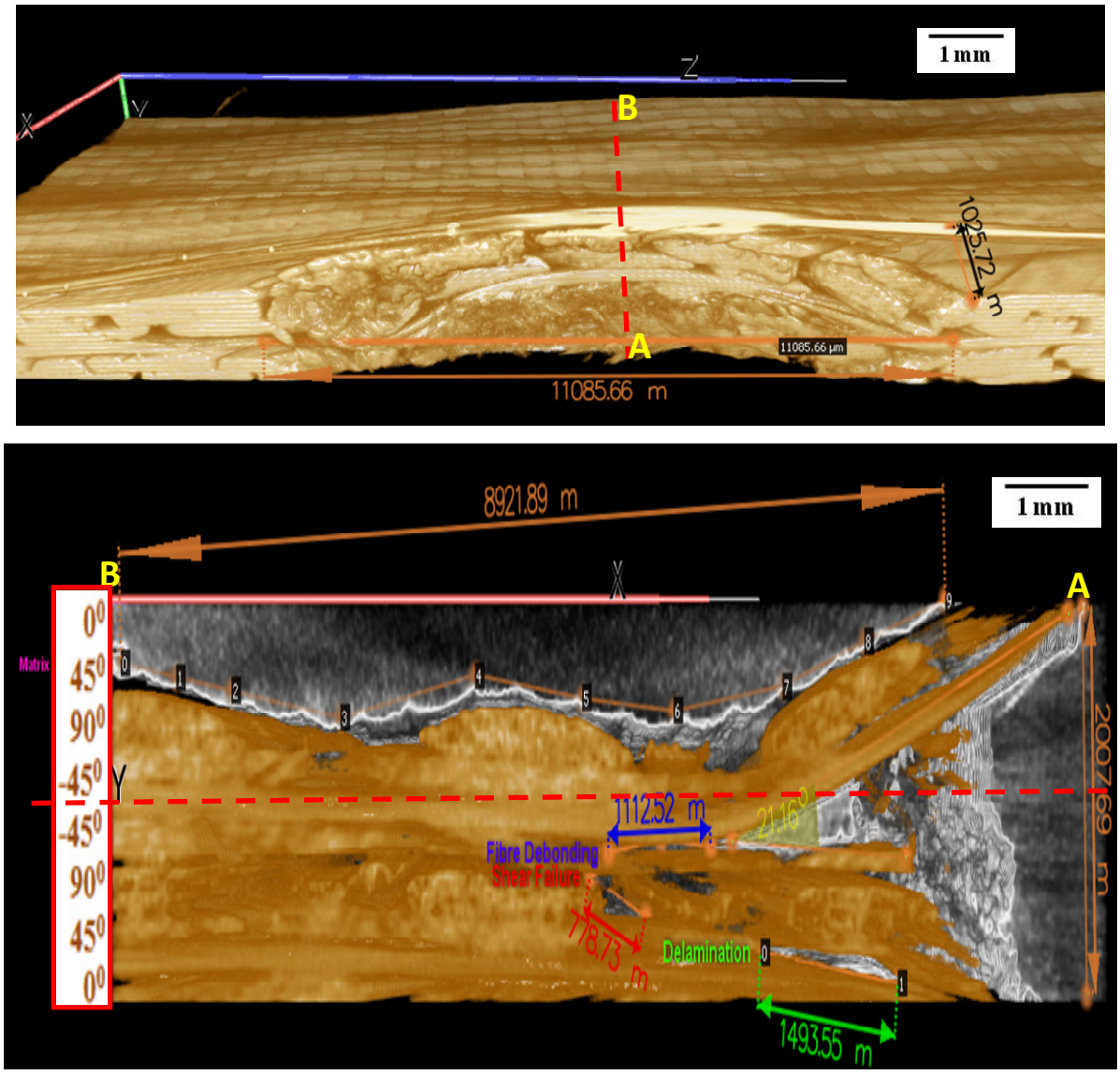

Figure 4.18 On-edge 4J impacted with 2mm thickness-through thickness multiple fibre/matrix damage zone

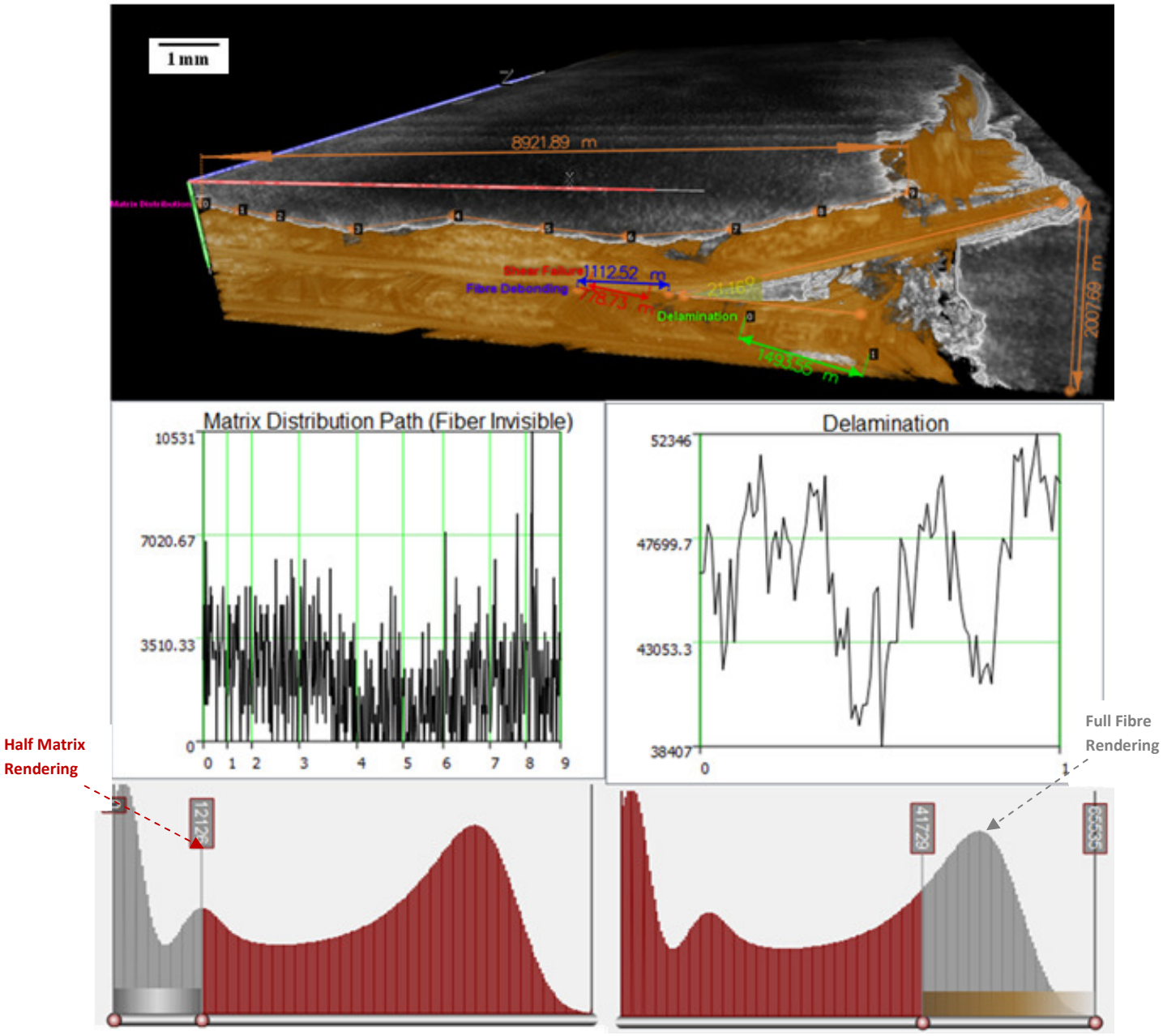

Figure 4.19 On-edge 4J impacted with 2mm thickness - different damage view and matrix distribution and embedded fibre histogram with profile data

4.4.3.2 Fibre/Matrix Fracture Zone

Figure 4.20 shows the front plies fibre and matrix fracture zone for the on-edge 4J impacted with thickness of 2 mm. The length of the matrix fracture is approximately around 13402 microns while for the fibre fracture zone length is approximately of 15805 microns. The fracture zone of matrix is much smaller than the fracture zone of the fibre. From the damage profile data it is clear that both types of fracture approaches the value of 0 around the middle of the profile indicating the removal of both the fibre and matrix around this area which is referred as an empty zone area. The maximum intensity value of the matrix zone is 47390 and for the fibre zone it is the much higher value of 56372.

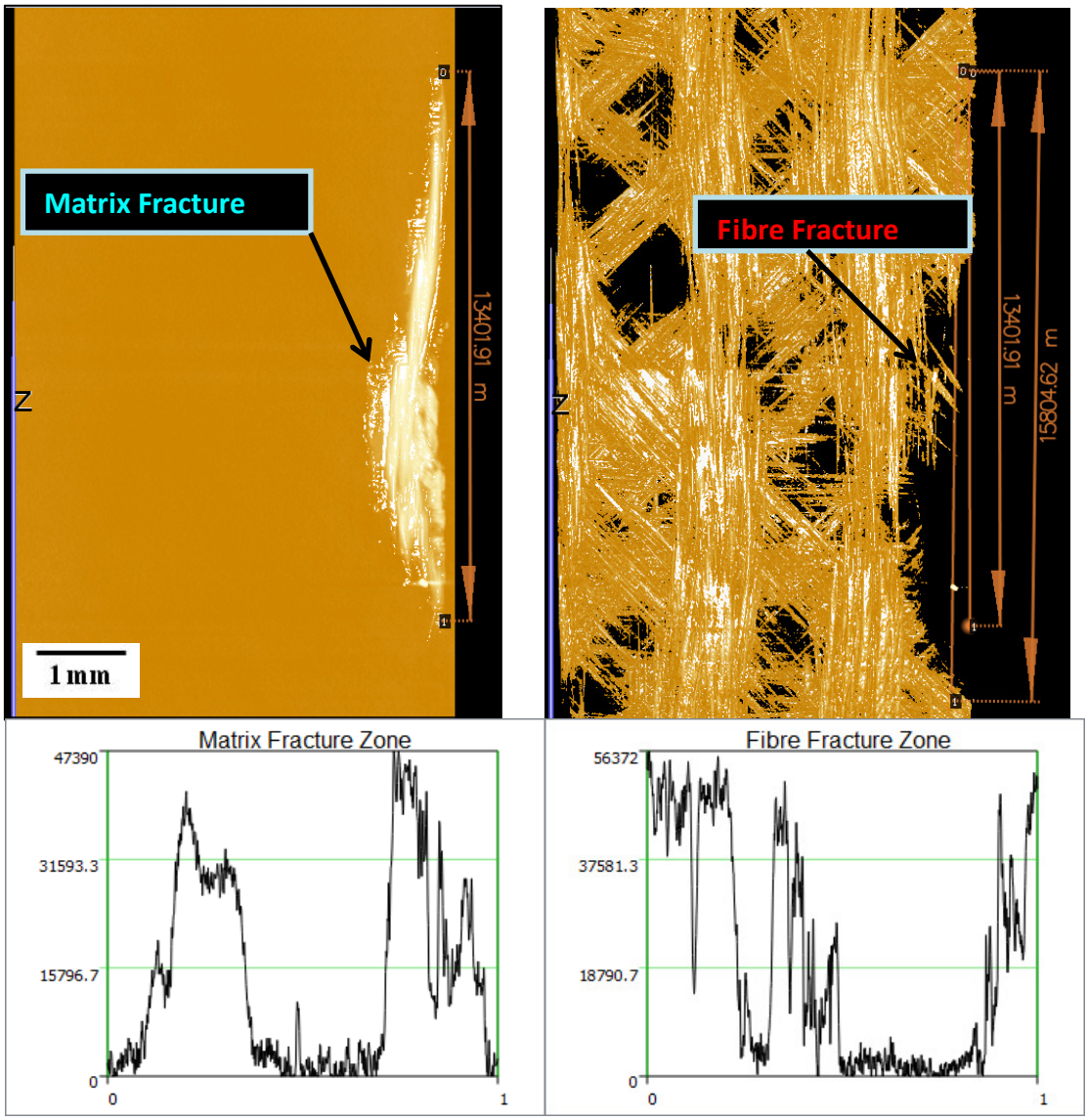

Figure 4.20 On-edge 4J impacted 2mm thickness-fracture fibre/matrix zone on the front plies

Along the profiles there is a zero phase indicating the removal of the matrix and fibre as the absorption coefficient is nearly zero at this point. Profile data helps to understand the behaviour of damage in detail. The profile values for fibre are always higher than the matrix due to the fact that every single fibre has different absorption coefficient and inhomogeneous state while matrix has a more homogenous state and thus low values are captured.

The bottom or the back plies have 0^0 and 45^0 plies removed around this area and is left with the 90^0 ply as shown in figure 4.21. Path A shows the bundle fibre damage path length with value of 12335 microns while the path B shows the crushed matrix damage path length with the value of 10754 microns. Profile data clearly shows that the damaged fibre bundle has the maximum intensity value of 54204. Between points 7 to 8 no fibre is present and matrix damage dominates as the value of the intensity approaches zero. The crushed matrix has the maximum value of 46770 and high frequency peaks are seen in this range due to matrix and fibre crushing behaviour.

Two transfer functions are used. The green colour shows the fibre rendering and the yellow colour shows the matrix rendering. The opacity levels are adjusted accordingly to capture the on-edge impact fracture damage data as shown in figure 4.21. The on-edge impact causes misalignment of the surface fibres and matrix crushing. Many fibres are broken to a considerable depth under the impactor. The misalignment caused by the impactor is expected to be always greater than any inherent fibre misalignment.

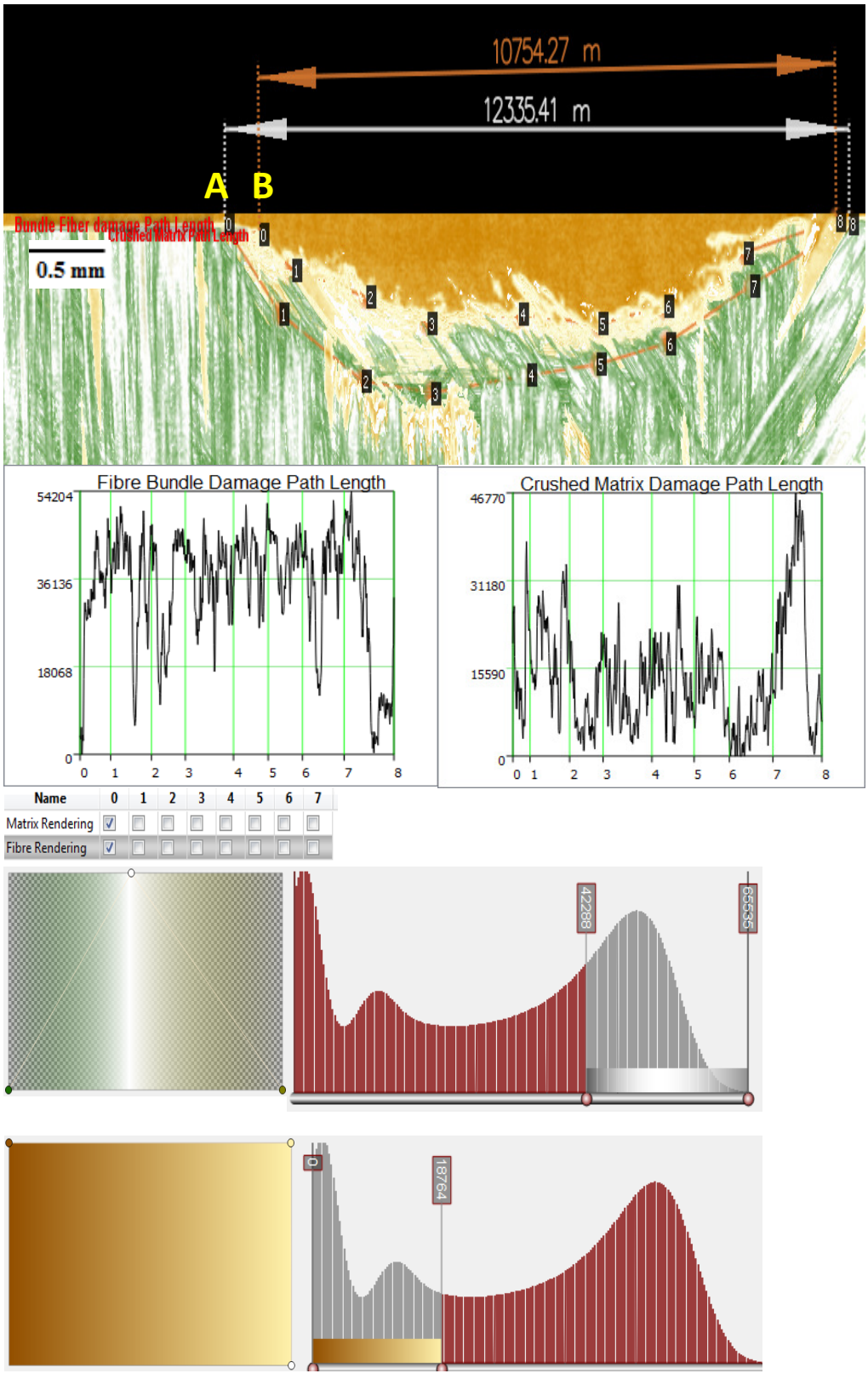

Figure 4.21 On-edge 4J impacted 2mm thickness-fracture fibre/matrix zone on the back plies with the transfer functions and opacity levels

4.5 Conclusions

For the near-edge impact fibre fracture is observed for the top 0^0 ply for the two tows nearest the edge. Further fibre fracture then occurs on the $+45^0$ ply. Delamination is most found at the $0^0/45^0$ interface and at the mid-section of the laminate, at the peak value of shear stress arising from the bending. For the on-edge impact, fibre fracture is observed through the entire thickness at the point of impact. Further fibre fractures in the 45^0 plies are observed throughout the area of examination. The amount of fibre fracture is far higher for the on-edge impact. Matrix damage for the on-edge impact is confined to a small area around the point of impact. Matrix damage for the near-edge impact is observed throughout the area of examination. This matrix damage leads to the growth of delaminations. The amount of matrix damage is far higher for the near-edge impact.

The same damage mechanisms are observed for on-edge impact for 2J and 4J impact energy, but with increasing severity at the higher energy level. At the higher energy level fibre/matrix crushing is observed, while at the lower energy level there is less crushing but more delaminations. Increasing the energy level for on-edge impact would probably lead to a similar trend, with more fibre/matrix crushing and less delamination. There is insufficient data from this study to produce a damage map but this data could contribute to future production of a damage map for on-edge impact.

This research can be compared with the other literature where similar damage mechanisms were observed under different impact conditions. Ullah et al (2012) investigated transversely fractured specimens of glass fibre reinforced polymers (GFRP) using computed tomography. These fractured specimen images were reconstructed in images in both 2D and 3D. Inter-ply and intra-ply damage at various locations across its width were extracted. Tomographic 3D images were used to detect laminate cracks and damages. Matrix cracks were developed first followed by delaminations and tow debonding; a similar pattern was observed in near-edge impact. Research by Ullah et al (2011) showed that the delaminations normally appeared near the matrix cracks area, which suggested that the formation of the cracks initiated delamination, similar to the observations for near-edge impact.

Later, Ullah et al (2014) investigated the damage behaviour of fabric-reinforced composites under dynamic bending using micro-CT scanning. Reconstructed 3D images of the carbon

fibre reinforced polymers (CFRP) specimens under bending and impact were investigated. Matrix cracks, delaminations and tow debonding were the primary damage modes that were detected at the specimen's impact location, whereas at the bending location, these modes were coupled with fibre fracture. Similar observations were observed in on-edge impact experiments where specimens suffered both matrix cracks, delaminations coupled with fibre fracture (Ullah et al 2014), as observed in this work.

Perret et al (2012) investigated an aircraft composite fuselage structure subjected to a compressive load. X-ray computed tomography was utilised to investigate the failure mechanisms during buckling test of a composite fuselage. At some locations no delaminations were detected while at other locations some delaminations were initiated and some of them were found to be fully delaminated. Similar damage mechanisms have been observed in this work for both the near-edge and on-edge impact where delaminations could be detected for both the on-edge and near-edge impact. For near-edge impact the delaminations were confined under the area of the impactor but some delaminations were invisible, whereas the delaminations were observed clearly around the area of on-edge impact.

Chapter 5

Residual Properties of Glass/Epoxy Laminate subjected to On-edge, Near-edge and Centre Impact

5.1 Introduction - Aim and Objectives

Impact damage has an adverse effect on the residual compressive strength and overall damage tolerance of composite structures. Impact reduces the residual strength/stiffness of composite structures and introduces several design problems. Results showed in the previous chapters indicate that the impacts on the edge of the laminate may lead to more severe damage than impact on the laminate plane. The presence of delamination can adversely affect the residual strength of the composite laminate. In this chapter the residual strength and failure mechanisms of the composite laminates subjected to compression and tension after impact will be investigated. The objective of this testing was to test the hypothesis that the different modes of testing would reveal the different failure mechanisms that had occurred for the different impact locations.

5.2 Compression after impact (CAI) - Centre, Near-edge and On-edge impact

5.2.1 Experimental Details

5.2.1.1 Compression After Edge Impact Testing Machine

Compression after impact tests were conducted on Instron 6025 mechanical test machine. For strength determination a load cell of 100kN was used with crosshead speed of 0.5mm/min. The CAI test set-up is shown in figure 5.1 (a) and (b).

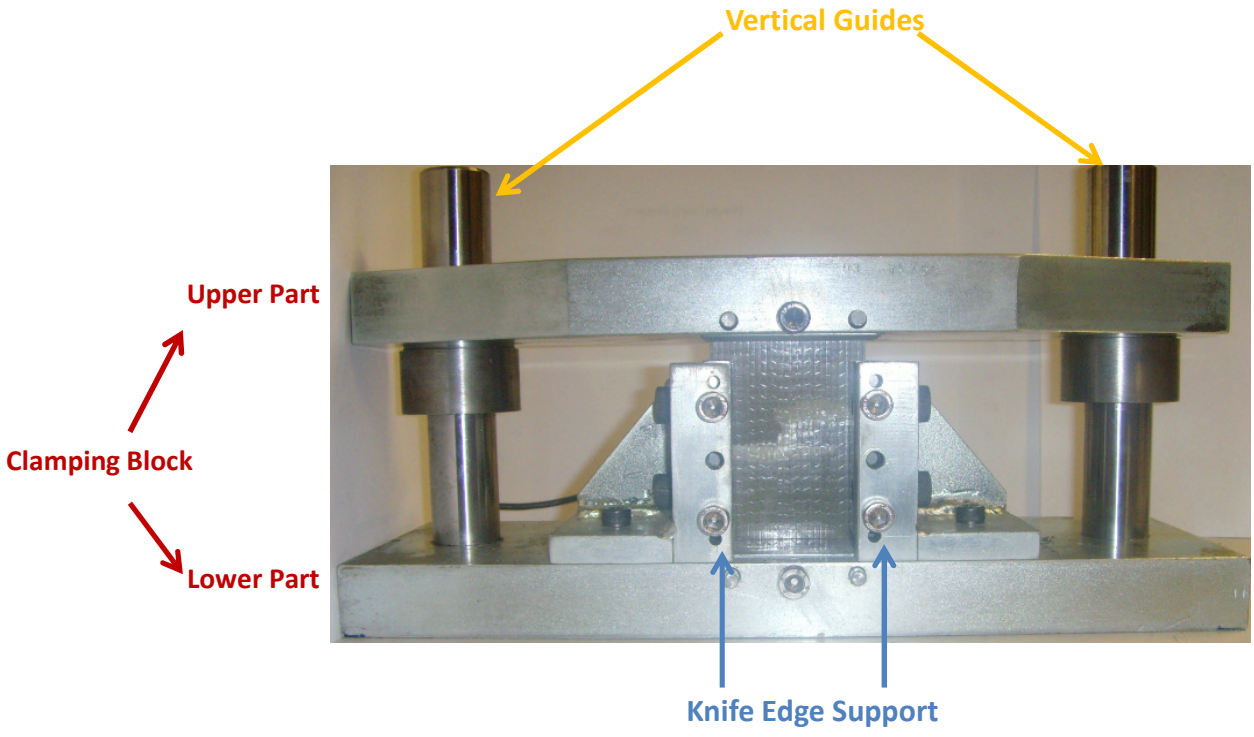

(a)

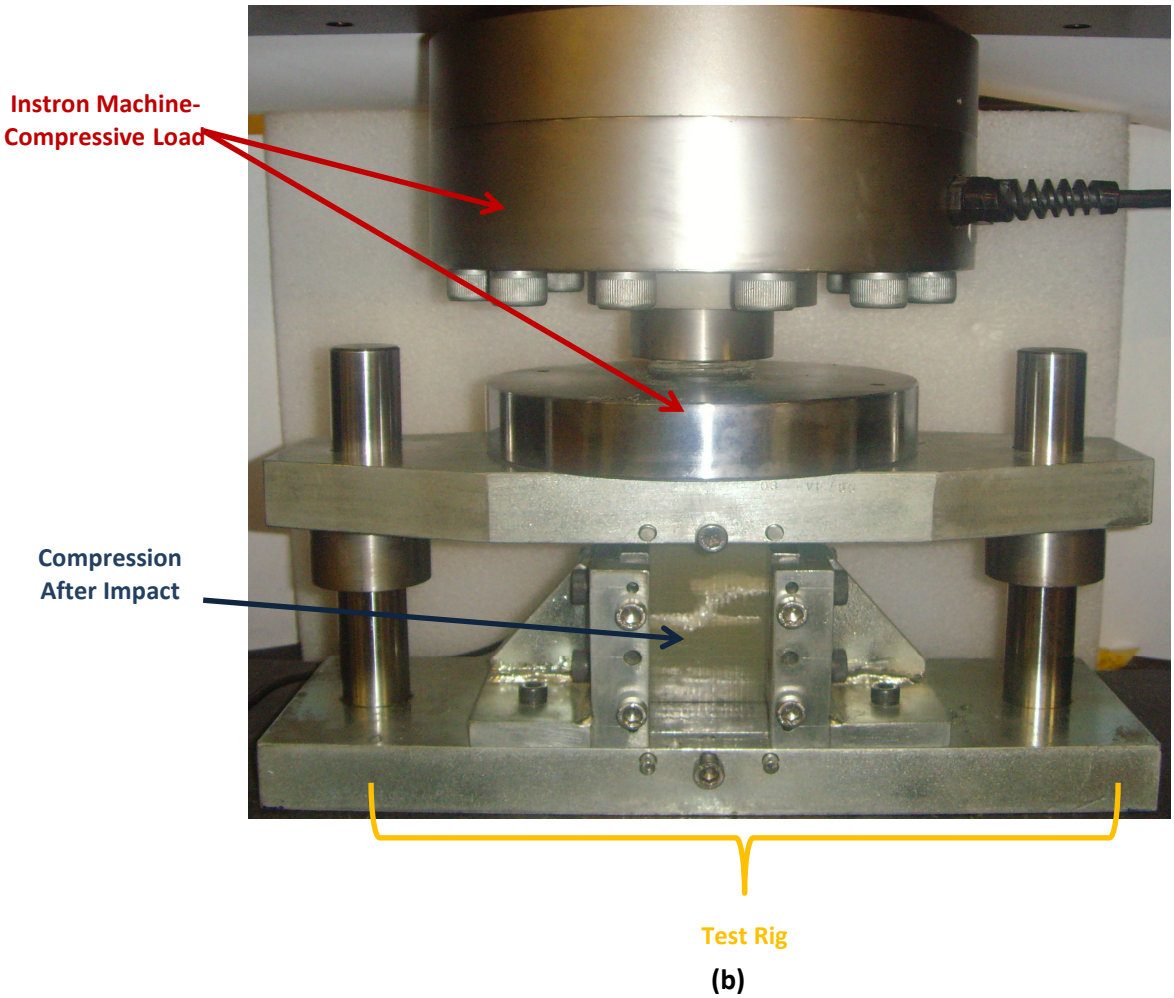

Figure 5.1 Compression after impact test rigs (a) CAI test rigs and fixtures (b) Compressive load on impacted test specimen

The QMUL fixture was developed by Hogg et al (1992). This fixture required further design changes such that the CAI experiments could be performed for laminates after edge impact. The new design allowed both thin and thick laminates to be tested. The specimen is clamped on the top and bottom undamaged ends.

5.2.1.2 Specimen Boundary Conditions

Boundary conditions were changed due to the nature of the edge impacted specimen. Anti-buckling guides were placed either side of the damage as shown in Figure 5.2. The specimen in-plane dimensions were kept the same at 55 mm by 89 mm.

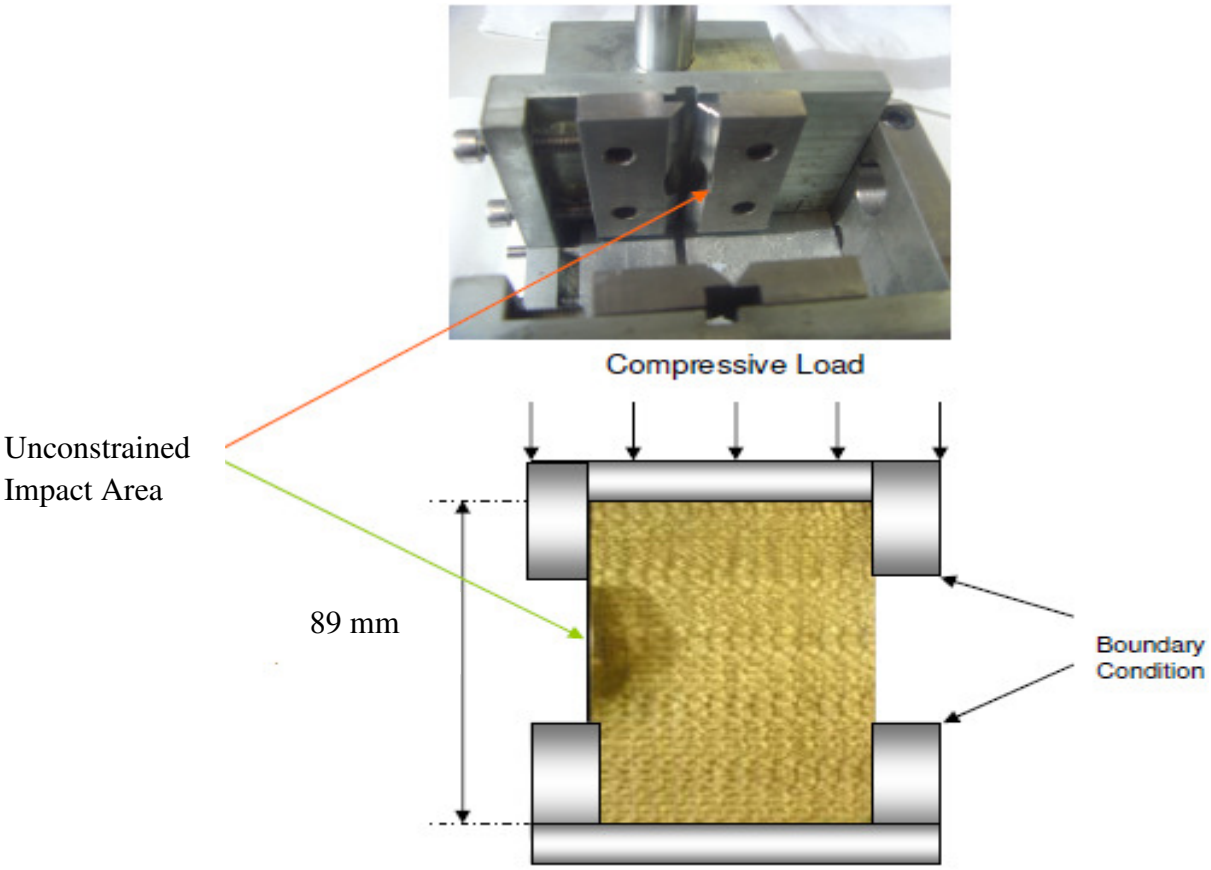

Figure 5.2 Constrained and unconstrained areas for edge impact

Specimens must be aligned properly in the vertical direction in order to prevent any bending and out-of-plane buckling.

5.2.1.3 Testing Parameters

Compressive tests were carried out at a constant crosshead-displacement rate of 0.5 mm/min. Three tests for each laminate impacted with centre, near and on-edge impact for both values of thickness and varying values of impact energy. Three non-impacted specimens were also tested. CAI machine calculates the force-time curve for each test. The maximum residual strength of the specimen can then be obtained by:

$$\sigma_c = \frac{F_{\max}}{w \times h} \tag{5.1}$$

Where σ_c is the ultimate compressive residual strength (MPa), $F_{\max}$ is the maximum force prior to failure (N), w is the width of the specimen (mm) and h is the thickness of the specimen (mm).

5.2.2 Results and Discussions

5.2.2.1 Effect of Compressive Load-Displacement

The compressive load-displacement is defined here as the maximum compressive load reached at a specific displacement. Thus figure 5.3 (a) and (b) show the comparison of load-displacement curves for the different incident energy levels from 1 to 5J for the different types of impact. It can be seen from figure 5.3 that the thin and thick laminates show different trends for compressive load with respect to displacement for centre, near and on-edge impacted specimens. The compressive load reaches its maximum value and the specimen is buckled under higher compressive load in all cases. Centre and near-edge impacts in figure 5.3 show less variation in compressive load at different energy levels as compared to on-edge impact.

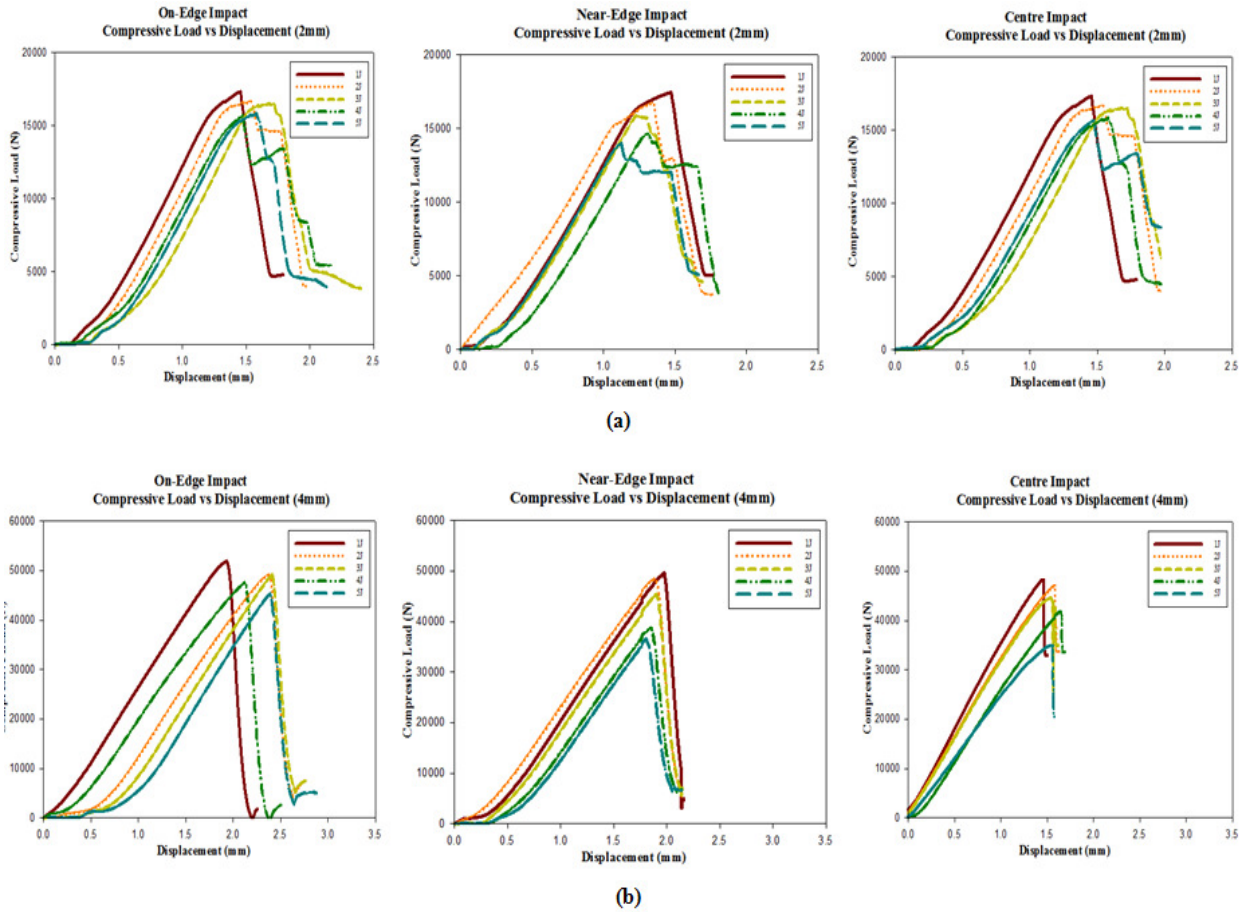

Figure 5.3 Comparison of compressive load vs displacement of composite laminates subjected to on-edge, near-edge and centre impact at various impact energies (a) Thin laminates (b) Thick laminates

The results shown in figure 5.3 are the representation of a single data specimen, which is the mid-range response for that condition. It provides useful information regarding how specimens behave for varying impact energy levels with respect to thickness and under different types of impact.

5.2.2.2 Effect of Thickness

Peak failure load is measured as the maximum compressive load sustained by a damaged specimen. Beyond these limits, the specimens buckle under compressive load. Figure 5.4 shows the comparison of failure loads as a function of various incident impact energies subjected to on-edge, near-edge and centre impacts. The thin laminates show different trends as compared to thick laminates.

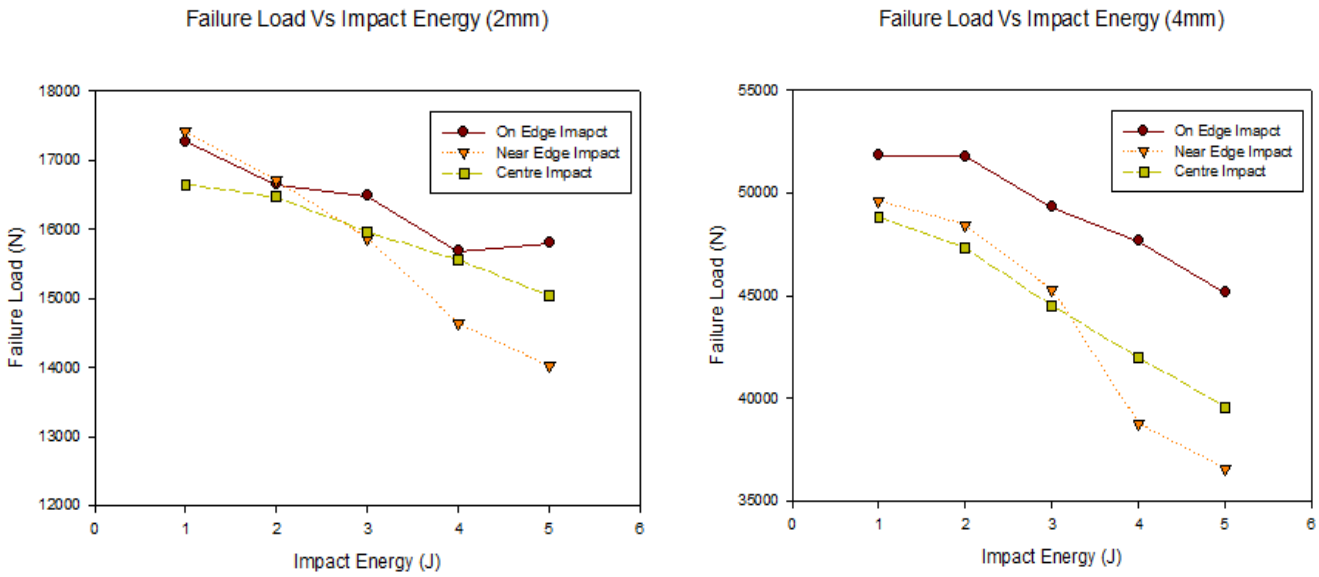

(a) (b)

Figure 5.4 Comparison of failure load vs impact energy of composite laminates subjected to on-edge, near-edge and centre impact at various impact energies (a) Thin laminates (b) Thick laminates

Incident Energy Level (J)	Peak Failure Load (N)					
	Thin Laminate (2mm)			Thick Laminate (4mm)		
	On-edge Impact	Near-edge Impact	Centre Impact	On-edge Impact	Near-edge Impact	Centre Impact
1J	17273	17414	16652	51825	49642	48830
2J	16654	16710	16469	51799	48467	47318
3J	16490	15870	15959	49305	45329	44517
4J	15681	14639	15557	47688	38789	42002
5J	15803	14019	15044	45162	36599	39590
% Reduction	8.5	19.5	9.7	12.9	26.3	18.9

Table 5.1 Peak load for thin and thick laminates

The trends for low impact velocity and thin laminates are hard to deduce due to the experimental difficulties. The results for the thick laminates show clearer trends. All values of failure load are higher for the on-edge impact. The values for the near-edge and centre impact cross over at 3J, for both thin and thick laminates. At lower impact energy levels, the centre impact has a higher area of damage. Thus the residual strength is lower than for the near-edge impact. At higher energy impact, above about 3J, the near-edge impact zone approaches the boundary conditions, causing more damage with the reflection of surface waves. Thus the percentage reduction in failure load over the whole impact energy range is highest for the near-edge impact as shown in table 5.1.

The effect of thickness is clearly seen from comparing values shown in table 5.1. All values of failure load for the thick laminate are around three times the corresponding value for thin laminates. The values of percentage reduction for the thick laminate are around 50% greater than the values for the thin laminate for on-edge and near-edge impact, but around double for centre impact.

5.2.2.3 Normalised residual strength

Normalised residual strength provides us the information of the load bearing capacity of composite laminate during impact and without impact. Normalised strength is the ratio between the average strength of the damaged specimen divided by that of the undamaged specimens during compression after impact tests. Figure 5.5 shows the normalised strength of the composite laminates during buckling with the various types of impact and all laminates undergo increased reduction in residual compressive strength at higher energy levels irrespective of thickness. Marked difference in the residual strength of near-edge impact is

seen when we double the thickness at energy level from 3J to 5J. At impact energy of 5J, the reductions in the compressive residual strength in near-edge impacted laminate for thin and thick laminate are approximately 26% and 35% respectively, while for centre impact it is 21.5% and 30.5% respectively and finally for on-edge impact it is 17.5% and 20 % respectively. However, at initial stage of lower energy levels at 1J all the residual compressive strengths lie between 10% to 15% in both cases of thin and thick laminates.

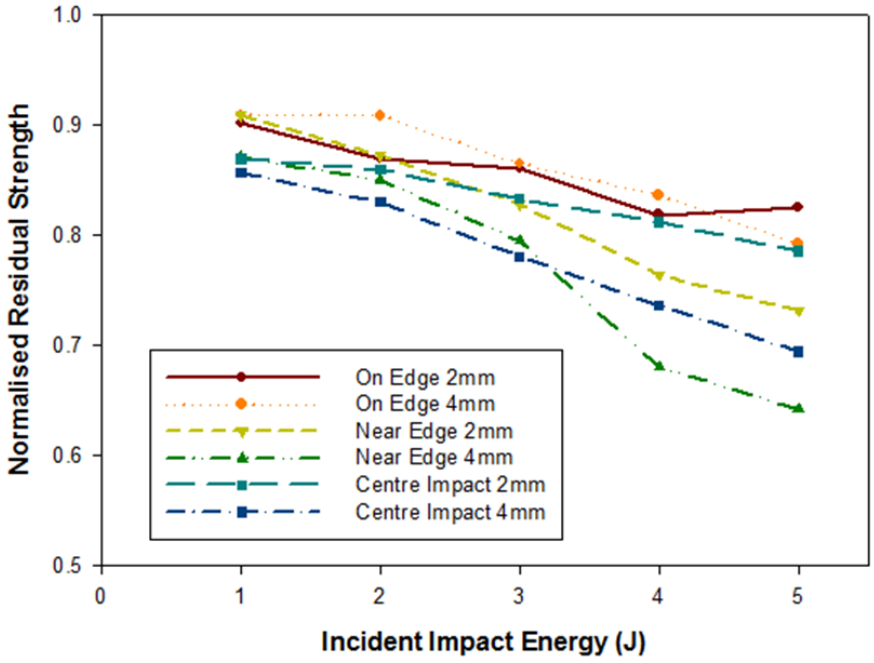

Figure 5.5 Normalised residual strength vs incident impact energy

The near-edge impacted laminate shows the greatest reduction of the normalised strength followed by centre impact and on-edge impacted specimens in both cases of thickness. The compressive damage progression of near-edge impacted specimen is governed by the bending deformation thus creates a ground for the initiation of the delaminations. The delamination is initiated when the impact force reaches critical value (Syr et al 2003). Delaminations in near-edge impacts occur just below the contact area of the impactor (see figure 4.12). Fewer delaminations are seen in the centre impacted specimen because of the damage controlled by the material boundary conditions (Reis et al 1997). Thus the initiation of delamination at low energy level creates interlaminar matrix cracks in upper plies (Aymerich et al 2007). This matrix cracking in the upper plies is thought to be caused by contact stresses during near-edge impact. With the increasing incident impact energies larger delaminations start developing and reside at the plies interface of the near-edge impacted specimen (Abrate

1998). During buckling composite laminate reduces its residual strength and increases shear cracking and enhance the growth of the delamination (Sanchez-Saez et al 2008). Interlaminar shear and tensile matrix cracks start spreading in the different plies and at the interface of near-edge impacted specimen. Thus during near-edge impact shear matrix cracks develop at the boundaries of the contact area between the impactor and laminate and causing shear deformation (de Freitas et al 2000). However thicker laminates show similar trends but greater resistance to the buckling because of the smaller damage area and higher stiffness of the composite laminate due to its increased thickness.

5.2.2.4 Damage assessment

The specimen geometry, loading conditions and damage width significantly affects the impact response in CAI tests of the composite laminates. Figure 5.6 (a)-(b) shows the side view of near and on-edge impacts at 5J and 3J for thin and thick laminate.

Figures 5.6 (a) show the compression after near-edge impact for thin and thick laminates. The effect of thickness can be clearly seen under compression in the near-edge impact; as the thickness is doubled the damage is also almost doubled. Near-edge impact area is shown for both thin and thick laminates. For the thin laminate just under this area the damage becomes narrower and further damage initiation starts under compression followed by the damage propagation. As the damage progresses further the shear damage starts developing and starts expanding toward the bottom of the laminate while for the thick laminate more extensive shear damage is seen under compression as shown in figure 5.6 (a).

Figures 5.6 (b) shows the compression after on-edge impact for thin and thick laminates. Also the effect of thickness can be clearly seen under compression in the on-edge impact; as the thickness is doubled the damage is also almost doubled. For the thin laminate just under the impact area the damage becomes very streamlined and progresses further under compression leading to more extensive damage. For the thick laminate the damage is more intensive and streamlined but damage has become double that of the thin laminate as shown in figure 5.6 (b).

The magnitude and intensity of the damage are different for the directions of impact. The impact damage zone is more intense for on-edge impact (see chapter 3 for more details). For near-edge impact, the impact damage leads to matrix cracks and multiple delaminations.

Under compressive load this damage propagates through the matrix cracks leading to further delaminations through the thickness. For on-edge impact, the impact damage causes more fibre failure across the whole thickness. Under compressive load this damage propagates at a high rate in a more streamlined manner. Near-edge impacted laminates fail through global buckling centred on the damaged zone. On-edge impacted laminates fail in a brittle manner from the growth of the damage.

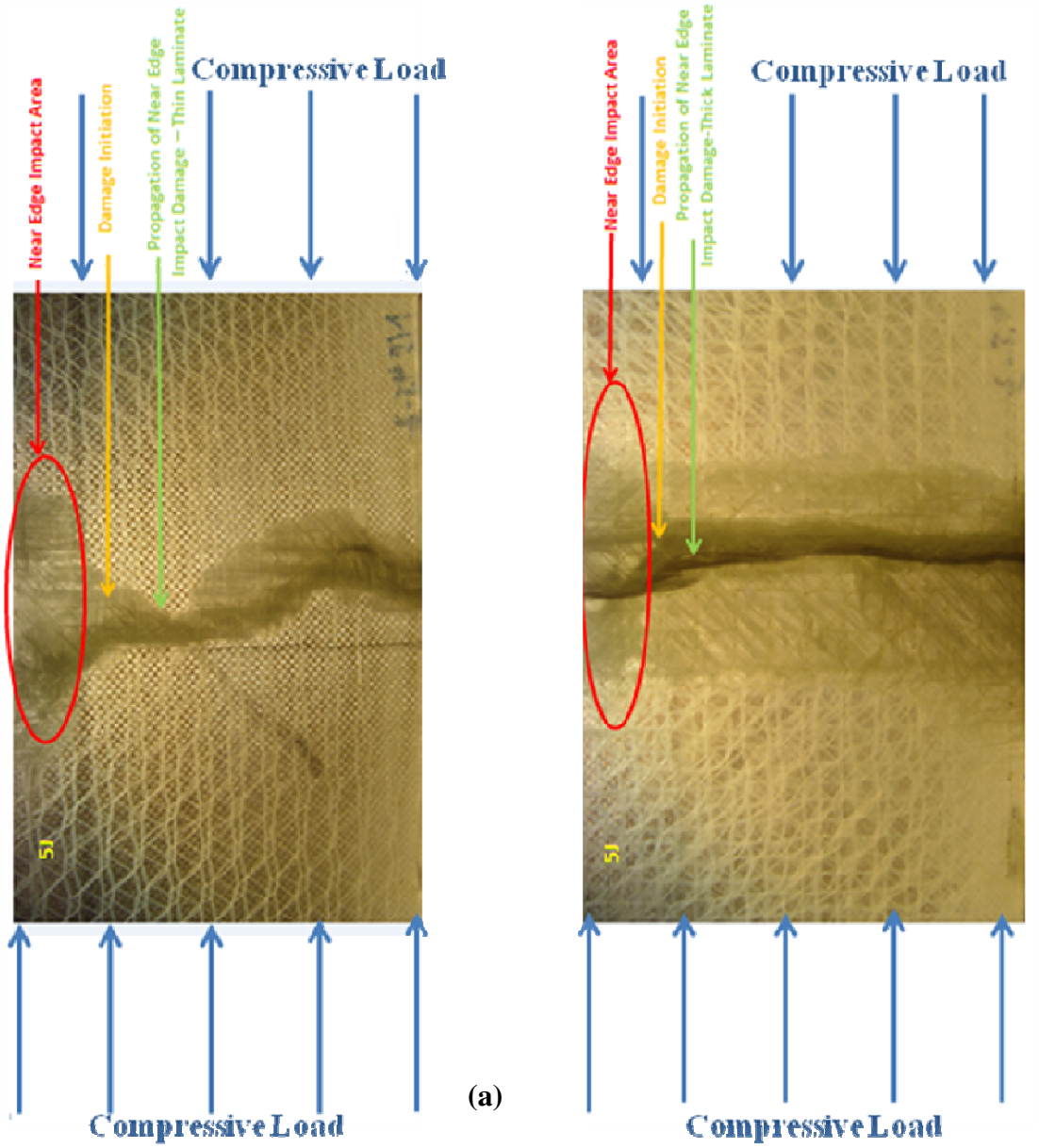

(a)

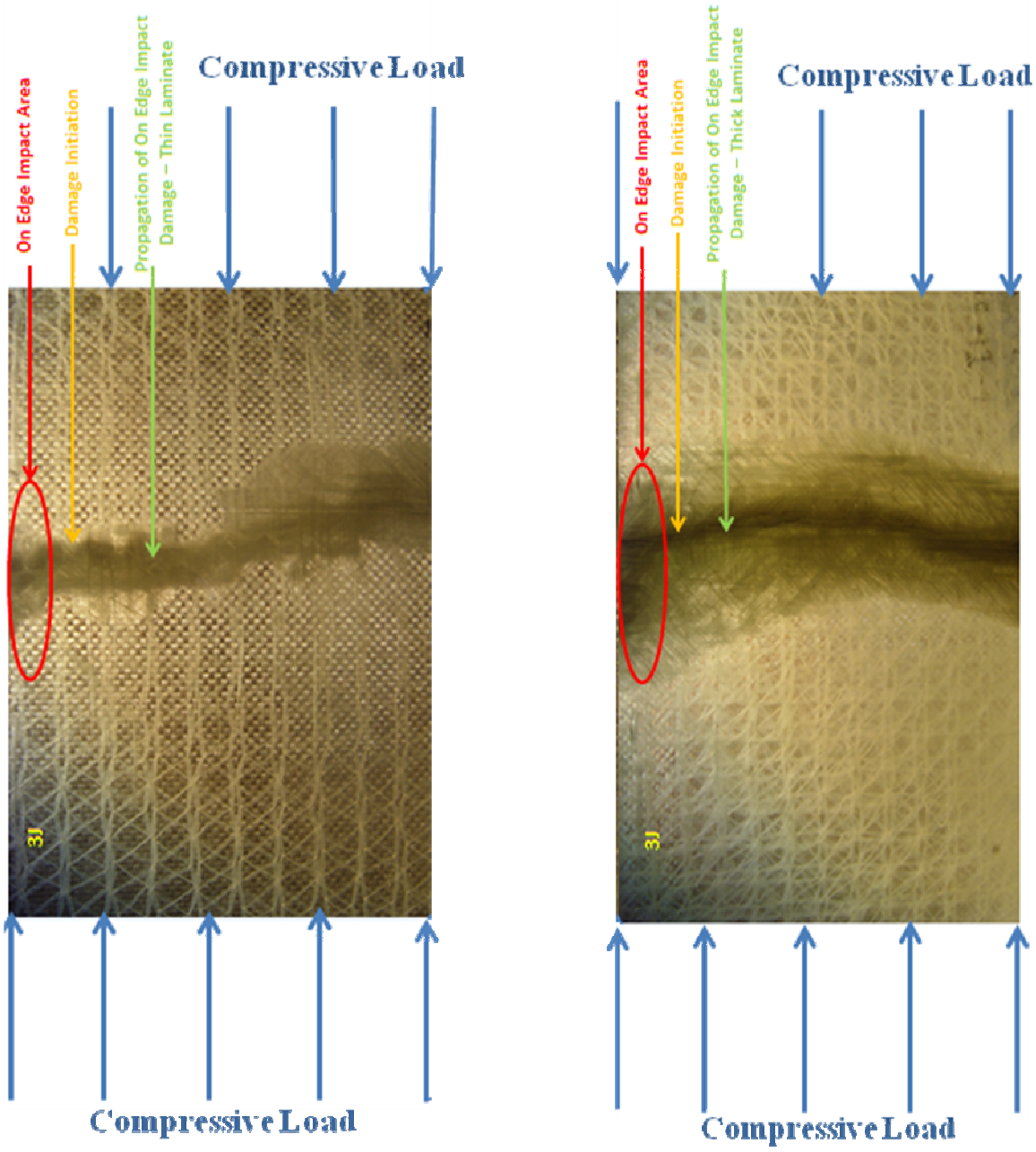

(b)

Figure 5.6 Damage side view of near-edge and on-edge compression after impact at 4J a) Near-edge impact thin and thick laminate b) On-edge impact thin and thick laminate

5.3 Tension after impact (TAI) - Centre, Near and On-edge impact

5.3.1 Experimental Details

5.3.1.1 Tensile Testing Machine

Tensions after Impact (TAI) tests were conducted to investigate residual tensile strength after impact damage, using an Instron 6025 mechanical test machine. For strength determination a load cell of 100kN was used with crosshead speed of 0.1mm/min. The TAI test set-up is shown in figure 5.7.

Figure 5.7 Tension after impact test experiment set-up

5.3.1.2 Specimen Preparation and Boundary Conditions

To conduct TAI tests, specimens are placed in the tensile testing machine. The specimens are loaded step by step up to failure loads in axial direction. The load-deflection curve is detected by the inbuilt software as the test is progressed and data is collected in the PC attached with the test machine. The area of the damage zone was unconstrained. Thus the 89 × 55 mm^2 specimens were cut with a diamond saw and the dimensions were reduced to 89 × 25 mm^2 (see figure 5.8 (b)). Undamaged specimens were also cut to the same dimensions. This width was required to allow testing. The damage width was always less than 20 mm (for more details please see chapter 3). The tabs were bonded to the specimen with an epoxy resin. The test specimens are firmly gripped with jaws of the tensile machine which ensure uniform tightening on the tabs during the tensile test. In order to avoid slipping between tabs and jaws

of the machine slower crosshead speed of 0.1 mm/min was used as shown in figure 5.8 (a). The tabs edges were completely fixed, and tensile load was applied in plane direction.

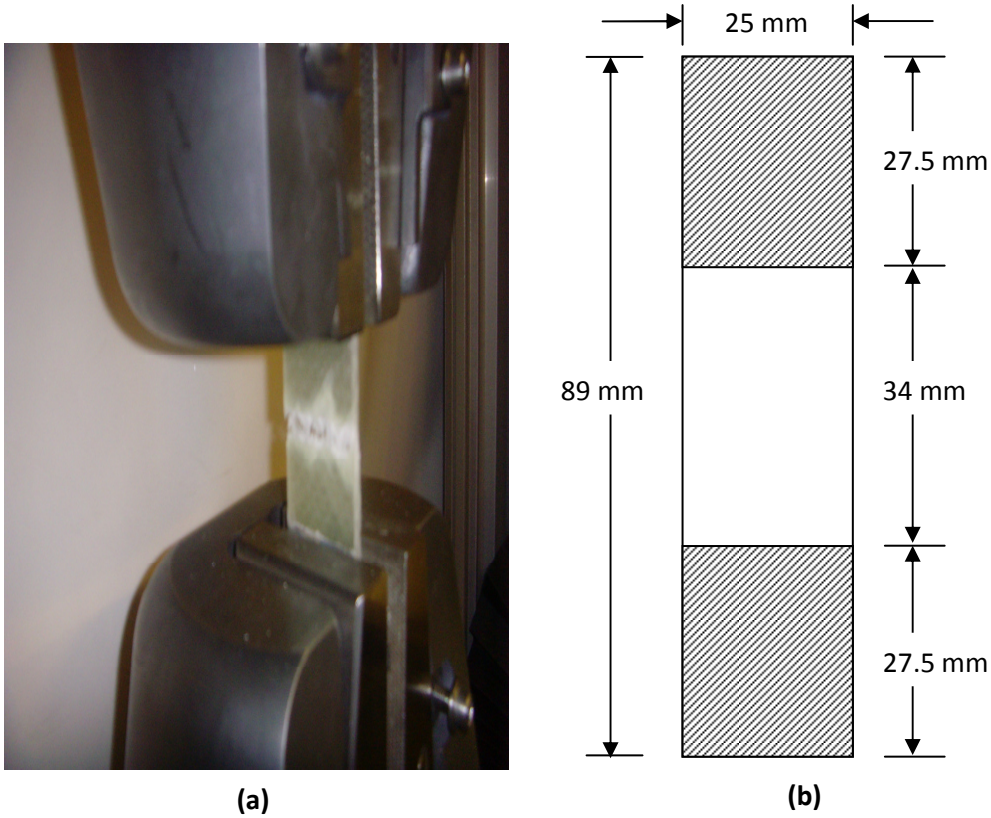

Figure 5.8 Tension after impact test rigs (a) TAI gripping jaw (b) Specimen dimensions

5.3.2 Results and Discussions

5.3.2.1 Effect of Tensile Load-Displacement Curve and Thickness

Tensile strength is measured as the maximum tensile strength sustained by undamaged and damaged specimen with respect to % strain. Figure 5.9 shows tensile strength of thin laminates at energy levels at 2J with respect to % strain for near-edge, on-edge and centre impact composite laminates. It is important to note that the strain values are inaccurate since slipping occurred in the grips. Thus stiffness cannot be reliably compared.

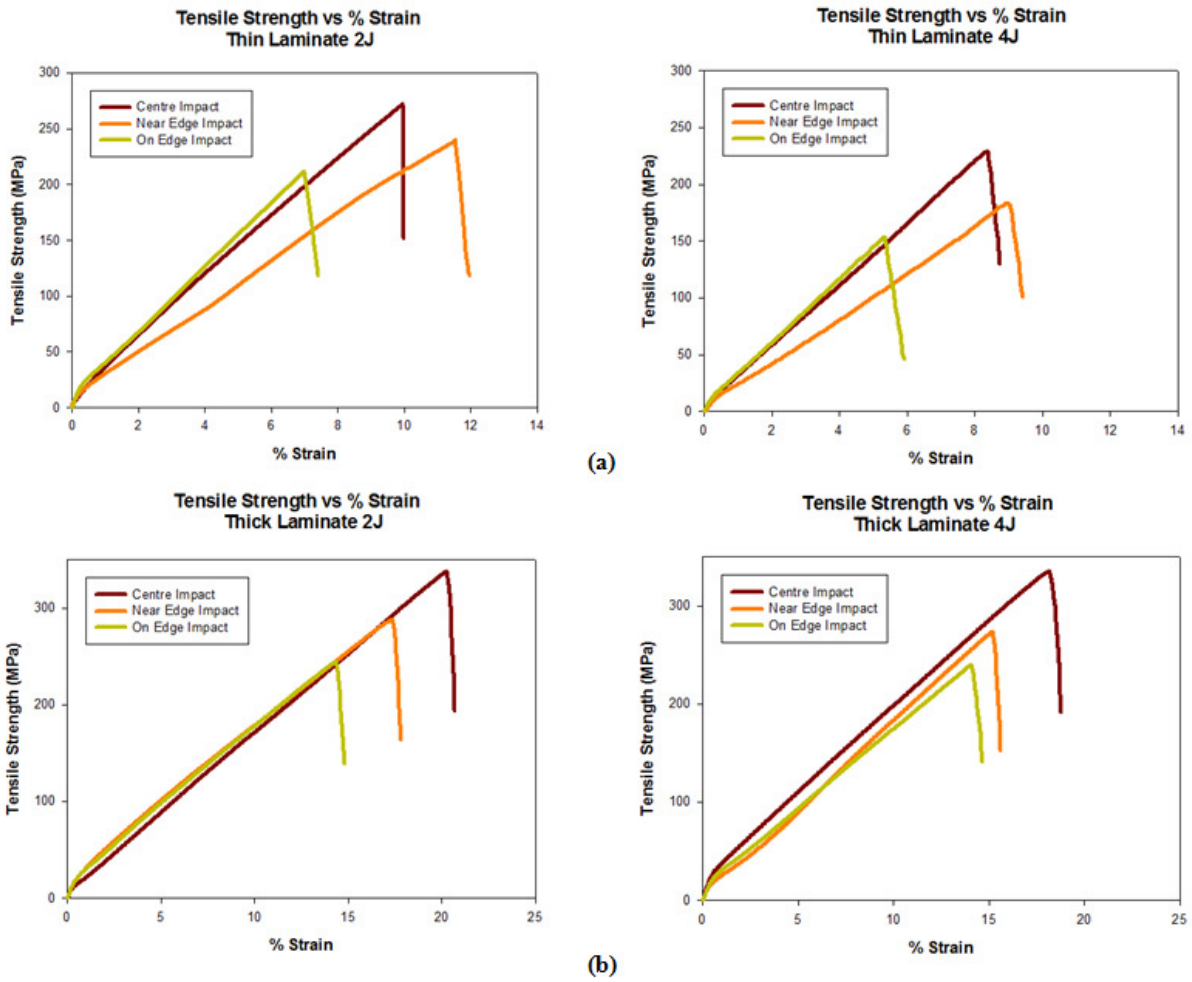

Figure 5.9 Comparison of tensile strength vs % strain of composite laminates subjected to on-edge, near-edge and centre impact at impact energies of 2J and 4J respectively (a) Thin laminates (b) Thick laminates

Maximum tensile strength of the on-edge impacted specimen is 211.6 MPa with strain 6.9% while for near-edge impacted specimen is 239.5 MPa with strain between 11.5% and finally centre impacted specimen the tensile strength is 271.2 MPa with strain between 9.9% at 2 J respectively.

Table 5.2 shows the effect of tensile residual strength with respect to thickness at incident energy level 4J. The thin laminates show a variation in the results indicating unstable behaviour while thick laminates show more stable behaviour and higher tensile strength at 4J. Thus we can deduce from table 5.2 that thicker laminates show higher tensile strength (approximately 1.5 times) than thin laminates. The strain at failure is approximately 1.6-2.6 times that of the thinner laminate. From this, it can be deduced that there is sharp reduction in tensile strength as the thickness of the composite laminates is reduced to half for all types of impact. Thus it indicates that thickness has a considerable effect on the residual tensile load

carrying capacity of the composite laminates. However it is seen that in thick laminates, the incident impact energy level has little effect on reduction of the tensile strength as compared to thin laminates. The higher tensile residual strength of the near-edge impact is due to the reduced fibre failure and higher matrix cracking while with on-edge impacted specimen the reduced tensile strength is due to fibre breakage found at several interfaces in the plane of the laminate and in the area of impact. When subjected to the same impact load, the centre and near-edge impacted laminates retain more of the load as compared to on-edge impacted specimen.

Impact Position	Tensile Strength (MPa)		% Strain	
	Thin Laminate 2mm	Thick Laminate 4mm	Thin Laminate	Thick Laminate
Undamaged	282	355	11	20
Centre Impact	229	335	8	18
Near-Edge Impact	183	274	9	15
On-Edge Impact	153	240	5	14

Table 5.2 Tensile strength load and % strain with respect to thin and thick laminates at 4J.

The depth of the dent was measured for the 4J on-edge impacted thin and thick laminates. The maximum depth for the thin and thick laminates was 3 mm and 1.5 mm. Assuming that these values of dent depth are equivalent to a change in cross-section of the laminate, the expected values of strength for the thin and thick laminates would be 248 MPa and 334 MPa. These values far exceed the values measured for the damaged specimens, 153 MPa and 240 MPa. Results from the TAI tests for the on-edge impact cannot be attributed to the presence of the dent.

5.3.2.2 Comparison of Results

Comparing the residual strength of both near-edge and on-edge impacted composite laminates it is clear that the compressive strength for near-edge impact is much lower than on-edge impact while the tensile strength for near-edge impacted specimen is much higher than for on-edge impacted specimens. Thus on-edge impact specimen fails in tensile mode while near-edge impact fails in compressive mode. This is due to the fact that compressive strength of the material depends upon the matrix behaviour. Since near-edge impact has larger area of damage, the damage starts occurring in the matrix phase so the bond in the epoxy matrix is broken in a more structured way. For on-edge impacted, the specimens

behave differently in tensile mode as failure is mostly driven through the fibre fracture and laminate fails at an early stage during damage progression which is through the fibre cracks instead of matrix cracks. The centre impacted specimens behave in more stable manner as compared to near-edge and on-edge impact because of the uniform boundary conditions from all sides leading to better load carrying capacity.

5.3.2.3 Damage Assessment

Figures 5.10 to 5.12 show the damage progression and damage pattern during tension after edge impact of thin and thick laminates. Figure 5.10 shows the tension after on-edge impact. The multiple fibre damage is clearly seen mostly on the upper and the bottom plies. The fibres are broken in these areas. Figure 5.10 (b)-(c) shows the comparison between the thin and thick laminate. The damage pattern is the same for both the thin and thick laminates. Both suffer extensive shear damage and the fibres are broken just under the point of on-edge impact.

The near-edge impact has different damage pattern as compared to on-edge impact. Figure 5.11 (a)-(b) shows the tension after near-edge impact for both the thin and thick laminates. The damage pattern is identical for both thicknesses. Here also extensive damage takes place just under the area of near-edge impact for both the thin and thick laminates. All the fibres are broken in the through thickness-width direction of the near-edge impacted specimens. For on-edge impacted laminates tested in tension the entire specimen between the grips whitens (see figure 5.10 (b) and (c)). Failure occurs by the growth of a shear cracks. For near-edge impact the damage is confined to the centre of the specimen around the impact damaged area (see figure 5.11). Failure occurs via a splitting process.

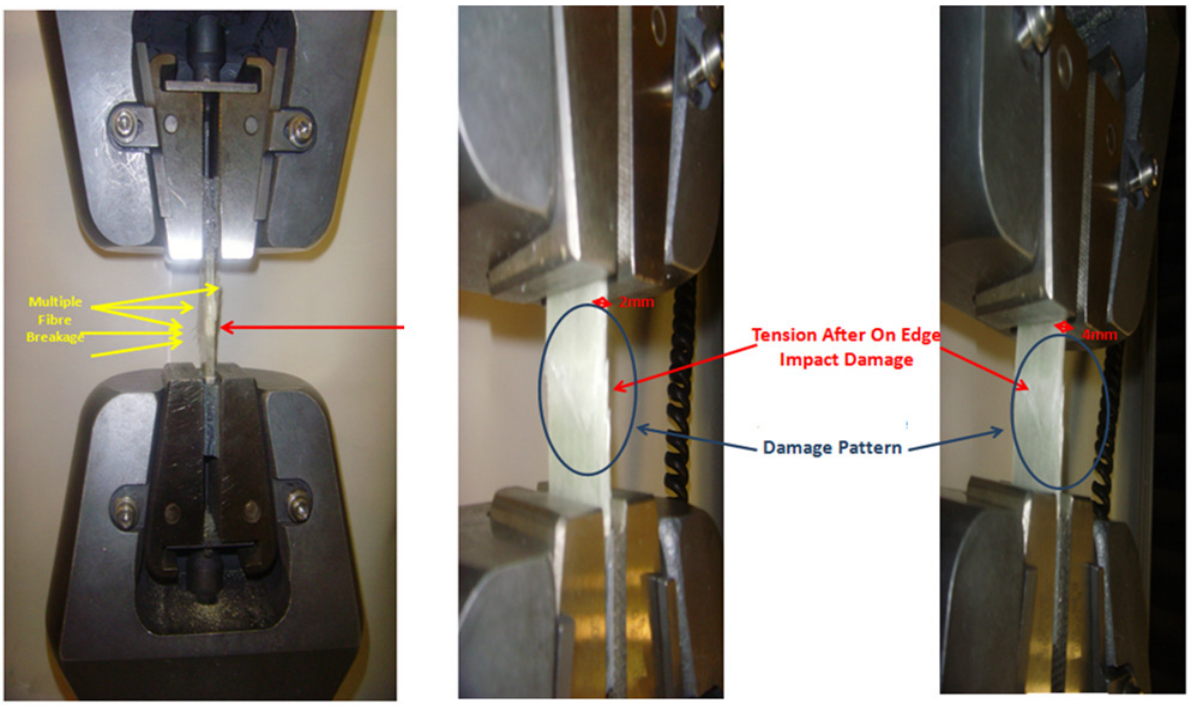

Figure 5.10 Different views of tension after on-edge impact at 4J (a) On-edge view- 2mm thickness (b) Thin laminate (c) Thick laminate

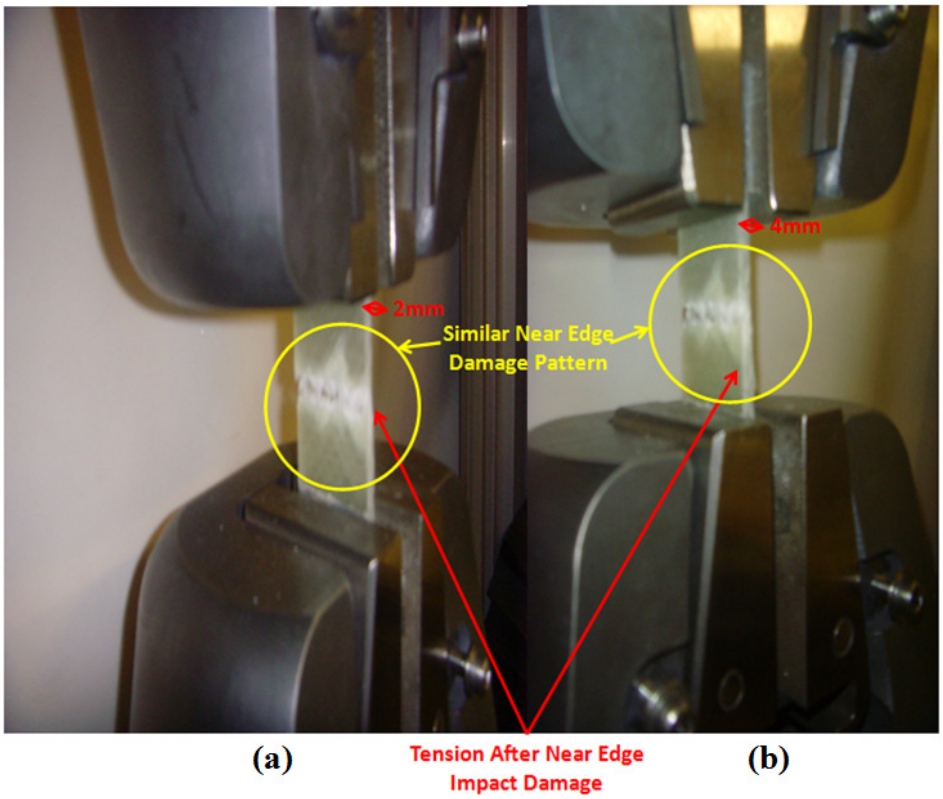

Figure 5.11 Different views of tension after Near-edge impact at 4J (a) Thin laminate (b) Thick laminate

It is seen that the TAI strength reduction is characterised by the increase in the damage size and area. Figure 5.12 (a)-(b) shows side view comparison of the near-edge and the on-edge tension after 4J impact. Effect of thickness can be seen from the figure 5.12 (c)-(f). It is clear that a similar damage pattern is seen for near-edge impact for both thicknesses (see figure 5.12 (c) and (e)). For on-edge impact (see figure 5.12 (d) and (f)) as the thickness is doubled more severe and extensive damage with broken fibres through the thickness of the specimen can be seen. It is noted that for near-edge and on-edge impact, a damage zone appears to have grown from the impact area. The area of delamination around the damage zone appears to be greater for the near-edge impact.

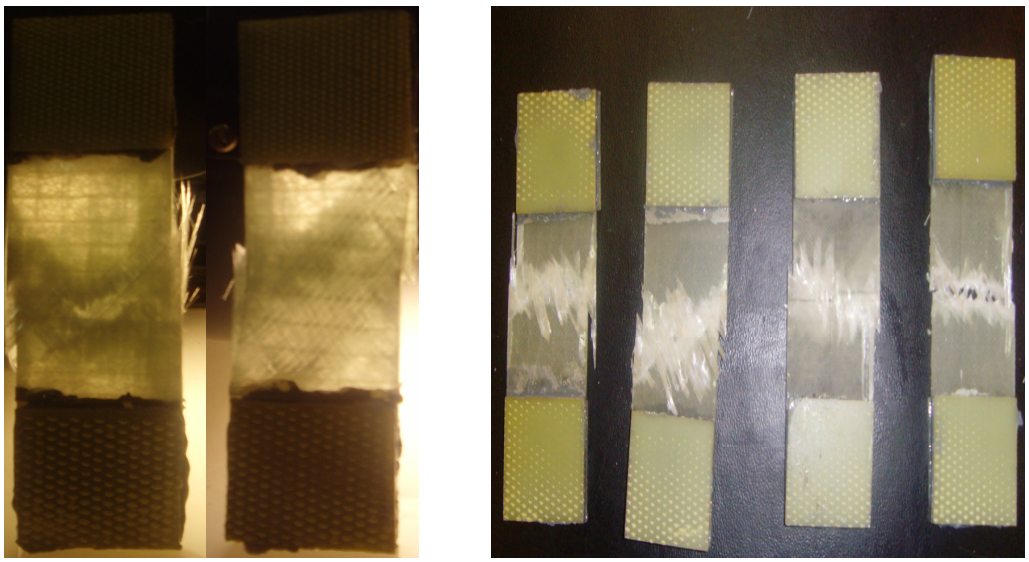

(a) (b) (c) d) (e) (f)

Figure 5.12 Damage side view of composite laminates subjected to tension after impact at 4J (a) Thick laminate: On-edge impact (b) Thick laminate: Near-edge impact (c) Thin laminate: Near-edge impact (d) Thin laminate: On-edge impact (e) Thick laminate: Near-edge impact (f) Thick laminate: On-edge impact

5.4 Conclusions

Residual strength of composite laminates has been carried out at three different impact locations. The impact response arising from on-edge impact was found to be very different from impacts on the plane of the laminate. The different failure mechanisms were highlighted from comparison of results from compression after impact and tension after impact tests. For the CAI tests, all values of failure load are highest for on-edge impact. Comparing the failure loads for central and near-edge impact show the amount of damage arising from the impact, and the interactions with the boundary conditions. The effect of thickness is clear since all values of failure load for the thick laminate are around three times the corresponding value for the thin laminate. For the TAI tests, all values of failure load are lowest for on-edge impact. The effect of thickness is less marked with the values for the thick laminate about 50% greater than the corresponding values for the thin laminate. The contrasting results from the CAI and TAI test highlight the different failure mechanisms for the different impact positions.

Chapter 6

Finite Element Analysis of Composite Laminate subjected to Low Velocity Edge Impact

6. Finite element analysis

6.1 Introduction

This chapter investigates the damage behaviour of composite laminates subjected to edge impact using finite element simulations. The same parameters have been used in the simulations as extracted from edge impact experiments. Laminate was modelled with thickness of 2mm and incident impact velocity of 2.85m/sec, equivalent to 3J impact energy. All the units used in Abaqus edge impact simulation are consistent in SI units.

Finite element simulations model for impact phenomena can be divided into three different sections:

- Pre-Processor
- Main Programme
- Post-Processor

As impact is a complicated and complex process, basic understanding of various impact parameters should be considered when modelling the impact. Figure 6.1 shows a description of the computational processes and parameters involved during impact simulation.

For accuracy of the results various parameters such as mesh density and element type are considered carefully. Since this project aims to validate experimental results, the variables are selected so that an accurate comparison can be made. The various parameters are:

- Element type
- Mesh density
- Boundary conditions
- Impactor size diameter
- Impactor mass
- Impactor velocity

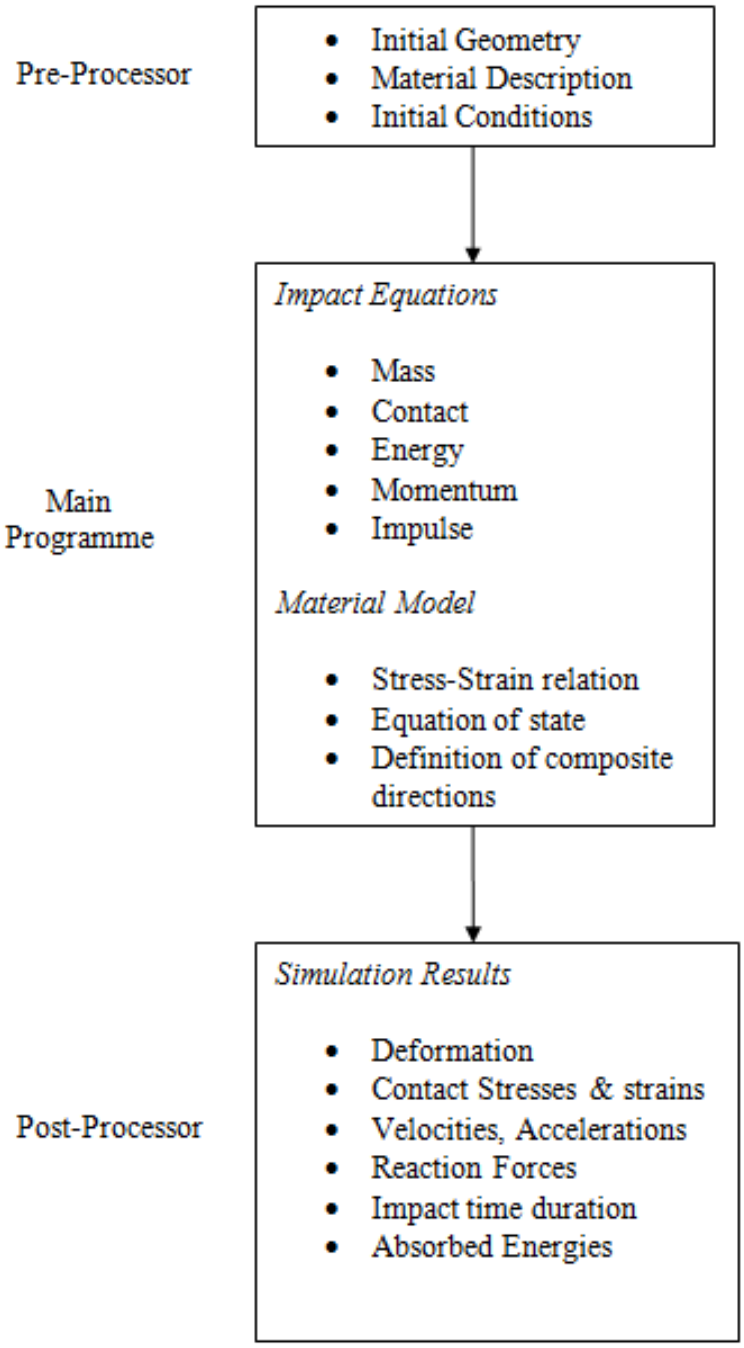

Figure 6.1 General description of the computational processes for impact

Modelling of the edge impact was approached by considering the following steps:

1. **Modelling Geometry:** The impactor and the laminate were modelled with similar geometric details used in the impact experiments. This is an important step in order to the validate the experimental results.
2. **Material properties:** Material properties for the laminate and impactor were defined in Abaqus/Explicit. More details of the laminate properties can be found in Appendix C. The impactor was modelled as a rigid body.
3. **Boundary conditions:** Initial conditions for the impactor such as impact velocity, acceleration, boundary conditions were defined at the reference node and the laminate was constrained around the boundary edges of the laminate.
4. **Contact conditions:** The contact algorithm was defined in Abaqus/Explicit using master-slave algorithm for simulating edge impacts.
5. **Mesh Density:** Correct element type and mesh density were defined for the edge impact for the accuracy of the results.
6. **Simulation:** The job is run in Abaqus/Explicit code. Results were extracted and compared with experimental results.

The following sections will now discuss more details about the modelling and simulation of edge impact.

6.2 Geometry Details

The following section will describe the geometry modelling for the impactor, followed by further details required for modelling the composite laminate for both near-edge and on-edge impacts.

6.2.1 Impactor Modelling

Impactor can be considered as a 3D discrete rigid body and is modelled with 3D rigid elements. The centre of gravity of the impactor is chosen as the reference point to define the impactor mass, velocity, boundary conditions and rigid boundary elements as shown in figure 6.2. For both near-edge and on-edge impactor discrete rigid elements have to be defined with body elements and the reference point as shown in figure 6.3.

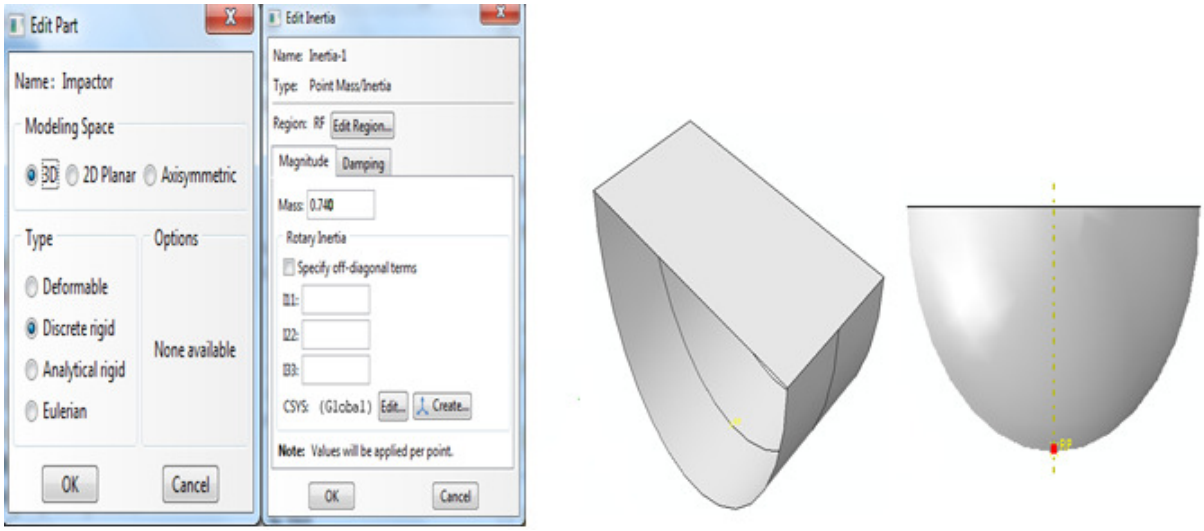

Figure 6.2 On-edge and near-edge impactor: Reference points and masses

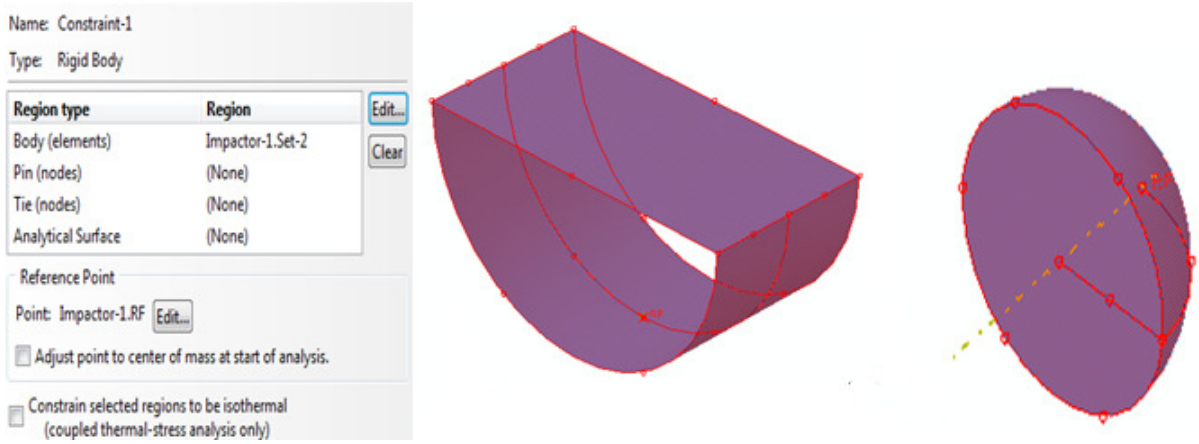

Figure 6.3 On-edge and near-edge impactor: Boundary elements and reference point

The boundary conditions for the near-edge and on-edge impactors are modelled at the reference point node. They are defined in different directions with respect to the global co-ordinate system, see figures 6.4. The two translational and three rotational degrees of freedom are constrained except displacement along the y-axis, U2, for the on-edge impact and displacement along the z-axis, U3, for the near-edge impact.

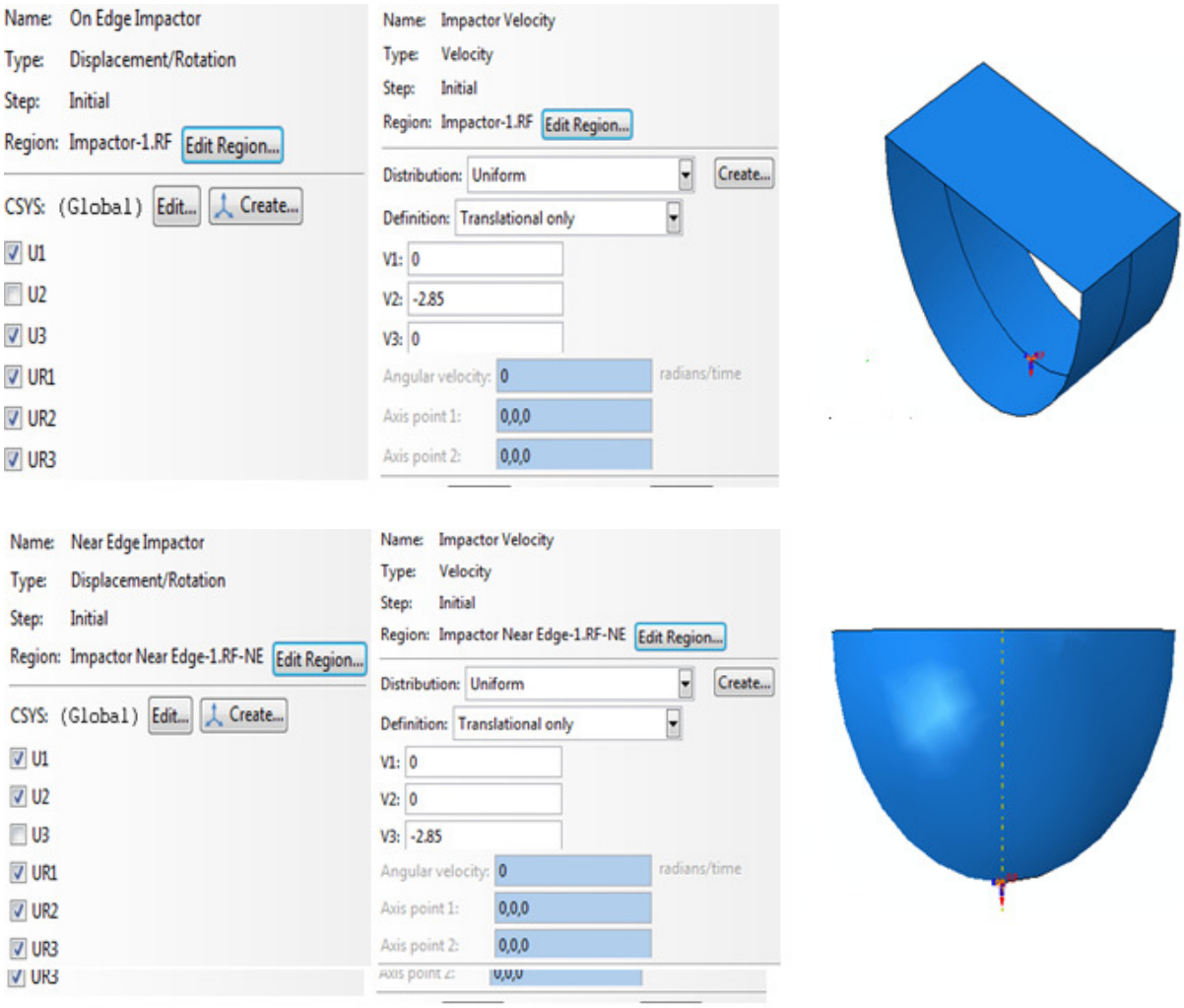

Figure 6.4 On-edge and near-edge impactor: Boundary conditions and impact velocity

The incident impact velocity for the edge impact simulation is given as v=2.85 m/s depending upon the direction of impact the sign has to be changed. Values assigned in the simulation are the same as measured in the experiments. The movement of the on-edge impactor is in negative y-direction and that of the near-edge impactor is in negative z-direction as shown in figure 6.4.

Figure 6.5 shows the meshing for both the near-edge and on-edge impactors. As both the impactors are of curved and round shape, the sweep meshing technique is utilised to obtain uniform meshes, see figure 6.5.

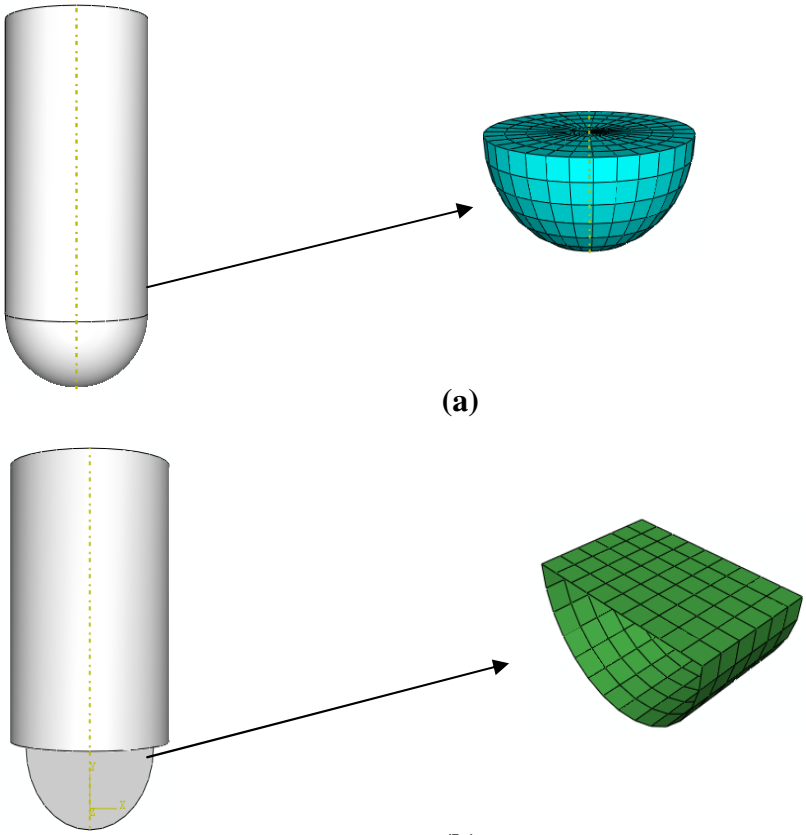

(a)

(b)

Figure 6.5 Modelling of impactor shape for a) Near-edge b) On-edge

6.2.2 Laminate Modelling

The glass/epoxy laminate is modelled using Abaqus 6.6. To model composite laminate the first step is to create partition. Partition is done in order to define the composite lay-up, the plies, plies orientation, material properties, thickness, number of integration points for each ply and to have uniform structural mesh around the critical areas. Following sections will discuss in detail the laminate modelling for both the near-edge and on-edge impact models.

6.3 Modelling Approach

6.3.1 Material Properties

The glass/epoxy material properties used for simulation are given in table 6.1. In this model, these properties are elastic, without the inclusion of failure mechanisms. The elastic composite materials properties of the glass/epoxy composite laminate were provided by the Saint-Gobain company. For more details please see Appendix C.

Glass/Epoxy Laminate Properties				
E_1 (GPa)	E_2 (GPa)	G_{12} (GPa)	G_{23} (GPa)	v_{12}
43.5	9.5	4.3	3.7	0.28

Table 6.1 Glass/Epoxy material properties (Appendix C)

6.3.2 Modelling Composite

The laminate was modelled for both the near-edge and on-edge impact. Thin laminate (2mm) is divided into 8 partitions in order to create eight individual plies. Partition of each plies is such that every ply has a thickness of 0.00025 m. CSYS method (Abaqus Manual 6.10) 3 point and rectangular datum is used to define the composite laminate axis where x-axis is aligned in 0^0 ply, y-axis is aligned as out of plane direction and z-axis is aligned through thickness direction as shown in the figure 6.6. The laminate is modelled initially with unidirectional 0^0 plies. Figure 6.6 shows the partition and global coordinates for laminate.

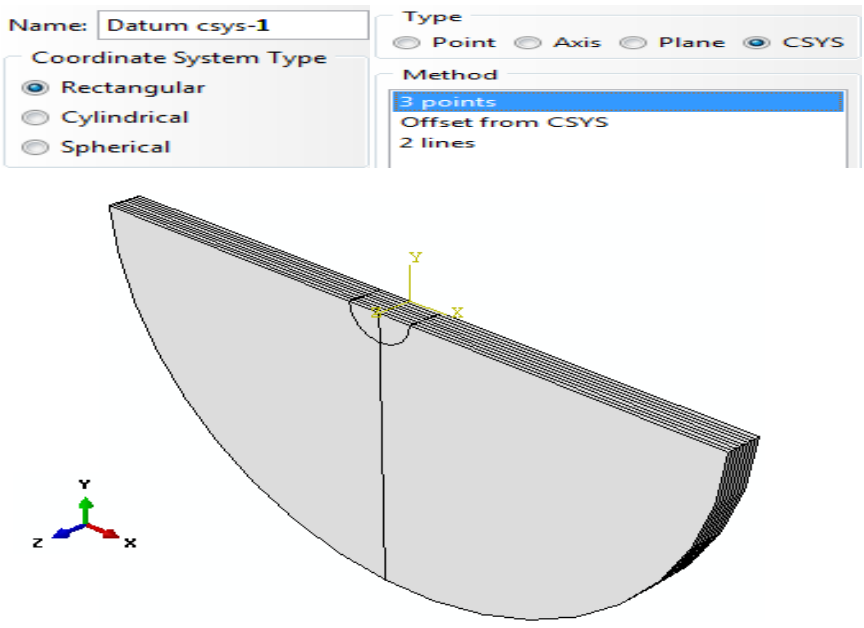

Figure 6.6 Partition and global co-ordinates for laminate

6.3.2.1 Section Assignment

Each ply is now assigned with composite material properties using section assignment method available in abaqus 6.6 and as shown in figure 6.7

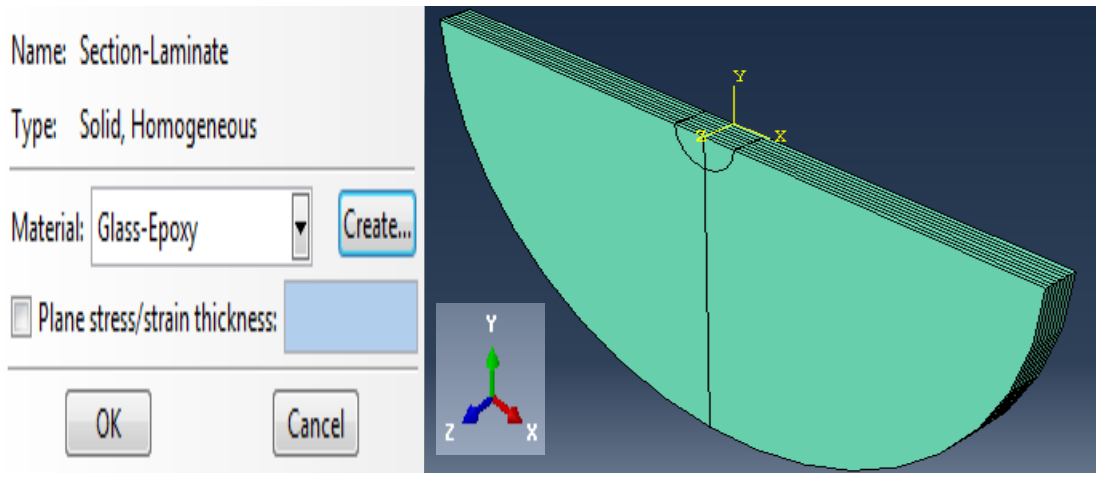

Figure 6.7 Plies section assignment

6.3.2.2 Co-ordinate Axes and Orientation

Once the plies are assigned material properties the next step is to define the orientation of the fibres within each ply of a composite layup. Initially by default we consider the laminate to have 0^0 fibre directions with respect to the reference coordinate system for each ply that is partitioned. In order to have layup of $[0/90/45/-45]_2$ datum created in section has to be selected. The selected datum defines the orientation of the fibres within each ply relative to the ply's coordinate system. The four ply orientations 0^0,45^0, 90^0,-45^0 with respect to the selected datum are shown in figure 6.8.

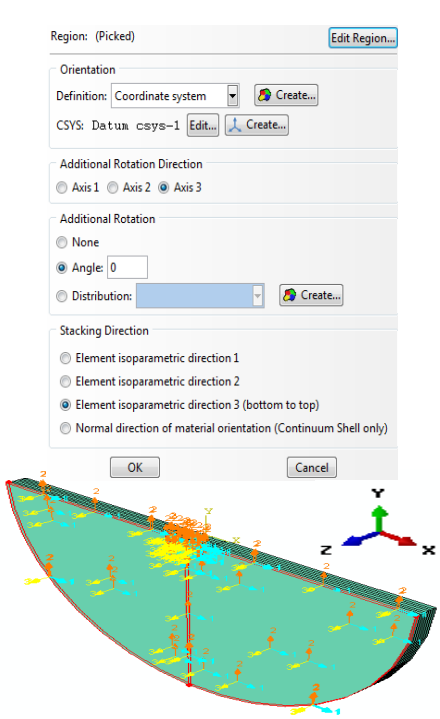

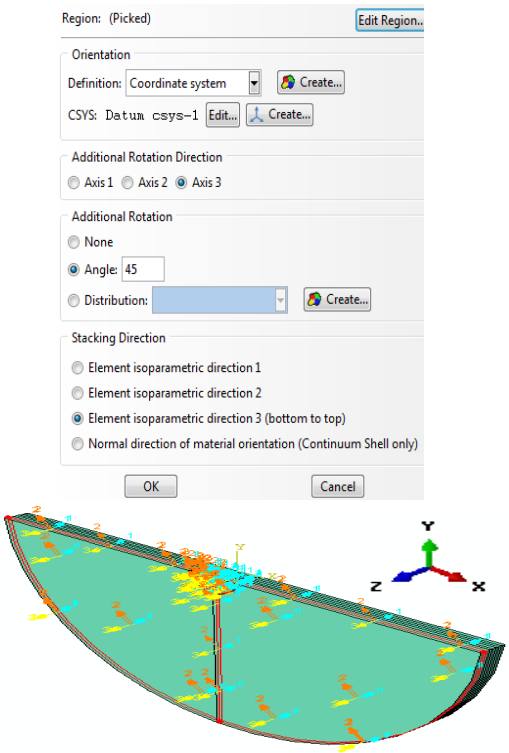

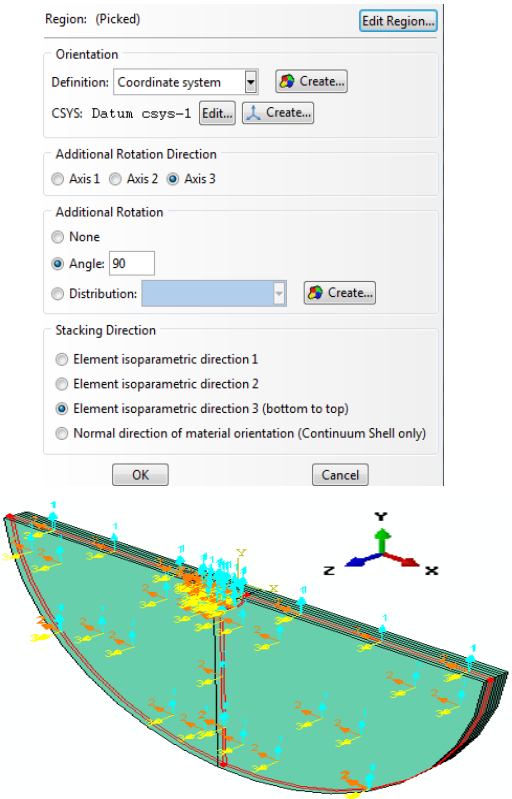

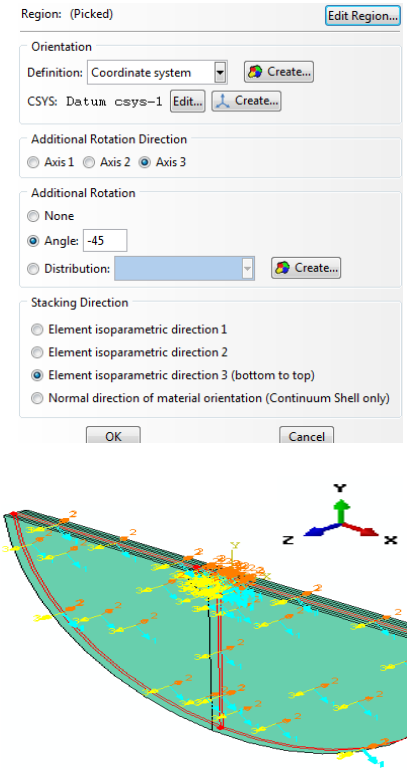

Figure 6.8 Ply orientations 0^0,45^0, 90^0,-45^0

6.3.3 Boundary Condition and Meshing

The laminate is constrained around the edge of the laminate. The encastre boundary method available in Abaqus is chosen. This condition enforces constrains for both translational and rotational degrees of freedom around the edge of the composite laminate during impact as shown in figure 6.9.

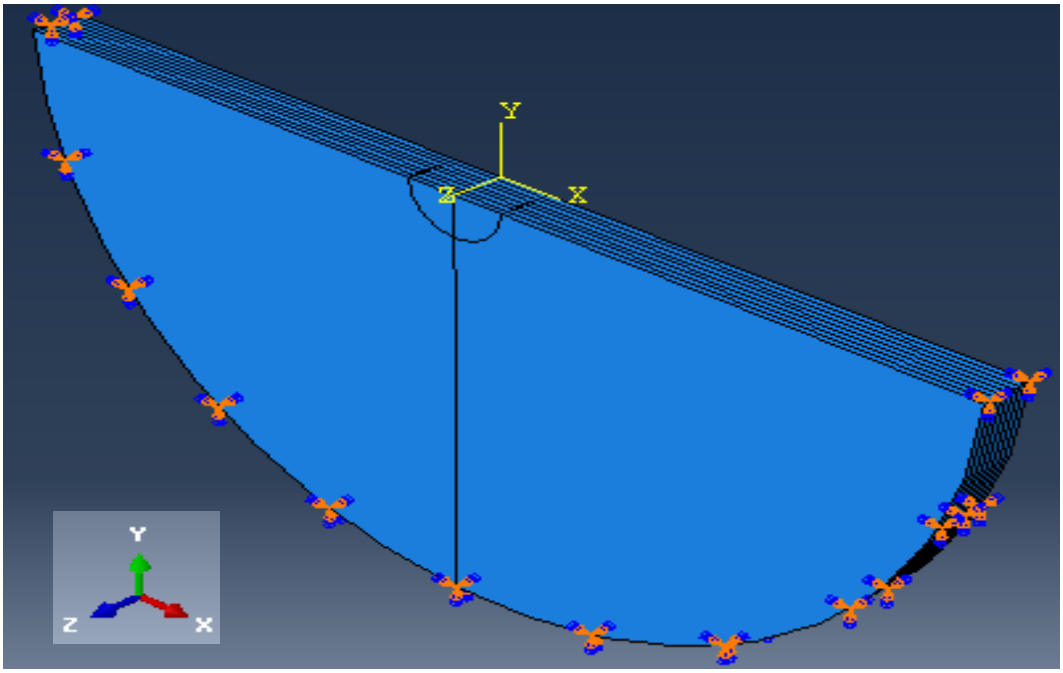

Figure 6.9 Laminate boundary conditions

In order to mesh the laminate global seeds are assigned of approximated size of 0.0004 m and structure technique is used for meshing the laminate. The composite plates are modelled with 3-D stress hexahedral element using reduced integration (C3D8R) with eight nodes brick elements. The plate is modelled at the ply level, with one layer of elements per ply; a typical mesh for a 2mm plate contains 24,000 elements. For on-edge impact relax stiffness hourglass method is used for the elements in order to reduce the distortion created by impact while for near-edge impact enhanced hourglass method is used for the elements in order to capture the desired damage behaviour. Figure 6.10 shows the laminate meshing. The same meshing conditions is used for both the on-edge and near-edge impact laminate.

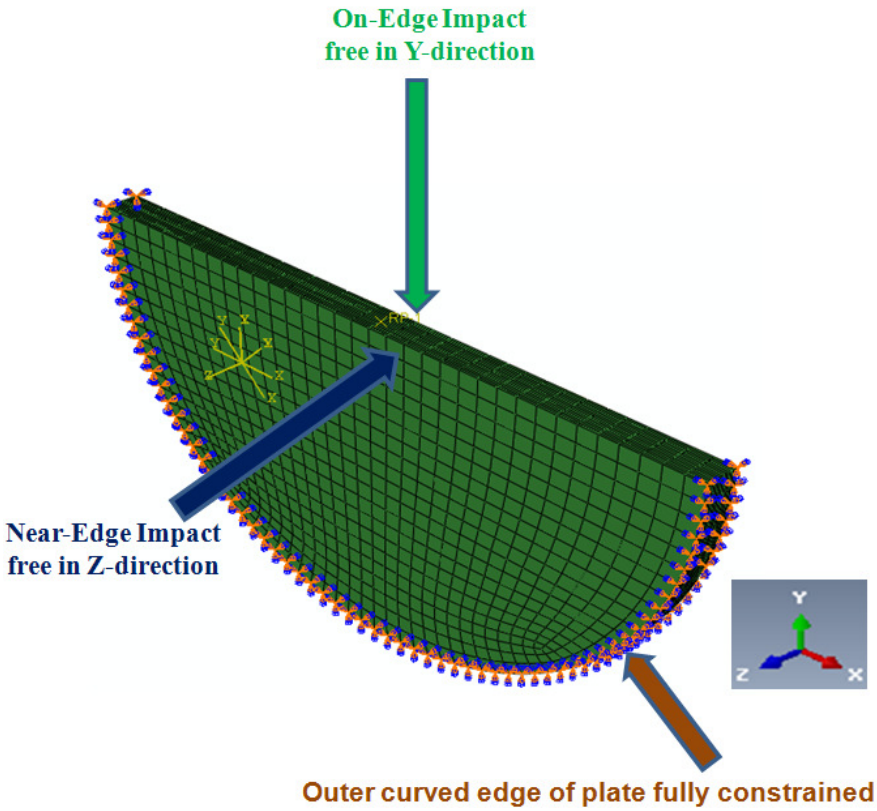

Figure 6.10 Laminate meshing

6.3.4 Contact Interactions

Abaqus/Explicit provides two algorithms for modelling contact. The first is general contact and the other one is surface to surface contact method to define contact between all regions of a model and impactor. In order to simulate impact, the general contact method is used for both the near-edge and on-edge impact analyses. The interaction between the impactor and the laminate surface is carefully selected and it is assumed that there is no friction between the impactor and the plate. We simulate the model by considering laminate as deformable body while impactor as rigid body. Impact velocity and density for rigid body are defined by reference nodes parameter. The contact should be such that the rigid impactor must be allowed to contact not only with the external surfaces of the laminate but also with its internal surfaces. By default, general contact in Abaqus/Explicit allows contact between all exterior surfaces in a laminate including a surface with itself. In the edit included pairs dialog box, choose the pairs that are to be included for general contact algorithm as shown in figure 6.11. Interaction properties must be defined in order to enforce the contact between the rigid impactor and the composite laminate. In interaction properties choose mechanical behaviour

and select the normal contact method in order for impactor to bounce back after impacting with the laminate. Abaqus/Explicit uses sophisticated search algorithms for tracking the motions of the surfaces. Balanced master-slave algorithm is considered by default method for this simulation. For on-edge and near-edge impact the same general contact conditions are used.

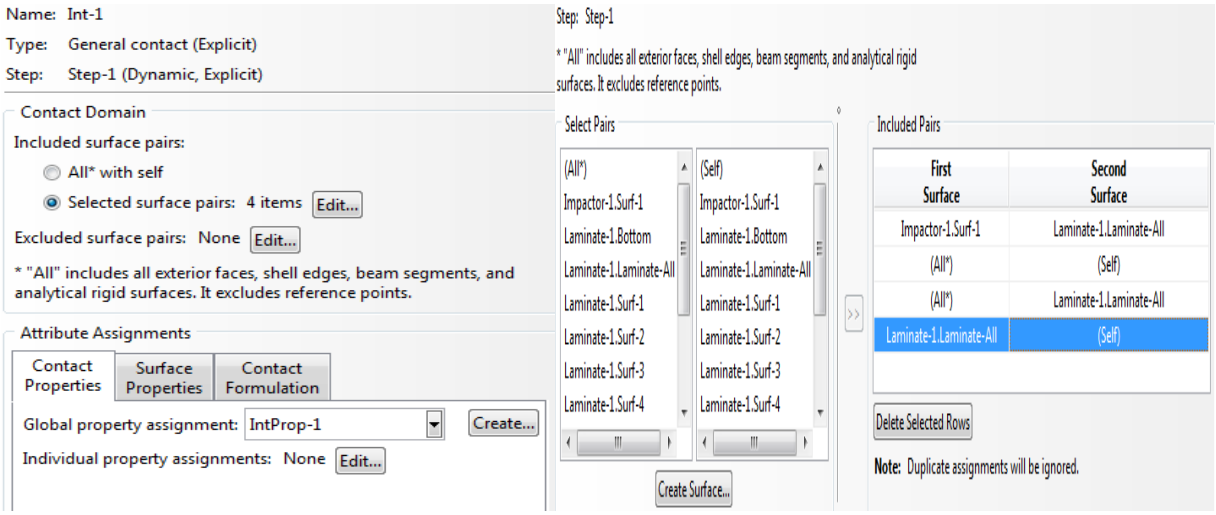

Figure 6.11 Contact algorithms for edge impact

6.3.5 Impact Damage History and Field Outputs

In history and field outputs the user has to define output variables required for validation with experimental edge impact results. In Abaqus/CAE field output request, the force and displacement is requested. In history output, the different sets created for the laminate model are selected. Sets should be selected around the critical or impact areas in order to extract the forces and displacements.

6.3.6 Impact Simulation

Abaqus/CAE was used as the pre-processor to create the input files that defines the geometry, loading conditions materials and the post-processor to process the results. The modelling of the contact-impact problem is governed by the fact that the impacting body and the target must not fully penetrate but bounce back. Simulation of the impact is investigated on the basis of the following assumptions:

- Impactor is assumed to be rigid.
- Ignoring the gravity force during the time period.
- Neglecting the damping effect in the composite structure.
- There is no friction between the impactor and composite structure.

Impact simulation approach is based on the central finite difference algorithm. During impact simulation the kinetic energy of impactor is converted into work done. Work is done by contact force and displacement of impactor. The contact force and acceleration are determined by displacement of the impactor. Displacement of impactor is determined mainly by structural deformation of the plate.

6.4 Results

6.4.1 Comparison of Edge Impact Experiments and Simulations

The accuracy of the simulations can be explored by comparison of force/time and displacement/time results; the comparisons are made for the impact event, up to maximum force or displacement.

6.4.1.1 Near-Edge Impact

Results for near-edge impact are shown in figure 6.12 (a) and (b). The near-edge comparisons show very good agreement for the maximum force and displacement. The values of impact event time are in very good agreement. Figure 6.12 (a) shows the variation of force with time and figure 6.12 (b) shows the variation of displacement with time. The experimental results initially show higher stiffness than the finite element simulations followed by apparent stiffness reduction, which is expected to arise from failure processes. The finite element results show near linear response as would be expected for these elastic simulations.

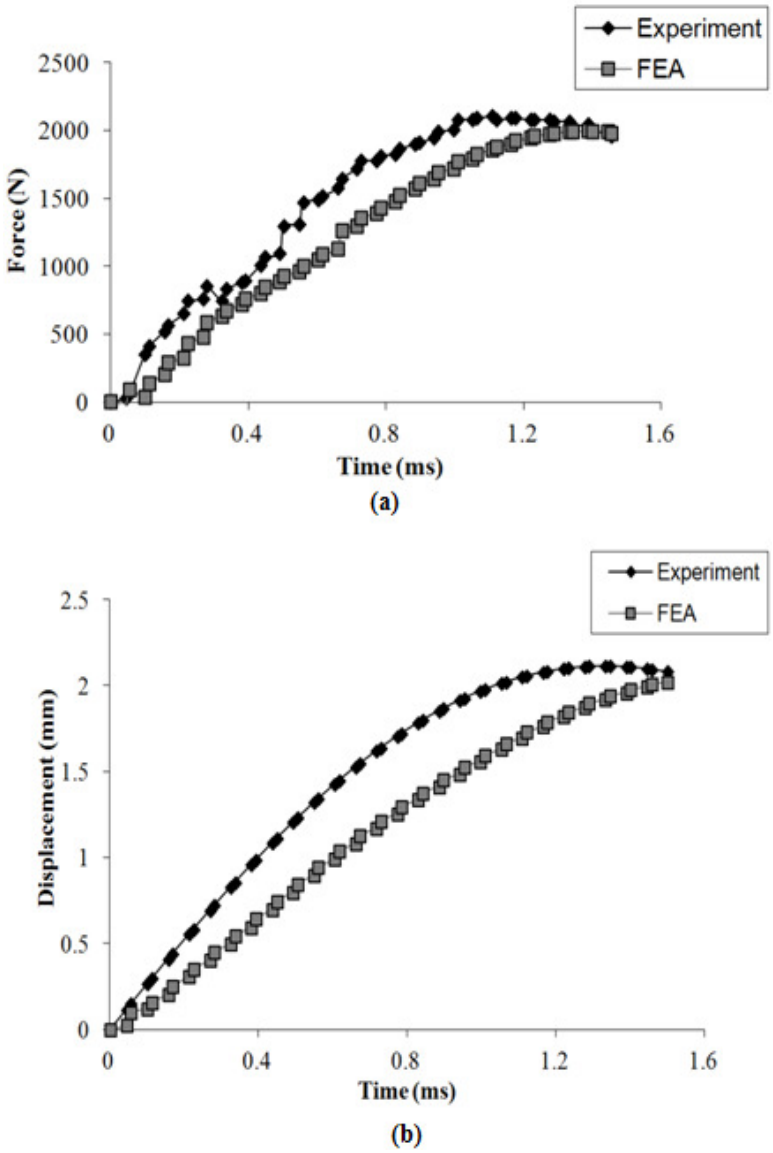

Figure 6.12 Comparison of experimental and predicted results for 3-J near-edge impact on 2-mm thin laminate (a) Variation of force with time (b) Variation of displacement with time

6.4.1.2 On-Edge Impact

Results for the on-edge impact are shown in figure 6.13. The on-edge comparison show good agreement for initial stiffness. Figure 6.13 (a) shows the variation of force with time and figure 6.13 (b) shows the variation of displacement with time. The predicted maximum force is in good agreement with the experimental results, but the experimental values of force increases at a faster rate, at times corresponding to the lower values of displacement. These differences must be associated with the onset of failure processes. The overall agreement between the results of the on-edge impact is reasonable for these elastic simulations.

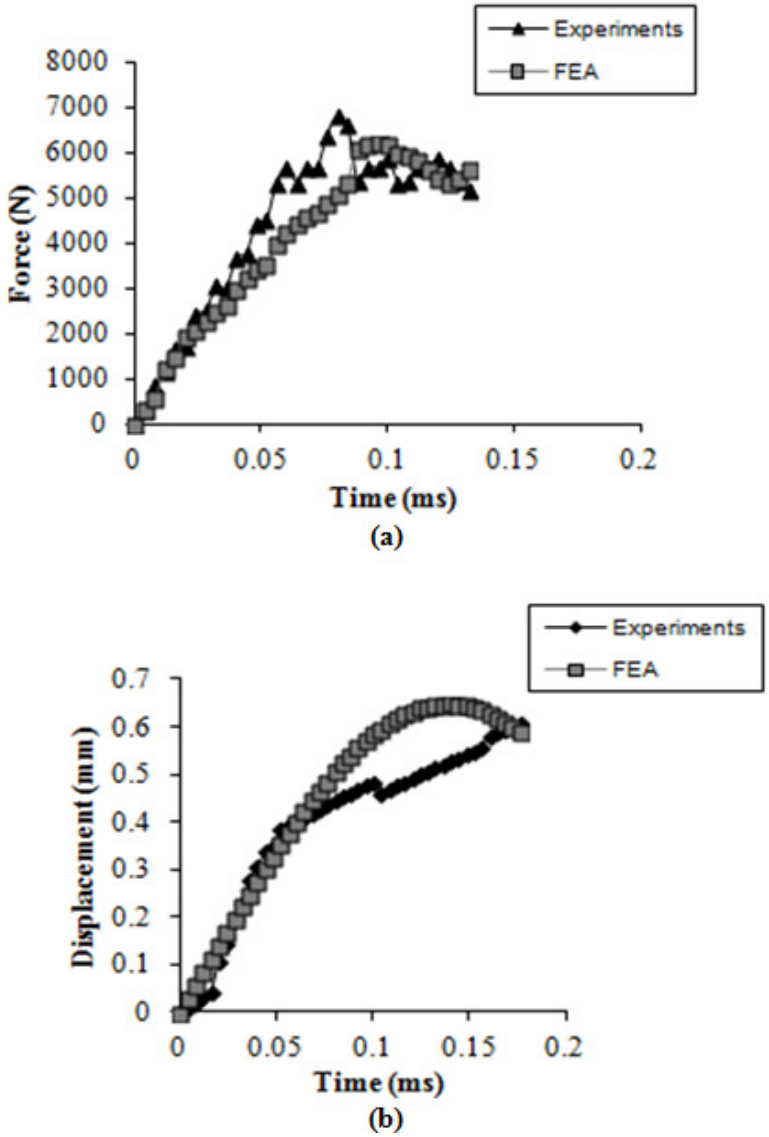

Figure 6.13 Comparison of experimental and predicted results for 3-J on-edge impact on 2-mm thin laminate (a) Variation of force with time (b) Variation of displacement with time

6.4.2 Stress Contours

Around the impact, the region of high stress is larger for the on-edge impact. Higher stresses arising from interaction with the boundary conditions at the edge of the plate are found for both types of impact. Figure 6.14 (a) shows side view of near-edge impact simulation. Simulation shows higher bending and flexural stresses as expected from the experimental results. For the near-edge impact, these high stresses exist all around the edge; for the on-edge impact they are only found on the edge of the plate below the impact (see figure 6.14 (b)).

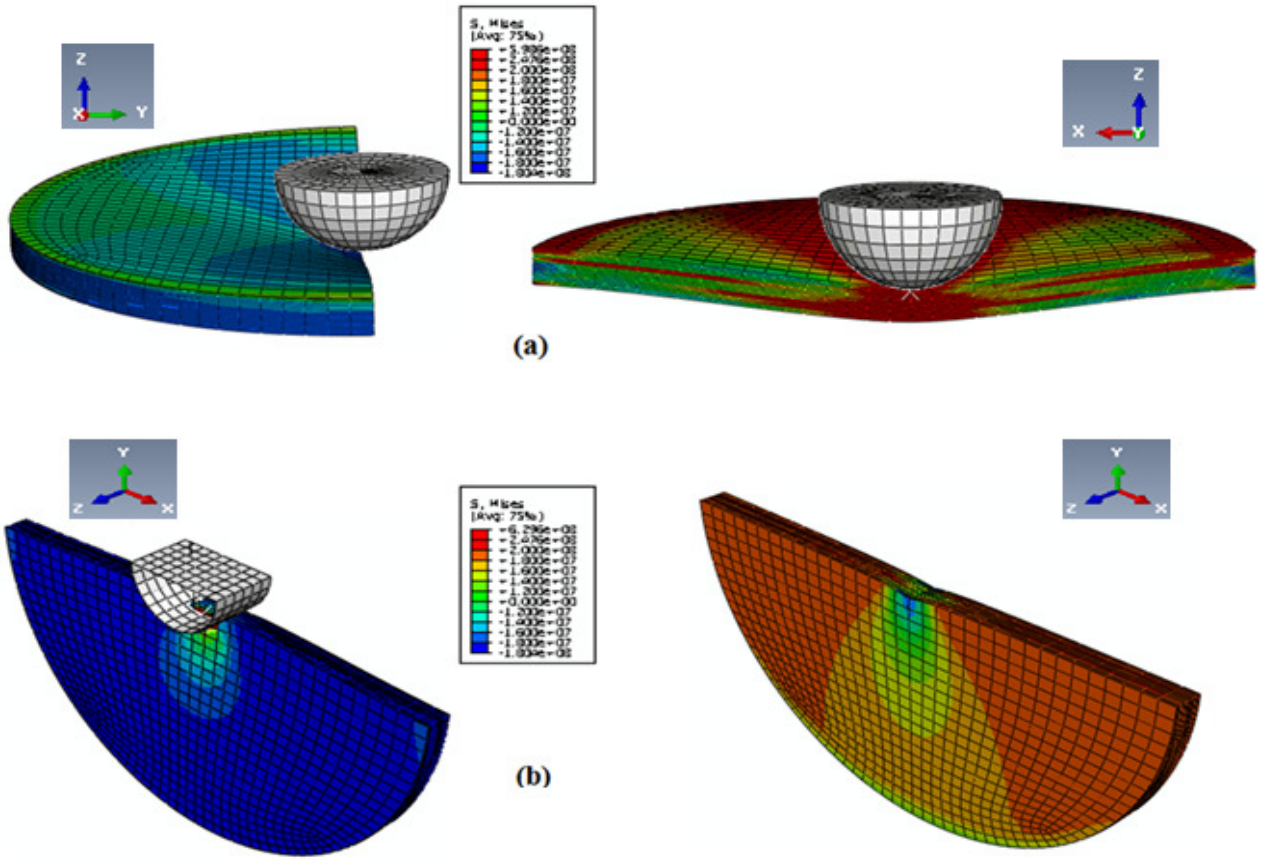

Figure 6.14 Different views of (a) Near-edge and (b) on-edge impact-initial contact and after 0.01 ms

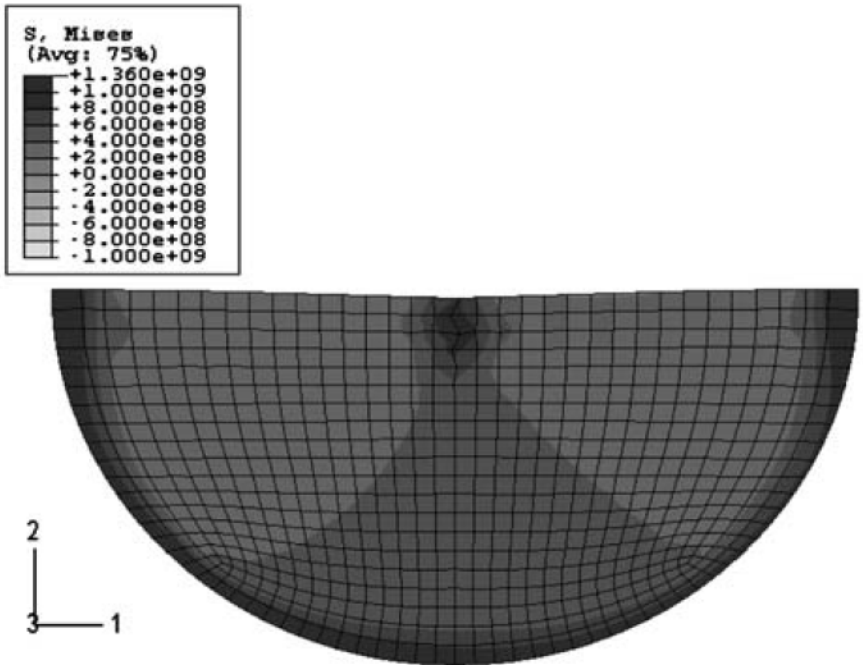

(a)

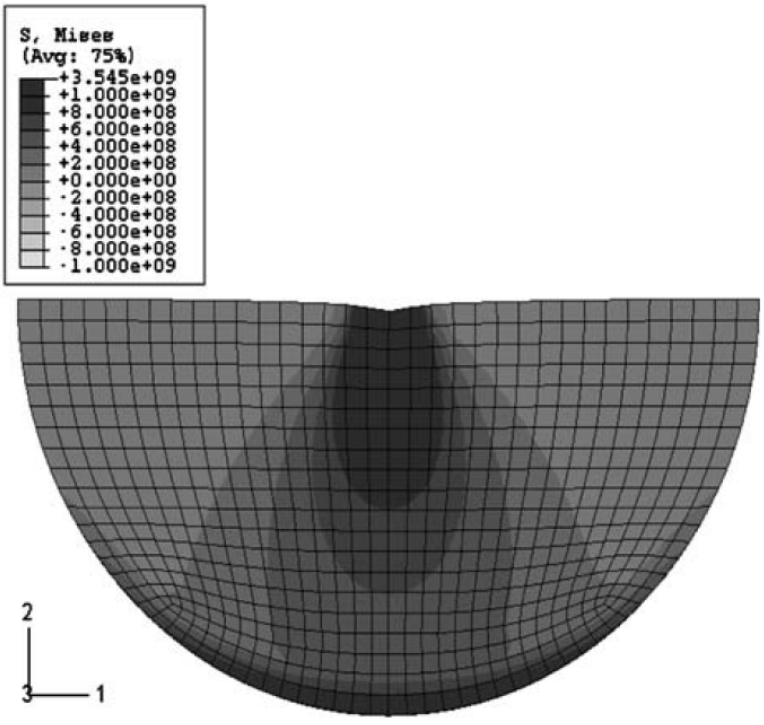

(b)

Figure 6.15 Predicted contours of von-mises stress on the top 0^0 ply for3-J impact on 2-mm thick laminate. (a) Near-edge impact (b) On-edge impact

Further stress contours were examined just after impactor contact to find maximum values for comparisons with the observed failure failures. As described above, all simulations are for 3-J incident energy impact on the 2-mm thin laminate. The response of the whole plate to the impact event can be assessed from the in-plane contours of Von-Mises stress in the top 0^0 ply. This is the impacted ply for the near-edge impact; for on-edge impact, identical results are found for the opposite, lower, 0^0 ply. The contours are shown in figure 6.15. The maximum stresses within the individual plies were examined; the directions of the stresses are all with respect to the fibre direction in that ply. For near-edge impact, maximum stress in the fibre direction is found in the lower 90^0 ply with respect to the impact. For on-edge impact, the maximum fibre stress is found in all the 45^0 plies. On-edge impact may lead to fibre failure in more plies. Delamination is expected to arise from transverse fibre stress and shear stress. For both the types of impact, maximum values of transverse fibre stress were found for the 45^0 plies. For the on-edge impact, maximum shear stress is also found for the 45^0 plies, but for the near-edge impact maximum shear stress is found for the 0^0 impacted ply. On-edge impact may lead to more extensive delamination.

6.4.3 Discussions

These preliminary finite element models do not include the failure mechanisms; the entire impact event has not been captured. The predicted force/time and displacement/time results are extracted, and are compared with the experimental results as discussed in section 6.4.1. Abaqus/Explicit captures the reaction force/time values by summation of all the reaction forces at the boundary conditions of the laminate only. Reaction forces are zero in the unconstrained areas of the laminate. As expected for these simulations assuming elastic material properties, displacement and force traces are all smooth and monotonic.

Examination of the stress contours has indicated that failure processes, including fibre failure and delamination, would be expected to be more severe for on-edge impact; the same comparison was found experimentally. The simulations can also be used to explain the fluctuations observed in the experimentally recorded force/time traces for on-edge impact. Out-of-plane vibration is clearly visible in this impact simulation. The frequency of the vibrations is approximately the same as that observed for the fluctuations in the force/time traces. We postulate that such out-of-plane lateral plate vibration is the cause of these fluctuations in load. So comparing FEA and experimental results it is clear that the expected

trends are in line with information gathered from FEA results. It provides a good overview and expected damage and force/displacement trends for both the on and near-edge impact results.

6.5 Development of Future Impact Damage Models

To analyse the strength of any laminated composite strength theories are required. Failure analysis is a tool for predicting the strength of a composite laminate containing several plies with different orientations and under complex loading conditions. Two finite element modelling approaches for impact problems have become very popular in academic research and industry. The first approach is using Hashin damage failure criteria for composites and the other approach is cohesive modelling approach. Hashin damage criteria provides greater insight to the tensile and compressive damage behaviour of fibre and matrix. The second approach, cohesive modelling, is more complex and uses one or two layers of elements per ply to represent each individual ply layer and each layer is bonded using cohesive elements. Individual plies with cohesive elements form a laminate stack. Cohesive modelling helps to model delamination. In the following sections we will discuss the future development of models for both near-edge and on-edge impact using these approaches.

6.5.1 Hashin Damage Criteria

There are numerous failure criteria for composite materials for different applications but the most widely used for impact on composites are the Hashin damage failure criteria. Hashin proposed a set of failure criteria for predicting failure of unidirectional composites based on each failure mode. An example of Hashin damage is shown in figure 6.16 in which the steel ball penetrates through the composite laminate. Matrix and fibre damage including reflection of stress waves can be seen clearly.

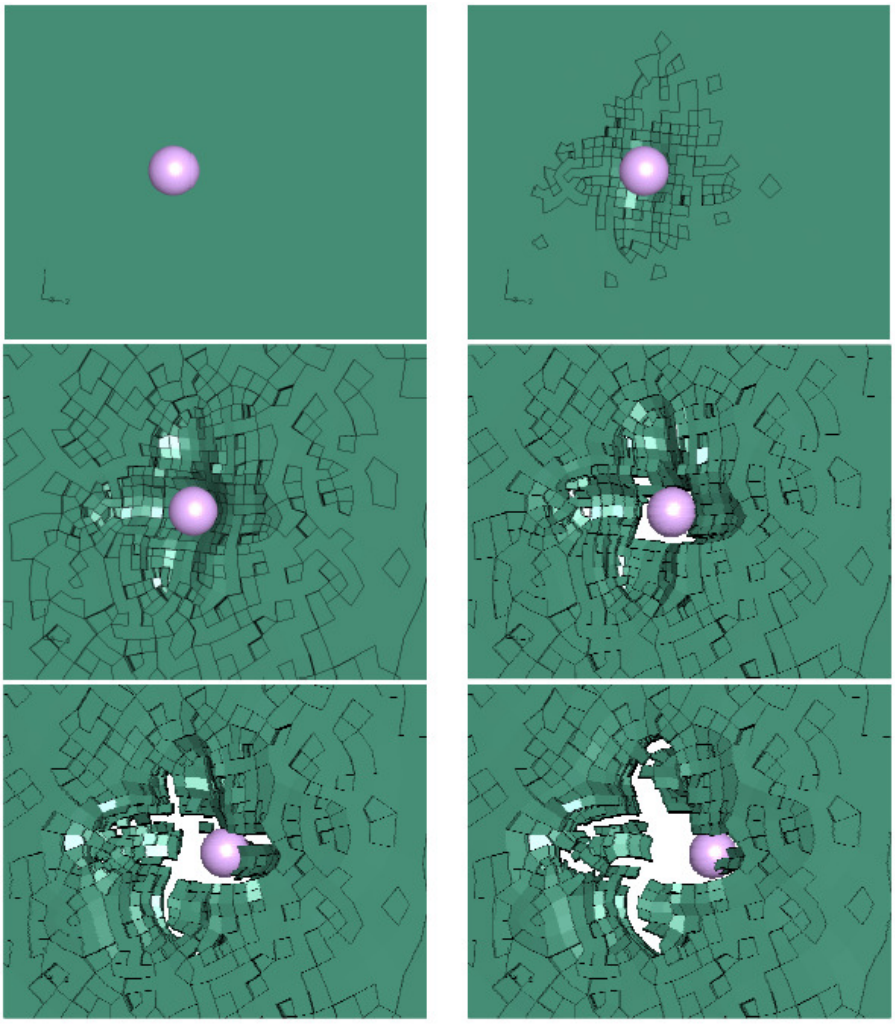

Figure 6.16 Projectile impact on a carbon fiber reinforced plate (Simulia 2007)

The near-edge and on-edge elastic models could further be developed to include Hashin damage failure criteria using the similar approach as described in the Simulia (2007) paper. This modelling approach will provide useful information regarding the reflection of stress waves, matrix and fibre damage, and locate the areas that are under high under compressive and tensile stresses. However this technique is limited to fibre and matrix damage as delamination is very difficult to predict using this technique.

In Abaqus Hashin damage criteria includes damage initiation and evolution. Damage criterion investigates four different damage modes: fiber tension, fiber compression, matrix tension, and matrix compression (Hashin and Rotem, 1973; Hashin, 1980). Usually Hashin criteria are implemented in two dimensions but the criteria are extended to three dimensions for complex problems. There are two approaches to simulate Hashin damage in Abaqus:

firstly using continuum shell and plane stress elements and secondly using 3D solid elements with VUMAT subroutine. The preselected default output in Abaqus does not include the damage output variables such as damage initiation and evolution so it is important to create sets and define them with output variables to extract the Hashin damage results. In Abaqus/Explicit by default, an element is removed from the mesh when either of the damage variables associated with fibre failure modes such as tensile or compressive reaches the value of 1.0. When damage in the matrix (tension or compression) or fibre (compression only) reaches unity, the stiffness component of that element is reduced to zero in all directions. When damage in the fibre tension direction reaches unity the element is deleted from the analysis.

6.5.2 Cohesive Modelling

The second approach for impact problems is cohesive modelling. Cohesive elements act like nonlinear springs and link volumetric finite elements which, when applied at the composite interfaces, will simulate delamination. Failure criteria are applied at these interfaces. Thus in academic research cohesive models are used to model delaminations for an accurate prediction of impact damage. An example of impact using cohesive layers at the interface is shown in figure 6.17 (Lopes et al 2009).

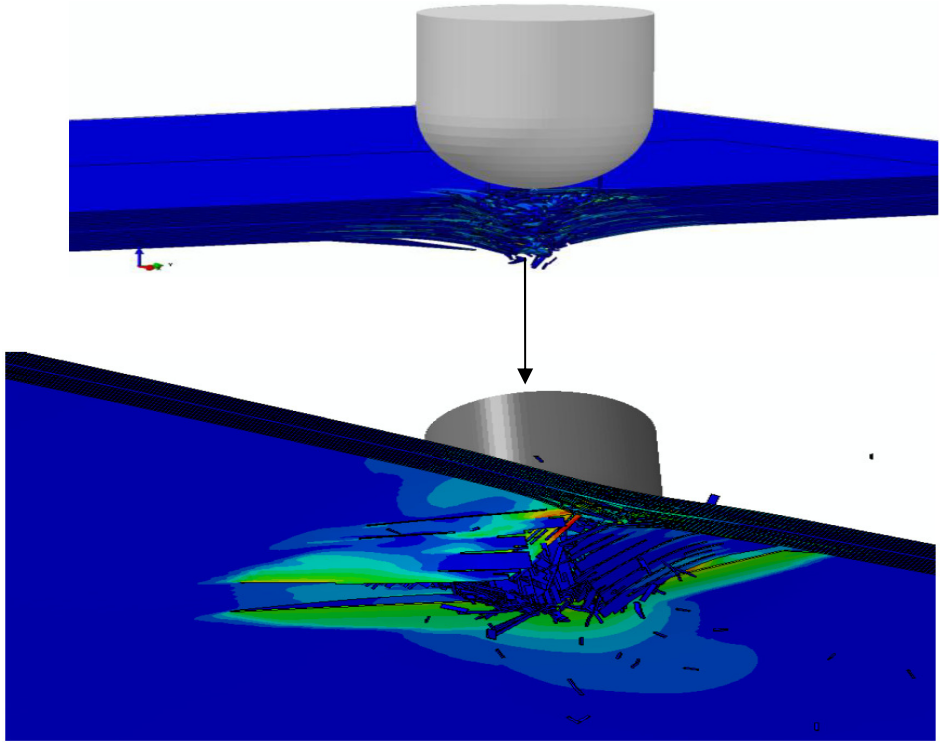

Figure 6.17 Simulation of 40J impact on a 32-ply composite laminate (Lopes et al 2009)

In figure 6.17 delamination and matrix and fibre damage can be seen clearly. Similar approach can be utilised for near-edge and on-edge models which could determine the sequence of delamination growth at different interfaces during edge impact. Cohesive layer of elements exists between interfaces of each ply in a laminate as these are the resin rich areas and thus promote delamination. After the job has run the visualisation post-processor allows the individual plies and interfaces be seen using CAE/visualisation which could provide useful information of the delamination and initiation and growth direction.

Failure laws in cohesive modelling consist of two parts:

- Damage Initiation Criterion.
- Damage Evolution Law.

Abaqus provides four damage initiation criteria: maximum stress, maximum strain, quadratic stress, and quadratic strain criterion. Once the damage initiation criterion of the cohesive element is met with the value of 1 or higher, the stiffness of the cohesive element is degraded. Abaqus/Explicit allows modelling of progressive damage and failure in cohesive layers using traction-separation behaviour. As the tractions approach value zero the opening increases thus creating damage/separation between the interfaces. Once the damage initiation criteria are reached, the traction displacement is degraded linearly. The damage evolution law describes the degradation of the material stiffness and propagation of delamination. A scalar damage variable is used as a damage parameter and can vary from 0 to 1, where 0 is for an undamaged and 1 is for a fully damaged material.

6.6 Overall Conclusions

Edge impact simulations were performed on 2mm thickness laminates with incident velocity of 2.85 m/sec^2 and incident energy of 3J. Widely spread stresses over the unconstrained area of the laminate were found for near-edge impact while high intensity stresses were located just under the area of impactor for on-edge impact. The simulations can also be used to explain the fluctuations observed in the experimentally recorded force/time traces for on-edge impact. Out-of-plane vibration is clearly visible in this impact simulation. The frequency of the vibrations is approximately the same as that observed for the fluctuations in the force/time traces. We postulate that such out-of-plane lateral plate vibration is the cause of these fluctuations in load. Models were then compared with force/time and displacement/time

curves. Both on-edge and near-edge impact were in very good agreement with the force/time and displacement/time experimentally measured values. These elastic simulations could not be expected to exactly match the experiments. Nevertheless, the validity of our approach has been demonstrated from the good agreement between predicted and measured maximum values of force and displacement, and the very good agreement for the impact time. Future simulations using two approaches i.e., Hashin damage failure criteria and cohesive models will lead to understanding of the sequence of damage events and development of an edge impact damage physical model. This chapter provides an initial overview of the impact damage processes for on-edge and near-edge impact.

Chapter 7

Overall Discussion

7.1 Introduction

In chapters 3 to 6, the results of this research were presented and discussed in detail. The experiments included edge impacts, compression and tension after impact and damage assessment techniques. These experiments were performed to meet the aims and objectives of this research. This chapter discusses the causes and dangers of edge impacts and how the impact location can affect damage tolerance during the life span of an aircraft. Further discussions will compare the results extracted from this research with other existing literature.

7.2 Dangers of Edge Impacts

Aircraft are designed to resist all ranges of impacts during operational flight cycles but there is still an on-going threat for the different types of impact. The greatest dangers for impact damage to an aircraft are during flight taxiing, take-off and landing and the probability of edge impacts is highest during this period. Once the aircraft has taken off safely and attained certain altitude the probability of low velocity edge impacts becomes less but the edge impact threat is still prevalent, for example edge impacts during lightening strike and hailstorms. These edge impacts can be termed as high velocity edge impacts. But the damage incurred by these impacts can be detected due to the visibility of the external damage and using NDT techniques. Aircraft nowadays are designed to resist these impacts.

The real threat of edge impact is during the ground handling and taxiing of an aircraft as impact can occur on the leading edge of the wing or fuselage sections. During this period minor damage may go unnoticed and generally is not recorded in the NDT inspection sheets. It is important to capture such damage, as delamination might have originated during these impacts which, during operational flight cycles, may lead to brittle failure. In this research the tomographic views of the near-edge and on-edge impacted laminate showed that for low energy impacts, delamination and matrix cracks are the initial damage mechanisms while at higher incident impact energy levels the damage is a combination of delamination, fibre and matrix failure. Similar damage patterns are seen in several references (see chapter 2 for more details) leading to the conclusion that low energy impacts events are a large threat. Edge impacts during manufacturing of composite spars are potentially more dangerous. Tools dropping or minor accidental impacts on the spars can go undetected which during operational flight cycles can initiate damage leading to failure. Currently, the major concern

in the aircraft industry for impact damage is the impact location. Generally impact tests are performed as centre impacts, and enough information is available in the literature to understand the damage process and the theory involved. But limited literature is available for edge impacts. Recently, there is growing interest in edge impacts (Rhead et al 2010, Gozluklu et al 2013, Ostre et al 2014). More impact and residual strength tests are being carried out to understand the damage processes from impact at an edge of the laminate. The following sections will now discuss the different types of potential accidental edge impacts locations occurring during ground service handling, spar manufacturing and in-flight service of aircraft.

7.3 Edge Impact Locations

Impact location is an important parameter to determine the damage incurred by a composite laminate. The impact scenarios addressed in this dissertation are focused on low velocity impacts at the edges of the composite laminates. An impact location determines the critical inspection areas that might have suffered causing significant levels of internal damage that is not visually detected. The impact data collected during these drop weight impact experiments provides an initial basis for the consideration of aircraft design and handling at different stages during the manufacture of aircraft. Now we will discuss various edge impact location areas during aircraft operational service and manufacturing of wingbox.

7.3.1 Ground Handling Accidental Low Velocity Impacts

Accidental impact location depends upon the direction of impact. Accidental impact can include debris such as rocks, runway pavement, dropped tools, fasteners and ground service equipment. Accidental low velocity impact damage to an aircraft can be caused by contact with various ground service equipments. As the aircraft is surrounded by different vehicles and equipments such as landing gear checks, NDT inspection equipment etc., mishandling can lead to impact edge damage when the aircraft turns towards the take-off location area. The probability of edge impact during this time is highest because of the multiple vehicles and equipments that can be a source of impact. Some airports have small turn around areas where the probability of edge impacts becomes higher. An example of such can seen in figure 7.1 (a) and (b) which is an example of an on-edge impact during aircraft towing. Figure 7.1 (a) shows that the tailing edge of the aircraft strikes the edge shelter roof leading to impact

damage and figure 7.1 (b) shows a pilot error causing the aircraft leading edge of the wing to strike a stationary aircraft tailing edge, leading to on-edge impact damage.

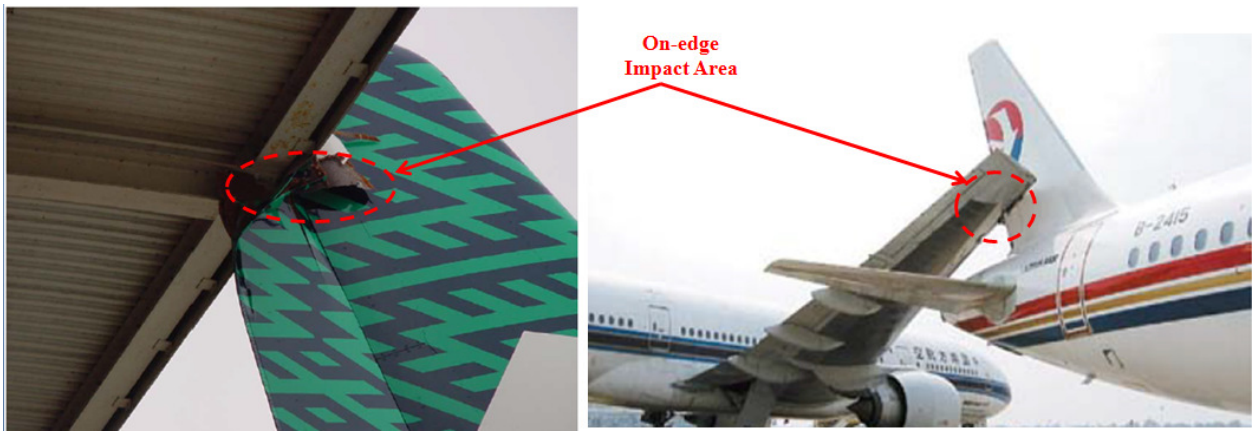

(a) **(b)**

Figure 7.1 (a) and (b) On-edge impact damage during aircraft towing (Blohm 2007)

Another example of edge impact damage locations caused by ground operations is shown in figure 7.2 (a) and (b). Figure 7.2 (a) shows the near-edge impact damage on the thrust reverser of the aircraft during ground operations and figure 7.2 (b) shows the near-edge impact damage caused by runway debris during taxiing of the aircraft. Similarly figure 7.3 (a) and (b) shows an example of centre impact. Figure 7.3 (a) shows centre impact by tyre separation debris and figure 7.3 (b) shows centre impact on the wing flaps caused by ground hail. Ground service vehicles can be another source of high energy and low velocity impacts. Impact location in this case is difficult to predict as they may be combination of edge and centre impacts as shown in figure 7.4 (a) and (b). Figure 7.4 (a) shows the cargo vehicle hitting the lower part of the fuselage and figure 7.4 (b) shows the cargo vehicle hitting the edge of the fan case. These vehicles have high mass leading to higher impact damage. These examples show that the edges of the composite components suffer significant damage. The repairs of these components are time consuming and costly.

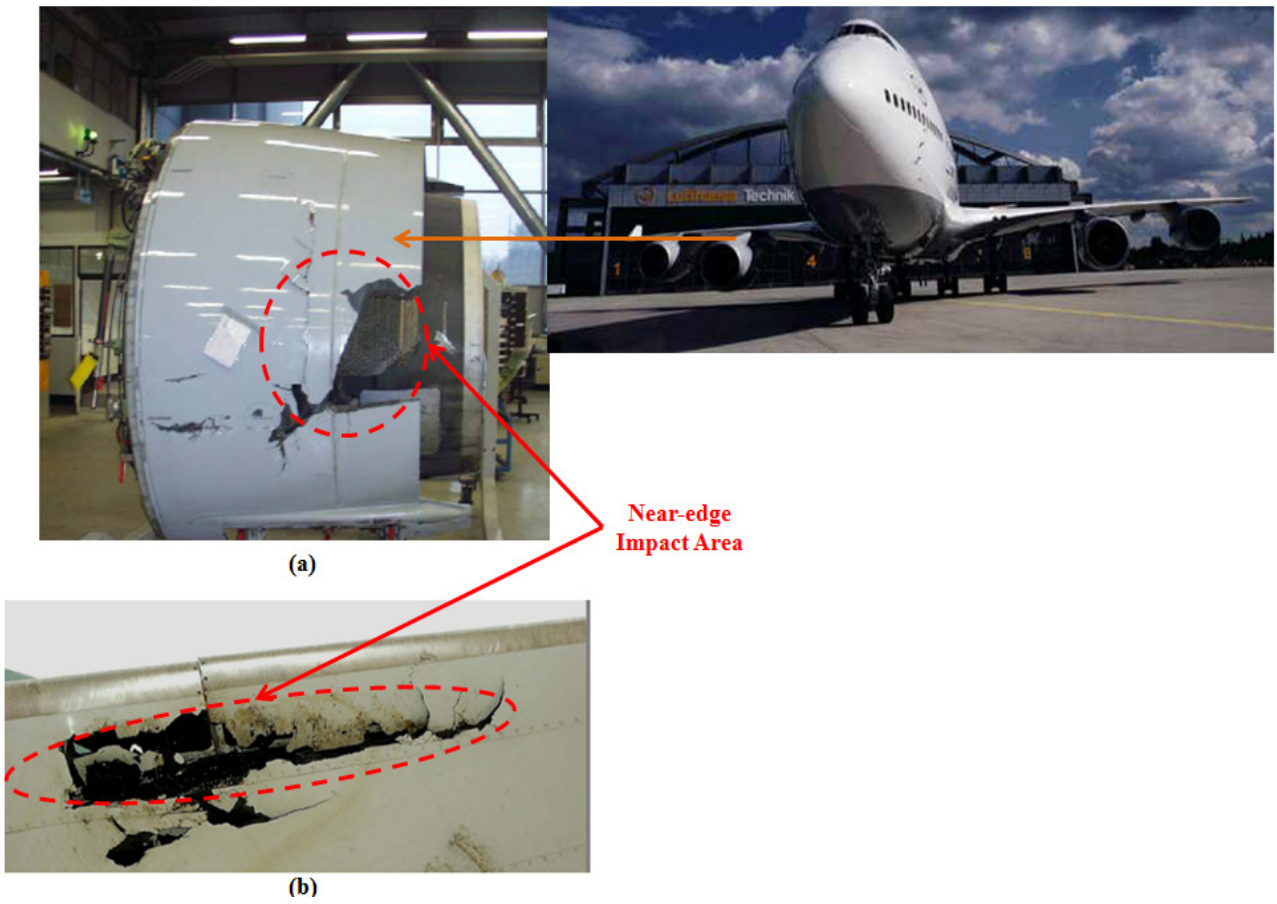

Figure 7.2 Near-edge impact areas (a) Near-edge impact damage to thrust reverser during ground operations (b) Near-edge impact damage during by runaway debris during taxing (Blohm 2007)

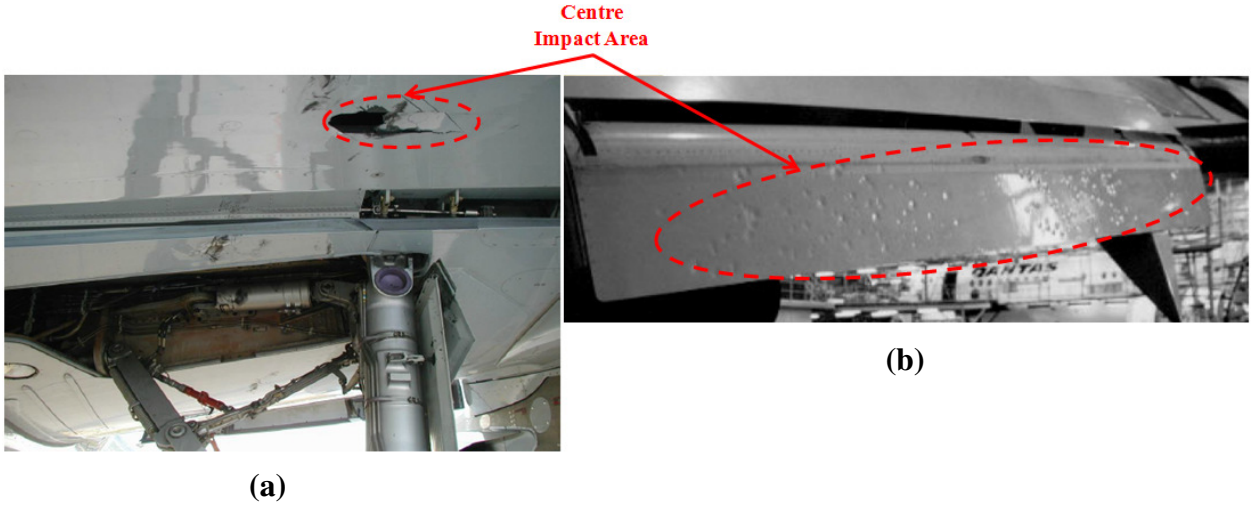

Figure 7.3 Centre impact (a) Tire separation debris (Lufthansa 2007) (b) Ground hail (Berner 2007)

Figure 7.4 Ground service vehicle edge impacts (a) Fuselage (b) Fan case (Blohm 2007)

7.3.2 Wing Spar Manufacturing Accidental Impact Areas

Nowadays, many new aircraft wings include composite materials to reduce costs and improve mechanical properties. However, the majority of accidental or minor impacts occur during manufacturing of the aircraft wings. Figure 7.5 shows a typical wingbox and its components. The aircraft wingbox is a combination of both metallic and composite materials. The areas of the wingbox such as front spar and rear spar, upper and lower covers are made of composite materials while ribs and rib posts are made of metallic components which are then attached to the front and rear composite spars. There is a high probability of edge impacts occurring

when attaching the upper and lower cover using metallic fasteners to the front and rear spars. The fasteners can be a source of impact during the manual handling which can lead to edge damage.

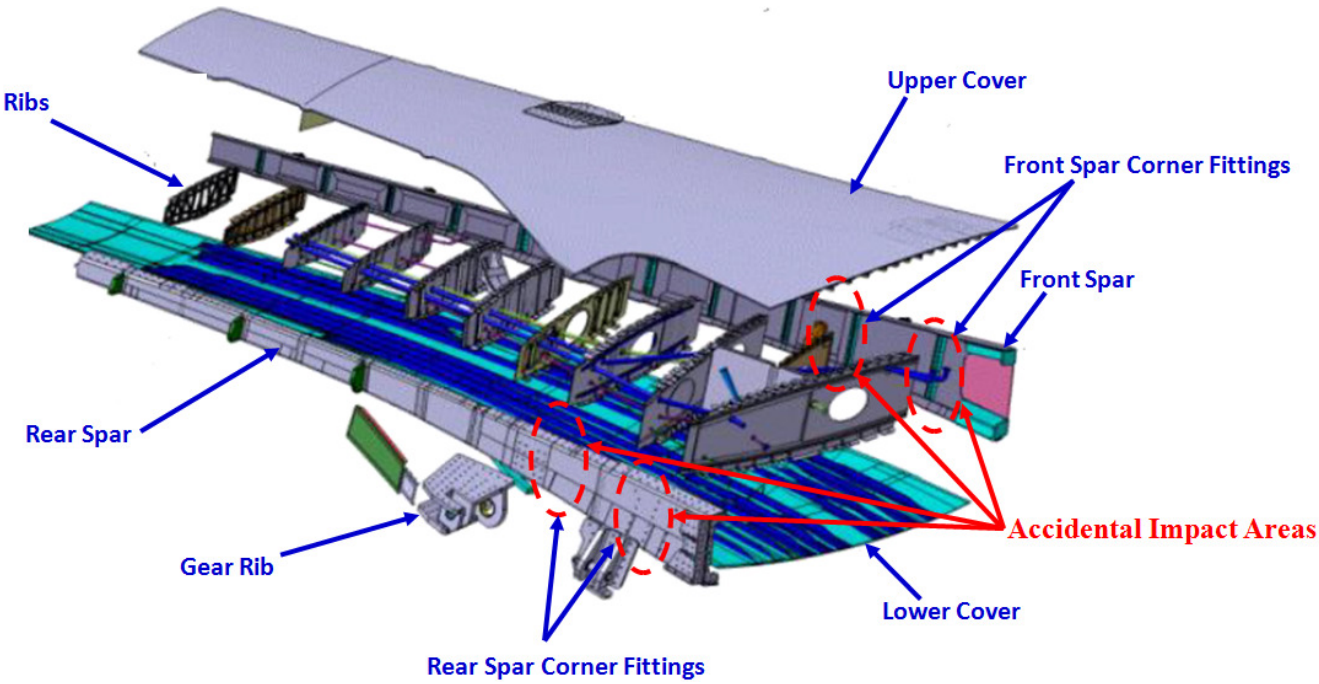

Figure 7.5 Typical aircraft wingbox (Maropoulos et al 2014)

A typical rear C-spar is shown in figure 7.6. This rear spar is made up of carbon/epoxy composite material. The rear spar consists of top/bottom flanges and the web. There are certain areas of the spar where the probabilities of impacts are highest. Figure 7.6 shows the different areas where the impacts can happen during manual handling. The top and bottom flanges in figure 7.6 are protected by impact absorbing covers, as these areas of the spar are likely to have on-edge impact. Near-edge impact is likely to occur around the cut-outs, small/large open holes and near the front edge of the spar. The spar web is most likely to have centre impacts during manual handling. Centre and near-edge impacts can occur very close to each other and could lead to the combination of impact damage. This research provides the initial insight of the damage processes arising from individual impacts; it would be interesting to investigate in future research combining different types of impacts. Other potential areas of impact include the corners of the spar which can lead to angle edge impact

damage. With the higher usage of composite materials in the manufacturing of aircraft wings, strict guidelines are in place to protect from the potential impact threats during the manufacturing of spars but still accidental impacts occur.

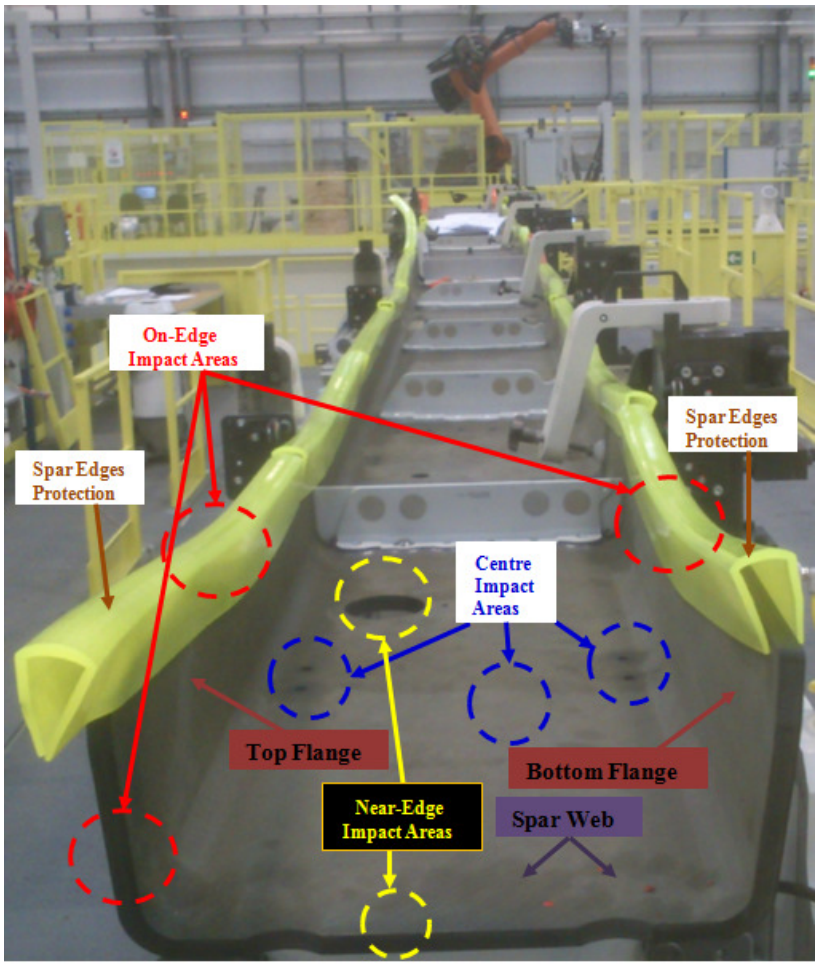

Figure 7.6 Carbon/Epoxy rear C-spar assembly: Impact location areas (GKN Aerospace 2013)

7.3.3 In-Flight Service Edge Impacts

In-flight service impacts can happen during the aircraft take-off, altitude cruising and landing. During aircraft take-off a flock of birds could come in the path of the speeding aircraft (see figure 7.7). Bird strikes involve high kinetic energy and thus become a source of high energy impact leading to severe damage to the aircraft. Multiple impacts by flock of birds around the same time at different locations of the aircraft create multiple stress waves which could generate the delamination and matrix cracks. The impact damage in these cases could be combination of on-edge, near-edge and centre impact. There are some critical areas of the

aircraft where the impact damage is highest for example bird strike on the aircraft jet engine fan blade which is still an on-going problem in aviation industry. Figure 7.8 shows the bird strike probabilities at different locations of the aircraft. The aircraft engine is likely to have more impacts followed by the leading edge of the wing and windshields.

Figure 7.7 Flock of bird strikes during aircraft take-off (Daily Mail 2014)

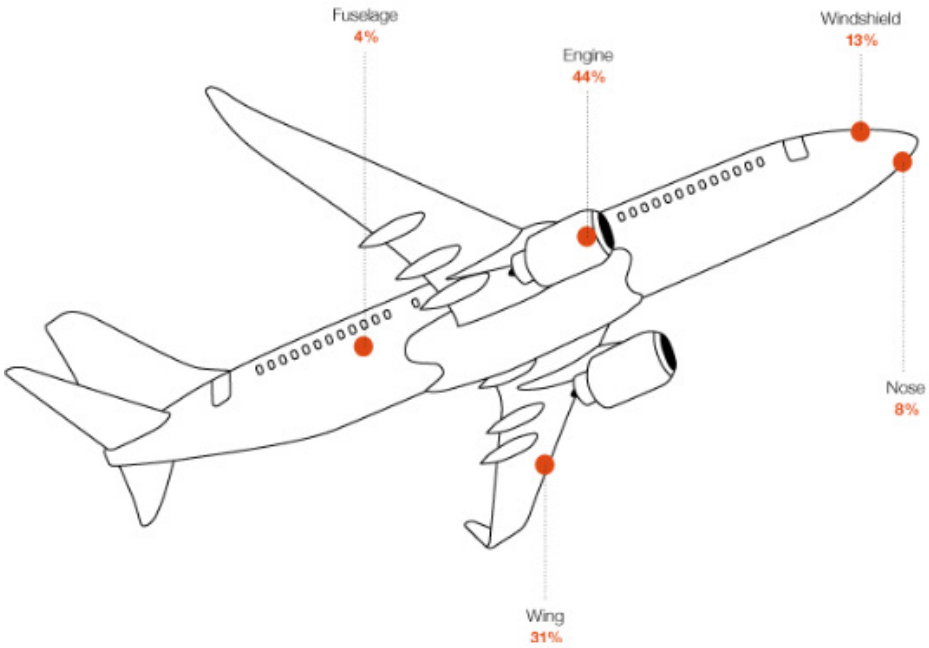

Figure 7.8 Locations of bird-strike damage (Boeing Magazine 2011)

Once the aircraft has taken off and attained high altitude, weather is the biggest threat. The source of impact at this altitude could be lightning and hail storm. Lightning strike is high velocity impact. An example of near-edge impact due to lightning strike is shown in figure

7.9. Lightning strike has damaged the near-edge of the fan reverser which is made of composite laminates. Impacts by lightning can be avoided by avoiding the thunderstorm path.

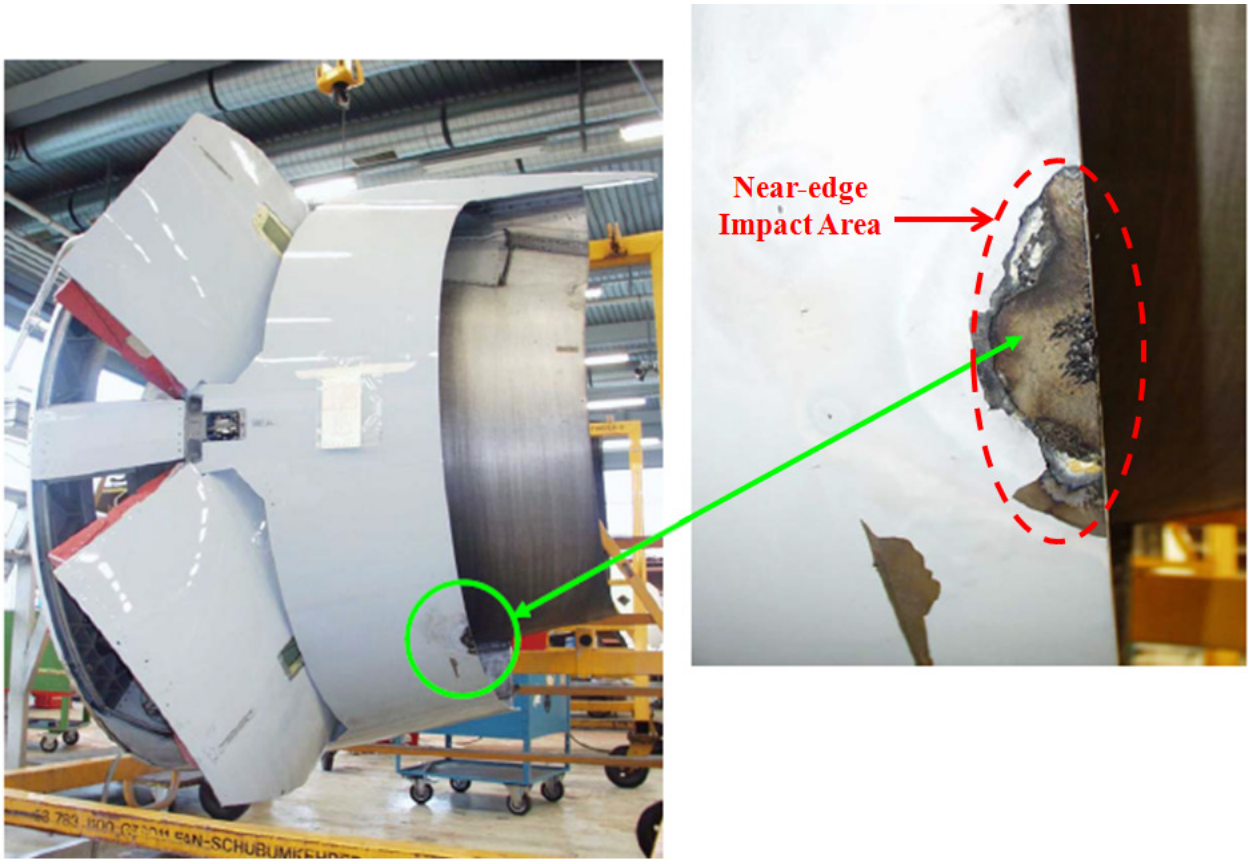

Figure 7.9 In-flight near-edge lightning strike on aircraft fan reverser (Blohm 2007)

Another source of impact during flight is hail strike. Hail can strike the aircraft with high velocity on critical areas of the aircraft. Aircraft are designed for all these types of high energy impacts but multiple impacts at critical locations could potentially damage the composite components leading to emergency landing or crash. An example of multiple on-edge hail strikes is shown in figure 7.10. Smaller hail can potentially damage the leading edges of the wings, inlets, windscreen and jet engines of the aircraft.

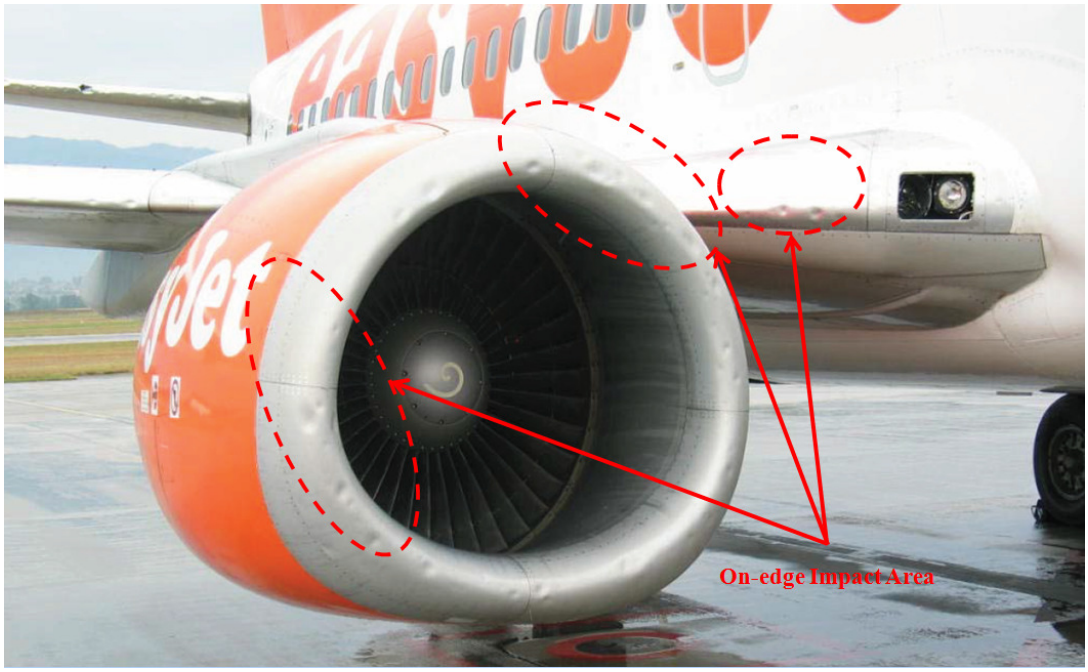

Figure 7.10 In-flight hail on-edge impacts on the aircraft wing and engine (Fawcett and Oakes 2006)

Aircraft are currently developed to make the nose section, leading edges of the wing and parts of the jet engine to withstand all these impact loads. However, there is still limitation of complete usage of composites in aircraft components due to high costs, time consumption and complex repairs of composite components. All examples discussed in this section conclude that edge impacts locations are critical in determining the severity of impact damage in the critical areas of the aircraft during ground and in-flight service.

7.4 Review of Edge Impact Results

This section will discuss the results obtained from this research at different impact positions and compare them with the literature.

7.4.1 Low Velocity Edge impacts

Three impact positions, on-edge, near-edge and centre were compared. The damage level can be predicted from force/time and force/displacement curves (Cantwell et al 1983). Damage initiation can be predicted from the first peak of the force/time and force/displacement curves (Abrate 1991,1998). Near-edge force-time curves showed smooth curve and small peaks indicating less damage. Multiple large fluctuations due to the propagation of elastic waves were detected for on-edge impacts indicating multiple delaminations and fibre/matrix damage. The peak force is critical in determining the damage severity of composite laminates

(Davies et al 1994). The maximum peak load was followed by the post peak region in which extensive damage developed around the impactor region.

From the edge impact experiments results it was clear that that there were three main factors that influence the damage process. These three principal modes of failure were:

- Matrix Cracks
- Delaminations
- Fibre Failure

Matrix Cracks

For near-edge impact matrix cracking occurs just under the impact position. The matrix cracks were detected using computed tomography. The top plies were in compression while the bottom plies were in tension. Shear stresses were detected in the middle ply. The on-edge impacts suffered matrix crushing just under the position of the impactor. It was observed that matrix cracks within the plies occurred first followed by the through thickness shear stresses. These matrix and shear cracks initiate delamination. For near-edge impact, interlaminar shear stresses were detected due to the bending of the laminate, as observed elsewhere (Park et al 2000). For on-edge impact, due to high localised stresses, fibre/matrix failure occurs just under the impactor, as found by Richardson et al (1996).

Delaminations

Delamination can affect the strength and stiffness of the composite laminate. From the results it was clear that the edge impacts could lead to edge delamination due to highly localised interlaminar stresses at the free-edge of the laminate; similar behaviour has been reported in the literature (Sihn et al 2007). Near-edge impacts suffered widespread delaminations and were detected in $+45^0/-45^0$ plies while on-edge suffered multiple delaminations in almost all the plies. For near-edge impact the delamination occurred in the through thickness direction of the laminate. For the thicker laminates delamination occurred just under the point of contact surface while for the thin laminates delamination occurred both on the top and the bottom face of the plies due to their higher bending stresses, as also reported by Pagano et al (2000).

Fibre Failure

On-edge impact suffered high fibre breakage compared to near-edge impact just under the location of the impactor. Large amount of matrix/fibre fracture was observed for the on-edge impact, particularly at high incident impact energies. Displaced fibres were observed for near-edge impact at lower impact energies.

Finite element simulations showed that near-edge impact suffered intralaminar damage and higher tensile stresses in the bottom plies while the top ply suffered higher compressive stresses in the contact surface. Simulations showed that impact damage for both on-edge and near-edge is mainly propagated by the transverse shear stresses. From the results, it was observed that during the near-edge impact the matrix failure in tension is the first and most critical failure mechanism of the plies. Near-edge impact was more susceptible to delamination, especially at the top ply and the interfaces of the plies. From the experiments and simulations it is clear that the on-edge impact response time duration is very small compared to near-edge impact. The peak force of the near-edge impact was much lower than the on-edge impacts and the trends of the curves obtained in the simulations agree with the experimental results for both near-edge and on-edge impacts.

Effect of thickness is an important parameter for understanding the damage process during edge impacts. At higher impact energies and velocities more damage is done to thinner laminate than to the thicker laminate for both types of edge impacts. From the results different trends in damage processes for near-edge and on-edge were observed for both the thin and thick composite laminates. As the critical peak force to create impact damage is directly proportional to laminate thickness (Davies et al 1994), the thicker laminate requires higher impact energy to cause damage (Stavropoulos et al 1997). The results for the thick laminates showed reduction in impact time and maximum displacement compared to the thinner laminate. The peak force is almost doubled for the thicker laminate; the increase in peak force with incident energy appears higher at lower incident energy. More energy is absorbed by the thicker laminate. A higher proportion of the incident energy is absorbed for higher energy impacts. For on-edge impacts the impact time decreases slightly for the thicker laminate. The value of peak force is increased for the thicker laminate, and the values appear to converge at higher incident energies.

7.4.2 Computed Tomography

Computed tomography technique has been successfully implemented to explore three dimensional views of the inner workings of biological properties (McElrone et al 2013). Using a similar approach, the internal damage of the composites has been investigated and the internal damage of the near-edge and on-edge impacted specimens was captured. A computer algorithm converts the large number of 2D projections to 2D slices. From these slices the three dimensional structure of the edge impacted laminate were reconstructed. On-edge and near-edge impacted damage were captured in three dimensions using the Drishti visualisation tool. The changes in number of pixels were investigated. The three phases: matrix phase, fibre phases and matrix/fibre phases were studied extensively to get an overall picture of the edge impact damage. Similar techniques are reported in the literature (Abel 2012). The fibre bundles, fibre cracks, displaced fibres were all fully captured using this technique. It was observed that the major damage mechanisms during edge impacts were shear damage and cracks at the interfaces of the plies. Matrix cracks were observed. Similar observations were made by Young (2009). Localised fractures of the on-edge impacted specimens were observed around the impact area. The fractured area was investigated first with the matrix phase and second with the fibre phase. It was observed that both the phases had similar contribution for the fracture area, as observed elsewhere (Crupi et al 2011). When the fibre was rendered invisible then the distribution of the matrix was mainly confined around the fibre bundles. From the results the shape and size of the matrix could be seen clearly, as observed in the work of Andersson (2011). Similarly when the matrix was rendered invisible we could see the fibre bundles and the potential damage areas of the fibre after the edge impact. Interface cracks were seen around the areas of fibre bundles. Two types of fibre breaks were observed:

- Shear cracks
- Fibre/matrix multiple crack load path

Load path was determined by the fibre/matrix crack interfaces. For on-edge impacted specimen splitting cracks along matrix/fibre interfaces were observed. Splitting cracks were driven by ply interfaces and the two types of cracks were observed: first the shear cracks and second the fibre breaks. Multiple fibre breaks were clearly visible. Shear cracks were found to be symmetric in position and direction. For near-edge impact the matrix crack formation

occurs at the front ply that is at the point of contact between the impactor and the laminate prior to fibre breakages, as reported in the literature (Scott 2010). Some fibre breaks were observed for the near-edge impact. Lots of displaced fibres were found for the near-edge impact and this could potentially lead to delamination because as the fibre displaces its position the matrix bonds are broken which can create peanut type delamination (Abrate 1991).

7.4.3 Residual Strength

The real strength of the composite laminate is measured from the damage tolerance to the edge impact damage. After edge impact, under compressive or tensile load, the strength will depend upon the type of edge impact, damage size, location and the laminate thickness. It was observed from the results that compression after near-edge impact suffered shear failure and fibre kinking; similar failure mechanisms were observed by Yuan (2000). Delamination played an important role in propagating the internal damage under compression after impact. Delamination between the plies was observed in near-edge impact. For near-edge impact internal delamination is mainly driven by shear stresses. The reduced compressive strength of the near-edge impacted laminate was directly related to the extent of the internal delamination, as found in the literature (Wiggenraad et al 1996; Park et al 2000). On-edge impact damage caused stress concentrations at the free edge of the laminate leading to both in plane and out-of-plane shear stresses in the region close to the point of impact thus creating fibre micro-buckling initiation at the edge; similar failure has been observed in the work of Edgren (2003). Higher residual strength was found in compression for the on-edge impacted laminates compared to the near-edge impacted laminates.

For tension after edge impact as the displacement is increased the load increased linearly until final fracture. When the fibres are broken there is a decrease in tensile strength. This reduction in the tensile strength depends upon the damage locations and the damage size of the composite laminate. Lower tensile residual strength for the on-edge impacted laminate was found; this is due to increased damage sizes and more fibre breakage compared to the near-edge impact, as observed in the literature (Li et al 2000). During tension after on-edge impact fibre cracks can be seen on the front and on the back face side of the specimen; similar cracks running perpendicular to the fibre direction have been found (Hoogsteden 1992).

The effect of thickness was also investigated. In the compression test, thinner laminates were found to have much lower reduced residual strength compared to thicker laminates for the on-edge, near-edge impacts and centre impact. This was due to the fact that the thicker laminates tend to have lower bending moment and thus higher residual strength than thin laminates under compressive load, as reported in the literature (Tai et al 1999). Residual tensile strength of thin laminates was reduced at higher incident energy levels. Thin laminates experience complete fibre breakage and fracture while for thick laminates less fibre breaks and fracture were observed.

7.5 Conclusions

The dangers of edge impact during aircraft taxiing, take-off, in-flight and landing have been discussed. The severity of the edge impacts depends upon the edge impact location and various real case studies of edge impacts have been discussed. The impact response arising from on-edge impact was found to be very different from impacts on the plane of the laminate. These observations were successfully explored using X-ray computed tomography. The different failure mechanisms were highlighted from comparison of results from compression after impact and tension after impact tests. Damaging fibre failure, caused by accidental low velocity impact on the edge of a composite laminate, is not readily detected in conventional compression after impact tests.

Chapter 8

Conclusions and Future Research

8.1 Introduction

In this section we will discuss about major findings, conclusions, recommendations and future research on the edge impact of composite structures.

8.2 Concluding Remarks

The causes and dangers of low velocity edge impacts have been discussed extensively in this research. The type of edge impact, impact location, the damage size and the laminate thickness all influence the damage initiation and damage evolution of the composite laminates. These parameters determine whether the damage can be visually inspected or requires non-destructive techniques for further investigations. The results presented in this research provide a good initial overview of the edge impact damage process for both the on-edge and near-edge impact. This research has shown that the edge impact damage zones have a very complex geometry.

Near-edge, on-edge and centre impacts have been investigated experimentally. Preliminary observations of the damage showed the severe nature of the damage arising from on-edge impact while for the near-edge impact the damage was found around the area of impact. Force-time histories at different incident impact energies and thicknesses were compared for on-edge and near-edge impacts and then later compared with centre impacted specimens. The experimental results showed that the impact damage increases as the incident impact energy increases irrespective of thickness. Thin laminates showed higher damage compared to thick laminates for all types of impacts. It has been found that both the on-edge and near-edge impact suffer delamination. Near-edge impact suffered shear failure/fibre kinking and delamination in-between the mid $-45^0/-45^0$ plies. This internal delamination in near-edge impact is mainly driven by shear stresses. On-edge impact suffered multiple delaminations and caused stress concentrations at the free edge of the laminate leading to both in plane and out-of-plane shear stresses in the region close to the point of impact. Later, the finite element models were compared with experimentally determined force/time and displacement/time curves. Both on-edge and near-edge impact is in fair agreement with the experimental measured values up to maximum peak force and displacement and for impact duration. Stresses in near-edge impact are more widely spread while on-edge impact stresses were more localised and confined to the point of impact. These models could further be

investigated using Hashin damage criteria and cohesive models to capture the full force-time and displacement time histories.

Initial damage assessment for near-edge, on-edge and centre impact were carried out using visualisation and optical microscopy techniques. Results showed that with increased incident energies, the damage tends to increase. Thus the observations from the initial damage lead to further investigation of edge impact damage process using computed tomography. Computed tomography technique was important in understanding the damage initiation, damage propagation and the position of delamination for both the on-edge and near-edge impact at different thickness and energy levels. Major damage mechanisms were explored such as fibre cracks, fibre/matrix cracks load paths, fibre bundle fracture, matrix damage and delamination. On-edge impact showed multiple delamination and fibre failure and near-edge impact showed more matrix damage around the area of contact.

The research further investigated the damage tolerance of the composite laminates for near-edge, on-edge and centre impacted laminates. When the laminate is loaded under compression and tension the edge impacts influence the failure and failure direction in the surrounding undamaged material. Results showed lower residual strength for increased incident energy for thin laminate for all types of impacts. On-edge impact laminate showed greater reduction in the tensile strength and less reduction in the compression tests while the near-edge and centre impact showed greater reduction in compression and less reduction in tension for the different thickness and incident energy levels. These reductions in the tensile strength were due to the damage locations, the damage type and the damage size of the composite laminate.

A final summary of the salient findings:

- On-edge impact leads to more fibre failure and matrix crushing.
  - Observed from 3D tomographic inspection and finite element simulations.
  - Higher stiffness is observed for on-edge impact laminate.
  - Out-of-plane vibration was seen in the on-edge impact finite element simulations.
  - Observed and predicted more fibre failure.
  - Maximum stresses are more concentrated through the thickness and around the area of on-edge impact.

- Severity of damage may not be detected using conventional CAI testing.

❖ Near-edge Impact leads to more internal delamination and matrix damage.
- Observed from 3D tomographic inspection and finite element simulations.
- Maximum stresses were found at the point of contact as seen from the finite element simulation results.
- Matrix damage and delamination were seen for both the thin and thick laminates followed by the fibre cracks/fibre displacement.
- Stresses are more distributed through the plane of the laminate and near the edges of the boundaries.
- Higher bending and flexural stresses are seen from the near-edge impact simulation.
- Larger area of delamination is observed inside the plane of the laminate due to larger area of contact.

❖ Centre impact also leads to delamination.
- Observed from maximum compressive stresses that are found at the point of centre impact.
- Behaved more like near-edge impact as the peak impact forces and residual strength were similar to near-edge impact.
- Higher impact duration was observed which directly relate to the higher bending and flexural stresses as compared to near-edge impacted laminate.
- Larger impact damage area was observed from the visualisation technique as the incident impact energy increased from 2J to 4J.

8.3 Future Research

The results from this thesis can lead to further research. Recommendations are as follows:

- Edge Impact can be further be investigated at various angles. This will lead to better understanding of the damage process involved. Finite element simulations could be carried out to capture various critical stress areas. Further, the damage tolerance of the angle edge impacted laminates could be investigated.

- Near-edge and on-edge impact damage could be further investigated using finite element simulations with various failure models such as Hashin damage and cohesive models. These could provide better understanding of the delaminations, fibre and matrix failures and could fully capture the force/time and displacement/time curves to compare with experimentally measured values.

- Research can be further extended to composite laminates with holes. It will be interesting to investigate the impact damage at the edge of a hole. This may provide wider interest for aerospace companies such as Airbus and Boeing. Holes and cut-outs are the major contributors to delamination around the free edge of the laminate. The hole in the composite spar associates with items such as various bolts fasteners, hydraulic fuel lines etc, which might interact with the hole edge and could lead to potential delamination. Further these investigations could include composite fatigue which can lead to lower reserve/safety factors.

- Further research can also be useful to study the effect of multiple edge impacts. These impacts could be carried out at both low and high velocity. These impacts could generate multiple stress waves which can great affect the damage process and strength of the laminate. Further compression and tension after edge impacts test could be carried out.

- Edge impact experiments could also be carried out using the different impactor shapes. Impactor shapes could greatly affect the damage process for composite laminates (for more details see chapter 2). Effect of thickness at different impact energies could be explored.

- High velocity edge impact which may occur during aircraft take-off and landing could also be investigated. Research could further investigate the effect of different boundary conditions and the effect of various impactor masses. Finite elements simulations could also be performed in order to detect the different damage states.

- Effect of different and lay-ups at different thicknesses and energy levels could be investigated for edge impacts. Computed tomography technique could be utilised for detecting delamination and impact damage processes of the composite structure.

Appendix-A

A.1 Analysis of Composite Laminates

Unidirectional Lamina:

Unidirectional Lamina can be represented as a single composite layer with continuous fibres perfectly aligned along the longitudinal direction. Unidirectional fibre composite has different strength and stiffness in different directions. In order to determine the mechanical properties of composites it is convenient to consider a composite in which all the fibres are aligned in one direction. This can then be used to predict the behaviour of continuous fibre multi directional laminates. Figure A.1 shows a unidirectional composite with the principal material axes. Coordinates x and y represent longitudinal and transverse in-plane directions.

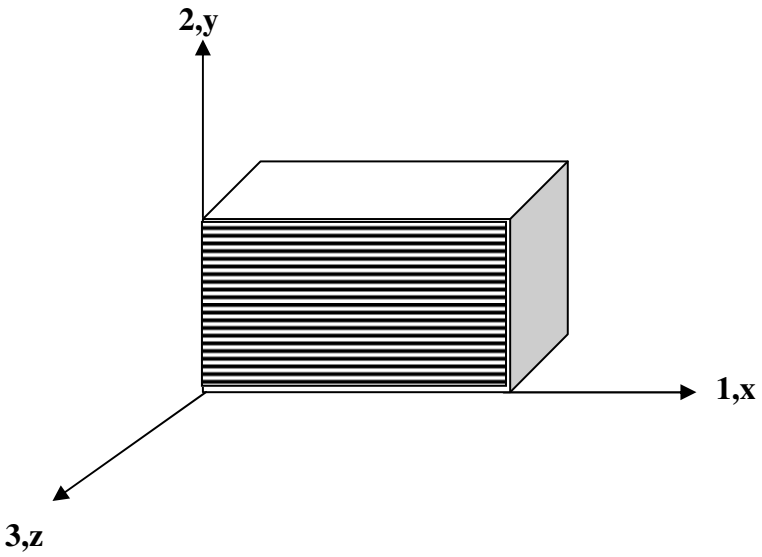

Figure A.1 Principal material axes for unidirectional lamina

The mechanical properties in the longitudinal (x-direction) are different from those in two transverse directions (y and z direction). In order to derive equation for longitudinal stiffness (E_1) and transverse stiffness (E_2), we will assume parallel arrangement of the fibres and the matrix as shown in figure A.2.

For this arrangement, the axial strain in the composite ε_1 is uniform such that the axial strains in the fibres and matrix are identical but the axial load P_1 in the composite is the sum of axial loads in the fibres and the matrix (Callister 2006, Matthews 2000).

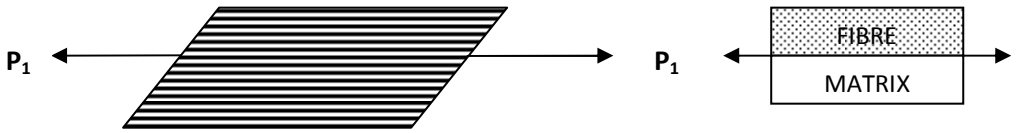

Figure A.2 Loading conditions parallel to fibre direction

$$\varepsilon_1 = \varepsilon_{m1} = \varepsilon_{f1} \quad \text{(A.1)}$$

$$P_1 = P_{f1} + P_{m1} \quad \text{(A.2)}$$

Where

ε_1 and σ_1 = Strain and stress in longitudinal direction

ε_{m1} and σ_{m1}= Matrix strain and stress in longitudinal direction

ε_{f1} and σ_{f1}= Fibre strain and stress in longitudinal direction

P_1= Applied load in longitudinal direction

P_{m1}= Applied matrix load in longitudinal direction

P_{f1}= Applied fibre load in longitudinal direction

Converting equation (A.2) into stress

$$\sigma_1 A_c = \sigma_{f1} A_f + \sigma_{m1} A_m \quad \text{(A.3)}$$

Where A_c, A_f and A_m are the cross-sectional areas of the composite, fibre and the matrix respectively ($A_c = A_f + A_m$). By rearranging equation (A.3) we obtain

$$\sigma_1 = \sigma_{f1} A_f/A_c + \sigma_{m1} A_m/A_c \quad \text{(A.4)}$$

Ratios A_f/A_c and A_m/A_c represent volume fractions of the fibres v_f, and matrix v_m, respectively. Thus the axial stress in the lamina is

$$\sigma_1 = \sigma_{f1} v_f + \sigma_{m1} v_m \quad \text{(A.5)}$$

Since $v_f + v_m = 1$, equation (A.5) can be expressed in terms of v_f only as

$$\sigma_1 = \sigma_{f1} v_f + \sigma_{m1} (1 - v_f) \quad \text{(A.6)}$$

i.e., the lamina stress in the axial direction is a linear function of fibre volume fraction. This equation is known as the "rule of mixtures for stresses".

Properties related to normal loading in the transverse direction (see figure A.3), is based on the assumption of a series arrangement between the fibres and matrix. For this arrangement, the transverse stress in the composite σ_2 or σ_3 is uniform such that the transverse stresses in the fibres and the matrix are identical but the axial strain ε_2 or ε_3 in the lamina is the sum of the axial strains in the fibre and the matrix (Matthews 2000).

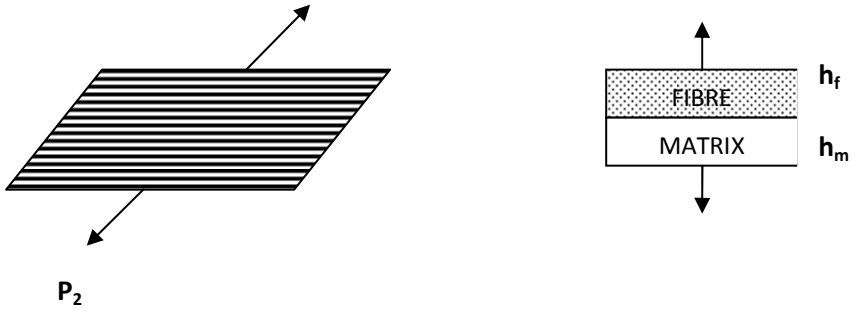

Figure A.3 Loading conditions normal to fibre direction

$$\sigma_2=\sigma_{m2}=\sigma_{f2} \quad \text{(A.7)}$$

$$\delta_2=\delta_{f2}+\delta_{m2} \quad \text{(A.8)}$$

Converting equation (A.8) into strain

$$\varepsilon_2 h_c=\varepsilon_{f2} h_f+\varepsilon_{m2} h_m \quad \text{(A.9)}$$

Where h represents ($h_c= h_f + h_m$). By rearranging equation (A.10) we obtain

$$\varepsilon_2=\varepsilon_{f2} h_f/h_c+\varepsilon_{m2} h_m/h_c \quad \text{(A.10)}$$

Ratios h_f/h_c and h_m/h_c represent volume fractions of the fibres ν_f and the matrix, ν_m respectively. Thus equation (A.10) can be written in terms of volume fractions as

$$\varepsilon_2=\varepsilon_{f2} \nu_f+\varepsilon_{m2} \nu_m \quad \text{(A.11)}$$

or

$$\varepsilon_2=\varepsilon_{f2} \nu_f+\varepsilon_{m2} (1-\nu_f) \quad \text{(A.12)}$$

i.e., the lamina strain in the transverse direction is a linear function of fibre volume fraction. This equation is known as “rule of mixtures for strains”.

So from equations (A.1) and (A.6) we obtain that

$$E_1 = E_f \nu_f + E_m \nu_m \quad \text{(A.13)}$$

i.e. axial modulus of the lamina is a linear function of the fibre volume fraction. This equation is known as "rule of mixtures for moduli". From equations (A.7) and (A.11) we obtain

$$\frac{1}{E_2} = \frac{v_f}{E_f} + \frac{v_m}{E_m}$$

or

$$\frac{1}{E_2} = \frac{v_f}{E_f} + \frac{(1 - v_f)}{E_m} \quad \text{(A.14)}$$

This equation is known as inverse "rule of mixtures for moduli".

Shear modulus of the lamina can be determined from the following relationship

$$\frac{1}{G_{12}} = \frac{v_f}{G_f} + \frac{v_m}{G_m}$$

or

$$\frac{1}{G_{12}} = \frac{v_f}{G_f} + \frac{(1 - v_f)}{G_m} \quad \text{(A.15)}$$

This equation is known as "inverse rule of mixtures for shear moduli".

Angle Ply Lamina:

In angle ply lamina the fibres are oriented at an angle θ with respect to x-direction. Figure A.4 shows the transformation of stress between the principal axes (1, 2) and global axes (x, y).

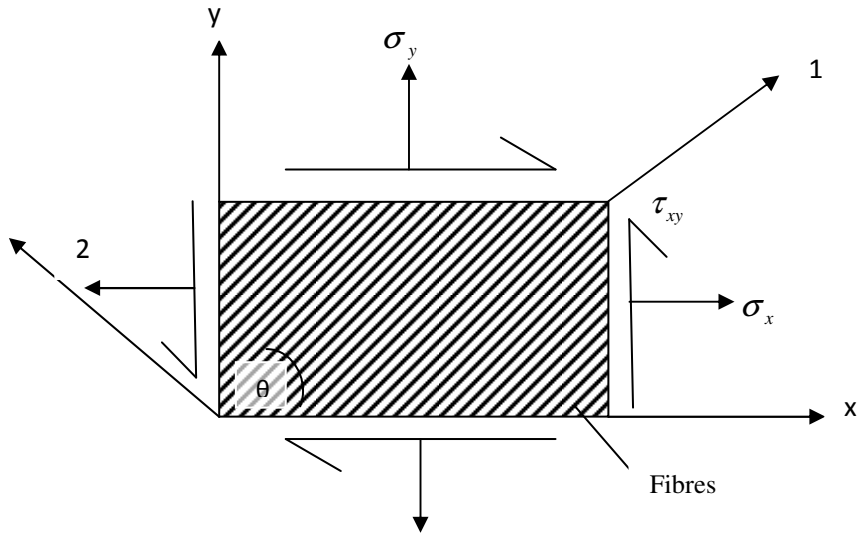

Figure A.4 Transformation of stresses from principal axes to global axes

Transformation of Stress:

The stresses in 1-2 system are related to the stresses in x-y system by

$$\begin{bmatrix}\sigma_1\\ \sigma_2\\ \tau_{12}\end{bmatrix}=\begin{bmatrix}m^2 & n^2 & 2mn\\ n^2 & m^2 & -2mn\\ -mn & mn & (m^2-n^2)\end{bmatrix}\begin{bmatrix}\sigma_x\\ \sigma_y\\ \tau_{xy}\end{bmatrix} \tag{A.16}$$

$$[T]_\sigma=\begin{bmatrix}m^2 & n^2 & 2mn\\ n^2 & m^2 & -2mn\\ -mn & mn & (m^2-n^2)\end{bmatrix} \tag{A.17}$$

With m= cos θ and n= sin θ

Putting equation (A.17) in (A.16) we have

$$\begin{bmatrix}\sigma_1\\ \sigma_2\\ \tau_{12}\end{bmatrix}=[T]_\sigma\begin{bmatrix}\sigma_x\\ \sigma_y\\ \tau_{xy}\end{bmatrix}\text{ or }[\sigma]_{1,2}=[T]_\sigma\,[\sigma]_{x,y} \tag{A.18}$$

The inverse of equation relates to stresses in the x-y system to stresses in the 1-2 system

$$\begin{bmatrix}\sigma_x\\ \sigma_y\\ \tau_{xy}\end{bmatrix}=[T]_\sigma^{-1}\begin{bmatrix}\sigma_1\\ \sigma_2\\ \sigma_3\end{bmatrix}\text{ or }[\sigma]_{x,y}=[T]_\sigma^{-1}\,[\sigma]_{1,2}\text{ Where}[T]_\sigma^{-1}=\begin{bmatrix}m^2 & n^2 & -2mn\\ n^2 & m^2 & 2mn\\ mn & -mn & (m^2-n^2)\end{bmatrix}$$

Transformation of Strain:

Similarly, the strains in the 1-2 system can be related to strains in x-y system

$$\begin{bmatrix} \varepsilon_1 \\ \varepsilon_2 \\ \gamma_{12} \end{bmatrix} = \begin{bmatrix} m^2 & n^2 & 2mn \\ n^2 & m^2 & -2mn \\ -mn & mn & (m^2 - n^2) \end{bmatrix} \begin{bmatrix} \varepsilon_x \\ \varepsilon_y \\ \gamma_{xy} \end{bmatrix} \tag{A.19}$$

This transformation matrix of trigonometric relations is used in plane-stress analysis of fibre-reinforced composites and is denoted by $[T]_\varepsilon$

$$\text{Where } [T]_\varepsilon = \begin{bmatrix} m^2 & n^2 & 2mn \\ n^2 & m^2 & -2mn \\ -mn & mn & (m^2 - n^2) \end{bmatrix} \tag{A.20}$$

Inserting equation (A.20) in (A.19) we have

$$\begin{bmatrix} \varepsilon_1 \\ \varepsilon_2 \\ \gamma_{12} \end{bmatrix} = [T]_\varepsilon \begin{bmatrix} \varepsilon_x \\ \varepsilon_y \\ \gamma_{xy} \end{bmatrix} \text{ or } [\varepsilon]_{1,2} = [T]_\varepsilon [\varepsilon]_{x,y} \tag{A.21}$$

The inverse of equation can be written as

$$\begin{bmatrix} \varepsilon_x \\ \varepsilon_y \\ \gamma_{xy} \end{bmatrix} = [T]_\varepsilon^{-1} \begin{bmatrix} \varepsilon_1 \\ \varepsilon_2 \\ \gamma_{12} \end{bmatrix} \text{ where } [T]_\varepsilon^{-1} = \begin{bmatrix} m^2 & n^2 & -2mn \\ n^2 & m^2 & 2mn \\ mn & -mn & (m^2 - n^2) \end{bmatrix}$$

Stiffness Transformation Matrix:

The stress-strain relationship in global system for plane-stress can be obtained by the constitutive equation in principal material coordinates and employing the stress and strain transformation given by equations (Matthews 2000).

$$\sigma_{12} = [Q][\varepsilon]_{1,2} \tag{A.22}$$

Putting equation (A.18) and (A.21) in (A.22) we have

$$[T]_\sigma [\sigma]_{x,y} = [Q][T]_\varepsilon [\varepsilon]_{x,y} \text{ or}$$

$$[\sigma]_{x,y} = [T]_\sigma^{-1} [Q][T]_\varepsilon [\varepsilon]_{x,y}$$

The product $[T]_\sigma^{-1}[Q][T]_\varepsilon$ is called the reduced stiffness transformation matrix and is denoted by $[Q]$. Thus the stress-strain relationship in the global system can be written as

$$\sigma_{x,y} = [\overline{Q}][\varepsilon]_{x,y} \tag{A.23}$$

$[\overline{Q}]$ is a matrix whose elements are related to the elements of $[Q]$

The transformed stiffness matrix is $\overline{Q}$, the elements of which are:

$$[\overline{Q}]=\begin{bmatrix} \overline{Q}_{11} & \overline{Q}_{12} & \overline{Q}_{16} \\ \overline{Q}_{12} & \overline{Q}_{22} & \overline{Q}_{26} \\ \overline{Q}_{16} & \overline{Q}_{26} & \overline{Q}_{66} \end{bmatrix}$$

Where $[\overline{Q}]$ is:

$$\overline{Q}_{11} = Q_{11}m^4 + 2(Q_{12} + 2Q_{66})n^2m^2 + Q_{22}n^4$$

$$\overline{Q}_{22} = Q_{11}n^4 + 2(Q_{12} + 2Q_{66})n^2m^2 + Q_{22}m^4$$

$$\overline{Q}_{12} = \overline{Q}_{21} = (Q_{11} + Q_{22} - 4Q_{66})n^2m^2 + Q_{12}(m^4 + n^4)$$

$$\overline{Q}_{66} = (Q_{11} + Q_{22} - 2Q_{12} - 2Q_{66})n^2m^2 + Q_{66}(m^4 + n^4)$$

$$\overline{Q}_{16} = (Q_{11} - Q_{12} - 2Q_{66})nm^3 + (Q_{12} - Q_{22} + 2Q_{66})n^3m$$

$$\overline{Q}_{26} = (Q_{11} - Q_{12} - 2Q_{66})n^3m + (Q_{12} - Q_{22} + 2Q_{66})nm^3$$

$$\varepsilon_{xy} = \overline{Q}^{-1}\sigma_{xy} \qquad \text{(A.24)}$$

Compliance Transformation Matrix:

Similarly for

$$\varepsilon_{12}=[S][\sigma]_{1,2} \qquad \text{(A.25)}$$

Putting equation (A.18) and (A.21) in (A.25) we have

$$[T]_{\varepsilon}[\varepsilon]_{x,y} = [S][T]_{\sigma}[\sigma]_{x,y} \ \ or$$

$$[\varepsilon]_{x,y} = [T_{\varepsilon}^{-1}][S][T]_{\sigma}[\sigma]_{x,y} \qquad \text{(A.26)}$$

The product $[T]_{\varepsilon}^{-1}[S][T]_{\sigma}$ is called the reduced compliance transformation matrix and is denoted by $[\overline{S}]$. Thus equation (A.26) is the stress-strain relationship in the global system and can be written as

$$\varepsilon_{x,y}=[\overline{S}][\sigma]_{x,y} \qquad \text{(A.27)}$$

$[\overline{S}]$ is a matrix whose elements are related to the elements of $[S]$

The transformed compliance matrix is $[\overline{S}]$, the elements of which are:

$$[\bar{S}]=\begin{bmatrix} \bar{S}_{11} & \bar{S}_{12} & \bar{S}_{16} \\ \bar{S}_{12} & \bar{S}_{22} & \bar{S}_{26} \\ \bar{S}_{16} & \bar{S}_{26} & \bar{S}_{66} \end{bmatrix}$$

Where:

$$\bar{S}_{11} = S_{11}m^4 + (2S_{12} + S_{66})n^2m^2 + S_{22}n^4$$

$$\bar{S}_{22} = S_{11}n^4 + (2S_{12} + S_{66})n^2m^2 + S_{22}m^4$$

$$\bar{S}_{12} = \bar{S}_{21} = (S_{11} + S_{22} - S_{66})n^2m^2 + S_{12}(m^4 + n^4)$$

$$\bar{S}_{66} = 2(2S_{11} + 2S_{22} - 4S_{12} - S_{66})n^2m^2 + S_{66}(m^4 + n^4)$$

$$\bar{S}_{16} = (2S_{11} - 2S_{12} - S_{66})m^3n + (2S_{12} - 2S_{22} + S_{66})mn^3$$

$$\bar{S}_{26} = (2S_{11} - 2S_{12} - S_{66})n^3m + (2S_{12} - 2S_{22} + S_{66})m^3n$$

Equation (A.23) can be written as

$$\begin{bmatrix} \sigma_x \\ \sigma_y \\ \tau_{xy} \end{bmatrix} = \begin{bmatrix} \bar{Q}_{11} & \bar{Q}_{12} & \bar{Q}_{16} \\ \bar{Q}_{12} & \bar{Q}_{22} & \bar{Q}_{26} \\ \bar{Q}_{16} & \bar{Q}_{26} & \bar{Q}_{66} \end{bmatrix} \begin{bmatrix} \varepsilon_x \\ \varepsilon_y \\ \gamma_{xy} \end{bmatrix} \text{ or} \qquad \text{(A.28)}$$

$$\sigma_x = \bar{Q}_{11}\varepsilon_x + \bar{Q}_{12}\varepsilon_y + \bar{Q}_{16}\gamma_{xy}$$
$$\sigma_y = \bar{Q}_{12}\varepsilon_x + \bar{Q}_{22}\varepsilon_y + \bar{Q}_{26}\gamma_{xy}$$
$$\tau_{xy} = \bar{Q}_{16}\varepsilon_x + \bar{Q}_{26}\varepsilon_y + \bar{Q}_{66}\gamma_{xy}$$

Equation (A.27) can be written as

$$\begin{bmatrix} \varepsilon_x \\ \varepsilon_y \\ \gamma_{xy} \end{bmatrix} = \begin{bmatrix} \bar{S}_{11} & \bar{S}_{12} & \bar{S}_{16} \\ \bar{S}_{12} & \bar{S}_{22} & \bar{S}_{26} \\ \bar{S}_{16} & \bar{S}_{26} & \bar{S}_{66} \end{bmatrix} \begin{bmatrix} \sigma_x \\ \sigma_y \\ \tau_{xy} \end{bmatrix} \text{ or} \qquad \text{(A.29)}$$

$$\varepsilon_x = \bar{S}_{11}\sigma_x + \bar{S}_{12}\sigma_y + \bar{S}_{16}\tau_{xy}$$
$$\varepsilon_y = \bar{S}_{12}\sigma_x + \vec{S}_{22}\sigma_y + \bar{S}_{26}\tau_{xy}$$
$$\gamma_{xy} = \bar{S}_{16}\sigma_x + \bar{S}_{26}\sigma_y + \bar{S}_{66}\tau_{xy}$$

Therefore equations (A.28) and (A.29) relate the stresses in the global coordinate system to strains in the same coordinate system.

A2. Classical Laminate Theory (CLT)

Consider a lamina of cross-section, A, under a simple normal load P (Tuttle 2013, Matthews 2000) as shown in figure A.5. The normal stress at any cross-section is given by

$$\sigma_x = P / A \tag{A.30}$$

Replacing stress and substituting the strain in equation (A.30), the corresponding normal strain for a linearly elastic isotropic rectangular plate is then given by

$$\varepsilon_x = P / AE \tag{A.31}$$

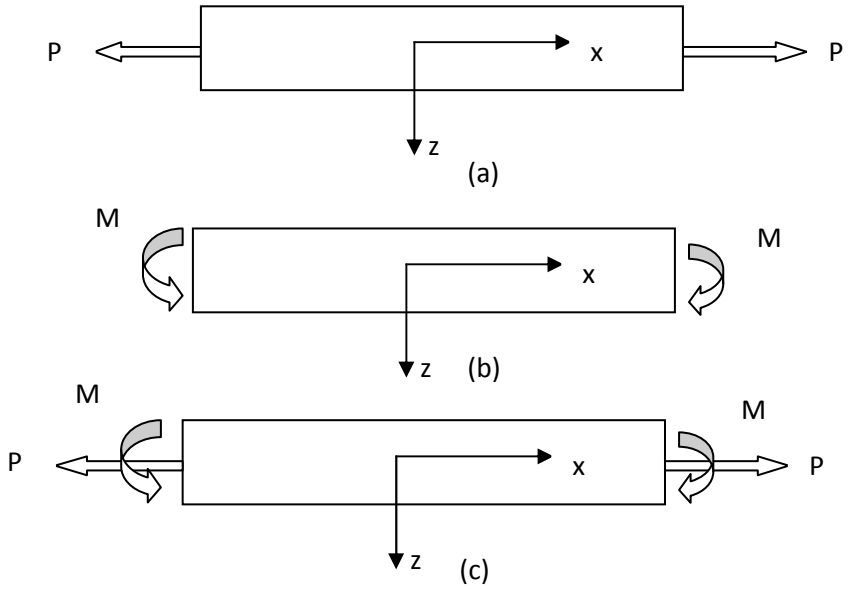

Figure A.5 A rectangular plate under (a) Axial load (b) Bending moment and (c) Combined bending

Let us now consider that the same rectangular plate is subjected to pure bending moment M, about its neutral axis as shown in figure A.5. At the distance z from neutral axis the stress in the beam in the x-direction is given by

$$\sigma_x = Ez / R \tag{A.32}$$

Where R is radius of curvature of beam. The strain in the x-direction is therefore

$$\varepsilon_x = z / R \tag{A.33}$$

Let us now consider that same rectangular plate is under the influence of both load P and bending moment M as shown in figure A.6.

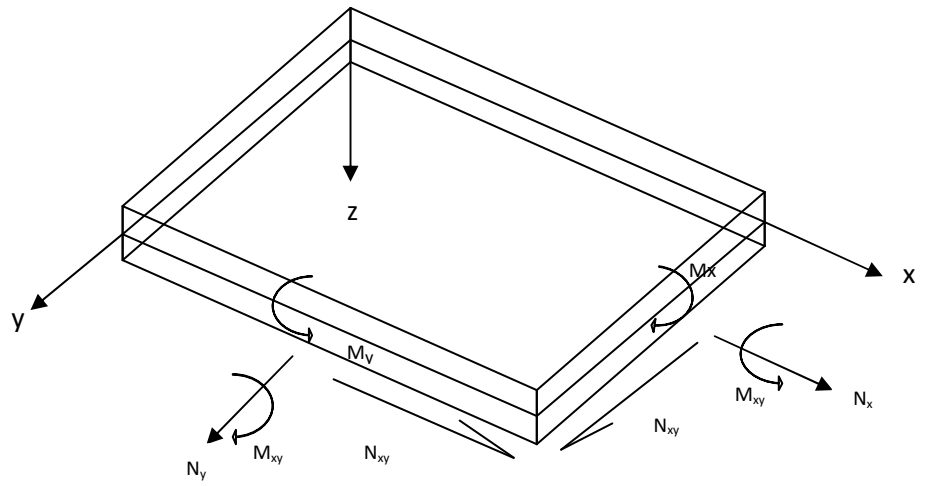

Figure A.6 Forces and moments in a laminate

From equations (A.32) and (A.33) the total strain in the x-direction is the algebraic sum of the two contributions i.e.

$\varepsilon_x = P/AE + z/R$ or

$\varepsilon_x = \varepsilon_0 + zk$

Where ε_0 is the strain at z=0 and κ=1/R (κ is called plate curvature). This equation shows that under a combined uniaxial and bending load, the strain is assumed here to vary linearly through the thickness of the rectangular plate.

Let us assume that the lamina is subjected to a loading system shown in figure A.7.

The global strain values in the k-lamina in two dimensions can be ascertained from the following relationship

$$\begin{bmatrix} \varepsilon_x \\ \varepsilon_y \\ \gamma_{xy} \end{bmatrix} = \begin{bmatrix} \varepsilon_x^0 \\ \varepsilon_y^0 \\ \gamma_{xy}^0 \end{bmatrix} + z_k \begin{bmatrix} \kappa_x \\ \kappa_y \\ \kappa_{xy} \end{bmatrix} \qquad \text{(A.34)}$$

κ_x = Bending curvature about the x-axis

κ_y = Bending curvature about the y-axis

κ_{xy} = Twisting curvature

$\varepsilon_x^0, \varepsilon_y^0, \gamma_{xy}^0$ = Mid-plane extensional and shear strains

Stress relations for a laminate:

If the strains at any point along the thickness of the laminate are known the global stresses in each lamina can be calculated from

$$\begin{bmatrix}\sigma_x\\ \sigma_y\\ \tau_{xy}\end{bmatrix}_k = \begin{bmatrix}\overline{Q}_{11} & \overline{Q}_{12} & \overline{Q}_{16}\\ \overline{Q}_{12} & \overline{Q}_{22} & \overline{Q}_{26}\\ \overline{Q}_{16} & \overline{Q}_{26} & \overline{Q}_{66}\end{bmatrix}_k \begin{bmatrix}\varepsilon_x\\ \varepsilon_y\\ \gamma_{xy}\end{bmatrix}_k \tag{A.35}$$

Substituting the equation (A.34) in equation (A.35)

$$\begin{bmatrix}\sigma_x\\ \sigma_y\\ \tau_{xy}\end{bmatrix}_k = \begin{bmatrix}\overline{Q}_{11} & \overline{Q}_{12} & \overline{Q}_{16}\\ \overline{Q}_{12} & \overline{Q}_{22} & \overline{Q}_{26}\\ \overline{Q}_{16} & \overline{Q}_{26} & \overline{Q}_{66}\end{bmatrix}_k \begin{bmatrix}\varepsilon_x^0\\ \varepsilon_y^0\\ \gamma_{xy}^0\end{bmatrix} + z_k \begin{bmatrix}\overline{Q}_{11} & \overline{Q}_{12} & \overline{Q}_{16}\\ \overline{Q}_{12} & \overline{Q}_{22} & \overline{Q}_{26}\\ \overline{Q}_{16} & \overline{Q}_{26} & \overline{Q}_{66}\end{bmatrix}_k \begin{bmatrix}\kappa_x\\ \kappa_y\\ \kappa_{xy}\end{bmatrix} \tag{A.36}$$

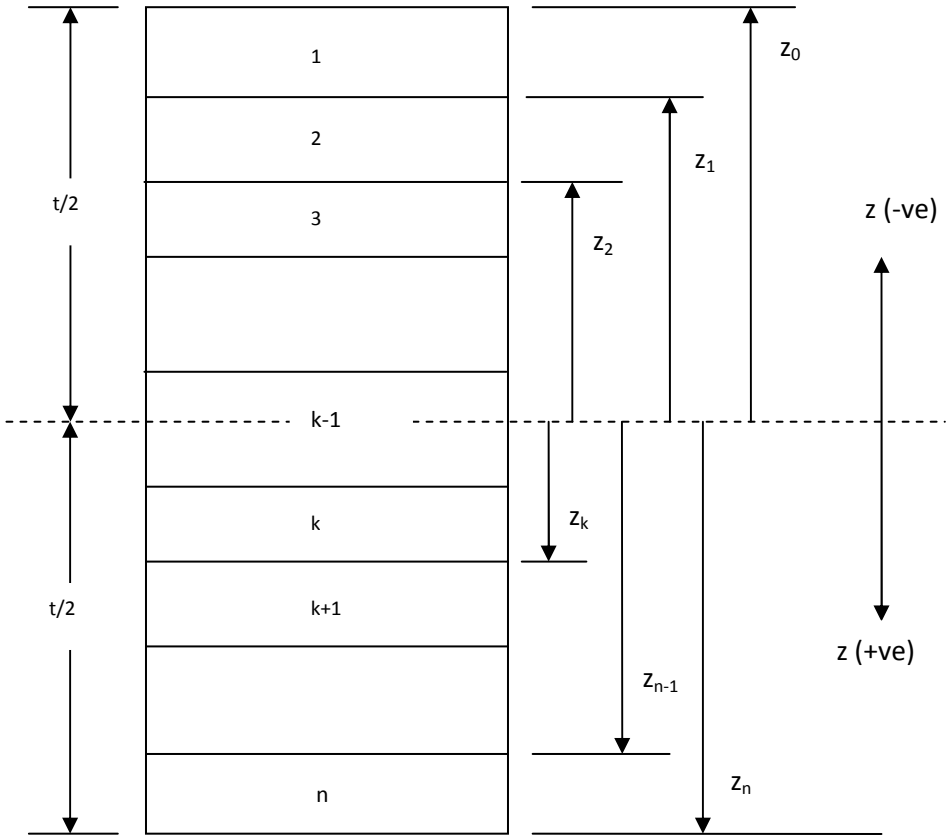

Figure A.7 Coordinate locations of plies in a laminate

Figure A.7 shows the coordinate locations of plies in a laminate. These global stresses can then be transformed into local stresses through the transformation matrix for stresses, $[T]_\sigma$. The global strains can also be transformed into local strains through the transformation matrix for strains, $[T]_\varepsilon$.

Mechanics of material show that in-plane forces per unit length N_x, N_y and N_{xy} and Moments M_x, M_y and M_{xy} per unit length are related to mid-plane strains and curvatures through three stiffness matrices

$$[N]=[A][\varepsilon^0]+[B][\kappa] \tag{A.37}$$

$$[M]=[B][\varepsilon^0]+[D][\kappa] \tag{A.38}$$

Equations (A.37)-(A.38) can be written in the form of

$$\begin{bmatrix} N \\ M \end{bmatrix}=\begin{bmatrix} A & B \\ B & D \end{bmatrix}\begin{bmatrix} \varepsilon^0 \\ \kappa \end{bmatrix} \tag{A.39}$$

Where [A],[D] and [B] in equation (A.39) relates to

[A] - Extensional stiffness matrix–in-plane forces to the in-plane strains

[D] - Bending stiffness matrix–moments to plate curvature

[B] - Coupling stiffness matrix–Couples the force and moment terms to the mid-plane strains and curvature.

$$[A]=\begin{bmatrix} A_{11} & A_{12} & A_{16} \\ A_{12} & A_{22} & A_{26} \\ A_{16} & A_{26} & A_{66} \end{bmatrix};[B]=\begin{bmatrix} B_{11} & B_{12} & B_{16} \\ B_{12} & B_{22} & B_{26} \\ B_{16} & B_{26} & B_{66} \end{bmatrix};[D]=\begin{bmatrix} D_{11} & D_{12} & D_{16} \\ D_{12} & D_{22} & D_{26} \\ D_{16} & D_{26} & D_{66} \end{bmatrix} \tag{A.40}$$

To evaluate laminate stiffness matrices, let us consider that the laminate is made of n plies. Each ply has a thickness of h_k (Tuttle 2013, Matthews 2000).

Then the thickness of the laminate t is given by

$$t=\sum_{k=1}^{n} h_k \tag{A.41}$$

The location of the mid-plane is t/2

[A], [B] and [D] matrices are defined from equations (A.36)-(A.41) and can be written as

$$[A]=\sum_{k=1}^{n}[\overline{Q}]_k(z_k-z_{k-1}) \tag{A.42}$$

$$[B]=1/2\sum_{k=1}^{n}[\overline{Q}]_k(z_k^2-z_{k-1}^2) \tag{A.43}$$

$$[D]=1/3\sum_{k=1}^{n}[\overline{Q}]_k(z_k^3-z_{k-1}^3) \tag{A.44}$$

Symmetric Laminates:

Laminates are symmetric if the material, angle and thickness of plies are the same above and below the mid-plane (Tuttle 2013). The symmetric laminate matrix is given by:

$$\begin{bmatrix} N_x \\ N_y \\ N_{xy} \\ M_x \\ M_y \\ M_{xy} \end{bmatrix} = \begin{bmatrix} A_{11} & A_{12} & A_{16} & 0 & 0 & 0 \\ A_{12} & A_{22} & A_{26} & 0 & 0 & 0 \\ A_{16} & A_{26} & A_{66} & 0 & 0 & 0 \\ 0 & 0 & 0 & D_{11} & D_{12} & D_{16} \\ 0 & 0 & 0 & D_{12} & D_{22} & D_{26} \\ 0 & 0 & 0 & D_{16} & D_{26} & D_{66} \end{bmatrix} \begin{bmatrix} \varepsilon_x^0 \\ \varepsilon_y^0 \\ \gamma_{xy}^0 \\ \kappa_x \\ \kappa_y \\ \kappa_{xy} \end{bmatrix}$$

Thus in plane loads will not generate bending and twisting curvatures. Thus if a symmetric laminate is subjected only to in-plane forces it will have zero mid-plane curvatures. We have used symmetric laminates in this research.

Appendix-B

B.1 Abaqus/Explicit Dynamics

The finite element method has become the most popular method in both research and industrial numerical simulations. Abaqus is a commonly used software for finite element analysis (Abaqus v6.10). Explicit methods are suitable for dynamic and non-linear problems. During impact, the duration of contact is very small so it is important to have detailed time history results of the force and displacements of the composite structure. High resolution solutions can be obtained effectively by using this method. The explicit algorithm provides an effective tool for simulating a wide variety of non-linear solid and structural dynamics events.

Abaqus/Explicit uses a central difference rule to integrate the equations of motion explicitly through time, using the kinematic variables at one increment to calculate them at the next increment (Abaqus/Explicit v6.10). At the beginning of the increment the program solves for dynamic equilibrium, which states that the nodal mass matrix, M, times the nodal accelerations, $\ddot{u}$, equals the total nodal forces (the difference between the external applied forces, P, and internal element forces, I).

$$M\ddot{u} = P - I \tag{B.1}$$

The accelerations at the beginning of the current increment time t are calculated and equation (B.1) can be written as

$$\ddot{u}_{(t)} = (M)^{-1}(P - I)_{(t)} \tag{B.2}$$

In Abaqus/Explicit each increment is inexpensive because there are no simultaneous equations to solve. Thus the acceleration of any node depends and is determined by its mass and the net force acting on it thus making the nodal calculations cost effective (Jacob et al 2002).

From equation (B.2) the accelerations are integrated through time using the central difference rule, which calculates the change in velocity assuming that the acceleration is constant. This change in velocity is added to the velocity from the middle of the previous increment to determine the velocities at the middle of the current increment:

$$\dot{u}_{\left(t+\frac{\Delta t}{2}\right)} = \dot{u}_{\left(t-\frac{\Delta t}{2}\right)} + \frac{\left(\Delta t_{(t+\Delta t)} + \Delta t_{(t)}\right)}{2} \ddot{u}_{(t)} \tag{B.3}$$

From equation (B.3) the velocities are integrated through time and added to the displacements at the beginning of the increment to determine the displacements at the end of the increment (see equation B.4).

$$u_{(t+\Delta t)} = u_{(t)} + \Delta t_{(t+\Delta t)} \dot{u}_{\left(t+\frac{\Delta t}{2}\right)} \tag{B.4}$$

Thus, satisfying dynamic equilibrium at the beginning of the increment provides the accelerations. Knowing the accelerations, the velocities and displacements are advanced "explicitly" through time. The term "explicit" refers to the fact that the state at the end of the increment is based solely on the displacements, velocities, and accelerations at the beginning of the increment. This method integrates constant accelerations exactly. For the method to produce accurate results, the time increments must be quite small so that the accelerations are nearly constant during an increment.

Implicit vs Explicit Analysis

There are two main kinds of direct time integration methods (Jacob et al 2002; Abaqus/Explicit v6.10).

These are:

1) Implicit methods
2) Explicit methods

Both procedures solve for nodal accelerations and use the same element calculations to determine the internal element forces. The biggest difference between the two procedures lies in the manner in which the nodal accelerations are computed.

Abaqus can solve a wide variety of linear and non-linear static and dynamic problems by using Abaqus/Standard and Abaqus/Explicit. Depending upon the problem and other parameters the user can use implicit or explicit methods. Generally Abaqus/Standard is more efficient for use for problems that are smooth and non-linear while Abaqus/Explicit is used for more dynamic events or for wave propagation analysis.

Direct time integration method is generally used in the calculation of a structure's response history using step-by-step integration in time without changing the form of the dynamic equations. Direct integration methods make use of a finite difference approximation to replace the time derivatives of the dynamic equation of motion.

B2. Contact Algorithm

Abaqus/Explicit provides two algorithms for modelling contact. General contact interactions allow definition of contact between the surfaces that can interact with one another. Contact pair interactions describe contact between a deformable surface and a rigid surface. An Explicit contact simulation is usually defined simply by specifying the surfaces that will interact with one another (Abaqus v6.10). Thus the contact algorithm works in the following steps:

- Determining all the surrounding nodes of the contact element
- Define the nodes in contact.
- Calculation of repelling force as a function of the distance of the node to the element
- Applying this force onto the node and the opposite force onto the contact element.

Thus the contact algorithm depends upon the contact formulation which includes constraint enforcement method, the contact surface weighting, the tracking approach, and the sliding formulation. Thus depending on the type of impact problem contact formulation can be approached.

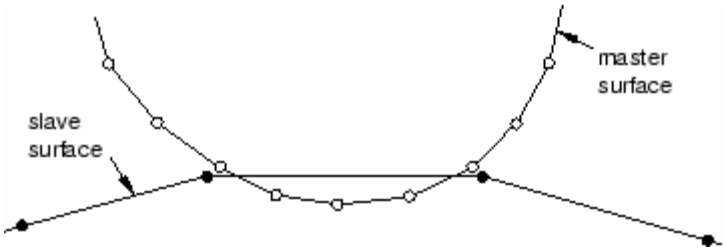

Figure B.1 Unbalanced master-slave contact (Abaqus v.6.10)

Figure B.1 shows penetration of master nodes into slave surface with pure master-slave contact. Master-slave approach is applied for impact in Abaqus/Explicit. In contact formulation, one of the surfaces is the master surface and the other is the slave surface. During the impact the master surface might penetrate into slave surface thus defining the

proper constraint enforcement methods such as kinematics balanced or penalty approaches is desirable. A pure master-slave weighting approach will resist penetrations of slave nodes into master faces (Abaqus v.6.10).

Kinematics balanced master-slave contact can be used to avoid penetration on the slave surface (see figure B.2). The balanced approach minimizes the penetration of the contacting bodies and, thus, provides more accurate results. Another way to avoid penetration is to ensure that the slave surface is adequately refined.

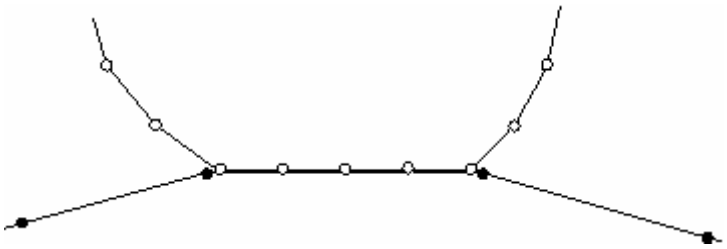

Figure B.2 Balanced master-slave contact

In the contact pair algorithm, the Abaqus/Explicit default method will automatically decide the type of weighting to be used for a given contact pair based on the nature of the two surfaces involved and the constraint enforcement method used. For most element types the default weight is 0.5. Setting weight to 1.0 specifies a pure master-slave relationship with the first surface as the master surface.

Appendix-C

C1. Composite Processing Details

Glass/Epoxy Composite Laminate Lay-Up

Lay-Up: Two laminate thicknesses have been used that is 2 mm and 4 mm for the low velocity edge impact programme. Each ply is approximately 0.25 mm thick.

Thickness

2mm $[0^0/+45^0/90^0/-45^0]_s$

4mm $[0^0/+45^0/90^0/-45^0]_{2s}$

In this section we will discuss about manufacturing and technical details of the composite laminate used during the low velocity edge impact programme.

Fabric Details

Multiaxial E-glass fabric is used for the project. Multiaxial fabric is made up of four layers of unidirectional fibres stitched together with a light thread. Being stitched, they do not exhibit the crimping effect as associated with the woven fabrics, when crimping leads to resin rich areas and thus leads to loss in the performance of the materials. Table C.1 shows aerial weight per ply with different orientation for E-glass fibre multiaxial fabric provided by Saint-Gobain company.

Type	**Layer Orientation**	**Layer Areal Weight (g/m2)**	**Total Areal Weight (g/m2)**	**Nominal Thickness (mm)**
E-Glass Fibre Multiaxial Fabric	0^0	283	1034	0.25
	$+45^0$	234		0.25
	90^0	283		0.25
	-45^0	234		0.25

Table C.1 Aerial weight per ply with different orientation for E-glass fibre multiaxial fabric

Table C.2 shows the details of the E-glass fibre fabric.

Fibre	**Fibre Diameter (µm)**	**Fibre Density (Kg/m^3)**
E-glass fibre Fabric	17	2.60

Table C.2 E-glass fibre fabric details

Resin Details

Following sections provide the details of epoxy resin and hardener used during the manufacture of composite laminates. Table C.3 and C.4 provide details of resin (Epoxy Araldite LY564) and hardener properties respectively.

Properties Data:

Resin Used	**Resin Properties**	**Resin Technical Data**
Epoxy Araldite LY564	Aspect (Visual)	Clear Liquid
	Colour	1-2
	Viscosity at 25^0C (mPa s)	1200-1400
	Density at 25^0C (g/cm^3)	1.1-1.2
	Flashpoint (^{0}C)	185
	Storage Temperature (^{0}C)	2-40

Table C.3 Epoxy Araldite LY564 properties details

Hardener Used	Hardener Properties	Hardener Technical Data
Hardener XB 3486	Aspect (Visual)	Clear colourless to slightly yellow liquid
	Viscosity at 25^0C (mPa s)	10-20
	Density at 25^0C (g/cm^3)	0.94 - 0.95
	Flashpoint (^{0}C)	123
	Storage Temperature (^{0}C)	2-40

Table C.4 Hardener XB 3486 properties details

It is very important to note that Araldite LY 564 and Hardener XB 3486 should be stored in a dry place in the temperature range of 2-40 ^{0}C. Containers should be properly closed at all times when not in use. Also, containers should be closed immediately after use for the restoration of the above mentioned properties.

Processing Data

Tables C.5 and C.6 provide the details of the mix ratio and initial mix viscosity data for Epoxy-Hardener.

	Components	Parts By Weight	Parts By Volume
Mix Ratio	Epoxy Resin-Araldite LY564	100	100
	Hardener XB 3486	34	41

Table C.5 Mix ratio for Epoxy-Hardener

Initial Mix Viscosity (mPa s) at 25^0C	Epoxy Resin-Araldite LY564/ Hardener XB 3486	200-300

Table C.6 Initial mix viscosity for Epoxy-Hardener

It is important to note that components are weighed with an accurate balance to prevent mixing inaccuracies which can affect these properties of the matrix system. The components should be mixed thoroughly to ensure homogeneity.

Gel Time

	Mixture	**Temperature^{0}C**	**Time (Mins)**
Gel Time	Epoxy Resin-Araldite LY564/ Hardener XB 3486	60	110-130
		80	33-43
		100	13-17
		120	5-9

Table C.7 Gel Time for Epoxy-Hardener

The values shown are for small amounts of pure resin/hardener mix. In composite structures gel time can differ significantly from the given values depending on the fibre content and laminate thickness (see table C.7).

C2. Laminate Preparation

In recent years, several low-cost manufacturing processes have evolved that can be used to manufacture structural composites as compared to autoclave moulding at the same time obtain high quality.

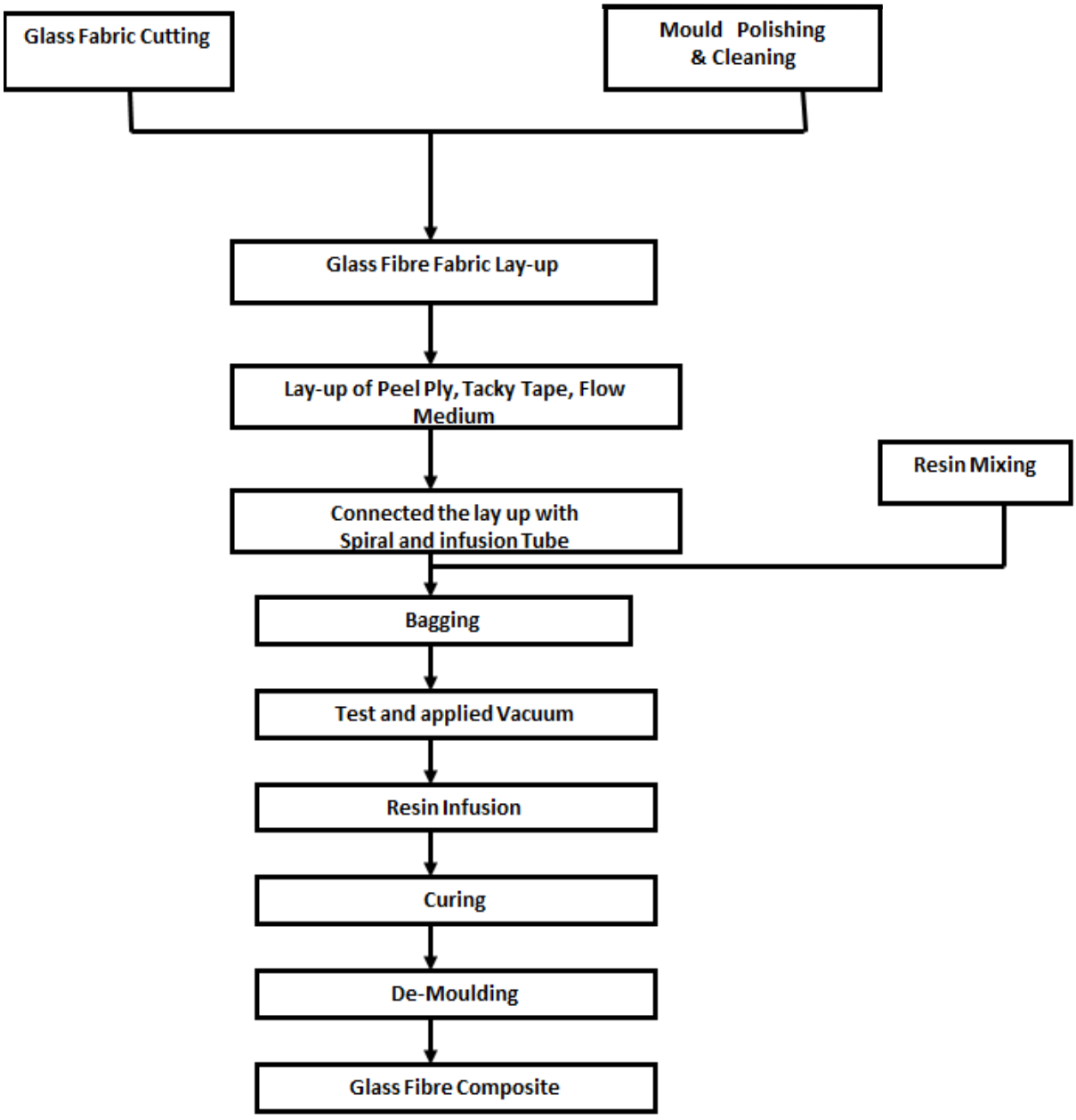

Figure C.1 Vacuum Assisted Resin Infusion Moulding (VARIM) process

Vacuum assisted resin infusion moulding (VARIM) is one such process and extensively used in composites industry. In the project we have used VARIM. It is a cost effective and at the

same time high quality process for the fabrication of composite materials. Glass fibre epoxy laminates were manufactured by using vacuum infusion process. Figure C.1 shows the flowchart for the laminate manufacture. The stages in the Vacuum assisted resin fusion moulding process are shown in figure C.2 (a)-(h).

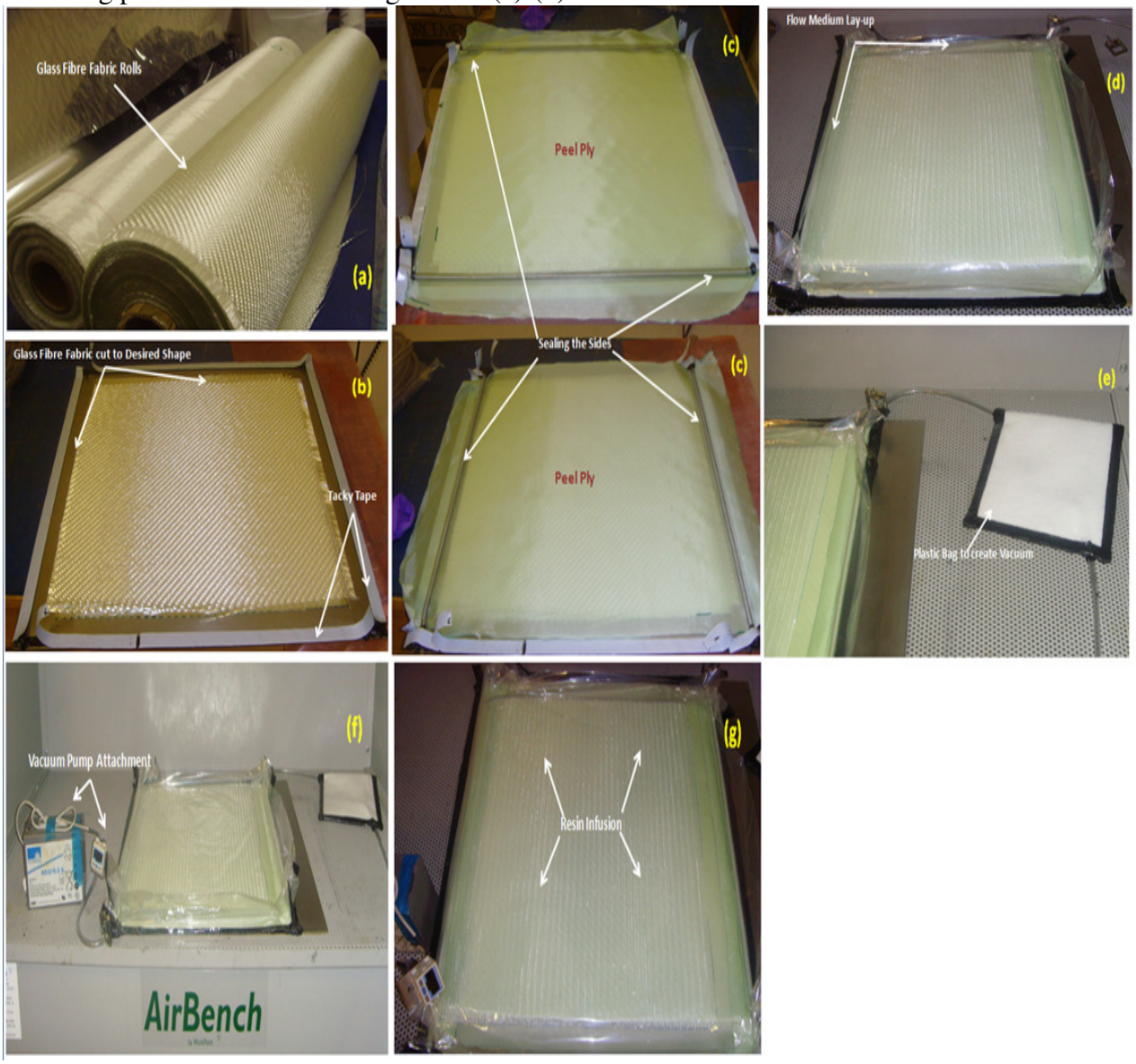

Figure C.2 Composite manufacturing process (a) Glass fibre fabric (b) Cutting glass fibre fabric as per desired size (c) Sealing the side around the mould stick black double-side tacky tape and covering the fabric with peel ply (d) Laying up the flow medium (e) Plastic bag to create vacuum (f) Attaching a vacuum pump to the bag (g) Fabric is covered with resin (h) Post curing in oven.

Figure C.1 shows the flowchart for the manufacture of laminate. The procedures for manufacturing the laminate are:

- Before we start, the flat mould should be cleaned first with mould cleaner Frekote PMC to remove the spare resin in the flat mould surface.
- Next coat the mould with semi-permanent mould release agent like polytetrafluoroethylene for 5 times. This is done so that the composite will not stick to the mould after it is being cured in final stage.
- Cut the glass fibre fabric as per desired size. Lay-up the cut fabric onto the cleaned flat mould.
- In order to seal the side around the mould stick black double-side tacky tape. Cover the fabric with peel ply, which is nylon cloth. This is done in order to prevent the composite from sticking to the mould.

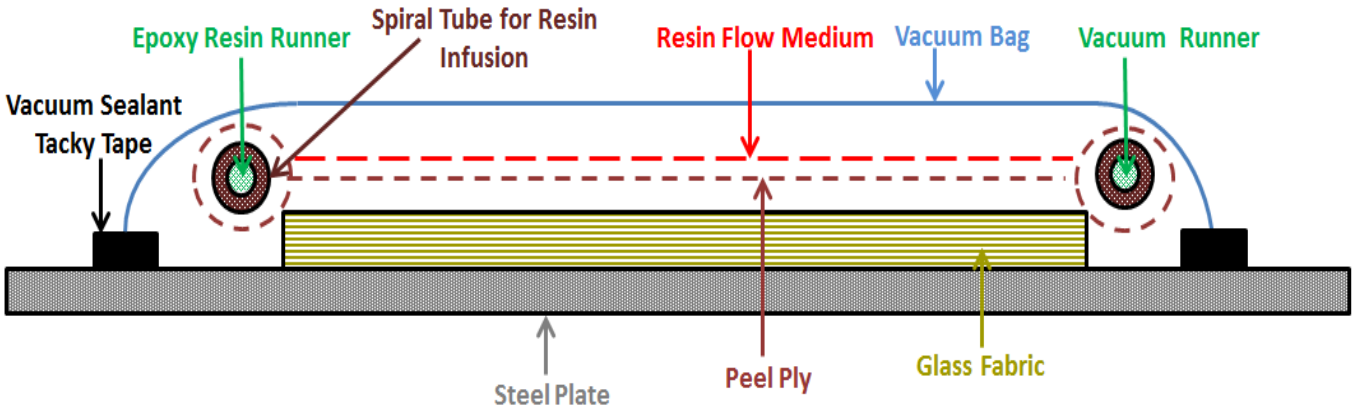

Figure C.3 Layup cross-section during manufacturing of glass fibre epoxy laminate

- Next stage involves, laying up the flow medium and then connect spirals to the two opposite sides of flow medium. So during the resin infusion process, the spiral directs the resin flow (see figure C.3).
- Resin then flows to the other side along the direction of the flow medium and thus during this whole process fabric is covered by resin rapidly assuring homogeneity of flow.

- In order to seal the side around the mould a plastic bag is put over the top. Precaution must be taken when bonding the edge of bag and tacky tape together. It is important to seal perfectly without any aperture so that vacuum can be created during resin infusion.

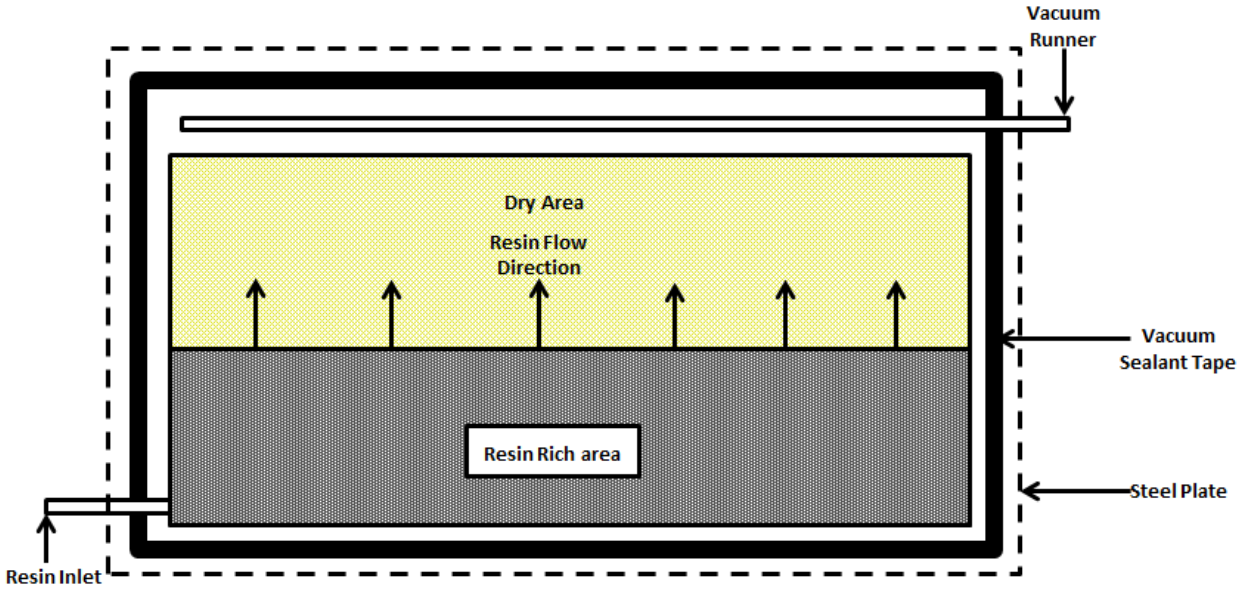

Figure C.4 Top view of laminate panel during infusion of resin

- Test vacuum repeatedly before infusing resin. Attach a vacuum pump to the bag and make sure that it sucks out all air from the mould. Apply vacuum for 15-20 minutes. To begin resin infusion open inlet tube (see figure C.4).

- As soon as the resin is reached the outlet runner clamp the inlet tube. Then slowly reduce vacuum to 800 bar.

- When the outlet runner is filled with resin clamp the tube tightly. Now, leave to cure at room temperature for 24 hours. Finally, post cure at 80°C for 3 hours.

C3. Multiaxial fabric details and technical datasheet

MULTIAXIALS

Introduction

MULTIAXIAL fabrics are made up of 2 or more layers of unidirectional fibres stitched together with a light polyester thread. Being stitched, they do not exhibit the crimping effect associated with woven fabrics - crimping that leads to resin rich areas, heavy print-through, and loss of performance.

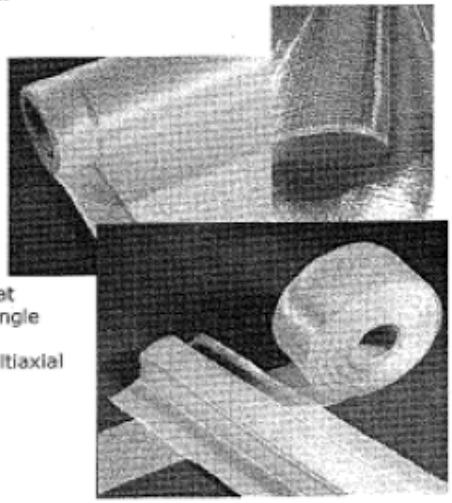

The result is a range of reinforcements that offer the ability to process multiple layers of unidirectionals (the ultimate reinforcement form) at varying angles in a single fabric form - giving the term 'multiaxial fabric'.

The advantages of Saint-Gobain **MULTIAXIALS**:

- Quick & easy to wet-out
- No resin-rich areas
- Minimum print-through
- Increased performance (tensile & flexural)
- Improved fatigue & impact resistance
- Easier handling - the fabrics stay intact even when cut
- Labour savings - by using fewer multi-layer, heavyweight fabrics

We can also offer MULTIAXIALS that are powder-bonded instead of stitched.

Performance Gains

The combination of straight fibres and easily achievable high fibre fractions allow MULTIAXIAL reinforcements to offer a performance advantage that is so important in any structural composite.

The unidirectional fibres can be loaded to their maximum potential before failure occurs, rather than suffer the premature kink-stress that is inherent in a woven fabric.

In any laminate, uncrimped fibres with high fibre fractions offer the following advantages over wovens or random mats:

- increased tensile & flexural strength
- increased tensile & flexural moduli
- less weight for the same strength
- improve impact performance
- improved resistance to fatigue

SAINT-GOBAIN
TECHNICAL FABRICS

SAINT-GOBAIN
TECHNICAL FABRICS

TECHNICAL DATA SHEET

SYDS 2404

TYPE : EQX 1034 - 3200

MATERIAL TYPE : E glass

CONSTRUCTION :

+/- 45° :

+ 45° : 2,85 y/cm x 600 Tex = 242 g/m² ± 5%
- 45° : 2,85 y/cm x 600 Tex = 242 g/m² ± 5%

90° :

: based on 600 Tex glass = 274 g/m² ± 5%

0° :

: based on 1200 Tex glass = 283 g/m² ± 5%

stitching :

Based on 76 dTex textured PES yarn = 10 g/m² ± 5%
stitch length = 2 mm / stitch type : tricot

TOTAL THEORETICAL WEIGHT = 1051 g/m² ± 5%

WIDTH : - including fringes : 1250 mm ± 50 mm or 300 mm ± 5 mm
- fringes : ≤ 10 mm

ROLL LENGTH : standard = 35 lm ± 5 lm
: max. 30% deviating length rolls allowed per consignement with a minimum of 40 % of given length

DIAMETER INNERCORE : 76 mm - cardboard

PACKAGING : rols individualy wrapped in PE film; on pallets

LABELLING : each roll contains 1 label mentioning :
- product type
- roll width (cm) + length (m)
- batch number + roll number

QUALITY DEMANDS : no missing stitch yarn(s) over a distance > 2 meter allowed
: no stains, contamination, . . allowed
: max. roll telescoping = 1 cm
: no missing +/-45° allowed over a distance > 20 mm

Saint-Gobain Isoglas N.V.

SAINT-GOBAIN
TECHNICAL FABRICS

HEALTH AND SAFETY DATA – Version 2001-03-05

Manufactured by:
Saint-Gobain BTI UK Limited
4/5 Crown Way Walworth Ind Est Andover Hants SP10 5LU England
Phone : +44 1264 333400 Fax : +44 1264 359610 e-mail: mspooner@sgbti.com

Manufacturers of COTECH® *multiaxial technology*

Products:
Relating to stitched fabrics assembled using E Glass:
E Lx / E LTx / E Bx / E TL x / E TT x / E QX x

Production composition:
Our products are manufactured from continuous glass fibre roving and / or yarn and with certain styles including Chopped Strand Mat. They include a small amount of sizing, and may include binder. The filament diameter size ranges from 9 to 24 microns.

Health hazards:
Skin and Eyes:
Particles of fibres entering the eyes may cause irritation. Rinse with copious amounts of water and seek medical assistance if the irritation persists.

Where a skin irritation occurs, copious amounts of water should be poured over the affected areas prior to washing with a mild soap.

Experience in handling the products should see a marked decrease in irritation of eyes and skin. However, if this fails to happen, then protective clothing and / or barrier cream should be used.

Care should be taken not to rub or scratch irritated areas.
Medical advice should be sought where an allergic reaction develops.

Inhalation:
The reinforcement fibres used in the manufactured of our fabrics are not respirable. However, irritation of the upper respiratory tract may be caused by high concentrations of airborne glass fibre dust. The effect should be temporary and cause no permanent disability.

Care should be taken to ensure that our fabric is not excessively abraded. Efficient ventilation and dust extraction should overcome these problems.

In June 1989 the International Agency for Research on Cancer (IARC) categorised fibreglass continuous filament as not classifiable with respect to causing human cancer. The evidence from human as well as animal studies was evaluated by the IARC as being insufficient to classify fibreglass continuous filament as a possible, probable, or confirmed cancer causing material.

Safety:
Glass fibre is incombustible; no decomposition occurs under the influence of high temperatures, therefore in the case of heating or fire, no noxious vapours arise.
Glass fibre also does not give off dangerous substances in water.
No precautions need be taken in the handling and storage.
Waste disposal should be made in accordance with local regulations.
Disposal is normally in an industrial landfill.

For further advice please contact Saint-Gobain BTI customer service on the numbers below.

Saint-Gobain BTI UK Limited
4/5 Crown Way • Walworth Ind Est • Andover • Hants SP10 5LU • England
Tel : +44 1264 333400 Fax : +44 1264 359610 • e-mail : mspooner@sgbti.com

Manufacturers of COTECH® *multiaxial technology*

Appendix-D

D. Computed Tomography

D.1 Histogram and Transfer Functions

The datasets of the edge impacts are loaded into Drishti import tool as a single file from .tom file. Drag and drop facility as it is available in the Drishti tool. First byte is considered as unsigned byte voxel type. This single byte is followed by three integers 4 bytes each. This determines the grid size of the specimen volume. The top values in the histogram graph are the raw values in the dataset from 0 to 255. As in the dataset we have unsigned byte therefore we have minimum and maximum values from 0 to 255 which are thus mapped in this range. Datasets are then saved in "Filename.plv.nc" format for 3D rendering. The dataset can be seen from two sides one from the top and second one from the bottom thus the option 0 in the histogram can be the defined as the top side or the bottom side. In the research we have used all the default values in-built in the Drishti tool.

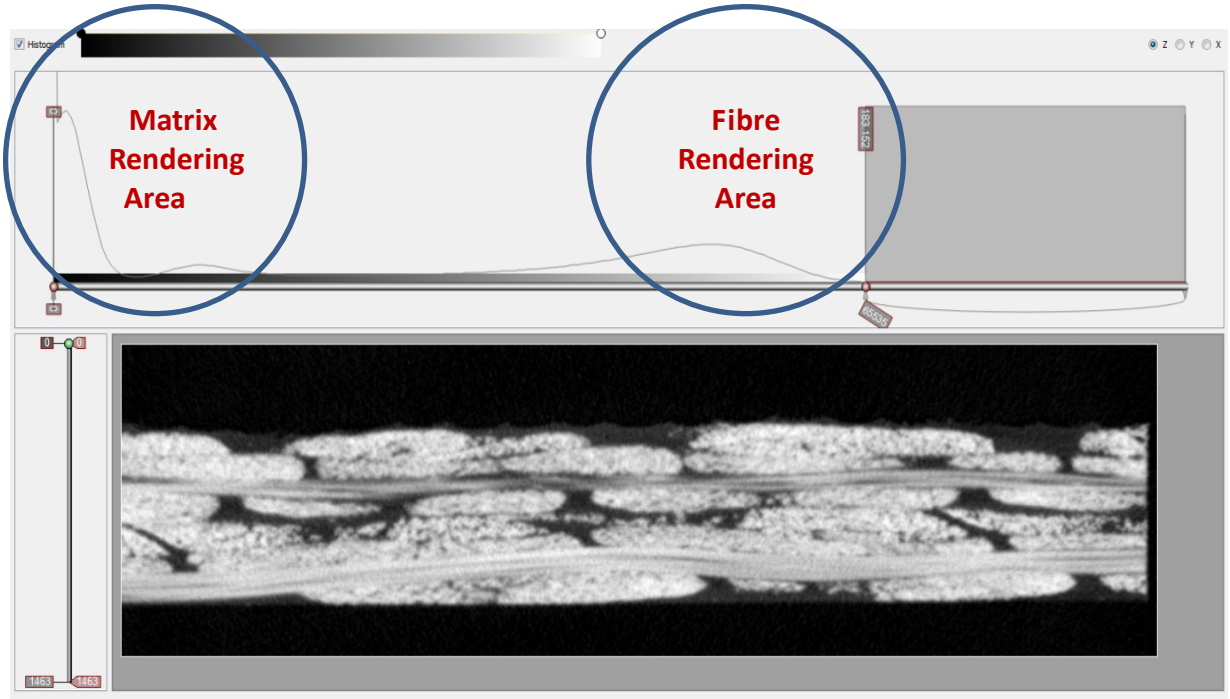

Figure D.1 Matrix and fibre rendering area in Drishti import tool

The left hand part of the histogram shows the matrix rendering areas while the right hand area shows the fibre rendering area as shown in figure D.1 highlighted in circles.

D1.1 8-Bit vs 16 Bit Histogram

Figure D.2 shows the difference between the 8-bit and 16-bit magnification for rendering the three dimensional edge impact damage image of the laminate. The horizontal and the vertical dimensions of the texture represent the gradient magnitude of 8-bit. 8-bit data has the maximum and minimum range for the entire dataset from 0 to 255 for unsigned character. 8-bit output type from Drishti importer can be saved into 16-bit datasets. Both the 8-bit and 16-bit dataset can be saved as pvl.nc or remapped as pvl.nc. The results presented in this chapter have originally by default 8-bit dataset which is then converted into 16-bit. This is done to obtain a higher resolution of the impacted damage image. 8-bit dataset has the two dimensional transfer function while the 16-bit has only one dimensional transfer function present. 8-bit has the texture size of 255 by 255 on either side.

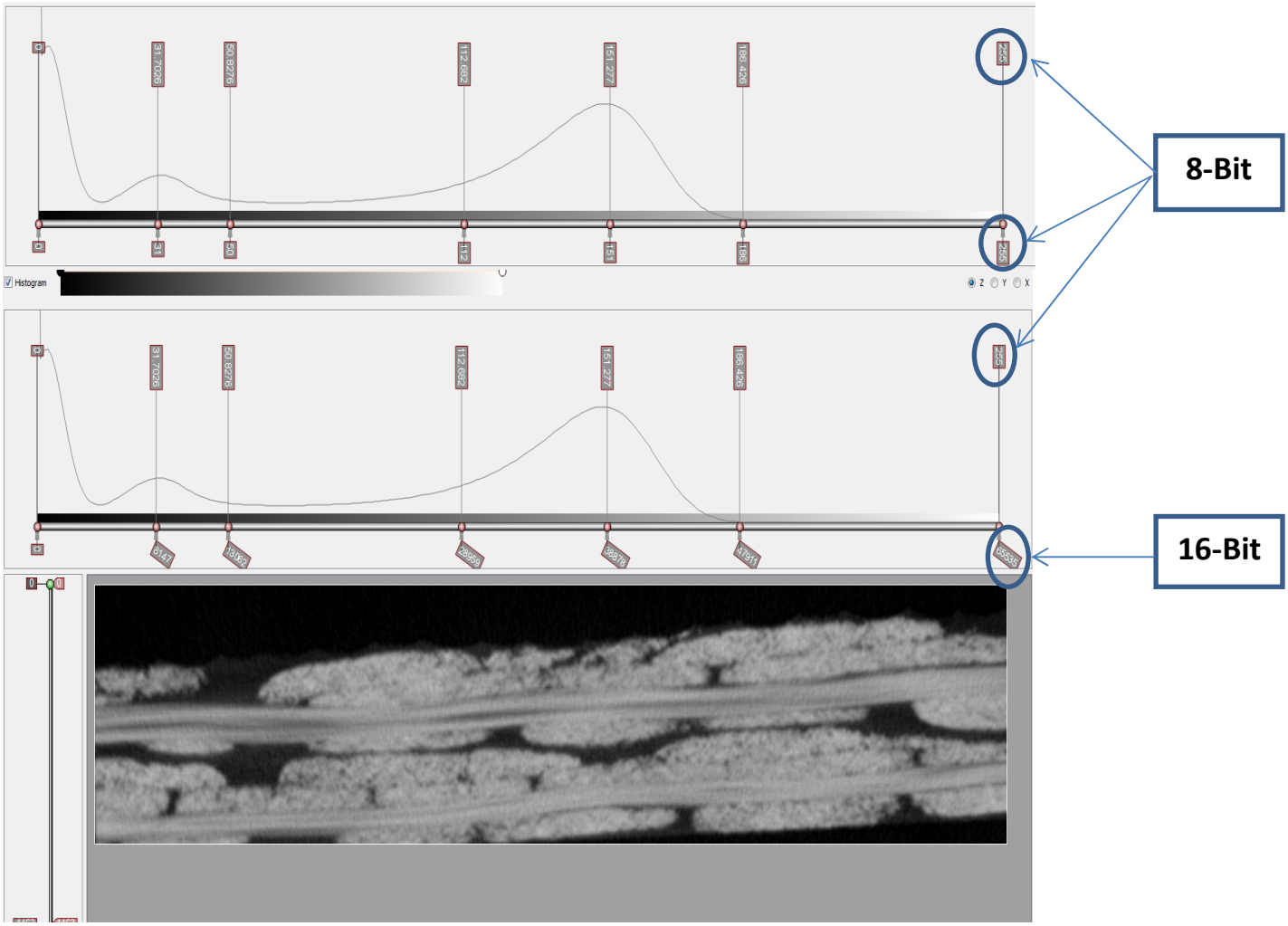

Figure D.2 Output type in 8-bit and 16-bit in Drishti import tool

The results in the following sections will be from 16-bit output. In 16-bit output type the two-dimensional texture from .tom file is loaded. The intensity magnitude at every voxel is calculated and thus produces the required colour and opacity. 16-bit restricted to use only in one-dimensional only and is purely voxel based rendering. There is restriction to multi-dimensional transfer function in 16-bit volumes. For 16 textures the amount of texture memory allocated becomes very large and the processor can become slow. So higher graphics and higher memory PC's are required to use this output data type. 16-bit output type offers high resolution image and high range of values in a single phase histogram and captures very close or multiple narrow range of values. For the 16-bit output type, the texture size is very large and the amount of texture memory allocated is very large compared to the 8-bit case.

D1.2 Transfer Functions

All the results presented in chapter 4 are 16-bit output results. Figure D.3 shows the 16-bit output transfer function. The one-dimensional fibre rendering is shown in figure D.3. There is a big chunk at the starting of the phase followed by a tiny graph. There are three phases in this dataset. The histogram in figure D.3 shows the relationship between these three phases. It is difficult to predict the relationship between these three phases. In the 8-bit case they are defined by the arches. The horizontal axis represents the voxel intensity and the vertical axis part represents the voxel value gradient magnitude. At every voxel the gradient magnitude is evaluated. Gradient magnitude indicates the rapid changes occurring in the voxel intensity value with respect to the neighbourhood of the given voxel.

High gradient values indicate major differences between the neighbouring voxel and the voxel under consideration. In inhomogeneous regions the gradient value/magnitude will be much higher compared to voxels in the homogenous regions. If the voxels are in homogenous regions or in areas with small changes, the gradient magnitude is becoming very small often close to zero. Generally the homogenous region can be referred as the matrix phase due to its low value while fibres can be referred as inhomogeneous regions. On the left there is a matrix phase and has a low magnitude indicating it is in the homogenous region and vice-versa for the fibre phase. The peak in the curve defines the number of voxels present in that particular phase and how close they are lying to the neighbouring voxel phase.

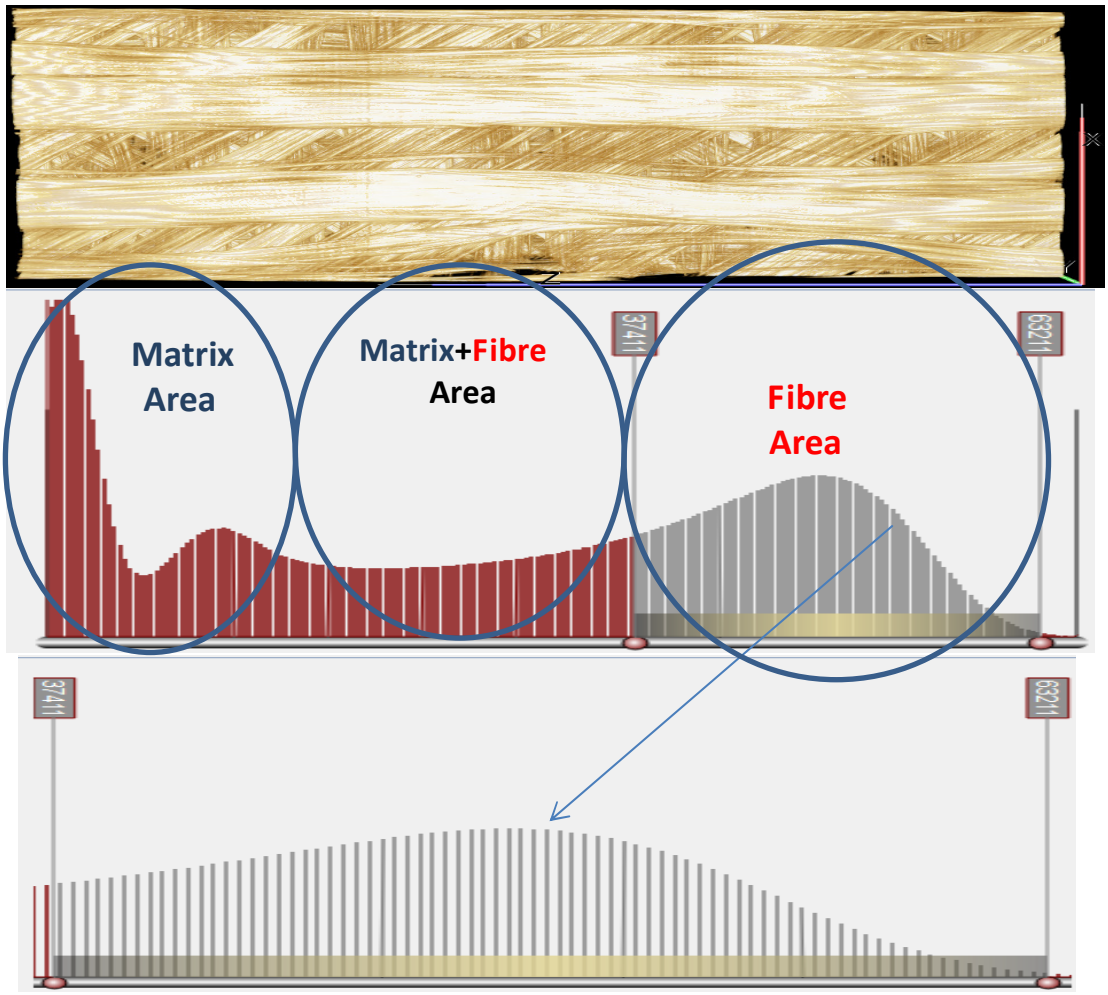

Figure D.3 Fibre rendering area for 16 bit output type

So there is a boundary between these two sets of voxels which is matrix and fibre phase. As we move from one region (matrix phase) to other region which is (fibre phase) the gradient magnitude starts rising as we approach the boundary and at the boundary will have the highest gradient magnitude. As an example figure D.3 shows the fibre rendering area for 16-bit output type. The fibre can be clearly seen in-between the histogram with the gradient value of 37411 to 63211 values.

D2. Histogram-Matrix/Fibre Phases

The histogram gives information about the absorption coefficient of the various fibre and matrix phases. Figure D.4 on the left hand part shows the matrix phase. There is one peak in the matrix phase with maximum gradient peak value of 31 (8-bit) and 8147 (16-bit). For values between 50 and 112 (8-bit) or between 13062 and 28959 (16-bit), both matrix and fibre can be observed. Similarly the value for fibre phase lies between 112 and 186. Higher peak is observed in the fibre phase indicating higher absorption coefficient while lower phase is observed in matrix phase. For values up to 255 there is no matrix and fibre phase. So depending upon the requirements the phases can be chosen. The following section will discuss the different phases for both on-edge and near-edge impacts with thin and thick laminates.

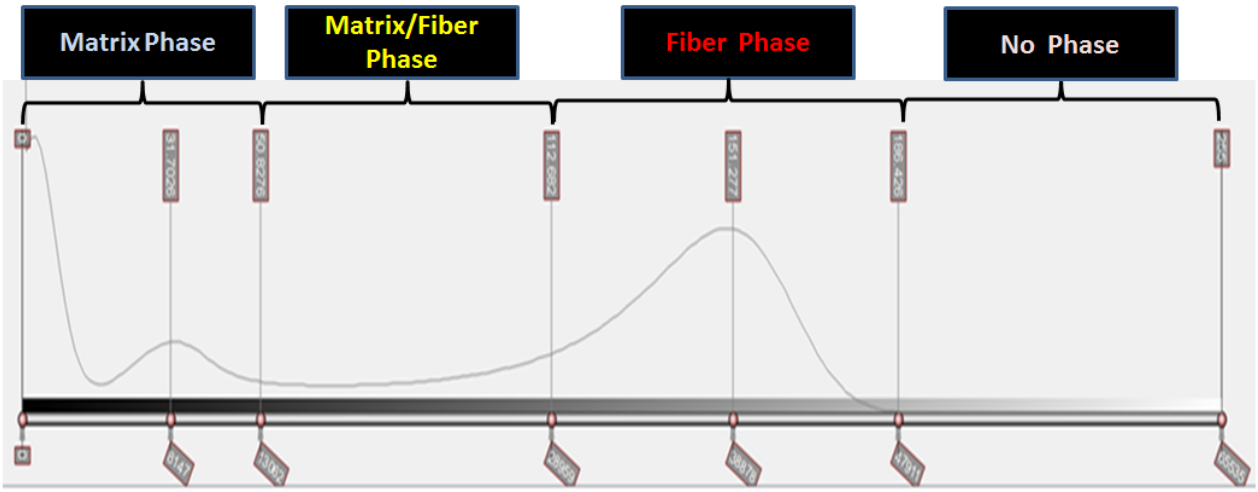

Figure D.4 Histogram-matrix/fibre phases

D3. On-edge and Near-edge Impact Histograms

The histogram for near-edge and on-edge impacts with varying parameters is shown in figure D.5. As can be seen the trend for both is nearly identical. A higher gradient peak is seen for thick laminates compared to thin laminates with respect to both types of edge impact. The matrix and fibre phases have shown these graphs and discussed in section D2. This approach is used to produce the 3D volume rendering for edge impact datasets. The main window is divided into two windows - histogram window and image window as shown in figure D.5. The histogram window is used for display of 1D histogram of the loaded volume.

Figure D.5 Histogram for near-edge and on-edge impact for various parameters

A transfer function is applied by mapping each coordinate on an intensity-gradient diagram to a particular colour and transparency on the composite laminate. Transfer functions map voxel information to optical properties. The horizontal axis represents the voxel intensities and the vertical axis represents the rate of change of voxel intensity.

D4. 3D-Edge Impact Rendering Results

This section will discuss the procedure followed to extract edge impact damage results in three dimensions (using Drishti tools).

D4.1 Image Acquisition and Processing

For 3D reconstruction the Drishti program allows easy volume rendering. The properties and each data point within these datasets are explored using this technique. The import utility converts the dataset volume files into the format that Drishti can understand - i.e. .pvl.nc format. Thus for the near-edge and on-edge .tom file datasets are first converted to plv.nc. Now another Drishti programme is opened which is referred as "Drishti 3D volume rendering". In this the saved project (plv.nc format) is imported into this Drishti tool for 3D volume rendering. Once the project is imported the next step is to define the transfer function which is the most important part in order to view the damage areas. This is already discussed in the earlier section D 1.2.

D4.2 Drishti Tool Measurements Units

Dimensions of all the results in chapter 4 are used in microns. This option is available in Drishti tool for various units. By default Drishti tool considers microns for the measurement of the different parts of the specimen under consideration. Thus in order to be consistent in the results all figures in the following section will have the measurement in microns.

D4.3 Opacity

In order to view the impact damage the opacity is an important tool to analyse the results. Figure D.6 (a)-(d) shows the different opacity levels with respect to changing colours. The laminate under consideration is near-edge 4J impacted with thickness of 2mm. We are only rendering fibre and thus the matrix is invisible. The histogram for all the figures is shown in figure D.6. Clearly we can see that there is considerable effect on 3D visualisation of near-edge impacted laminate by changing the opacity levels in Drishti tool. Moving down the left hand opacity graph will result in low opacity while moving up right hand of the opacity graph will result in high opacity. Thus opacity changes linearly from bottom to top.

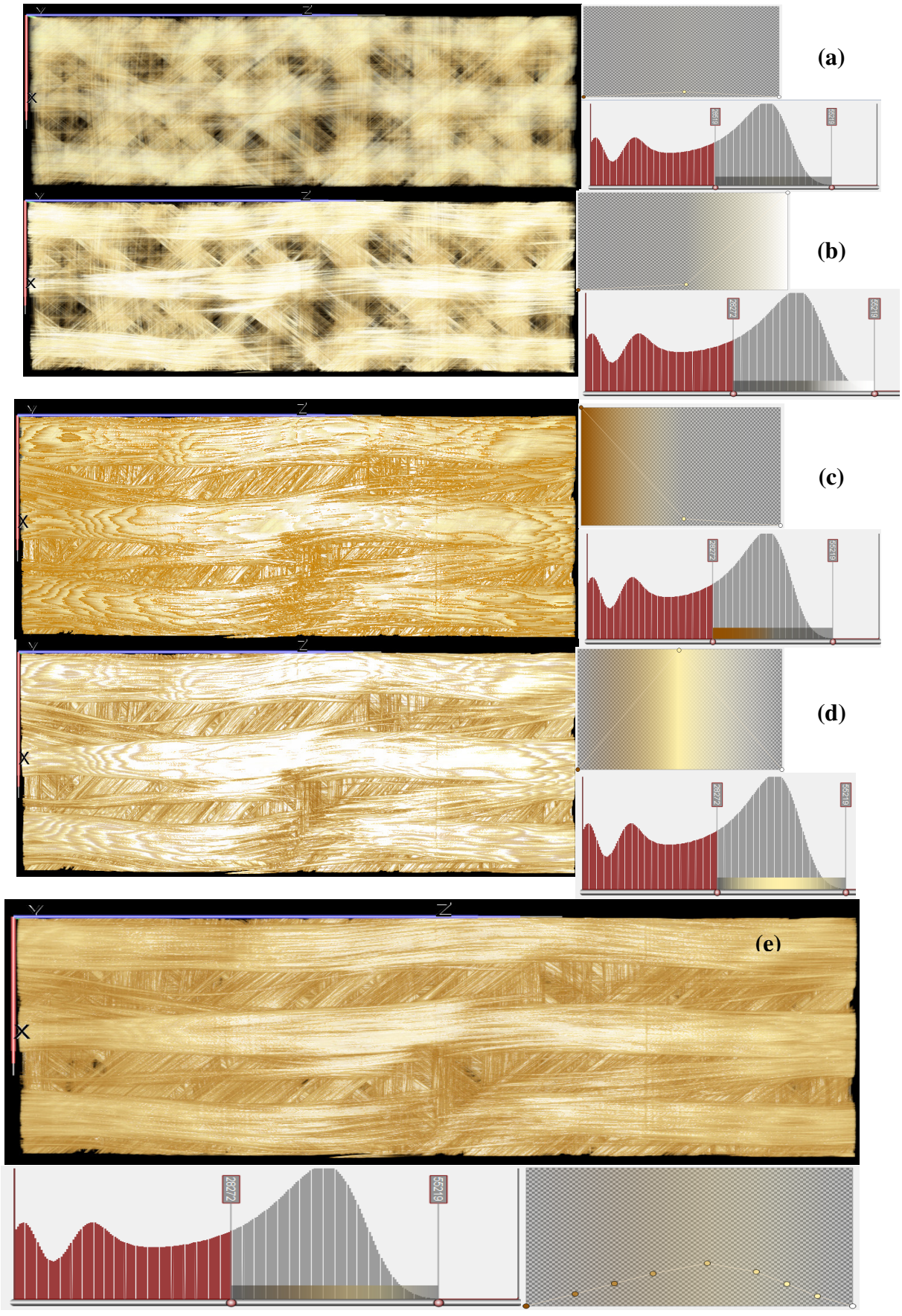

Figure D.6 (a) to (e) Opacity histogram for near-edge 4J impact with thickness 2mm

Figure D.6 (e) shows the multiple opacity points for better detection of impact damage and delamination areas. Thus depending upon the project requirements one can choose the opacity levels. The results in chapter 4 are based on different opacity levels.

Abaqus (http://www.3ds.com)

Abaqus Analysis User's Manual, Version 6.10, 2010.

Abaqus/Explicit Analysis User's Manual, Version 6.10, 2010.

Abel,R.L.,Laurini,C.R.,Richter,M. (2012), 'A palaeobiologist's guide to virtual micro-CT preparation', *Palaeontologia Electronica.* Vol. 15, Issue 2.

Abrate, S. (1991), 'Impact on Laminated Composite Materials', *Applied Mechanics Reviews*, Vol. 44(4), pp: 155–190.

Abrate, S. (1998), '*Impact on Composite Structures*', Cambridge University Press.

Airbus A3XX, European Aeronautic Defence and Space Company (www.airbus.co.uk)

AIRBUS, CAI mounting fixture, AITM 1-0010, ISO 18352, EN 6038.

Andersson,L. (2011),'Shaping macroporous ceramics - templated synthesis, X-ray tomography and permeability', *Department of Materials and Environmental Chemistry Stockholm University*, Doctoral Thesis.

Aoki, Y., Samejima, H., Suemasu, H., Nagao, Y. (2009) 'Effect of thickness on impact damage and CAI behaviour', *Proc. ICCM17*, Edinburgh, UK.

Ashby, M., Johnson, K. (2009) *'Materials and Design: The Art and Science of Material Selection in Product Design*', 2nd Edition, Butterworth-Heinemann.

Aslan, Z., Karakuzu, R., Sayman, O. (2002), 'Dynamic Characteristics of Laminated Woven E-Glass-Epoxy Composite Plates Subjected to Low Velocity Heavy Mass Impact', *Journal of Composite Materials*, Vol.36, pp: 2421-2442.

Aslan, Z., Karakuzu, R., Okutan, B. (2003), 'The response of laminated composite plates under low velocity impact loading.' *Journal of Composite Structures,* Vol.59, pp: 119-27.

Australian Transport Safety Bureau (2010), Airbus A380-842, ATSB Transport Safety Report – AO-2010-089.

Aymerich, F., Pani, C. and Priolo, P. (2007), 'Effect of Stitching on the Low-Velocity Impact Response of $[0_3/90_3]$s Graphite/Epoxy Laminates', *Composites: Part A,* Vol. 38, No. 4, pp: 1174-1182.

Beaumont, P.W.R., Riewald, P.G., Zweben, C. (1974), 'Methods for improving the impact resistance of Composite Materials', *Foreign Object Impact Damage to Composites*, ASTM STP 568, pp: 134-158.

Belingardi, G., Vadori, R. (2002), 'Low Velocity Impact Tests of laminate glass-fibre epoxy matrix composite materials plates', *International Journal of Impact Engineering*, Vol.27, pp: 213–229.

Berner,J. (2007), 'Bolted Repair Design and Process Considerations', *Commercial Aircraft Composite Repair Committee (CACRC) Meeting and Related Industry/FAA/EASA Workshop,* Amsterdam.

Blohm, C. (2007), 'Lufthansa Perspectives on Safe Composite Maintenance Practices.' *Composite Damage Tolerance and Maintenance, Commercial Aircraft Composite Repair Committee (CACRC) Meeting and Related Industry/FAA/EASA Workshop,* Amsterdam.

Boeing, BSS 7260 Boeing Specification Support Standard (1988), 'Advanced Composite Compression Tests.', *The Boeing Company: Seattle*, Washington.

Boeing787, 'Composite Materials Application: Exterior surfaces' (http://www.compositesworld.com/articles/boeing-sets-pace-for-composite-usage-in-large-civil-aircraft)

Boeing Magazine (2011),
(Website: http://www.boeing.com/commercial/aeromagazine/articles/2011_q3/4/)

Bradshaw, F.J., Dorey G., Sidey. G.R. (1973), 'Impact resistance of carbon fibre reinforced plastics', *Royal Aircraft Establishment*, Farnborough, Technical Report No.: 72240.

Breen, C., Guild, F.J., Pavier, M.J. (2006), 'Impact Damage to thick Carbon Fibre Reinforced Plastic Composite Laminates', *Journal of Material Science,* Vol.41, pp: 6718–6724.

Brown,T. (2006), 'Crashworthiness of Aircraft for High Velocity Impact (CRAHVI)', Airbus (UK).

Butcher, B.R. (1979), 'The impact resistance of unidirectional CFRP under tensile stress', *Fibre Science Technology*, Vol.12, pp: 295-326.

Callister, W.D. (2006), 'Materials Science & Engineering', John *Wiley & Sons*.

Cantwell, W.J. (1981), 'The influence of target geometry on the high velocity impact response of CFRP', *Journal of Materials Science Letters*, Vol.7, pp: 756-758.

Cantwell, W.J., Morton, J. (1989), (a), 'Geometrical Effects in the Low Velocity Response of CFRP', *Composites Structures*, Vol. 12, pp: 39-59.

Cantwell, W.J., Morton, J. (1989), (b), 'Comparison of the low and high velocity impact response of CFRP', *Composites*, Vol. 20, pp: 545-551.

Cantwell, W.J., Morton, J. (1989), (c), 'The Influence of Varying Projectile Mass on the Impact Response of CFRP', *Composite Structures*, Vol. 13, pp: 101-114.

Cantwell, W.J., Morton, J. (1990), (a), 'Impact Perforation of Carbon Fibre Reinforced Plastic', *Composites Science and Technology*, pp: 119-141.

Cantwell, W.J., Morton, J. (1990), (b), 'An Assessment of the Residual Strength of an Impact-Damaged Carbon Fibre Reinforced Epoxy', *Composite Structures*, Vol. 14, pp: 303-317.

Cantwell, W. J., Morton, J. (1991), 'The Impact Resistance of Composite Materials- A Review', *Composites*, Vol. 22, No. 5, pp: 347-362.

Capriotti, E.D., Silvestri, P., Trivisonno, G. (2000), 'NDT Techniques for the Evaluation of Impact Damage on Aeronautical Structures', *Aeronautica Militare Italiana*, WCNDT Roma, Italy. (Website: http://www.ndt.net/article/wcndt00/papers/idn697/idn697.htm)

Carlsson, L.A., Adams, D.F., Pipes, R.P. (2014), *'Experimental Characterization of Advanced Composite Materials*', 4th Edition, CRC Press, Taylor and Francis Group.

CCP Composites,
(Website:http://www.ccpcomposites.eu/products-top/application-processes/hand-lay-up-a-spray-up)

Cesari, F., Dal Re,V., Minak, G., Zucchelli, A. (2007), 'Damage and residual strength of laminated carbon–epoxy composite circular plates loaded at the centre', *Composites: Part A,* Vol.38,pp:1163–1173.

Chamis, C.C., Hanson, M.P., Serafini, T.T. (1972), 'Impact Resistance of Unidirectional Fiber Composites', *Composite Materials: Testing and Design (Second Conference)*, ASTM STP 497, pp: 311-323.

Chaturvedi, S.K., Sierakowski, R.L. (1997), '*Dynamic loading and characterization of fiber-reinforced composites*', A Wiley-Interscience publication, ISBN 047113824X, pp: 257.

Cho, C., Zhao, G. (2002), 'Effects of geometric and material factors on the mechanical response of laminated composites due to low velocity impact', *Journal of Composites Materials*, Vol.36, pp: 1403-28.

Choi, H. Y., Wu, H.Y. T., Chang, F.K. (1991), 'A New Approach to Understanding Damage Mechanisms and Mechanics of Laminated Composites Due to Low-Velocity Impact: Part II– Experiments', *Journal of Composite Materials*, pp: 1012-1038.

Choi, H.Y. (1991), 'Damage in Graphite/Epoxy Laminated Composites Resulting From Low Velocity Impact', *AIAA-91-1081-CP*, pp: 1153-1161.

Chun, L., Lam, K.Y. (1998), 'Dynamic Response of Fully-Clamped Laminated Composite Plates Subjected to Low-Velocity Impact of a Mass.', *International Journal of Solid Structures,* Vol.35-11, pp: 963-977.

Columbia Accident Investigation Board (2003), 'Space Shuttle Columbia-Flight STS 107', NASA (USA).

Composite Primer, 'Composites-by-design',
(Website: http://66.147.244.180/~carbonbo/compositesbydesign/primer/)

Cormack, A.M. (1963), 'Representation of a function by its line integrals, with some radiological applications', *Journal of Applied Physics*, Vol.34, pp: 2722–7.

Crupi, V., Epasto, G., Guglielmino, E. (2011), 'Computed Tomography analysis of damage in composites subjected to impact loading', '*V. Crupi et alii, Frattura ed Integrità Strutturale'*, Vol. 17, pp: 32-41.

Dalvi, R., Abugharbieh, R., Wilson, D.C., Wilson, D.R. (2007), 'Multi-Contrast MR for Enhanced Bone Imaging and Segmentation', *In Proc. 29th Annual International Conference of the IEEE Eng. Med. Biol. Soc*., pp: 5620-5623.

Daily Mail (2014), 'Bird Strike'. (Website: http://www.dailymail.co.uk/news/article-1217035/Bird-strike-The-moment-200-starlings-sucked-passenger-jet-engine-off.html)

Davies, G.A., Hitchings, D. (1996), 'Impact Damage and Residual Strength of Woven Fabric Glass/Polyester Laminates', *Composites*, Vol. 27A, pp: 1147-1156.

Davies, G.A.O. and Zhang, X. (1994), 'Impact Damage Prediction in Carbon Composite Structures', *International Journal of Impact Engineering,* Vol. 16, No. 1,pp: 149-170.

Davies, G.A., Hitchings, D., Zhang, X. (2000), 'Damage Tolerance to Low Velocity Impact of Laminated Composites', *Defense Technical Information Center Report ADP010638.*

De Freitas, M., Silva, A., Reis, L. (2000), 'Numerical Evaluation of Failure Mechanisms on Composite Specimens Subjected to Impact Loading', *Composites: Part B*, Vol. 31, pp. 199-207.

DeMorais, W.A., Monteiro, S.N., D'Almeida, J.R.M. (2004), 'Effect of the laminate thickness on the composite strength to repeated low energy impacts', *Composite Structures,* Vol: 70 Issue 2, pp: 223-228.

Djordjevic, B. (2000), 'Remote Non-Contact Ultrasonic Testing of Composite Materials.' *Proceedings 15th World Conference on NDT*, Rome, Italy.
(Website: http://www.ndt.net/article/wcndt00/papers/idn358/idn358.htm)

Dowling, N.E. (1999), '*Mechanical Behaviour of Materials Engineering*', Methods of Deformation, Fracture, and Fatigue 2nd Edition, Prentice-Hall Inc.

Doyle, J. F. (1989), *'Wave propagation in structures: an FFT-based spectral analysis methodology*', Springer-Verlag, New York.

Drishti software. (Website: http://sf.anu.edu.au/Vizlab/drishti/)

Dunkers, J.P., Zimba, C.G., Flynn, K.M., Hunston, D.L. (1999), 'Characterization of Composite Microstructure and Damage Using Optical Coherence Tomography', *Polymers Division, National Institute of Standards and Technolog*y, Gaithersburg, MD 20899-8543.

Edgren, F., Asp, L.E. (2003), 'Compressive Failure of Impacted NCF Composite Sandwich Panels–Characterisation of the Failure Process', *Journal of Composite Materials*, Vol. 38, No. 6/2004.

Fawcett, A.J., Oakes, G.D. (2006), 'Boeing Composite Airframe Damage Tolerance and Service Experience.' *Proceedings FAA Workshop for Composite damage tolerance and maintenance*, Chicago, IL, USA.

Federal Aircraft Accident Board (2003), Boeing 737-33V Aircraft, Final Report No. 1950.

Fidler, I. (2007), 'Airline Operational Composites', Composite Damage Tolerance and Maintenance, *Commercial Aircraft Composite Repair Committee (CACRC) Meeting and Related Industry/FAA/EASA Workshop*, BA Structures, British Airways, Amsterdam.

Ganapathy, S., Rao, K.P. (1998), 'Failure analysis of laminated composite cylindrical/spherical shell panels subjected low velocity impact.' *Computer and Structures,* Vol 68, pp: 627-641.

Geandier, G. (2003), 'Microstructural analysis of alumina chromium composites by X-ray tomography and 3-D finite element simulation of thermal stresses', *Scripta Materialia*, Vol. 48(8), pp:1219–1224.

Geubelle, P.H., Taylor, J.S.(1998), 'Impact-induced delamination of composites: a 2D simulation', *Composites Part B,* Vol.29B, pp: 589–602.

Ghaffari, S., Tan, T.M., Awerbuch, J. (1990), 'An experimental and analytical investigation on the oblique impact of graphite/epoxy laminates', *22nd International SAMPE Technical Conference,* Covina, CA, USA, AMPE Symposium*,* 6–8 November 1990, pp: 494–508.

Ghomi, M.T. (2011), 'Modelling and simulation of elastic & plastic behaviour of propagating impact wave', *Mälardalen University Sweden, School of Sustainable Development of Society and Technology*, Press Dissertations No.117, ISSN 1651-4238.

GKN Aerospace (2013), C-Spar Photograph, Filton, UK.

Goldsmith, W. (1960), 'Impact: The Theory and Physical Behaviour of Colliding Solids', *Edward Arnold, London.*

Gowariker, V.R., Viswanathan, N.V., Sreedhar, J. (1986), 'Polymer Science', *New Age International Limited Publishers*.

Gozluklu,B., Oncul,G., Koseoglu, U. (2013), 'Design Concept of a CFRP External Trailing Edge for Ailerons', *Advances in Aerodynamics*, *ASME Proceedings*, Vol.1., Paper No.IMECE2013-66066, pp: V001T01A028.

Graham, R.A. (1972), 'Strain Dependence of longitudinal piezoelectric, elastic, and dielectric constants of X-cut quartz.' *Physical Review B*, Vol.6, pp: 4779–4792.

Graham, R.A. (1974), 'Shock-wave compression of x-cut quartz as determined by electrical response measurements.' *Journal of Physics and Chemistry of Solids* Vol.35, pp:355–372.

Greszczuk, L.B. (1975), 'Foreign object impact damage to composites: A symposium', *American Society for Testing and Materials*, pp: 244.

Habib,F.A. (2001), 'A new method for evaluating the residual compression strength of composites after impact.', *Composite Structures*, Vol.53, pp: 309-316.

Hashin, Z. (1980),'Failure criteria for unidirectional fiber composites', *Journal of Applied Mechanics*, Vol.47, pp: 329-334.

Hashin, Z., Rotem, A. (1973), 'A fatigue failure criterion for fiber-reinforced materials', *Journal of Composite Materials*, Vol.7, pp: 448.

Hoogsteden,W. (1992), 'Compression after impact behaviour of ARALLO-1 laminates', *Material Engineering Branch, Wright Laboratory*, AD-A259 203.

Hounsfield, G.N. (1973), 'Computerized transverse axial scanning (tomography): Part I. Description of system', *Journal of Radiology*, Vol.46, pp: 1016.

Impact-Echo Instruments (2001), '*A Self-Teaching Course and Reference for the Impact-Echo Method and Software*', Impact-Echo User's Manual v2.2a, (USA).

Jacob, P.,Goulding, L. (2002), 'An Explicit Finite Element Primer',*NAFEMS,* ISBN187437645X.

Justice, I. (2003), 'Characterisation of void and reinforcement distributions in a metal matrix composite by X-ray edge-contrast microtomography', *Scripta Materialia*, Vol.48, pp: 1259 - 1264.

Kapdia, '*Non Destructive Testing of Composite Materials'*, National Composites Network, TWI Ltd.

Koo, J.M., Choi, J.H., Seok, C.S.(2013), 'Evaluation for residual strength and fatigue characteristics after impact in CFRP composites', *Composite Structures*,Vol.105,pp: 58–65.

Kreculj, D., Rasuo, B. (2013), 'Review of impact damages modelling in laminated composite aircraft structures', *Technical Gazette,* Vol. 20, pp: 485-495.

Kuhl,E, Edwards,R.Q.(1963), 'Image separation radioisotope scanning., *Radiology*, Vol.80, pp: 653–61.

Lagace, P.A., Wolf, E. (1993), 'Impact Damage Resistance of Several Laminated Material Systems', *34th Structures, Structural Dynamics and Materials Conference, AIAA*, USA doi:10.2514/6.1993-1524.

Lakshminarayana, H.V., Boukhili, R., Gauvin, R. (1994), 'Finite element simulation of impact tests of laminated composite plates.' *Composite Structures*, Vol.28, pp: 47–59.

Li, C.F., Hu, N., Cheng, Y.G., Fukunaga, H., Sekine, H. (2002), 'Low-velocity impact-induced damage of continuous fiber-reinforced composite laminates. Part II Verification and numerical investigation', *Composites: Part A*, Vol.33: 1063–72.

Li, C.F., Hu, N., Yin, Y.J., Sekine, H., Fukunaga, H. (2002), 'Low-velocity impact damage of continuous fiber-reinforced composite laminates. Part I An FEM numerical model', *Composites: Part A,* Vol.:33:1055–62.

Li,G.,Pang,S.,Helms,J.E. (2000), 'Low Velocity Impact Response of GFRP Laminates Subjected to Cycling Moistures', *Polymer Composites*, Vol.21, No.5.

Lopes, C.S., Camanho, P., Gurdai, Z., Maimi, P., Gonzalez, P. (2009), 'Low-velocity impact damage on dispersed stacking sequence laminates. Part II Numerical simulations', *Composites Science & Technology*, Vol. 69 pp: 937-947.

Maia, L., de Oliveira, P. (2005), 'Crashworthy Composite Fuselage Section Concept for Next Generation General Aviation', *SAE Technical Paper*, 2005-01-4011.

Malhotra, A., Guild, F.J., Pavier, M.J. (2008), 'Edge impact to composite laminates: experiments and simulations', *Journal of Materials Science*, Vol.43, Iss.20, pp: 6661-6667.

Maropoulos, P.G., Muelaner, J.E., Summers, M.D., Martin, O.C. (2014), 'A new paradigm in large-scale assembly-research priorities in measurement assisted assembly.' *The International Journal of Advanced Manufacturing Technology*, Vol. 70 (1-4), pp: 621-633.

Matthews, F. L., Rawlings, R.D. (2000), *'Composite Materials: Engineering and Science'*, Woodhead Publishing Limited.

McElrone,A.J.,Choat,B.,Parkinson,D.Y., MacDowell,A.A.,Brodersen,C.R. (2013), 'Using High Resolution Computed Tomography to Visualize the Three Dimensional Structure and Function of Plant Vasculature', *Journal of Visualized Experiment,* Vol. 74, pp: 1-11.

Meo, M., Morris, A., Vignjevic, R., Marengo, G. (2003), 'Numerical simulations of low-velocity impact on an aircraft sandwich panel', *Composite Structures*, Vol.62, pp: 353-360.

Mikkor, K.M., Thomson, R.S., Herszberg , I., Weller,T. and Mouritz, AP. (2006), 'Finite element modelling of impact on preloaded composite panels'*, Composite Structures,* Vol. 75, Issue 1–4, pp: 501–513.

Mines, R.A.W., Roach A.M., Jones, N. (1999), 'High velocity perforation behaviour or polymer composite laminates', *International Journal of Impact Engineering*, Vol.22, pp: 561–588.

Mitrevski, T., Marshall, I.H., Thomson, R.S. and Jones,R. (2004), 'Low-velocity impacts on preloaded GFRP specimens with various impactor shapes', *Composite Structures*, Vol.76 Issue 3, pp: 209-217.

Moon, F.C. (1973), 'A critical survey of wave propagation and impact in composite materials', *NASA Lewis Research Centre*, Grant No. NGR 31-001-267.

NASA, NASA Reference publication 1092 (1983)–'Standard tests for toughened resin composites', USA.

Olsson, R. (2000), 'Mass criterion for wave controlled impact response of composite plates', *Composites Part A,* Vol.31, pp: 879–887.

Olsson, R. (2003), 'Closed prediction of peak load and delaminations onset under small mass impact', *Composite Structures,* Vol. 59, pp: 341–349.

Oster.R (1997), 'Computed Tomography as a Non-Destructive Test Method for Fibre Main Rotor Blades in Development, Series and Maintenance', *23rd European Rotorcraft Forum, Dresden, Germany.*

Ostre,B., Bouvet,C., Lachaud,F., Minot,C., Aboissiere,J. (2014), 'Edge impact damage scenario on stiffened composite structure', *Journal of Composite Materials,* Vol. 48, Issue:21.

Pagano, N.J.,Schoeppner, G.A. (2000), 'Delamination of Polymer Matrix Composites: Problems and Assessment', *Polymer Matrix Composites*, Pergamon Press, Oxford, UK, pp: 433-528.

Park, R. and Jang, J. (2000), 'Effect of Stacking Sequence on the Compressive Performance of Impacted Aramid Fiber/Glass Fiber Hybrid Composite', *Polymer Composites,* Vol. 21, No. 2, pp: 231-237.

Pavier M.J., Clarke M.P. (1995), 'Experimental techniques for the investigation of the effects of impact damage on carbon-fibre composites', *Composite Science and Technology,* Vol.55, pp: 157-69.

Perreta,A., Mistoub,S., Fazzinib,M., Braultb,R. (2012), 'Global behaviour of a composite stiffened panel in buckling. Part 2: Experimental investigation', *Composite Structures*, Vol.94, Issue 2, pp: 376–385.

Phoenix Airport Bird Control Services
(Website: http://www.airport-int.com/suppliers/phoenix-bird-control.html)

Prichard, J.C., Hogg, P.J., Stone, D.L. (1992), 'A Miniaturized Post Impact Compression Test', *ECCM-Composites Testing and Standardisation,* EACM, Bordeaux, France.

Reis, L., de Freitas, M., 'Damage Growth Analysis of Low Velocity Impacted Composite Panels, *Composite Structures*, Vol.38 (1-4), pp: 509-515.

Rhead, A.T., Marchant,D., Butler,R. (2010), 'Compressive strength of composite laminates following free edge impact', *Composites Part A: Applied Science and Manufacturing*, Vol. 41, Issue 9, pp: 1056–1065.

Richardson, M.O.W. and Wisheart, M.J. (1996), 'Review of Low-Velocity Impact Properties of Composite Materials', *Composites Part A,* Vol. 27, No. 12, pp: 1123-1131.

Richardson, M.W., Wisheart, M. J. (1996), 'Review of low-velocity impact properties of composite materials', *Composites A Vol. 27 pp 1123-1131.*

Sanchez-Saez, S., Barbero, E, Zaera, R., Navarro, C. (2005), 'Compression after impact of thin composite laminates', *Composites Science and Technology*, Vol. 65, Iss.13, pp: 1911–1919.

Sankar, B.V. (1996), 'Low velocity impact response and damage in composite materials', *Key Engineering Materials*, Vol.121–122, pp: 549–82.

Sansalone, M., Carino, N.J., Hsu, N.N. (1987), 'A Finite Element Study of Transient Wave Propagation in Plates', *Journal of Research of the National Bureau of Standards*, Vol. 92(4), pp: 267-278.

Schilling,P.J.,Prakash,B., Karedla,R.,Tatiparthi,A.K.,Verges,M.A., Herrington,P.D.(2005), 'X-ray computed micro tomography of internal damage in fiber reinforced polymer matrix composites', *Composites Science and Technology*, Vol.65, pp: 2071–2078.

Schoeppner, G.A., Abrate, S. (2000), 'Delamination threshold loads for low velocity impact on composite laminates.' *Composites: Part A*, Vol. 31, pp: 903-915.

Scott,A.E.,Sinclair,I.,Spearing,S.M.,Mavrogordato,M.,Bunsell,A.,Thionnet,A.(2010), 'Comparison of the accumulation of fibre breaks occurring in a unidirectional carbon/epoxy composite identified in a multi-scale micro-mechanical model with that of experimental observations using high resolution computed tomography', *Matériaux*, Nantes, France.

Shim, V.P.W., Yang, L.M. (2005), 'Characterization of the residual mechanical properties of woven fabric reinforced composites after low-velocity impact.' *International Journal of Mechanical Science*, Vol.17, pp: 647–65.

Short, G.J., Guild, F.J., Pavier, M.J. (2001), 'The effect of delamination geometry on the compressive failure of composite laminates', *Composites Science and Technology,* Vol. 61, Issue 14, pp: 2075–2086.

Short, G.J., Guild, F.J., Pavier, M.J. (2002), 'Delaminations in flat and curved composite laminates subjected to compressive load', *Composite Structures*, Vol.58, Issue 2, pp: 249–258.

Shyr, T.W., Pan, Y.H. (2003), 'Impact resistance and damage characteristics of composite laminates'. *Composite Structures*, Vol. 62, pp: 193-203.

Sihn, S., Kim, R.Y., Kawabe, K. and Tsai, S.W. (2007), 'Experimental Studies of Thin-Ply Laminated Composites', *Composite Science and Technology,* Vol. 67, No. 6, pp: 996-1008.

Simulia (2007), 'Projectile Impact on a Carbon Fiber Reinforced Plate', Abaqus Technology Brief, TB-06-CRP-1.

Slaney, M., Kak, A. C., Larsen, L. E. (1984), 'Limitation of imaging with first-order diffraction tomography', *IEEE Trans. Microwave Theory and Tech.,* Vol.8, 860–874.

Sosa, J.L.C., Phaneendra, S., Munoz, J.J.(2012), 'Modelling of mixed damage on fibre reinforced composite laminates subjected to low velocity impact', *International Journal of Damage Mechanics,* Vol. 22 (3), pp: 356-374.

'Standard Guide for Computed Tomography (CT) Imaging' (1995), *American Society for Testing and Materials,* ASTM E1441-11.

Stavropoulos, C.D. and Papanicolaou, G.C. (1997), 'Effect of Thickness on the Compressive Performance of Ballistically Impacted Carbon Fibre Reinforced Plastic (CFRP) Laminates', *Journal of Materials Science,* Vol. 32, No. 4, pp: 931-936.

Summerscales, J. (1990), 'Non-destructive testing of advanced composites: a review of recent advances', *British Journal of Non-Destructive Testing*, Vol.32 (11), pp: 568-577.

Sun, C.T., Chattopadhyay,S. (1975), 'Dynamic response of anisotropic laminate plates under intial stress to impact of a mass.', *Journal of Applied Mechanics*, Vol.42, pp: 693-698.

Sutherland, L.S., Soares, C.G. (2004), 'Effect of laminate thickness and of matrix resin on the impact of low fibre-volume, woven roving E-glass composites', *Composites Science and Technology,* Vol.64, pp: 1691-1700.

Symons, D.D. and Davis, G. (2000), 'Fatigue Testing of Impact-Damaged T300/914 Carbon-Fibre-Reinforced Plastic', *Composites Science and Technology,* Vol. 60, No.3, pp: 379-389.

Tai, N.H., Ma, C.C.M., Lin, J.M. and Wu, G.Y. (1999), 'Effects of Thickness on the Fatigue-Behavior of Quasi-Isotropic Carbon/Epoxy Composites before and after Low Energy Impacts', *Composites Science and Technology,* Vol. 59, No. 11, pp: 1753-1762.

Tiberkak, R., Bachene, M., Rechak, S., Necib, B. (2008),'Damage prediction in composite plates subjected to low velocity impact.' *Composite Structures*, Vol. 83 (1), pp: 73-82.

Toland, R.H.(1974), 'Impact testing of Carbon-Epoxy Composite Materials', *Instrumented Impact Testing*, ASTM STP 563, American Society for Testing and Materials, pp:133-145.

Tuttle,M.E.(2013), *'Structural Analysis of Polymeric Composite Materials'*, CRC Press, Taylor and Francis Group.

Ullah,H., Harland,A.R., Silberschmidt,V.V. (2012), 'Experimental and Numerical Analysis of Damage in Woven GFRP Composites Under Large-deflection Bending', *Applied Composite Materials*, Vol.19, pp: 769–783.

Ullah, H., Harland, A.R., Silberschmidt, V.V. (2014), 'Evolution and interaction of damage modes in fabric-reinforced composites under dynamic flexural loading', *Composites Science and Technology,* Vol.92, pp: 55–63.

Wang, C.J., and Jang, B.Z. (1991), 'Deformation and Fracture Mechanisms of Advanced Polymer Composites under Impact Loading', *Journal of Thermoplastic Composite Materials*, Vol. 4, pp. 140-172.

Wang, H., and Vu-Kanh, T. (1998), 'Low-Velocity Impact Damage in Laminated Composite Materials, Impact Response and Dynamic Failure of Composites and Laminate Materials', *Key Engineering Materials*, Vol.141-143 (Part 1), pp: 277-304.

Wang, S.X., Wu, L.Z., Ma, L. (2010), 'Low-velocity impact and residual tensile strength analysis to carbon fiber composite laminates', *Materials and Design,* Vol.31, pp:118–125.

Wang,X.W., Pont-Lezica,I., Harris,J.M., Guild,F.J., Pavier,M.J. (2005), 'Compressive failure of composite laminates containing multiple delaminations', *Composites Science and Technology,* Vol.65, pp: 191–200.

Wardle, M.W., Tokarsky,E.W. (1983), 'Drop Weight Impact Testing of Laminates Reinforced with Kevlar Aramid Fibres, E-Glass and Graphite.', *Composite Technology Review,* Vol. 5 (1), pp: 4-10.

Wiggenraad J.F.M., Zhang X., Davies, G.A.O. (1999), 'Impact damage prediction and failure analysis of heavily loaded, blade-stiffened composite wing panels', *Composite Structures*, Vol.45, pp: 81-103.

Wiggenraad, J.F.M., Aoki, R., Gaedke, M., Greenhalgh, E., Hachenberg, D., Wolf, K., Buebl, R. (1996), 'Damage Propagation in Composite Structural Elements-Analysis and Experiments on Structures', *Report no. TP 96341, NLR*, Amsterdam, Netherlands.

William, H.G.,Wells,.J.M. (2001), 'Non-destructive Characterization of Impact Damage in Metallic/Non-metallic Composites Using X-ray Computed Tomography Imaging', *ARL-TR-2399, Army Research Laboratory*, Aberdeen.

Winkel, J. D. and Adams, E. H. (1985), 'Instrumented Drop Weight Impact Testing of Cross-Ply and Fabric Composites.' *Composites* Vol.4, pp: 268-278.

Wright.P, Fu,X., Sinclair,I.,Spearing,S.M.(2008), 'Ultra High Resolution Computed Tomography of Damage in Notched Carbon Fiber Epoxy Composites', *Journal of Composite Materials*, Vol.42, pp:1993-2002.

Wu, H.Y. T., Chang, F.K. (1989), ' Transient dynamic analysis of laminated composite plates subjected to transverse impact.', *Computers and Structures*, Vol. 31(3), pp: 453–466.

Young,S.A. (2009), 'High Resolution X-ray Tomography of Fiber Reinforced Polymeric Composites', *University of Tennessee – Knoxville,* Master thesis.

Yuan,J.,Takedai,N.,Waas,A.M. (2000), 'Compressive Failure Mechanism and Impact Behavior of Unidirectional Carbon-Fiber/Vinyl Ester Composites', *Journal of Composite Materials*, Vol. 35, No.16/2001.

Zaretsky,E., DeBotton,G., Perl,M. (2004), 'The response of a glass fibres reinforced epoxy composite to an impact loading', *International Journal of Solids and Structures, Vol.*41,pp: 569-584.

Zhang, X. (1998), 'Impact damage in composite aircraft structures experimental testing and numerical simulation', *Journal of Aerospace Engineering*, Vol. 212, pp: 245–259.

Zhou, G. (1995), 'Damage Mechanisms in Composite Laminates Impacted by a Flat-Ended Impactor', *Composites Science and Technology*, Vol.54, pp: 267-273.

Zhou.G, S.R. Reid (2000), *'Impact Behaviour of Fibre-reinforced Composite Materials and Structures'*, Woodhead Publishing Limited, Cambridge.

Zukas, J.A. (1982), *'Impact Dynamics'*, John Wiley & Sons.